ANALYSIS, MODELING AND OPTIMUM DESIGN OF SOLAR DOMESTIC HOT WATER SYSTEMS

LIN QIN

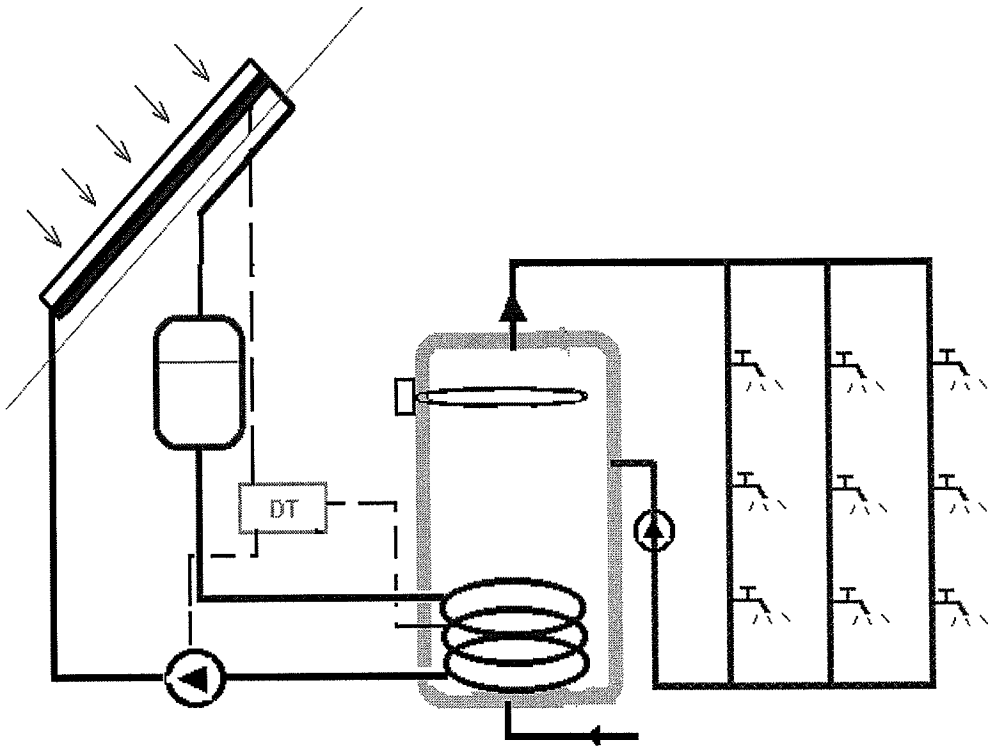

REPORT
R-22
1998

ISSN 1396-4011
ISBN 87-7877-023-8

DEPARTMENT OF BUILDINGS AND ENERGY
TECHNICAL UNIVERSITY OF DENMARK

Analysis, Modeling and Optimum Design of Solar Domestic Hot Water Systems

Lin Qin

Department of Buildings and Energy
Technical University of Denmark
July 1998

ISBN 87-7877-023-8

Preface

This thesis has been prepared at the Department of Buildings and Energy, Technical University of Denmark, as a part of the requirements for the Ph.D. degree. The research presented in this thesis has been carried out under the guidance of my supervisor Simon Furbo and Professor Svend Svendsen at the Department of Buildings and Energy, Technical University of Denmark.

My thanks are due to Simon Furbo for his encouragement and guidance throughout the study, and to Professor Svend Svendsen for inviting me to work in his Laboratory and supporting and directing me during this study.

Thanks are also due to Hans Lund, Morten Carlsen, Jens Rahbek, Louise Jivan Shah, Niels Kristian Vejen, Department of Buildings and Energy, Technical University of Denmark, for numerous fruitful discussions and advice during the course of this work.

I would also like to use the opportunity to sincerely thank all the members of the staff of the Department of Buildings and Energy, Technical University of Denmark for their friendship, kindness and great help during my stay at this Department. Special thanks to Anne Rasmussen for her kind help with the proofreading and correction of this thesis.

My study has been partly founded by Daloon Foundation, Technical University of Denmark and Department of Buildings and Energy. I would like to submit my thanks to these organizations.

Finally, I thank my family and friends for their great support during this study.

April 1998

Lin Qin

Summary

This study focuses on the analysis, modeling and simulation of solar domestic hot water (DHW) systems. Furthermore, problems related to the system operation, such as input weather data and hot-water load conditions are investigated.

The magnitude and the monthly variation of solar radiation in Beijing (China) and in Denmark are analyzed both by theoretical calculations and the analysis of long-term measurements. Based on the weather data from the Beijing Meteorological Station during the period of 1981-1993, a Beijing Test Reference Year has been formulated by means of statistical analysis. A brief introduction about the Danish Test Reference Year and the Design Reference Year is also presented.

By means of a literature study, the hot-water load and the load pattern for domestic hot water systems are discussed. In order to investigate the heat loss as a part of the total heat load, dynamic models for distribution networks have been developed, and simulations have been carried out for typically designed distribution networks of the circulation type. The influence of operation parameters such as the tank outlet temperature, the hot-water load and the load pattern, on the heat loss from the distribution networks is presented. It was found that the tank outlet temperature has a significant influence on the heat loss from a circulation type of distribution network, while the hot-water load and the load pattern have no obvious effect.

Dynamic models of drain-back tanks, both as a separated tank and combined with a mantle tank, have been developed and presented. Models of the other basic components commonly used in solar DHW systems, such as flat-plate collectors, connection pipes, storage tanks with a heat exchanger spiral, and controllers, are also described.

For the dynamic simulation of thermosyphon solar DHW systems, a thermosyphon loop model with the thermosyphon loop directly connected to a storage tank has been put forward. Based on the program SOLSIM, simulations have been carried out to investigate the effects of the design parameters on the thermal performance of the system. Several recommendations are given for the optimum design of such type of systems.

Dynamic models for drain-back solar DHW systems, both with spiral heat exchanger tank and mantle tank, have been developed. To make sure that the models may be used to describe the real thermal process, they have been verified by means of comparison of the simulated temperature and energy quantities with measured data. Based on the verified models, the long-term thermal performances of the two tested systems have been predicted. To investigate the influence of design parameters on the thermal performance of the system, a number of simulations have been carried out and recommendations have been given for optimum design of these types of drain-back systems.

In order to gain a better understanding of the impact of the drain-back design and of different working fluids on the system performance, simulations were also performed for parallel systems, both with normal and with drain-back design. It was found that the usage of water instead of a water/glycol mixture as a working liquid in a drain-back system makes the contribution to the improvement of the system thermal performance.

Based on 10 *min* measurements of weather parameters in Denmark during 1996, the impact of the time scale of input weather data on simulation results was investigated. It was found that the time scale of input weather data has a small effect on the simulated system thermal performance. However, the influence is relatively strong on the low-flow combi tank systems as compared to systems with preheating tank design.

Key words: ***Solar heating, climatic data, domestic hot water, heat load, distribution network, thermosyphon, drain-back, thermal performance, modeling, simulation.***

Resumé

Dette studie fokuserer på analyse, udformning og simulering af solvarmeanlæg til brugsvandsopvarmning. Derudover undersøges blandt andet hvorledes vejret og varmtvandsforbruget påvirker anlæggenes driftsforhold.

Mængde og månedlig variation af solstråling i Beijing (Kina) og Danmark analyseres, både ved hjælp af teoretiske beregninger og ved bearbejdelse af målinger fra langvarige perioder. Baseret på vejrdata fra Beijing Meteorological Station for perioden 1981-1993 er der udarbejdet et Test Referenceår for Beijing ved hjælp af statistiske analyser. Der gives også en kort introduktion til Det Danske Test Referenceår og Design-referenceåret.

Ved hjælp af et litteraturstudie gøres der rede for varmtvandsforbrug og forbrugsmønsteret for anlæg til brugsvandsopvarmning. For at undersøge varmetabet som en del af det totale varmebehov er der udviklet dynamiske modeller for distributionsnet, og simuleringer er udført for karakteristisk udformede distributionsnet med en cirkulationsledning. Driftsparametres indflydelse på varmetabet fra distributionsnettene, såsom fremløbstemperaturen fra tanken, varmtvandsforbruget og forbrugsmønsteret, er bestemt. Det har vist sig at fremløbstemperaturen fra tanken har en betydelig indflydelse på varmetabet fra et distributionsnet med en cirkulationsledning, hvorimod varmtvandsforbruget og forbrugsmønsteret ikke har nogen særlig effekt.

Dynamiske modeller af tømmetanke, både som separat tank og kombineret med en kappebeholder, er blevet udviklet. Modeller af andre komponenter der er almindeligt benyttede i solvarmeanlæg til brugsvandsopvarmning, såsom solfanger, rørkreds, lagertanke med indbygget varmevekslerspiral og styresystemer, bliver også beskrevet.

Der er opbygget en simuleringsmodel for selvcirkulerende solvarmeanlæg til brugsvandsopvarmning. Den selvcirkulerende kreds er direkte koblet til en varmtvandsbeholder. Baseret på programmet SOLSIM er der udført simuleringer for at undersøge designparametrenes effekt på anlægsydelsen. Der gives mange forslag til optimal udformning af denne type anlæg.

Der er udviklet simuleringsmodeller for solvarmeanlæg til brugsvandsopvarmning udformet efter tømmesystemprincippet. Anlæg både med spiralbeholdere og kappebeholdere er taget i beregning. For at sikre at modellerne kan bruges til at beskrive virkeligheden, er de blevet efterprøvet ved at sammenligne simulerede temperaturer og energimængder med målte data. Ved hjælp af de efterprøvede modeller er de årlige ydelser for de to afprøvede tømmeanlæg blevet bestemt. For at undersøge designparametrenes indflydelse på anlægsydelsen er der udført en del simuleringer og der er givet forslag til optimal udformning af disse typer tømmeanlæg.

For at få en bedre forståelse af den indvirkning tømmeanlæggets udformning og forskellige solfangervæsker har på anlægsydelsen, blev der også udført simuleringer for anlæg, både

med normal udformning og med tømmeanlægs-udformning. Det blev konstateret at tømmeanlæggets ydelse er højere end ydelsen af det normale anlæg fordi der benyttes vand som solfangervæske i tømmeanlægget, mens der benyttes en glycol/vand-blanding med dårligere termiske egenskaber i det normale solvarmeanlæg.

Baseret på 10-minuts-målinger af vejrparametre i Danmark i 1996, blev det undersøgt hvorledes det anvendte tidsskridt for de benyttede vejrdata påvirker simuleringsresultaterne. Det blev konstateret at tidsskridtet for vejrdata har en lille effekt på den simulerede anlægsydelse. Indflydelsen er størst for low-flow kombi tank-anlæg.

Nøgleord: ***Solvarme, klimadata, varmt brugsvand, varmtvandsforbrug, distributionsnet, selvcirkulation, tømning, anlægsydelse, udformning, simulering.***

Contents

Preface

Summary

Resumé (summary in Danish)

Contents

Chapter 1

Introduction

1.1 Background

Solar radiation is our abundant permanent source of energy, and the application of solar energy is expected to play an important role in the future. By means of different mechanisms, solar radiation may be converted into other forms of energy, such as photovoltaic conversion into electric energy, photochemical conversion into chemically bound energy, and photothermal conversion into heat. The heat converted from solar radiation is well suited to provide domestic hot water and space heating. In most parts of the world, the yearly solar radiation received by a single family house is several times greater than the energy needed for domestic hot water and space heating.

For many years, solar domestic hot water (DHW) systems have gained great attention due to their considerable energy conservation, environmental protection and relatively good economy. The purpose of using a solar DHW system is to convert the solar radiation into thermal energy, and then to use it for domestic hot water heating, thus reducing the consumption of conventional energy. Recently, environmental issues have led to an even greater interest in solar DHW systems.

Several fundamental conditions make solar DHW systems very different from conventional fossil-fuels systems. First, the power density of solar radiation is relatively low and the collector has to cover a large area. Thus the solar DHW systems cannot be as compact as conventional units. Secondly, the solar radiation varies considerably during the day, in the course of a year and between different locations. Therefore, the solar energy received by a collector is an irregular function of time and location, and the power output of the collector cannot be controlled in the same way as conventional heating systems. Consequently, heat storage and auxiliary energy are required to match the supply to the load. Furthermore, a solar DHW system will never operate under steady-state condition.

One major problem related to solar DHW systems is that they are not competitive economically to conventional ones. So far, the heat produced by burning fossil fuels still costs less than solar heat. In the future, the cost of conventional energy will probably increase due to energy shortage and adverse environmental effects. However, the most efficient way out of the problems should be to increase system efficiency and to decrease the cost of the systems. This indicates the importance of optimum design of solar DHW systems.

When designing a solar DHW system, both the magnitude and the pattern of the heat load should be analyzed to determine the necessary heat production. Normally the heat load is calculated according to the total daily hot water consumption, and the dynamic behaviour of the load is only rarely focused on. However, research has shown that the heat load is a very important factor in the operation of solar DHW systems where the solar fraction largely depends on the load level and the load pattern. Therefore, an investigation of how different parameters affect the heat load is necessary.

A detailed investigation of the solar energy resources for a specific region is also important, due to the irregular local behaviour of solar radiation. Together with the heat load, solar radiation forms the most important basis for system design. As far as the optimum design of a system is concerned, the system location has to be specified. In this study both Denmark and Beijing in China are chosen as the given locations.

Normally, a typical solar DHW system consists of a collector loop, a storage tank and an auxiliary heating system. The solar collector works as a photothermal conversion device and the capacity of the collector should be carefully matched to the load, in order to keep the investment as low as possible. Heat storage is another major issue for solar DHW systems. Basically, heat from the collector is transferred to the storage tank and stored as sensible heat of water. However, the storage of heat cannot be done without heat losses to the surroundings, and this influences the system efficiency considerably.

In the last decades, many typical designs of solar DHW systems have been developed all over the world, and many investigations on the performance of these systems have been carried out both theoretically and experimentally. However, there is still insufficient information on the dynamic behaviour of many of those types of systems. To carry out an optimum design, the dynamic properties of the system have to be investigated. In the present project, thermosyphon and drain-back solar DHW systems have been chosen as the types of systems to be studied.

Thermosyphon systems have been and still are one of the most popular systems in many parts of the world, especially in developing countries, due to their simple construction and good economy. Different from other types of design, the operation of such systems depends on a large number of design and climatic variables, which makes the theoretical analysis difficult. Although many authors have conducted studies on the effect of individual variables on the performance of the system, it is necessary to conduct a comprehensive study on the impact of most of the design parameters.

In most parts of the world, freeze-protection is the common problem that faces the solar DHW system design. To solve this problem, one general solution is the use of an anti-freeze working liquid in the collector loop. However, from both the efficiency and the environmental point of view, the anti-freeze liquid should be avoided. The other possible solution is then the mechanical method that is the drain-back design of the system. During the course of time, many different types of drain-back solar DHW systems have been introduced into the market, but only a few investigations on drain-back systems have been reported. To predict the system performance and optimize the system design, it is necessary to perform a detailed study on this type of systems.

The design of solar DHW systems is a complex process, due to characteristics inherent in the solar heating technology. Recently, computer simulation has become a widely used technique to improve the understanding of the thermal processes in the system, and to support the optimum design. Many simulation programs of various degree of detail have been developed during the last twenty years by different research groups. Since none of these programs are able to include every kind of system design, dynamic models for new systems are needed. The simulation in this study was mainly based on several simulation programs that have been developed at the Department of Buildings and Energy, Technical University of Denmark.

When the optimization of a system is to be performed, not only the appropriate simulation models are needed, but also the related operation conditions have to be studied. Therefore, the investigation of the solar energy resource for certain locations, the study of dynamic modeling of the system and the heat load, and the analysis of the optimum design of thermosyphon and drain-back systems via the models form the background of this study.

1.2 The scope of the study

This study concentrates on the development and the verification of models for carrying out the simulation and evaluation of the dynamic performance of solar DHW systems. Conditions related to system operation, such as heat load and weather influence are also investigated.

Basically, a complete DHW system consists of four major parts: ① the hot water consumer, ② the distribution network, ③ the hot water storage, and ④ the heat production unit (for solar DHW system, this is the solar collector loop). The basic principle of the solar DHW system design is to fulfill the hot water need of the consumer under all conditions of normal use.

In order to carry out the simulation of solar DHW systems, it is necessary to develop dynamic models of the basic components used in these systems. The models for some fundamental components such as solar collector, heat storage and pipes have been analyzed comprehensively in previous work, and were adopted in this study. The component models which are going to be developed in the present study are the thermosyphon loop model and drain-back tank models. To make sure that the developed models represent the physical reality, the models will be verified by means of comparisons of the simulated results with measurements from laboratory tests.

To carry out the simulation of solar DHW systems, the weather data of the specified region have to be studied in order to generate a weather data file. Here, we use a so-called Test Reference Year (TRY), which may represent the typical weather conditions of the region. In this study climatic conditions in both Beijing and Denmark are analyzed and long-term climatic data from Beijing are studied to generate a Beijing TRY. The Danish TRY and Design Reference Year (DRY) (which were set up in previous work) will also be used for the system simulation under Danish conditions.

As mentioned before, the heat-load calculation is the basis for general work concerning any DHW system design. One purpose of this project is to investigate the total heat load which commonly includes both hot water load from the consumer and heat loss from the distribution

networks. In order to simulate how the network affects the total load conditions, a dynamic model of distribution networks will be developed.

System evaluation is a central element in the design process. The main scope of this project is to build up a certain type of system models (thermosyphon and drain-back systems) which are suitable for system simulation and evaluation, the main interest focusing on an appropriate description of the thermal processes. To ensure that the developed models are able to describe a real situation, they will again be verified by means of measured data if the latter are available. After the system models have been set up, the influence of each design parameter on the system efficiency may then be evaluated via a series of system simulations.

The most important fact of system simulation is that the simulated results should accurately represent the physical reality. However, the commonly used hourly input weather data are not taking the short-term variation of the radiation (due to changing cloud coverage) into consideration. Therefore, using hourly input weather data may, to some degree, lead to an error in the simulation result. The impact of the time scale of input weather data on the simulation results is investigated by using 10-minute measurements from Denmark in 1996.

1.3 The structure of the report

Chapter 2 analyses the climatic conditions in both Beijing and Denmark. Long-term (1981-1993) climatic data from the Beijing Meteorological Station are studied, and a Beijing TRY is generated based on statistical analysis. A brief introduction to the Danish TRY and DRY is also presented.

Chapter 3 presents an investigation on the total heat load of solar DHW systems. The dynamic model of the distribution network is developed, and the influence of the heat loss from the distribution net work on the total heat load is presented. Based on literature studies, the hot water load of the consumer is also investigated.

Chapter 4 describes the dynamic models of fundamental components for solar DHW systems. Models for drain-back tanks are developed in this project. Other component models, such as solar collector, spiral heat exchanger, storage tank with heat exchanger spiral, and control systems are based on previous work.

Chapter 5 presents the dynamic model of thermosyphon systems. System simulation and evaluation are carried out for the thermosyphon system with a thermosyphon loop directly connected to the storage tank. Several recommendations are made for optimum design parameters of this type of system.

In **Chapter 6,** dynamic models of drain-back solar DHW systems with both a spiral heat exchanger tank and a mantle tank are studied. The system models are verified by comparing the simulated energy quantities to measured results from a laboratory test. System simulations are carried out to investigate the effect of the design parameters on the thermal performance of the system for both types.

Chapter 7 investigates the impact of the time scale of input weather data on the simulation results. The short-term (10 min) measurements of climatic data from Denmark in 1996 are used for the simulation. Time scales of 10 to 60 minutes are used for the input weather data.

Chapter 8 includes conclusions and further discussions.

Chapter 2

Solar radiation and meteorological Test Reference Year

2.1 Introduction

The solar radiation is the basic premise and fundament for the application of solar energy. Analysis of the solar radiation is therefore the most important work for the design of any type of solar energy systems.

Besides radiation data, the operation of solar thermal systems is also largely dependent upon other climatic variables, such as ambient temperature, relative humidity, wind speed and sunshine duration. All these climatic variables can be described as irregular functions of time and location, both on small (hourly or daily) and large (monthly or yearly) time scales. It is the irregularity and the local behaviour of the weather which complicate the analysis and design of solar heating systems. To carry out the system optimization and performance prediction, specified locations have to be defined. In this study Denmark and Beijing, China are chosen as the specified areas where the design of solar DHW systems is performed.

After the geography locations have been decided, the performance prediction and optimum design of solar DHW systems could be done by series of long-term simulations under the local climatic conditions. To carry out such simulations, sufficient long-term hourly weather data must be provided, and significant computational work is involved. In reality, the simulation is often limited by a lack of long-term hourly data.

Viewed on a short-term basis, and in a certain area, meteorological variables often seem to be highly random and irregular. However, long-term statistical analysis indicates that these variables are predictable to some degree. Therefore, the dynamic nature of weather data can be smoothed out by formulating a representative year which can characterize the mean-value behavior of the weather over a long period. Based on this idea, meteorological "Test Reference Years (TRY)"[12] (in Europe) and "Typical Meteorological Years (TMY)"[40] (in America), which represent the typical weather conditions for certain regions, have been developed.

Basically, a TRY is a collection of climatic data for a given location and for one year, arranged as hourly, simultaneous weather parameters. The data from a TRY can be used as input weather data for computer simulations to predict the typical annual performance of

solar energy systems. Therefore, by using a TRY, the prediction of long-term performance may be greatly simplified.

In this chapter, the effort is concentrated on the analysis of climatic data and the setup of a TRY for Beijing. Long-term weather data from Beijing Meteorological Station are used as the basic data for statistical analysis and construction of a TRY for Beijing.

For Denmark, the TRY and its later version Meteorological Design Reference Years (DRY) [44] have been developed in previous work. Here, only a brief introduction about Danish TRY and DRY is presented.

2.2 Solar radiation for Beijing and Denmark

The intensity of the solar radiation received at the ground surface in a certain area depends on the position of the sun in the sky, and on various atmospheric effects. Furthermore, the solar energy reaching a solar collector at a certain location depends on the relative position of the collector.

The geometrical aspects, namely the sun's apparent movement in the sky, the rotation of the earth and their effects on the incidence angle of radiation on a surface are the fundamental influence facts of solar radiation in a certain area. Extraterrestrial radiation (with no atmosphere) on any surface can be simply determined by these geometrical aspects. However, not all the extraterrestrial radiation is available at ground level due to various atmospheric effects such as scattering of short-wavelength radiation by atmosphere molecules, scattering by aerosols or dust and absorption by some atmospheric gases. If the sky is totally or partly overcast, the reflection, scattering and absorption by clouds will have further influence.

Since the atmospheric effects are highly random and impossible to predict, the real available solar radiation in a certain area has to rely on the measurements. However, the extraterrestrial radiation and the theoretical maximum possible values on ground level may still be of great importance for obtaining a brief view of the basic solar radiation and its changing patterns for certain areas.

2.2.1 Geography position and climate

Beijing is located in China at the continent of east Asia at about 39.5° northern latitude and 116.4° eastern longitude with a total area of 16,800 square kilometers. In most time of the year, it receives dry, temperate continental air-masses. The yearly sunshine duration (beam irradiance larger than 200W/m^2) is about 2800 hours.

Denmark is, apart from Greenland, situated in the northern temperate zone and its geography location is about 55.5° northern latitude and 12.5° eastern longitude. Air-masses of maritime origin are most common in Denmark, however, for approximately 2000 h a year, Denmark receives dry, continental air-masses. Both situations are possible in all months, with easterly

winds most frequent in the first half of the year. Further, because the temperature is generally rising in the first half of the year, humidity and precipitation are generally low during the spring.

2.2.2 Maximum possible global radiation

The maximum possible global radiation on horizontal surface can be calculated from the extraterrestrial radiation and maximum clearness index. Extraterrestrial solar irradiance on any surface is simply the product of the solar constant and the cosine of the incidence angle θ of the sun ray with respect to the surface. According to [8], it can be determined as:

$$B_{s0} = B_0 \cdot r \cdot \cos\theta \tag{2.2.1}$$

Where B_{s0} and B_0 are the extraterrestrial irradiance on a surface and the solar constant, respectively. r is the sun-earth distance correction factor, and can be calculated according to the day number (dn=1 to 365) in a year:

$$r = 1 + 0.034 \cdot \cos(0.986 \cdot dn - 2°) \tag{2.2.2}$$

For horizontal plane, incident angle θ can be derived from solar altitude γ. Daily extraterrestrial irradiation on a horizontal surface can then be computed by integrating the irradiance with respect to time between sunrise and sunset by the following equation.

$$G_{0d} = \frac{24}{2 \cdot \pi} \cdot B_0 \cdot r \cdot \int_{-\omega_0}^{\omega_0} \sin\gamma \cdot d\omega \tag{2.2.3}$$

Rearrangement of Eqn. 2.2.3 yields:

$$G_{0d} = \frac{24}{\pi} \cdot B_0 \cdot r \cdot (\frac{\pi}{180} \cdot \omega_0 \cdot \sin\phi \cdot \sin\delta + \sin\omega_0 \cdot \cos\phi \cdot \cos\delta) \tag{2.2.4}$$

Here, G_{0d} is the daily extraterrestrial irradiation on a horizontal surface and ω_0 is the sunset hour angle. δ, ϕ and ω are declination, latitude and hour angle, respectively.

The declination is the angle between the sun-earth axis and the equatorial plane. It varies from +23.45° at summer solstice to -23.45° at winter solstice. At a certain day of the year, the declination may be computed from a more accurate formula which was proposed by Bourges[8].

$$\begin{aligned} \delta = {} & 0.3723 + 23.2567\sin w\psi + 0.1149\sin 2w\psi \\ & - 0.1712\sin 3w\psi - 0.7580\cos w\psi \\ & + 0.3656\cos 2w\psi + 0.0201\cos 3w\psi \end{aligned} \tag{2.2.5}$$

where

$$\psi = dn - 79.301 - 0.2422(Y - 1969) + INT((Y - 1969)/4)$$

$$w = 360/365.2422$$

Here, Y is the year and INT is the integer part function.

The clearness index k_T is defined as the ratio of global irradiance on a horizontal plane to the extraterrestrial value. It normally ranges between 0.05 for a heavily overcast sky to 0.75 for a very clear sky[8]. From this maximum clearness index (0.75) the theoretical maximum global daily radiation for Beijing and Denmark are calculated. The results are shown in figures 2.1 and 2.2.

From Fig. 2.1 and 2.2 it can be seen that the monthly mean of daily irradiation in Beijing and Denmark shows a similar changing pattern during a year, with maximum in June and minimum in December. In the months of May to July, Beijing and Denmark may receive similar amount of solar irradiation, while during the winter period, the solar energy resource in Denmark is considerably less than that in Beijing.

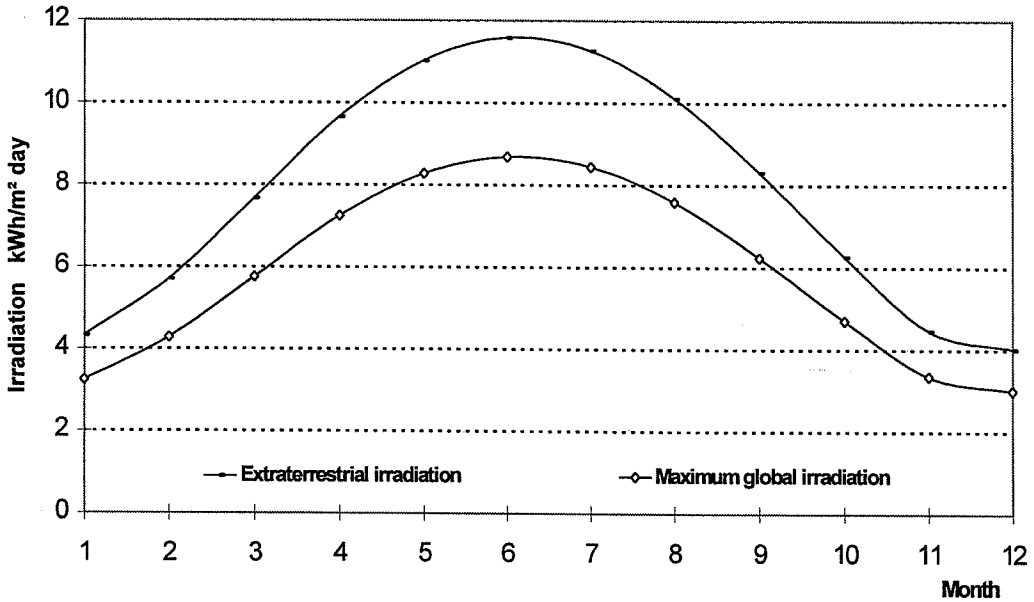

Figure 2.1 Monthly mean of daily extraterrestrial and maximum possible radiation in Beijing.

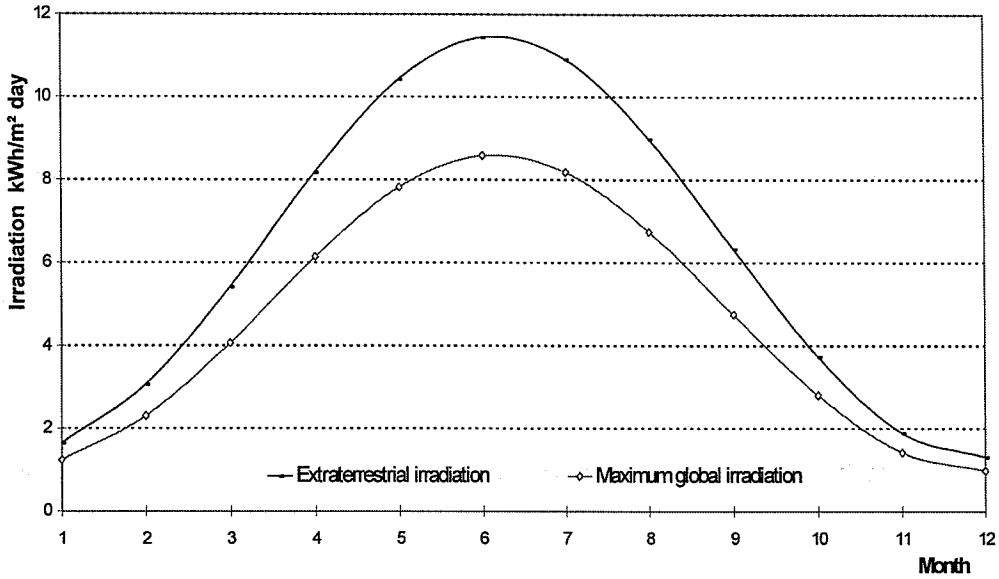

Figure 2.2 Monthly mean of daily extraterrestrial and maximum possible radiation in Denmark.

2.2.3 Solar radiation measurements

In reality the daily maximum possible irradiation can be rarely achieved due to the air pollution and cloud cover effects. The real available solar radiation in a certain area still has to rely on the real measurements.

The observations of the daily global solar radiation on ground surface during the period of 1981 to 1993 in Beijing have been studied. By computing this thirteen-year average of the monthly global irradiation and integrating the averages over a one-year period, the mean value of the annual global irradiation in Beijing was found to be 1390 kWh/m^2. The thirteen-year average of the annual diffuse radiation is about 50% of the global radiation. Likewise, based on the measurements the monthly mean value of daily global and diffuse irradiation was also calculated and the results are shown in table 2.1. Just as the theoretical prediction, the maximum solar radiation appears in June and the minimum radiation period is in December.

Solar radiation in Denmark is heavily influenced by climate effects. From measurements over a 15-year (1975-1989) period, it was found that the average annual sunshine hours (G > 200W/m^2) are about 1700 hours and annual global irradiation is about 1000 kWh/m^2 [44] on horizontal surface. The proportion of the diffuse radiation is about 50% of the total radiation on a yearly basis.

Table 2.1 Monthly means of daily global and diffuse radiation in Beijing (kWh/m^2 day)

		Jan	Feb	Mar	Apr	May	Jun	Jul	Aug	Sep	Oct	Nov	Dec	Year
1981	G	2.45	3.06	4.14	5.35	5.74	5.72	5.33	4.74	4.33	3.64	2.47	1.88	4.07
	D	1.04	1.45	2	2.25	2.7	2.58	2.77	1.99	1.94	1.36	1.02	0.77	1.82
1982	G	2.31	2.74	3.82	5.32	5.37	5.24	4.68	4.63	4.42	2.77	1.86	1.92	3.76
	D	0.98	1.28	1.79	2.19	2.56	2.63	2.74	2.52	1.57	1.4	0.88	0.98	1.80
1983	G	2.38	3.27	4.27	5.03	5.83	6.16	5.42	4.59	4.27	3.21	2.59	2.31	4.11
	D	1.2	1.55	2.25	2.74	3.14	2.72	2.49	2.62	1.92	1.45	1.11	0.96	2.02
1984	G	2.53	3.33	4.55	4.55	5.83	5.62	5.21	4.92	4.47	3.56	2.18	2.02	4.07
	D	1.11	1.55	2.09	2.55	2.81	2.66	2.77	2.28	1.86	1.34	1.14	0.91	1.92
1985	G	2.16	2.54	4.03	4.97	4.46	5.71	4.37	3.91	3.71	3	2.53	2.07	3.62
	D	0.9	1.13	1.85	2.39	2.51	2.77	2.55	2.13	1.62	1.35	1.08	0.91	1.77
1986	G	2.43	3.51	4.15	5.28	5.69	5.67	4.12	4.51	4.71	3.17	2.5	1.79	3.96
	D	1.02	1.22	1.9	2.21	2.64	2.67	2.8	2.08	1.72	1.31	0.99	0.9	1.79
1987	G	2.04	3.05	3.92	4.19	5.37	5.13	5.38	4.38	4.36	2.91	2.14	2.03	3.75
	D	0.93	1.53	1.84	2.46	2.68	2.87	2.73	1.93	1.85	1.44	1.09	0.96	1.86
1988	G	2.32	3.28	4.03	5.3	5.13	5.1	4.02	3.57	3.7	2.99	2.77	1.92	3.67
	D	1.04	1.61	2.09	2.45	2.27	2.59	2.42	1.77	1.81	1.28	0.99	0.86	1.76
1989	G	2.01	2.9	4.32	4.98	5.41	5.3	4.09	4.4	3.56	3.28	2.19	1.71	3.68
	D	1.02	1.46	1.76	2.39	2.46	2.53	2.22	2.37	1.59	1.29	1.03	0.95	1.76
1990	G	2.02	2.03	3.61	4.87	5.48	5.63	3.97	4.23	3.91	8.32	2.07	1.84	4.01
	D	1.23	1.4	2.39	3.1	2.81	3.19	2.94	2.59	2.03	5.12	1.23	0.99	2.43
1991	G	2.02	2.92	3.28	4.93	5.24	6.05	4.79	5.15	3.82	3.2	2.17	1.43	3.75
	D	1.20	1.84	2.32	2.89	3.16	3.24	2.87	3.21	2.21	2.64	1.8	1.15	2.38
1992	G	1.95	3.31	3.11	4.81	5.46	5.64	4.63	4.05	4.01	3.02	2.08	1.58	3.63
	D	1.01	1.36	1.69	2.1	2.16	2.81	2.42	2.54	1.82	1.43	1.02	0.86	1.76
1993	G	2.15	2.89	3.85	4.98	5.69	5.18	4.34	4.62	4.31	3.14	1.81	1.91	3.74
	D	1.02	1.37	1.93	2.33	2.63	2.31	2.81	2.08	1.73	1.28	0.82	0.77	1.76
Aver	G	2.21	2.99	3.93	4.97	5.44	5.55	4.64	4.44	4.12	3.17	2.26	1.88	3.83
	D	1.14	1.56	2.16	2.62	2.88	2.96	2.88	2.51	1.97	1.89	1.18	1.00	1.91

* G - global radiation D - diffuse radiation

The monthly means of daily global irradiation for both Beijing (from 1981-1993) and Denmark (from 1975-1989) are presented in figure 2.3. It shows that in both Beijing and Denmark the monthly mean of daily irradiation gets maximum in June and minimum in December, just as the prediction made from the theoretical analysis. In May, June and August, the monthly irradiation in these two areas is similar as expected, but in July, the monthly irradiation in Beijing is considerably less than one would expect. This may be due

to the fact that in July rainy days often occur in Beijing. Figure 2.3 also shows that, in winter, the solar energy received per unit area in Beijing is nearly three times as high as that in Denmark.

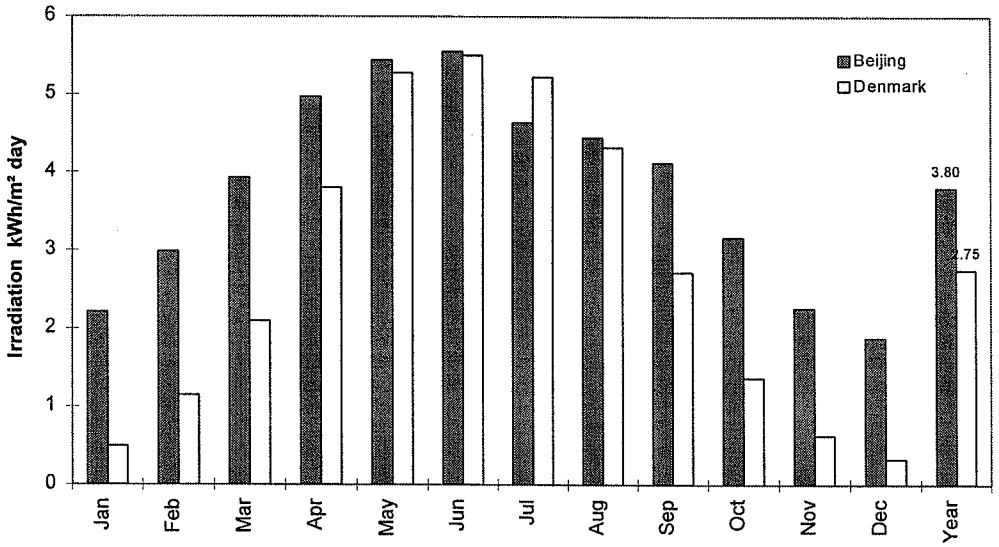

Figure 2.3 Monthly mean of global irradiation in Beijing and Denmark

2.3 Test Reference Year for Beijing

Meteorological TRY's have been developed for many European countries based on hourly data that were either measured or synthetically generated. The basic requirements for a TRY are that it corresponds to an average year, both regarding the monthly or seasonal mean values and occurrence and persistence of warm, cold, or sunny periods. The data available for Beijing TRY are 13 years' (81-93) monthly or daily averages, and 4 years' (90-93) hourly data. Although the methodology to generate hourly weather data from limited (daily or monthly) data has been introduced by many authors[4,40,48], no feasible method handles the correlation between many parameters, and many of the relations between individual parameters cannot yet be described mathematically. The use of real measured data in the TRY is therefore chosen as the priority method to obtain the desired quality.

Based on the "Danish method"[44], Beijing TRY is generated from a combination of monthly sequences of measurements which are selected from available hourly data. The selection of the months is done by statistical comparison of 13 years' data.

2.3.1 Basic climatic data for Beijing TRY

The data base for Beijing TRY is 13 years' (1981-1993) measurements from Beijing Meteorological Station. However, during the period from 1981 to 1989, the weather data which was recorded is only in the form of monthly or daily values. Continuous records of hourly data (or every 6 hours data) are only available for the 1990-1993 period.

The observations of the weather parameters, which include global and beam radiation, ambient temperature, relative humidity and wind speed, made between 1990 and 1993 are at an hourly or six hours' basis. Radiation data was recorded as hourly mean value between 6 am and 6 pm in the winter period and between 5 am and 7 pm in the summer. There are some days where possibly the sun rises before 5 am and sets after 7 pm. However, this fact does not have a considerable effect on the accuracy of the data, since the irradiation in these periods is very low. The ambient temperature and relative humidity were recorded every 6 hours, at 2 am, 8 am, 2 pm and 8 pm, every day and wind speed was measured at an hourly basis.

2.3.2 Check of original data

The climatic variables such as solar irradiation and ambient temperature, which are of special interest for solar energy system calculations, were critically examined through computer processes. Consequently, corrections were made according to certain principles.

First the missing values were checked and it was found that some data were missing at certain hours. These missing data were recovered by using the data interpolated from neighboring hours. For radiation data, some zero daily values were detected. Since the zero irradiation day may be caused by a heavily overcast or rainy day, these radiation data were carefully inspected before any change was made. The obviously wrong daily radiation data was replaced by monthly average values.

After checking for missing data, the difference between daily mean and maximum temperature was compared with the limit values which were derived from long-term statistic analyses for each month. The limit values are 5K, 5K, 6K, 6K, 6.5K, 6.5K, 5K, 5K, 6K, 6.5K, 5K, 5K for the 12 months. The temperature difference between consecutive days is also checked and the critical limit is 4 K. All the days reported by the program with error data were carefully inspected. For the hourly data with error, corrections were made manually by using the interpolated data from the neighboring hours. For the daily data with error the monthly mean value was used.

2.3.3 Radiation data

As mentioned before, solar radiation is both scattered and absorbed by the earth's atmosphere. The total radiation received at ground level is therefore the sum of two components: direct and diffuse radiation. Since both the intensity of the global radiation and the proportion of its components have an influence on the efficiency of the photo-thermal conversion, it is necessary to have detailed information about the direct and diffuse radiation.

In the 1990-1991 period, the measured hourly radiation data were the global and beam radiation. The direct and diffuse radiation on the horizontal surface was not recorded. To fulfill the requirement of the TRY data base, the hourly direct and diffuse irradiation were computed from global and beam irradiation by the following equation:

$$I_{dir} = I_{DN} \cdot (\cos\phi \cdot \cos\delta \cdot \cos\omega + \sin\phi \cdot \sin\delta) \qquad (2.3.1)$$

where I_{dir} (W/m^2) is the direct radiation on horizontal surface and I_{DN} $(W/m^2)$is the beam (normal) radiation.

2.3.4 Ambient temperature

The ambient temperature, which mainly depends on the solar radiation, is continuously changing. It is also one of the important parameters on the operation of solar DHW systems, because the efficiency of a collector heavily depends on the ambient temperature.

The monthly means of daily maximum, mean and minimum temperature in 1981-93 were investigated and the results are shown in Figures 2.4-2.6. These figures show that the daily mean temperature in Beijing changes greatly throughout the year, with the maximum in July and the Minimum in January. The variation of the monthly means of daily values in each month is about 5 K over these 13 years. Since the effect of temperature change is of importance to the solar DHW system operation, temperature has to be taken as one of the important parameters in Beijing TRY.

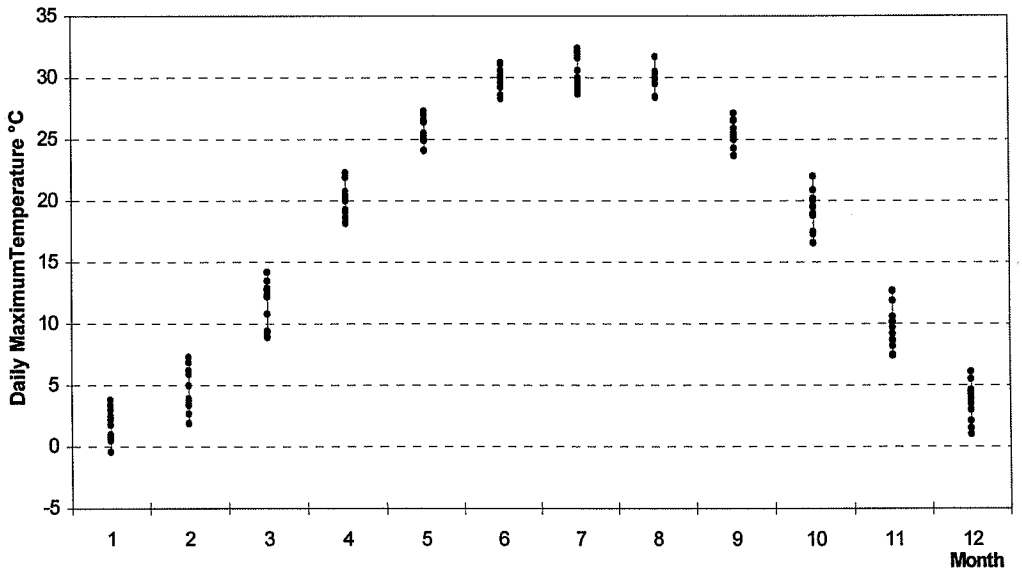

Figure 2.4 Monthly mean of daily maximum temperature in the period 1981-1993

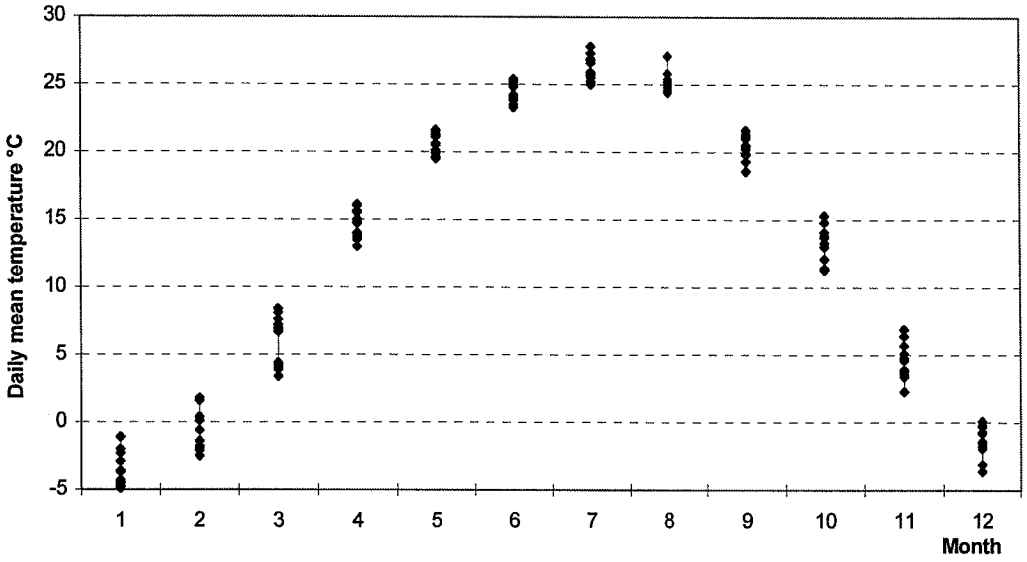

Figure 2.5 Monthly mean of daily mean temperature in the period 1981-1993

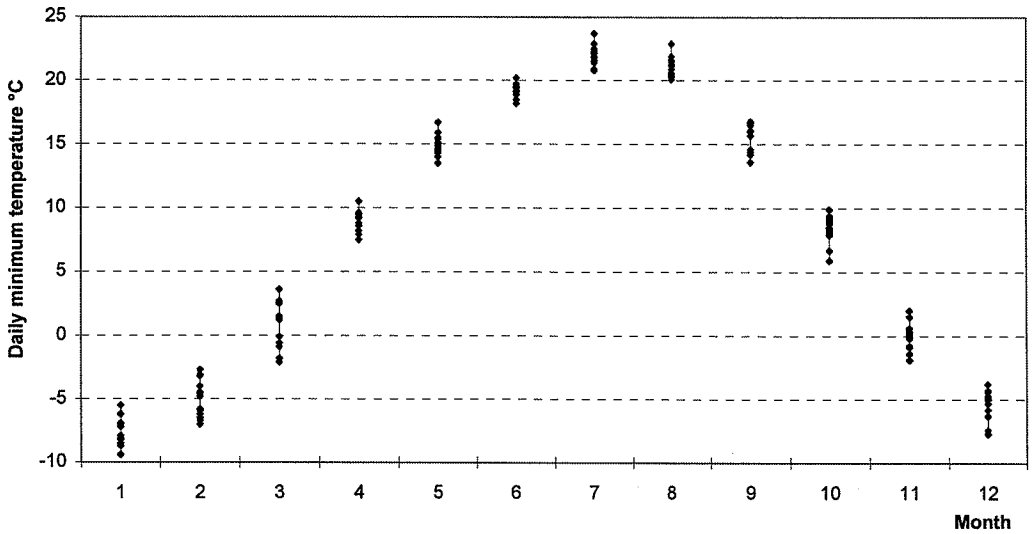

Figure 2.6 Monthly mean of daily minimum temperature in the period 1981-1993

The available short-term ambient temperature data from Beijing Meteorological Station are 6-hour records during the 1990 - 1993 period. The data were taken at 2 am, 8 am, 2 pm, and 8 pm every day. Since the minimum and maximum temperature are constantly observed at 5 am to 7 am and 1 pm to 3 pm, these 6 hours values are suitable as the data base to generate the hourly values for the TRY. The hourly data generation is conducted by means of the interpolation method.

The basic idea about interpolation is to estimate a function $T(h)$ for an arbitrary hour h, in some sense, draw a smooth curve through the existing points [h_i , $T(h_i)$]. There are several interpolation methods in existence. The cubic spline interpolation method is considered to be especially practical, and the detailed explanation of it may be found in [53].

Therefore, the cubic spline interpolation was employed to generate the hourly temperature data from the existing 6-hour values. The computed daily maximum, mean and minimum temperature was compared with measured data, and the result shows a good agreement. The hourly temperature patterns for 3 example days in January, July and October are shown in Figure 2.7. The minimum and maximum temperature are constantly observed at 5 am to 7 am and 2 pm to 3 pm, as expected.

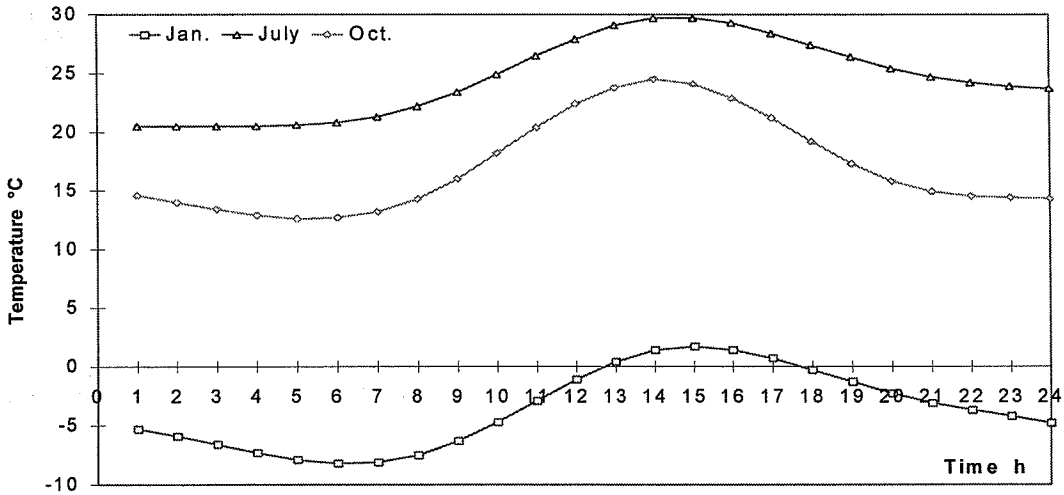

Figure 2.7 Hourly temperature patterns for 3 example days in January, July and October

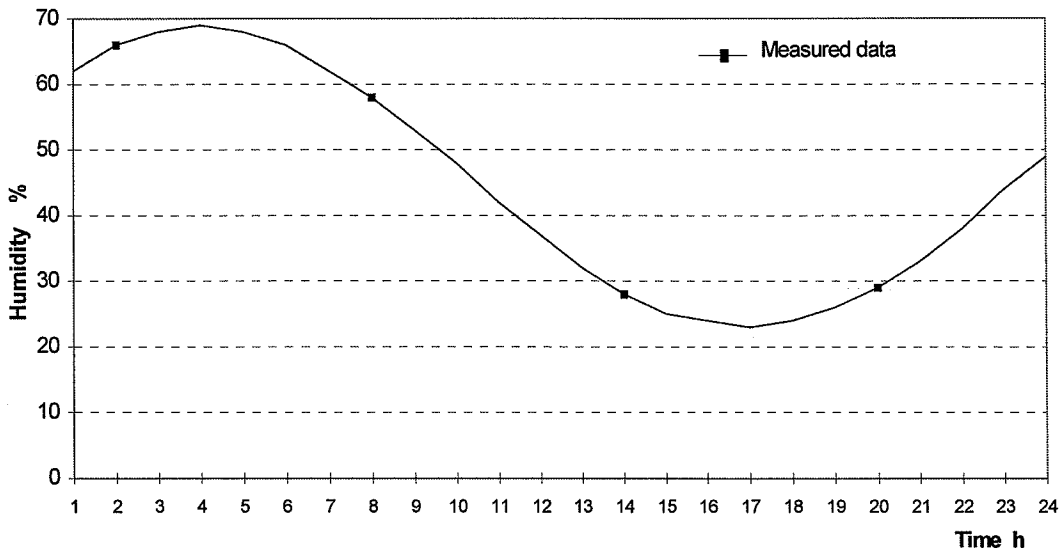

Figure 2.8 Hourly relative humidity (Date: 1990.06.15)

2.3.5 Relative humidity and wind speed

For the calculation of the dew point temperature, relative humidity is the most frequently used parameter. In the 90-93 period, relative humidity was recorded at certain hours (at 2

am, 8 am, 2 pm and 8 pm). The cubic spline interpolation method was used and the hourly relative humidity data were then obtained by fitting a curve between the existing values. Figure 2.8 shows the hourly relative humidity created from existing 6-hour value for 15 June 1990.

Wind speed is one of the important parameters in the simulation of heating and ventilation systems. The hourly measurements of wind speed in the 90-93 period are direct adopted in the TRY data base.

2.3.6 Selection months for Beijing TRY

The basic requirement for a TRY is that it should show a typical annually variation of the most important weather parameters, and further show typical deviation from this regular variation. Several adequate selection methods have been proposed for generation of TRY's (in Europe) or TMY's (in USA)[1, 40, 44, 48,]. The method used for Beijing TRY is based on the "Danish" method [44] which has been used for some of the EEC TRY's.

The months for Beijing TRY are chosen from the 4-year (1990-1993) period with hourly data. The selection is based on the 13 years' (1981-1993) daily data and following three criteria.

1. Months with abnormal weather condition were excluded.
2. Selection of months with typical mean values of the three most important weather parameters: daily mean temperature, daily maximum temperature and daily total global radiation.
3. Selection of month with typical variations of the three parameters.

Typical means and variation

For each month during a year in the 1981-1993 period, the monthly mean value of the daily mean and maximum temperature and daily global radiation is compared with the mean value of all 13 months. The deviations are normalized with the standard deviation of the 13 monthly values. For each month, the standard deviation and the normalized value are calculated by the following equations:

$$S_{i,j} = \sqrt{\left(\sum_{81}^{93} \left(D_{i,j} - \left(\sum_{i=81}^{93} D_{i,j} \right) / 13 \right)^2 \right) / 12} \qquad (2.3.2)$$

$$F_{i,j} = \left| \frac{D_{i,j} - \left(\sum_{i=81}^{93} D_{i,j} \right) / 13}{\sqrt{\left(\sum_{81}^{93} \left(D_{i,j} - \left(\sum_{i=81}^{93} D_{i,j} \right) / 13 \right)^2 \right) / 12}} \right| \qquad (2.3.3)$$

Where i and j are the year and month. $S_{i,j}$ and $F_{i,j}$ are the standard deviation and normalized value for the i year and the month j. $D_{i,j}$ is the monthly mean of daily value.

Therefore, each month in these 13 years has one normalized value for each of the three important parameters which characterize the month. The largest normalized standard deviation of these three important parameters is used as a classification number for the month. The best suited month is then the one with the lowest classification number, that is with the smallest deviation from the typical month. Since the TRY months have to be chosen from the 1990-1993 period, the comparison of the classification number is carried out only within these 4 years. The normalized values for the three important parameters in 1990-1993 are given in Table 2.2-2.4.

Table 2.2 Normalized deviations of daily global irradiation for the 81-93 period

Year	Jan	Feb	Mar	Apr	May	Jun	Jul	Aug	Sep	Oct	Nov	Dec
1990	1.0	2.4	0.8	0.3	0.1	0.2	1.2	0.5	0.6	0.8	0.7	0.2
1991	1.0	0.2	1.6	0.1	0.5	1.5	0.3	1.7	0.8	0.1	0.3	2.0
1992	1.3	0.8	2.0	0.5	0.1	0.3	0.0	0.9	0.3	0.6	0.6	1.3
1993	0.3	0.2	0.2	0.0	0.7	1.1	0.6	0.4	0.5	0.1	1.5	0.1

Table 2.3 Normalized deviations of daily mean temperature for the 81-93 period

year	Jan	Feb	Mar	Apr	May	Jun	Jul	Aug	Sep	Oct	Nov	Dec
1990	1.2	0.1	0.9	1.0	1.3	0.3	0.5	0.3	0.2	1.6	1.5	0.3
1991	1.0	0.4	1.0	0.8	0.9	0.8	0.3	2.8	0.1	0.3	0.1	0.6
1992	2.0	1.5	0.4	0.8	0.1	1.5	0.8	0.8	0.2	1.1	0.8	0.8
1993	0.2	1.4	1.2	0.7	1.3	1.0	1.0	0.1	1.2	0.3	0.7	0.4

Table 2.4 Normalized deviations of daily maximum temperature for the 81-93 period

Year	Jan	Feb	Mar	Apr	May	Jun	Jul	Aug	Sep	Oct	Nov	Dec
1990	1.7	0.7	0.6	1.1	0.9	0.1	0.5	0.4	0.5	1.9	1.3	0.5
1991	0.5	0.2	1.2	0.8	1.0	0.8	0.3	2.3	0.3	0.2	0.0	1.1
1992	1.6	1.5	0.3	0.1	0.8	1.8	0.2	1.3	0.7	1.3	0.9	0.1
1993	0.7	0.9	0.7	1.1	0.5	0.3	1.2	0.1	0.9	0.3	1.3	0.1

2.3.7 Structure of the Beijing TRY

After the selection process, the month components of the TRY were determined. It consists of the following months:

January	1993	May	1992	September	1990
February	1991	June	1990	October	1991
March	1990	July	1991	November	1991
April	1991	August	1993	December	1993

The weather parameters which are included in the Beijing TRY are solar radiation (global, direct and diffuse radiation), ambient temperature, relative humidity and wind speed. All data are presented as hourly mean values. Global radiation and wind speed are measured at Beijing Meteorological Station. Other parameters are either partly or totally computed from the relevant existing data. The Beijing TRY format follows the recommendation of Danish Test Reference Year[1] and it shows in Table 2.5.

Table 2.5 Beijing TRY format

Position	parameters	Unit	Format	Col.
1	Station name	-	A3	1-3
2	Ambient temperature	0.1°C	I4	4-7
3	Global radiation	W/m^2	I4	8-11
4	Diffuse radiation	W/m^2	I4	12-15
5	Direct radiation	W/m^2	I4	16-19
6	Relative humidity		I3	20-23
7	Wind speed	0.1m/s	I3	24-26
8	month, day, hour		I2	27-32
9	continuation 0		I2	33-34

2.3.8 Application examples of Beijing TRY

For the design of solar DHW systems, the monthly irradiation on the collector plane and its variation during the year is the important basic information. Based on the TRY, the typical monthly mean of daily global radiation on horizontal surface can be determined. Figure 2.9 shows the monthly mean of daily global radiation from TRY and its variation in the 1981-1993 period.

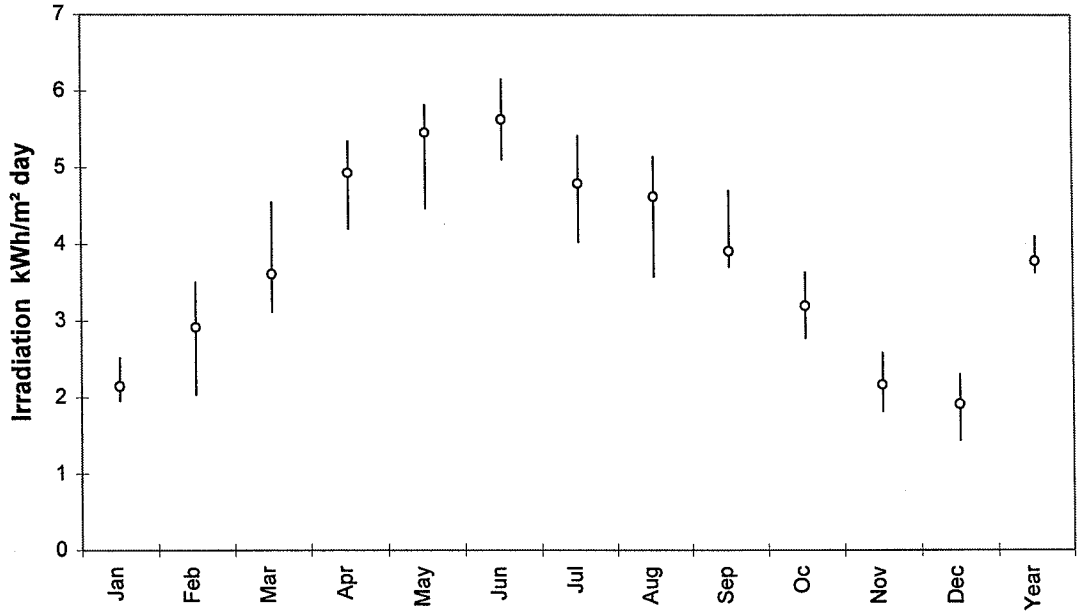

Fig. 2.9 Monthly mean of the daily global radiation in the years 1981-93
o Monthly mean value in TRY | indicates highest and lowest

The irradiation on a surface with a certain tilt angle is seldom measured by meteorological services, but it can be computed from the measured values on the horizontal surface. Based on Beijing TRY, the annually total irradiation on a tilted surface facing south was also investigated and the result is shown in Figure 2.10. It was found that the plane with 38° tilt angle receives the highest solar radiation over a year in Beijing.

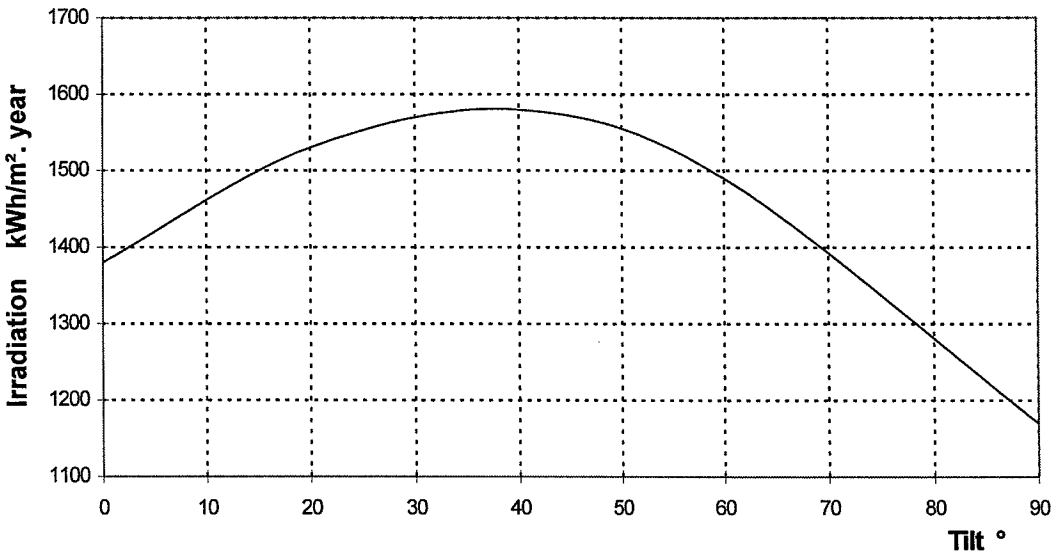

Figure 2.10 Yearly total irradiation on a tilted surface facing south (from Beijing TRY)

2.3.9 Remark

In this section, limited climatic data available for Beijing were analyzed and organized into typical annual records of hourly data - a TRY. The cubic spline interpolation method was used to generate the hourly temperature and relative humidity data from the existing six-hour values. The result shows a good agreement with measured daily mean and maximum data.

To set up a TRY by statistical methods, generally, long-term (more than 10 years) hourly data are expected. Therefore, the Beijing TRY which was limited by the available 4 years' hourly data may have a large deviation in some months. But, since the selection of months was done by 13 years' data, the deviation was smoothed out to some degree.

In Lund[44], the area of validity for a TRY was estimated as about 1600 $(km)^2$ for uniform landscapes, and considerable less in mountainous areas. Therefore, the Beijing TRY may have a limited use for the north-skirts mountainous area.

2.4 Danish TRY and DRY

The Danish TRY was composed of twelve typical months chosen from a 15-year period (1959-1973). It provides values of 33 weather parameters measured simultaneously and shows the natural variation of the parameters throughout the year. The individual months of the Danish Test Reference Year have been selected from observations made at Værløse Air Base and at Højbakkegård in Tåstrup. The months chosen are typical regarding monthly mean values and variations of important parameters throughout the month. For many years, the Danish TRY has been widely used in solar energy system simulations and heat balance calculations for buildings in Denmark.

The Danish Design Reference Year (DRY) is, like earlier TRY, a collection of climatic data for one year, arranged as 8760 sets of hourly, simultaneous weather parameters. The data for the Danish DRY are taken from 16 years' (1975-1990) measurements at Værløse, a military Air Base which is 17 km north-west away from Copenhagen. Irradiation data are from the Agricultural Research Station Højbakkegaard in Tåstrup 12 km south of Værløse. The DRY contains, as hourly data: dry bulb and dew point temperature, global, diffuse and beam irradiance, wind speed and direction, cloud cover and some new parameters which were not included in the TRY. These new parameters include illuminance, 5-minute values of direct irradiance, weather forecast data and long-wave sky radiation.

2.5 Conclusion and discussion

Solar radiation for both Beijing and Denmark are investigated. It was found that the average annually available global solar radiation is about 1380 kWh/m^2 in Beijing and 1000 kWh/m^2 in Denmark. In these two areas, the changes of monthly mean of daily irradiation show a similar pattern with maximum in June and minimum in December. In the months of May, June and August Beijing and Denmark receive similar amount of solar energy, but in other

months, solar irradiation for Denmark is considerably less than that in Beijing, except July. Beside the geography impact, the atmospheric aspects make a great contribution.

Climatic data measured in Beijing Meteorological Station during the 1981-93 period were analyzed. By statistical methods, typical months for each month of the year were selected from the period of 1990-1993 when hourly (or six hours') data are available. By combining these typical months, an annual record of hourly data - a Test Reference Year (TRY) is set up for Beijing.

Based on Beijing TRY, it was found that the surface with tilt angle 38° receives the maximum solar radiation over a one-year period in Beijing.

Chapter 3

Dynamic modeling of the heat load

3.1 Introduction

The heat load of a domestic hot water (DHW) system is the heat supplied from its hot water storage tank to the distribution network of the service building. It generally consists of two parts, the heat consumption for domestic hot water and the heat loss from the pipes of the distribution network. The determination of the heat load forms the most important basis of the system design for any type of DHW system.

In recent years, research on domestic hot-water services has received increasing attention, but in many cases, the simulation and optimum design of hot-water systems for various conditions have been complicated by the fact that there was insufficient knowledge of the heat load. To optimize the capacity rate of the heat production units, it is necessary to have detailed information about the requirements of hot-water consumption, the pattern of the hot-water load, and the heat loss from the distribution networks.

Unlike conventional fossil fuel DHW systems, solar DHW systems rely on time-dependent solar energy. The solar fraction of such systems is strongly influenced by their heat load and load pattern. Research has shown that for the same amount of daily hot-water consumption, the solar fraction of a system may show variations of up to 30% [22], due to varying load patterns. To optimize the design and operation of such systems, it is vital to have some models to predict the heat-load condition.

Dynamic modeling and analysis of the heat load are therefore of general interest for both solar and conventional DHW systems.

3.2 Hot water load

For a solar DHW system, each apartment or household is an individual hot-water consumer. In order to determine the hot-water requirements for a single household, it is necessary to know the magnitude of the requirement and its variations. Normally, the hot-water consumption in a household is largely dependent on the number, age, profession and customs of the inhabitants. Although the former are not predictable during the system design, it is possible to get some idea of individual requirements by forming mean values. In

this chapter, a mean-value behavior model of hot-water consumption, based on a literature study, is presented.

In the last decades, research on the DHW hot-water load has gained great attention. Results from various theoretical and experimental investigations may be found in the literature, see Lawaetz [42], Werner [63], Yang [64], Holmberg [34], Carlsson [10] and Otto [51]. Lawaetz (1985) carried out measurements on the hot-water load of a large number of apartment buildings and family houses in Denmark. Holmberg (1987) introduced an analytical model for the dimensioning of flow requirements to apartment units. Measurements of the hot-water load in apartment buildings in Brøndby, Ishøj and Glostrup in Denmark were also reported in [64] and [10].

3.2.1 Average daily hot-water load

The average domestic hot-water loads for one-family houses or apartment buildings are normally found from experimental measurements. A number of results from several different regions have been reported. From these results, it was found that the average daily hot-water consumption differs considerably for different areas. This may due to many effects such as the use of water saving equipment, climate differences and the life style.

In Lawaetz [42], investigation results of the average DHW load for one-family houses and multi-apartment buildings are presented (see Table 3.1). The results are obtained from measurements in 240 one-family houses and 20 apartment buildings, with a total of 999 apartments in Copenhagen in 1984. It appears from Table 3.1 that the variation in the average domestic hot-water load in one-family houses is large, whereas within an apartment building, the variation of the average consumption in the different flats is relatively small.

Table 3.1 Average domestic hot-water load of 240 one-family houses and 999 apartments in twenty buildings in Copenhagen, From [42].

	Mean Value	Variation	Unit
One-family house	6	1.9 - 12.5	kWh/day
	105	70 - 270	l/day
	2200	700 - 4600	kWh/year
	38	20 - 100	m^3/year
Apartment building	5.0	3.6 - 7.6	kWh/day
	81	50 - 160	l/day
	1800	1300- 2800	kWh/year
	30	20 - 60	m^3/year

Recently, Otto and Nielsen (1997) [51] carried out measurements for 16 one-family houses in Denmark. It was found that the average daily hot-water (50°C) load is about 32 liters per person, which is lower than the commonly accepted design value of 40 liters/person. The yearly heat load for a single-family house was found to be about 1800kWh, which is about 20% lower than the consumption found a decade ago by Lawaetz [42].

In 1994, Harrison and Carpenter [31] conducted an investigation on 60 solar DHW systems for single-family houses in Canada. It was found that the average daily hot-water load for a family is 290 *l* in the winter and 244 *l* in the summer, which is rather high compared to the Danish conditions.

3.2.2 The variation of hot-water load

In order to obtain a better understanding of the hot-water load, it was deemed necessary to perform a study of the variation of the daily load over an extended period. Werner [63] analyzed various measurements from Sweden and found that the relative net energy consumption for a hot-water supply is great during the winter, and considerably less during the summer (see Fig. 3.1). Carlsson [10] and Yang [64] carried out measurements for apartment buildings in Denmark (Glostrup and Bøndby) and obtained results similar to those of Werner [63]. Yang (1994) also found that the net heat load is about 10-40% higher than the mean level in the winter period and about 10-30% lower in the summer period. This variation may be due to, among others, the temperature change of the cold water and summer holidays. Schultz [54] presented a measurement of the cold water temperature over a year in Denmark (see Fig. 3.2). It shows that the monthly average temperature of the cold water changes greatly from a low of 2°C in March to a high of 15.5°C in August.

Both Lawaetz [42] and Yang [64] also carried out measurements of the weekly variation. It was found that the hot-water load is low on working days, and high during the weekend. Homonnay and Brana [35] investigated the measurements in several apartment buildings in Hungary and found that the domestic hot-water load during weekends is approximately 2 to 5 percent higher than on working days. In 1995, Carlsson [10] conducted a measurement in an office-resident building. The result shows that for this building type, the hot-water load is lower during the weekend than on working days.

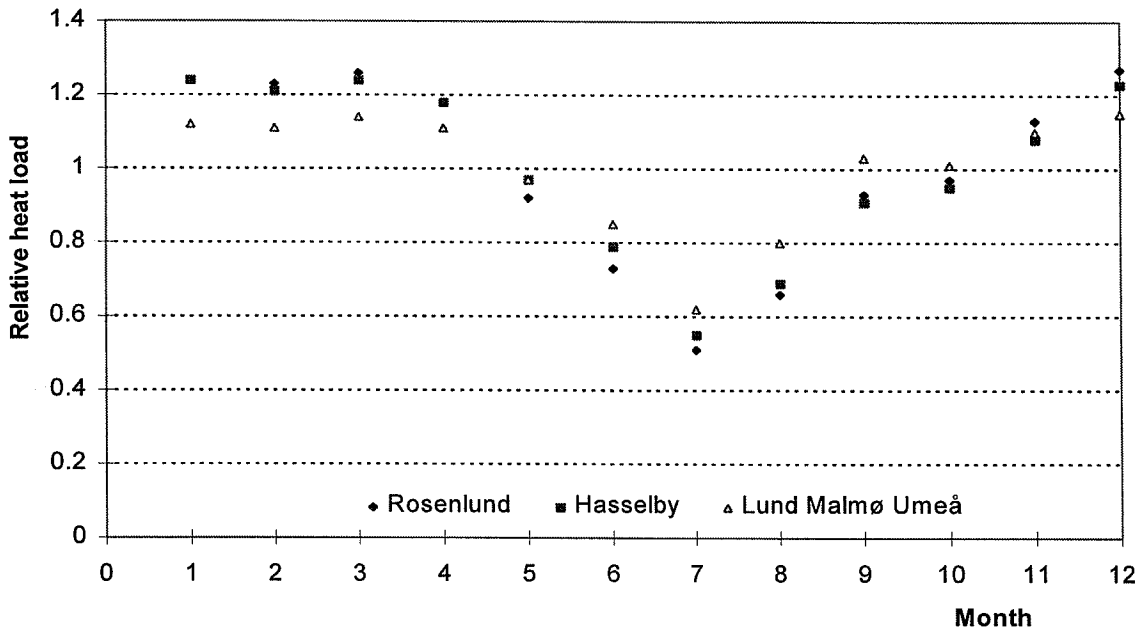

Figure 3.1 Relative variation of the heat load during a year, from [63].

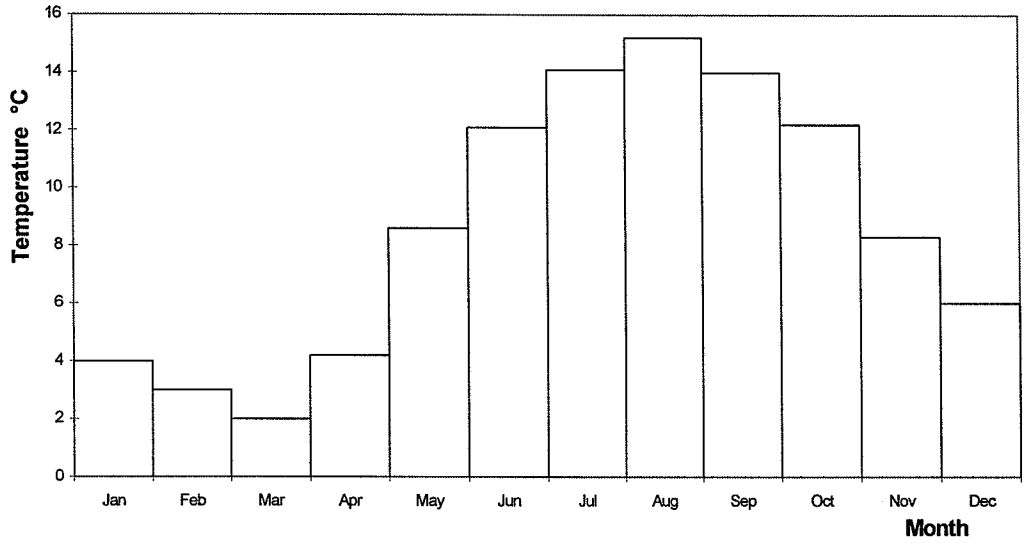

Figure 3.2 Cold water temperature during the year in Denmark, from Schultz [54].

3.2.3 Peak load and load pattern

The design of solar DHW systems is based on average and maximum hot-water load. Consequently, knowledge about the domestic hot-water peak load is also important. According to measurements, peak loads occur approximately every twelve hours, the larger one in the morning, and another one in the evening.

Obviously, the design peak load for an apartment building with a large number of apartments should be corrected by aggregation factors. In the German DIN 4708 standard [41], the peak load for an arbitrary number of apartments is calculated using the following equation:

$$Q_Z = Q_b\left(N \cdot K(u_1)\right) + \sqrt{N} \cdot K(u_2) \qquad (3.2.1)$$

Here Q_z total net heat demand in time period Z, Wh
Q_b heat demand for an apartment, Wh
N number of apartments
$K(u_1)$ time and N dependent factor
$K(u_2)$ time and N dependent factor

In the German standard, it is assumed that a normal apartment has 3.5 residents, and one tapping place with a daily heat demand of 5820 Wh, i.e. Q_b=5820 Wh. The determination of $K(u_1)$ and $K(u_2)$ value can be found in Lawaetz [41].

Although the hourly based tapping of hot water varies from one household to another, it shows a certain pattern for a definite location. The idea of a consumption pattern is that it should yield as accurate a picture of the heat load during the day as possible. Often, the

weekly variation is discussed as well when such a load pattern is considered. Figure 3.3 shows the weekly load pattern from a measurement [42].

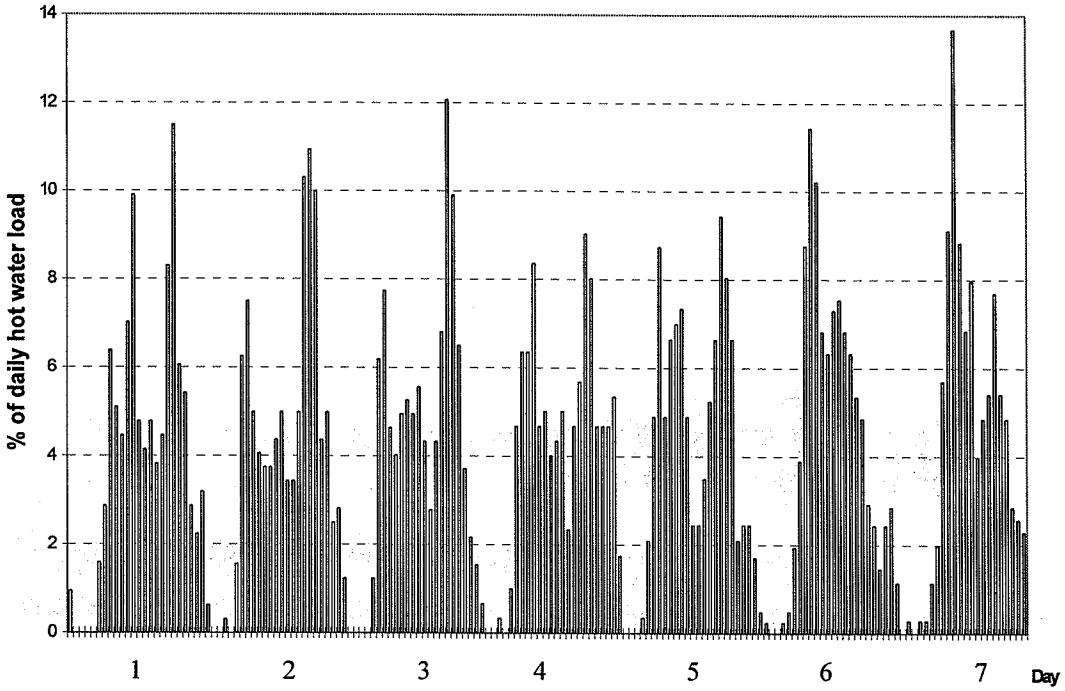

Figure 3.3 Hourly load pattern during a week, from [42].

Based on the existing measurements, Mazin [45] demonstrated the typical hot-water load patterns for weekdays and the weekend under Danish conditions; see Figs. 3.4 and 3.5.

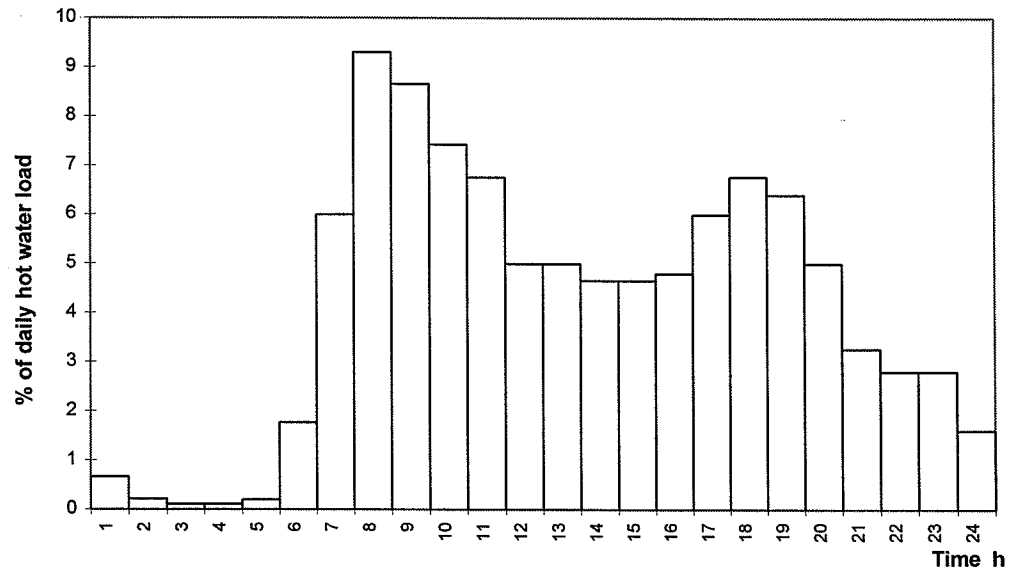

Figure 3.4 Average hourly based load pattern of working day, from [45].

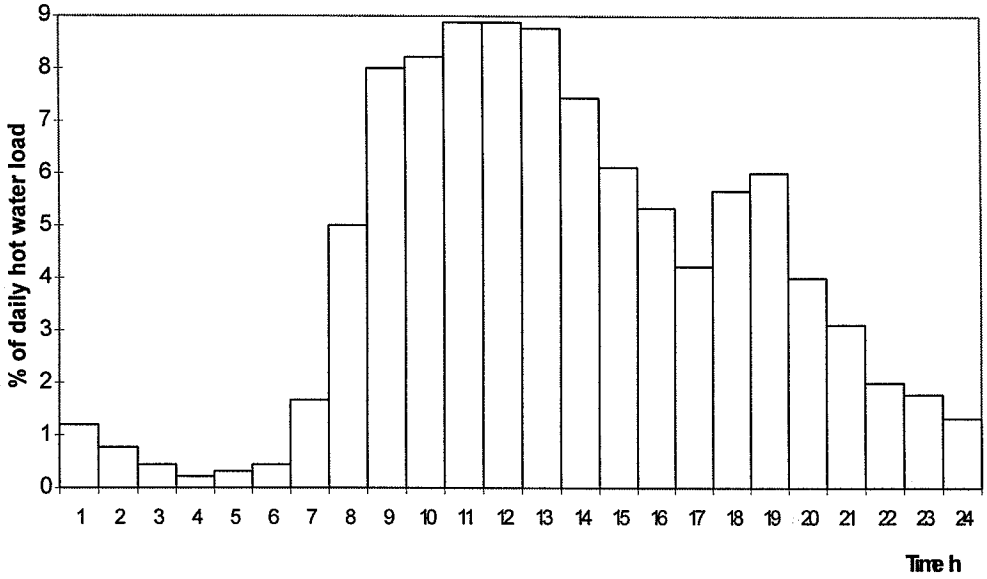

Figure 3.5 Average hourly based load pattern of holiday/weekend, from [45].

3.3 Heat loss from the distribution network

3.3.1 Introduction

For the design and simulation of solar DHW systems, the heat load is often calculated according to the hot-water consumption which is directly dependent upon the life style of the consumers. Heat loss from the distribution network is only taken into account in large installations, by increasing the effective value of the hot-water load by a percentage. However, many investigations show that in circulation-type DHW distribution networks, the heat loss may be significant: from 30% to 60% of the total heat load [64]. Therefore, together with the dynamics of the consumers, the distribution network strongly affects the heat load of the DHW systems.

The design of the networks used to distribute hot water may vary from building to building. However, the network must deliver an adequate water pressure, volume and temperature at any point within a building under all circumstances, to meet the conditions of normal use. Basically, there are two types of distribution networks that are most commonly used in domestic buildings, namely networks with or without a circulation loop. Figure 3.6 shows a circulation type of distribution network which is commonly used in apartment buildings.

To investigate the heat loss from distribution networks, it is vital to have some models to simulate the thermal process. These models should be used to determine the influence of the design and operation parameters on the total heat loss of a hot-water distribution network. Some papers [5, 13, 28, 29, 50, 59, 65] have been dealing with similar problems, such as district heating networks and gas supply networks, but in all cases there are some differences from a DHW distribution network.

In the present study, a complete model which describes both the hydraulic and thermal behavior of a hot-water distribution network is developed.

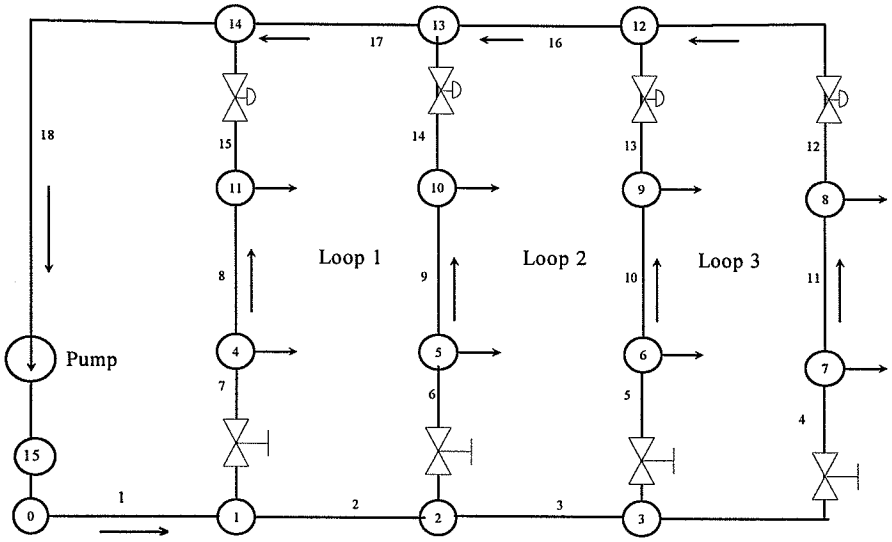

Figure 3.6 Schematic view of a DHW network (with circulation loop).

3.3.2. Strategy for distribution network modeling

A DHW distribution network can be described as an inner connected insulated pipe system, with m pipes, a reservoir node (storage tank) and n interior nodes, through which the hot water in the storage tank is delivered to the consumers. The flows through the networks are controlled by the difference between the pressure heads at the input point (storage tank) and the pressure heads at the draw-off points. The temperature in the network depends on the input (storage tank) temperature, the heat capacity of the net, the heat loss from the pipes, and the flow conditions.

Like gas and electrical networks, a DHW distribution network obeys three fundamental principles: conservation of mass, energy and momentum. In order to carry out a simulation and determine the heat loss, it is necessary to develop fully dynamic models with which the basic energy, mass and heat balance equations are solved simultaneously to calculate both the flow in the network and the dynamic change in temperature.

For an existing distribution network the following data may be determined:

- Lengths, diameters, materials, roughness and insulation of the pipes.
- The draw-off from the interior nodes, $q_1, \ldots, q_n$.
- The head and temperature at the reservoir node (hot-water tank), h_0 and T_0

The unknown quantities are:

- The flows in each pipe, $m_1, \ldots, m_m$.
- The heads at the interior nodes, $h_1, \ldots, h_n$.
- The temperature of each pipe and node, T_i and T_j

3.3.3. Steady-state analysis of hydraulic

Steady-state analysis of flow and pressure in piping systems was, and still is, a major subject in the engineering area. There are many methods, and various calculation programs exist for solving the problem (see Cross (1936) [13], Nielsen (1987) [50], Hansen (1988) [28], Casey (1992) [11]).

Unlike in other pipe networks, such as for gas and cold water, the flow and pressure distribution in a DHW network are also controlled by the temperature variation in the network, through temperature-controlled valves or flow balance devices. Therefore, it is necessary to further analyze the flow in DHW networks. Furthermore, knowledge of the flow distribution in the net work is a precondition for a dynamic simulation.

3.3.3.1 Modeling of distribution networks

In any pipe network, the number of unknown flows correspond to the number of pipes in the network, and their evaluations involve the solution of an equal number of simultaneous continuity equations and energy equations (if the network features loops). These equations are of two types:

1. Continuity equations: the algebraic sum of the flows at any node must be Zero.
2. Energy equations: the integrated head loss around any loop must be Zero.

In 1987, Nielsen [50] first set up the governing equations for general networks. To satisfy continuity, the mass flow into a junction (node) must be equal to the mass flow out of it. Let the ith pipe connect with the nodes j_{i1} and j_{i2}, indicating the inlet and outlet nodes of pipe i. The flow is positive when its direction is from j_{i1} to j_{i2}. For each interior node j, a continuity equation is set up;

$$\sum_{i=1}^{m} a_{ij} \cdot \dot{m}_i = q_j \qquad j=1, \ldots, n \qquad (3.3.1)$$

$$a_{ij} = \begin{cases} -1 & \text{if} \quad j = j_{i1} \\ 1 & \text{if} \quad j = j_{i2} \\ 0 & \text{otherwise} \end{cases}$$

Here, m_i is the mass flow in the ith pipe, and q_j is the external flow at the interior nodes j (demand). If the network contains n nodes and all external flows (demands) are known, then n continuity equations may be written;

$$\begin{pmatrix} a_{11} & \cdot & \cdot & a_{m1} \\ \cdot & \cdot & \cdot & \cdot \\ \cdot & \cdot & \cdot & \cdot \\ a_{1n} & \cdot & \cdot & a_{mn} \end{pmatrix} \begin{pmatrix} \dot{m}_1 \\ \cdot \\ \cdot \\ \dot{m}_m \end{pmatrix} = \begin{pmatrix} q_1 \\ \cdot \\ \cdot \\ q_n \end{pmatrix} \qquad (3.3.2)$$

Defining $\mathbf{M}=[m_1,\cdots,m_m]^T$, and $\mathbf{Q}=[q_1,\cdots,q_m]^T$ and using a matrix formalism, Eqn.3.3.2 becomes

$$\mathbf{A}^T\cdot\mathbf{M}=\mathbf{Q} \qquad (3.3.3)$$

Because of the conservation of energy, the integrated pressure loss around any loop must be Zero.

Let S_k be the set of numbers for the pipes in loop k and S_{kl} the set of numbers for the pipes in this loop with clockwise flow. Then, one can write the following energy equation for loop k:

$$\sum_{i=1}^{m} b_{i,k}\,\Delta h_i = 0 \qquad (3.3.4)$$

$$b_{i,k} = \begin{cases} -1 & if \quad i \in S_k / S_{kl} \\ 1 & if \quad i \in S_{kl} \\ 0 & if \quad i \notin S_k \end{cases}$$

Here Δh_i is the head loss of pipe i.

For a network consisting of n interior nodes, m pipes and L_n loops, the equation $L_n=m-n$ will always be satisfied.

In a distribution network, the reservoir node (storage tank) is taken as the reference. The pressures at the other nodes are evaluated with respect to this reference node pressure. It is easily seen that the relation of node pressure and pipe pressure loss can be described as:

$$\Delta h_i = \sum_{j=1}^{n} a_{ij} h_j \qquad (3.3.5)$$

Here, h_j is the energy head on node j.

In the matrix formalism, the system of equation to calculate the energy head in each node takes the form:

$$\mathbf{A}\cdot\mathbf{H}=\Delta\mathbf{h} \qquad (3.3.6)$$

$\mathbf{H}=[h_1,\cdots,h_n]^T$ is the node pressure vector, and $\Delta\mathbf{h}=[\Delta h_1,\cdots,\Delta h_m]^T$ is the pipe pressure loss vector.

3.3.3.2 Solution procedure - Linear theory method

As mentioned before, the network equations consist of a set of n continuity equations (for nodes) which are linear in $\dot{m}$ and a set of m-n energy equations (for loops) which are linear in Δh.The head loss Δh_i of pipe i may be related to the mass flow rate $\dot{m}_i$ by a power expression [11];

$$\Delta h_i = Rf_i \cdot m_i^{\beta} + \Delta h_{ei} \qquad (3.3.7)$$

where Rf_i is a pipe resistance coefficient whose value depends on the pipe parameters. The exponent β is a constant for a given kind of fluid, and Δh_{ei} is the head loss caused by the elevation difference of the pipe. Then, Eqn.(3.3.4) becomes

$$\sum_{i=1}^{m} b_{i,k} Rf_i \cdot m_i^{\beta} = 0 . \qquad (3.3.8)$$

For example: The Hazen-Williams equation [32] is often used for purposes of water network computation. The correlation of frictional head loss and mass flow in water pipe i is found to be:

$$\Delta h_i = \frac{10.704 \cdot L_i}{C_i^{1.852} \cdot d_i^{4.871}} \cdot \dot{m}_i^{1.852} \qquad (3.3.9)$$

Here, d_i and L_i are the diameter and length of the pipe i. C_i is the Hazen-Williams coefficient. Then, for pipe i the resistance coefficient Rf_i becomes:

$$Rf_i = \frac{10.704 \cdot L_i^*}{C_i^{1.852} \cdot d_i^{4.871}} \qquad (3.3.10)$$

Here, L_i^* consists of two parts, the physical length L_i and the equivalent length L_i^e which is converted from the devices, such as valves, bends and tees, in the pipe. For control valves, L_i^e is a function of the temperature of the pipe.

For an open network, the pipe number equals the number of interior nodes. Therefore, the number of continuity equations corresponds to the number of unknown flows, and the flow rate in each pipe may be computed by solving the above system of continuity equations. For a network with loops, such as the one shown in Fig.3.6, the number of continuity equations (15 nodes) plus the number of energy equations (3 loops) equals the number of the unknown flows. Because of the nonlinear nature of the relation between flow and pressure, the calculation of flow in this system requires the solution of a system of nonlinear equations. Although a direct solution is not feasible, several iterative methods have been introduced, such as the Harday-Cross (1936) method, the Newton-Raphson method and the Wood and Charles (1972) method.

Here, the Wood and Charles linearization method is employed. The basic idea of the linear theory is to transform nonlinear energy equations into linear equations and solve them together with linear continuity equations. Then Eqn.(3.3.8) may be written in a modified form:

$$\sum_{i=1}^{m} b_{i,k} Rf_i \cdot m_i^{\beta-1} \cdot \dot{m}_i = 0 \qquad (3.3.11)$$

or

$$\sum_{i=1}^{m} b_{i,k} Rf_i^* \cdot \dot{m}_i = 0 \,. \qquad (3.3.12)$$

Here, $Rf_i^* = Rf_i \cdot \dot{m}_i^{\beta-1}$ is treated as a numerical coefficient, based on the current value of $\dot{m}_i$. To start the calculation, it is necessary to assume an initial flow distribution.

Let $d_{i,k} = b_{i,k} \cdot Rf_i^*$, then the energy equations may be expressed as:

$$\sum_{i=1}^{m} d_{i,k} \cdot \dot{m}_i = 0 \qquad (3.3.13)$$

Now, the L_n energy equations can be written in a matrix form,

$$\mathbf{D^T M = 0}. \qquad (3.3.14)$$

Combined with the continuity equations, the system of equations for determining the flow rate may be written as:

$$[A^T \; D^T]^T \cdot M = [Q \; 0]^T \qquad (3.3.15)$$

It has to be noted that Eqn.(3.3.15) is a combination of the linearized energy equations and the continuity equations. These system equations can be solved by linear algebra, but the first solution will usually not be correct, because the initial guess for the m_i is not necessarily equal to the m_i produced by the solution. However, the process may be repeated until the correct m_i is obtained.

3.3.4. Thermal analysis of DHW distribution networks

The changes of pressure and flow may spread in the distribution network with the speed of sound, while the variations of the temperature travel with a speed close to the flow velocity of the distributed water. This leads to the fact that there is a time delay of the temperature change in the network. Beside the transport time, the distribution network pipes also affect

these time delays, as the pipes alternatively give and take heat to and from the water as the temperature of the water changes. The temperature change through a DHW network is also strongly influenced by the load of individual consumers. All these facts indicate that the heat transfer in a distribution network is a highly dynamic process.

In order to have a better understanding of the thermal process to investigate the heat loss, it is desirable to have a dynamic model for DHW distribution networks.

3.3.4.1 Dynamic models of DHW network pipe

Dynamic modeling of distribution networks is based on the modeling of pipes which are the fundamental elements of DHW networks. Several pipe models have been found in the literature, see Bøhm [9], Rahbek [52], Dutre [18] , Benonysson [5], and Isakson [36].

Generally, the following assumptions are made in these models:

- The axial heat conduction is neglected.
- Instant mixing is assumed in nodes where two or more flows meet.
- The heat resistance between the water and the steel pipes is neglected.
- The heat capacity of the insulation is neglected.

Model 1 - Plug flow model

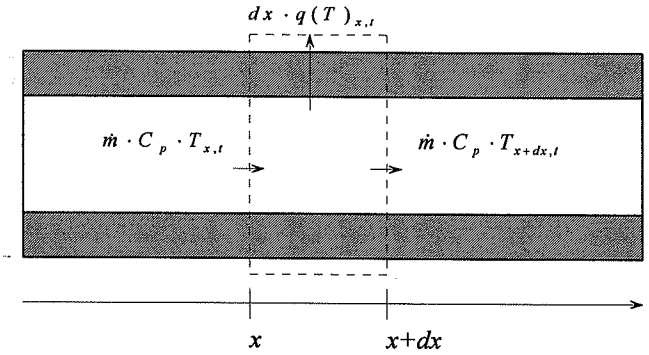

Figure 3.7 Plug flow model of a pipe.

The model was built on the basis of the diagram shown in Fig 3.7. To determine the temperature change along the pipe, the energy balance of the pipe as a whole may be formulated by writing down the energy equations for a segment with length *dx*. Thus, within a time period, the internal energy increase of this segment must equal to the heat transferred into the segment, minus the heat coming out of it. The energy balance of the element during the time *dt* can be presented as:

$$C_{pw} \cdot (T_{x,t+dt} - T_{x,t}) \cdot dx = \dot{m} \cdot C_p \cdot (T_{x,t} - T_{x+dx,t}) \cdot dt - q(T_{x,t}) \cdot dx \cdot dt \qquad (3.3.16)$$

Division by $dx \cdot dt$ and rearranging yields

$$\dot{m} \cdot C_p \cdot \frac{(T_{x+dx,t} - T_{x,t})}{dx} + C_{pw} \cdot \frac{(T_{x,t+dt} - T_{x,t})}{dt} = -q(T_{x,t}) \qquad (3.3.17)$$

Based on the energy balance of this segment, letting $dx \to 0$ and $dt \to 0$, one arrives at a partial differential equation:

$$\dot{m} \cdot C_p \frac{\partial T}{\partial x} + C_{pw} \frac{\partial T}{\partial t} = -q(T) \qquad (3.3.18)$$

Here,

t	time	s
dx	length of element	m
T	element temperature	°C
C_p	heat capacity of water	J/Kkg
C_{pw}	heat capacity of water and pipe	J/m K
$q(T)$	the energy exchange with surroundings $q(T) = U_p \cdot (T - T_a)$	W/m
U_p	Heat loss coefficient of the pipe	W/mK
T_a	Temperature of the surroundings	°C

Rearranging Eqn.(3.3.18) yields

$$V \frac{\partial T}{\partial x} + \frac{\partial T}{\partial t} = U_p (T_a - T) \qquad (3.3.19)$$

Here $V = \dot{m} \cdot C_p / C_{pw}$

By Laplace transformation, the water temperature at time t and location x in the pipe may be obtained as:

$$T(t,x) = T(t - x/v, 0) \cdot e^{-U_p \cdot \frac{x}{V}} + T_a \cdot (1 - e^{-U_p \cdot \frac{x}{V}}) \qquad (3.3.20)$$

Model 2 - Element method

In the element method, a pipe is assumed to be divided into a number of n elements along the flow direction, and each element is considered to have a uniform temperature. The energy equation for each element i may then be written as:

$$C_{pw} \cdot l_i \cdot \frac{dT_i}{dt} = \dot{m} \cdot C_p \cdot (T_{i-1} - T_i) - U_p \cdot l_i \cdot (T_i - T_a) \qquad (3.3.21)$$

Here, l_i is the length of element *i*.

Therefore the temperature change along the pipe can be determined by solving a set of *n* differential equations. According to Benonysson [5] and Bøhm [9], when using the element model, it is necessary to take the so-called Courant number into account to avoid numeric dispersion. Detailed descriptions of the Courant number may be found in [5] and [9].

Model 3 - Node method

Instead of dividing a pipe into a number of elements, the node method considers the energy balance in the pipe as a whole. This method has been widely applied in the dynamic modeling of solar DHW systems and district heating networks. Different versions of this method can be found in Rahbek [52], Benonysson [5] and Dutre [18]. In each time step, the energy balance of the pipe can be presented as:

$$C_{pw} \cdot L \cdot \frac{d\overline{T}}{dt} = \dot{m} \cdot C_p \cdot (T_i - T_u) - U_p \cdot L \cdot (\overline{T} - T_a) \qquad (3.3.22)$$

Here, $\overline{T}$	mean temperature of the pipe $\overline{T} = (T_u + T_i)/2$	°C
T_u	outlet temperature of the pipe	°C
T_i	inlet node temperature	°C

3.3.4.2 Dynamic model of DHW networks by the node method

In DHW distribution networks, long pipes are rarely used. Therefore, the node method that considers the energy balance in each pipe as a whole is justified. The principle of the node method is that, based on the known inlet temperature (from the inlet node), the outlet temperature of the pipe is calculated from the energy-balance equation of the whole pipe in each time step. Then, the new temperature for each node is obtained. According to equation 3.3.22, the heat balance for each pipe in the network can be written in finite-difference form:

$$C_{pwi} \cdot L_i \cdot (\overline{T}_{i,l} - \overline{T}_{i,l-1}) = \dot{m}_{i,l} \cdot C_p \cdot dt(T_{j_{i1},l-1} - T_{j_{i2},l}) - U_{pi} \cdot L_i \cdot dt(\overline{T}_{i,l-1} - T_a) \qquad (3.3.23)$$

Where, dt is the time step. The subscripts i and j indicate the pipe and node number, respectively. j_{i1} and j_{i2} indicate the inlet and outlet nodes of pipe i, while the subscripts l and l-1 denote values at time t and t-dt, respectively.

By Equation 3.3.23, the mean and the outlet temperature of each pipe can then be determined explicitly. The mean temperature of the node j in the time interval dt is therefore:

$$T_{j,l} = \frac{\sum_{i=1}^{m} a_{i,j} \cdot \dot{m}_{i,l} \cdot T_{i,l}}{\sum_{i=1}^{m} a_{i,j} \cdot \dot{m}_{i,l}} \quad if \quad a_{i,j} = 1 \qquad (3.3.24)$$

3.3.4.3 Heat loss coefficient

The heat loss from the network is proportional to the difference between the temperature of the pipe water and the temperature of the surroundings. Thus the heat losses increase when the temperature of the hot water rises. The actual heat loss per unit length pipe also depends on the insulation of the pipes, as well as on their diameter.

The pipes in the DHW distribution networks should be well insulated. Then the heat loss coefficient of each pipe can be calculated by the following equations:

$$U_{pi} = \frac{1}{\frac{1}{2 \cdot \pi \cdot \lambda_{ins}} \cdot \ln(\frac{D_{pi} + 2 \cdot e_{pi}}{D_{pi}}) + \frac{1}{\pi \cdot (D_{pi} + 2 \cdot e_{pi}) \cdot \alpha_{air}}} \qquad (3.3.25)$$

Where

D_{pi}	the outer diameter of the pipe i	m
e_{pi}	the thickness of the insulation material of pipe i	m
α_{air}	heat transfer coefficient between pipe insulation surface and air	W/m^2 K

The total heat loss Q_{loss} from a network with a number of m pipes may thus be found by:

$$Q_{loss} = \sum_{j=1}^{m} U_{pi} \cdot L_i \cdot (\overline{T}_i - T_a) \qquad (3.3.26)$$

3.4 Analysis of total heat load - A case study

Dynamic models of the hot water load and the distribution networks have been discussed in Sections 3.2 to 3.3. These models will be used to simulate the real heat load conditions by

using a typical design network configuration and mean-value consumption data under Danish conditions. The major interest of this simulation is to study the influence of the heat loss on total heat load. Therefore, a number of simulations will be carried out to investigate the heat loss under different operation and hot-water load conditions.

The temperature changes of the draw-off points and return water are important parameters in the design of distribution networks. Therefore, simulations will be carried out to examine the temperature distribution in the network.

3.4.1 Data of reference distribution network

Simulations were carried out for a DHW distribution network in a two-storey apartment building with 8 apartments. The network was chosen to be an up-feed circulation design. The corresponding diagram is shown in Figure 3.6. The geometric and thermal parameters which are used in the simulation are defined in Table 3.2. The outlet temperature of the tank is maintained at 50°C, and the surrounding temperature of the network is taken to be 20°C.

Table 3.2 Data for the pipes in the reference network.

Pipe no.	Node 1	Node 2	Length (m)	Diameter (mm)	Roughness (mm)	Heat loss (W/m K)	Heat capacity (J/m K)
1	0	1	10	22	0.03	0.23	1551.5
2	1	2	10	22	0.03	0.23	1551.5
3	2	3	10	22	0.03	0.23	1551.5
4	3	7	15	18	0.03	0.20	1033.8
5	3	6	3.5	18	0.03	0.20	1033.8
6	2	5	3.5	18	0.03	0.20	1033.8
7	1	4	3.5	18	0.03	0.20	1033.8
8	4	11	3.5	18	0.03	0.20	1033.8
9	5	10	3.5	18	0.03	0.20	1033.8
10	6	9	3.5	18	0.03	0.20	1033.8
11	7	8	3.5	18	0.03	0.20	1033.8
12	8	12	15	18	0.03	0.20	1033.8
13	9	12	3.5	18	0.03	0.20	1033.8
14	10	13	3.5	18	0.03	0.20	1033.8
15	11	14	3.5	18	0.03	0.20	1033.8
16	12	14	10	15	0.03	0.18	714.4
17	13	14	10	15	0.03	0.18	714.4
18	14	15	25	15	0.03	0.18	714.4

CirCon valves were chosen for the operation control. A CirCon valve is a thermostatic valve for the regulation of domestic hot water. The proportional regulator automatically ensures the distribution of the water in the system and maintains a given temperature. The working principle of these valves is that if the temperature of water reaches a certain value (e.g. 45°C), the pressure drop through the CirCon will be high, and if the temperature is reduced, the CirCon opens and increases the flow.

3.4.2 Hot water load of consumer

According to the investigation of Lawaetz [42], the average domestic hot-water (50 °C) load for each apartment is chosen as 81 *l*/day. For each apartment, the daily hot-water consumption pattern is as shown in Fig 3.4.

3.4.3 Simulation procedure

To apply the models described in sections 3.2 and 3.3 as a tool for analyzing the dynamic thermal process in a distribution network, a computer simulation program was developed in *Pascal* [66].

In order to carry out the dynamic simulation of a DHW network, sufficient boundary conditions must be specified. For the DHW networks shown in Fig.3.6, data for the pressure and outlet temperature of the tank, the circulation pump, the temperature-controlled valves, and the hot-water consumption are know.

In each time step, for given boundary conditions and temperatures in the network, the flow can be computed by Eqn.(3.3.15). To start the simulation, it is necessary to assume an initial flow and temperature in the network. After the flow has been determined, Eqns.(3.3.20) and (3.3.21) for each pipe and node may be solved implicitly, based on the known temperature from the last time step. For example, the value of $T_{i,l}$ may be calculated in terms of the known values $T_{i,l-1}$ and $T_{jil,l-1}$ from the previous time step. The time step should be chosen such as to give a stable solution.

Short time steps (less then 10 seconds) should be used in the simulation. This is mainly because of the temperature control strategy.

3.4.4 Simplifications in the simulation

The physical properties of the supply water and return water are assumed to be constant in the simulation. The cold water is set as 10°C, and the tapping program for the 8 draw-off points, which is shown in Fig 3.6, is applied simultaneously.

To determine the change of the circulation flow in the operation conditions, a preliminary calculation was carried out. Fig 3.8 shows the system head variations with the control valve operation. It can be seen that the circulation flow varies between 0.07 l/s and 0.08 l/s corresponding to the "open" and "closed" of the control valves.

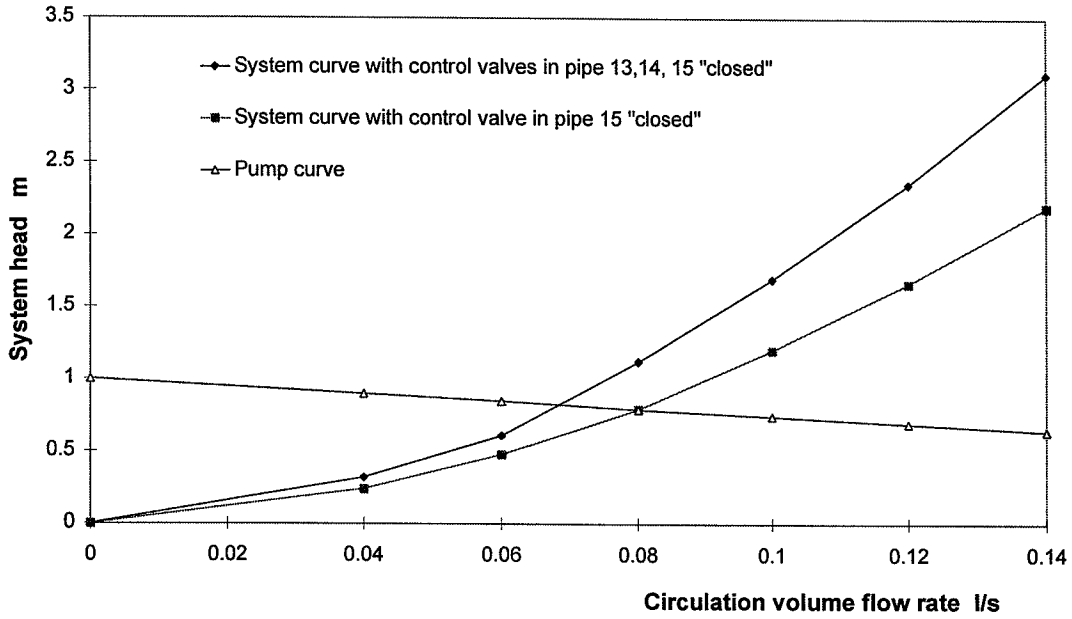

Figure 3.8 system curve variation during operation.

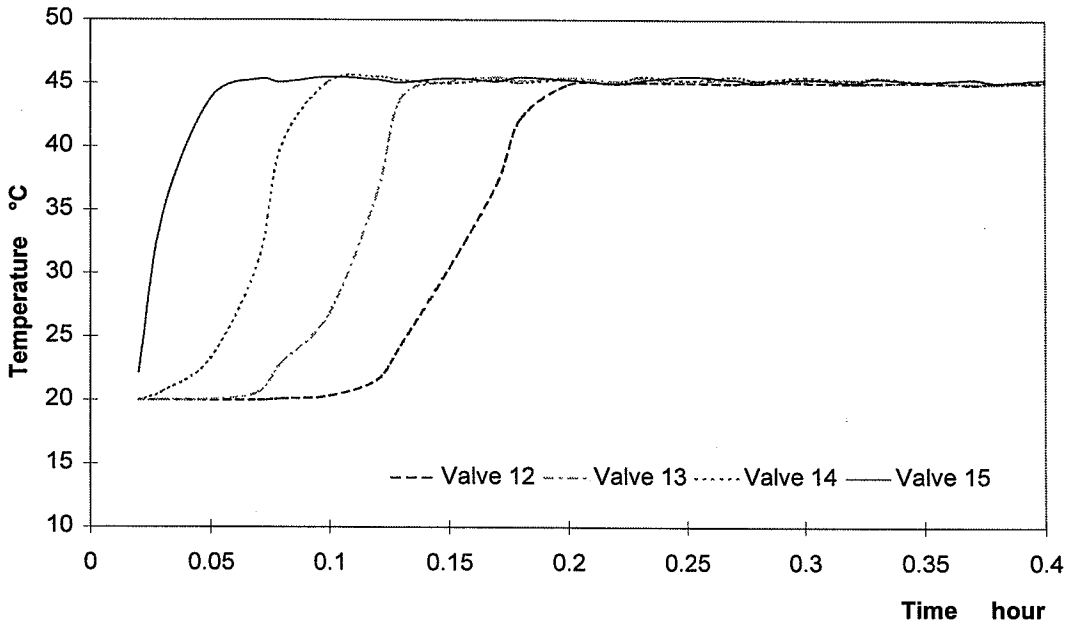

Figure 3.9 The temperature change in each control valve under starting conditions. The circulation flow rate is 0.08 l/s, and the output temperature of the tank is 50°C.

3.4.5 Analysis of the results

To investigate the total heat load and thermal performance of the network, a number of simulations were carried out. Figure 3.9 illustrates the time delay of the temperature change at the control valves correspond to the change of tank outlet temperature. With the circulation flow rate 0.08 l/s, the transmission of the temperature change to the control valve 12 takes about 0.2 hour. As expected, the distance makes a major contribution to this time

delay. The daily temperature changes at the draw-off nodes 8 to 11 and the return point are presented in Fig. 3.10. It shows that the daily temperature variation in each draw-off node is very small.

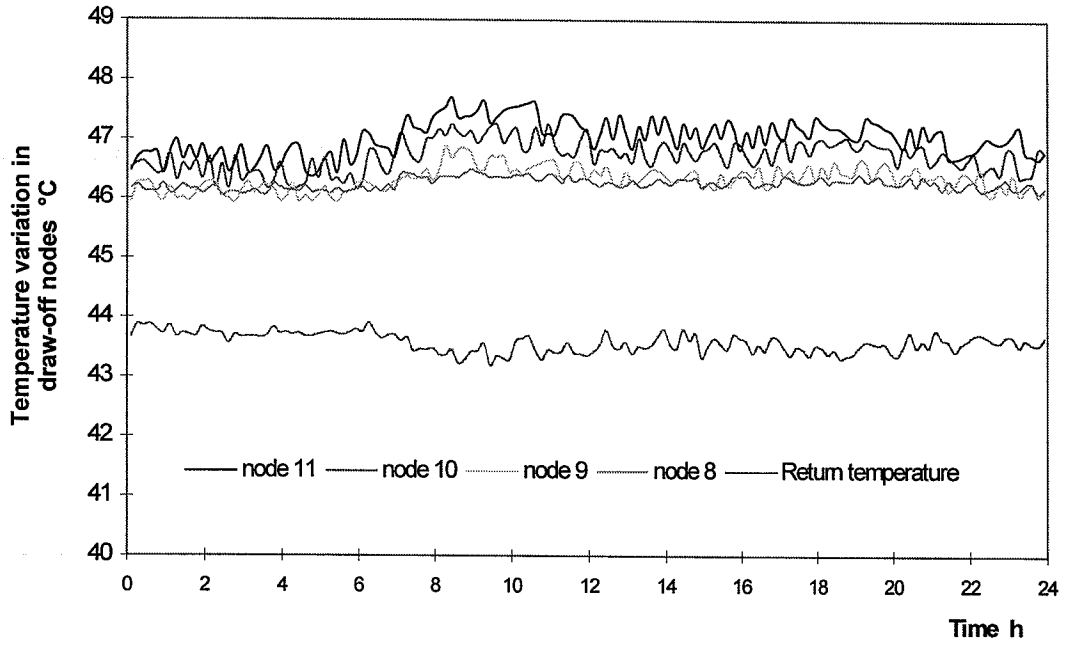

Figure 3.10 Temperature variation of draw-off nodes 8 to 11, and of the return water.

The effect of outlet temperature of the tank on the total heat loss from the network is shown in Figure 3.11. It is obvious that the heat loss from the distribution network increases with the increase of the tank outlet temperature. As the tank outlet temperature changes from 50°C to 70°C, the daily total heat loss from the network increases from 20 kWh/day to 25 kWh/day corresponding to 41% and 52% of the total heat load.

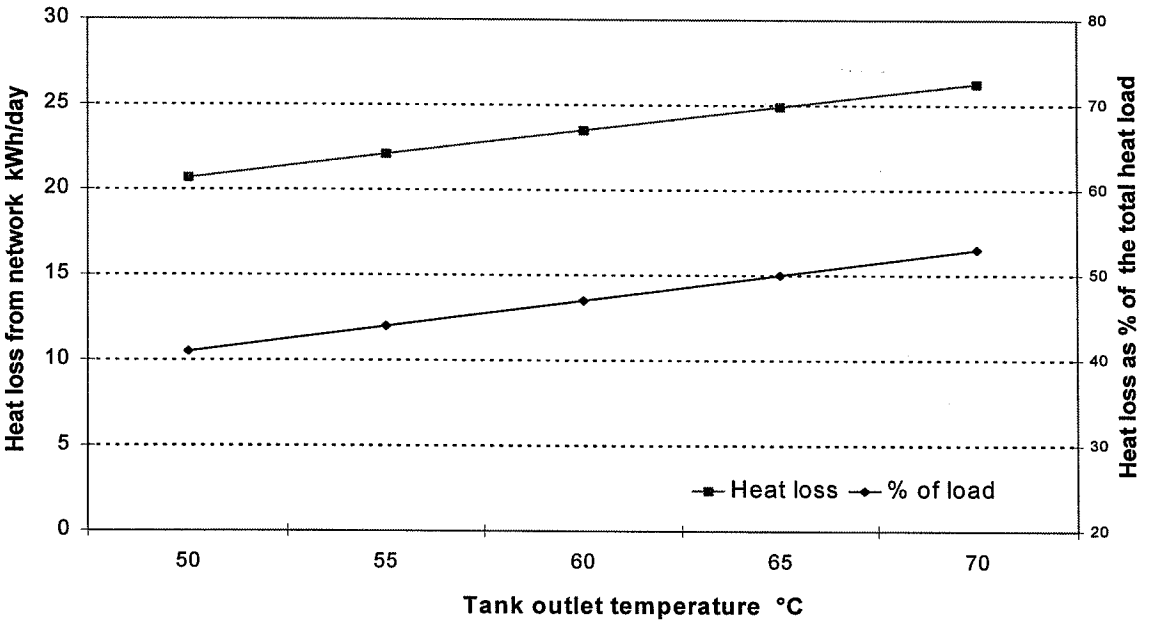

Figure 3.11 Daily heat loss as a function of tank outlet temperature.

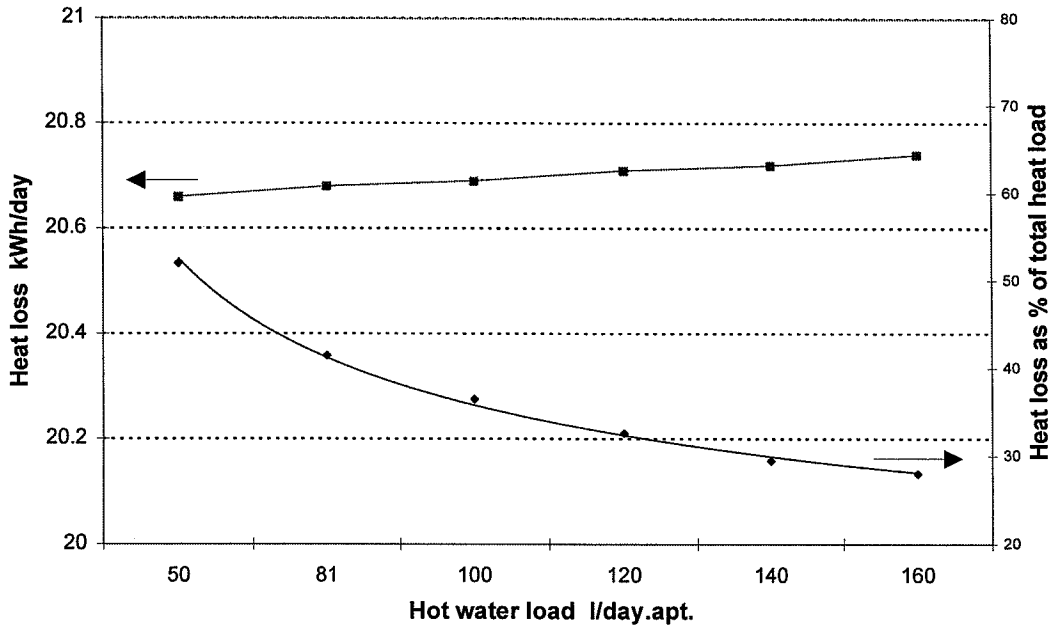

Figure 3.12 The daily heat loss as a function of the hot-water load.

Figure 3.12 shows the daily heat loss as a function of the hot-water load under operation condition with a tank outlet temperature of 50°C and a control temperature of 45°C. It can be seen that the daily hot-water load has only a very slight influence on the heat loss from the network. The difference of total daily heat loss is less than 0.1 kWh when the hot water load changes from 50 l/day.apt. to 160 l/day.apt. However, the increase of daily hot-water consumption results in an increase of total heat load. As a consequence, the percentage of the heat loss in the total heat load decreases.

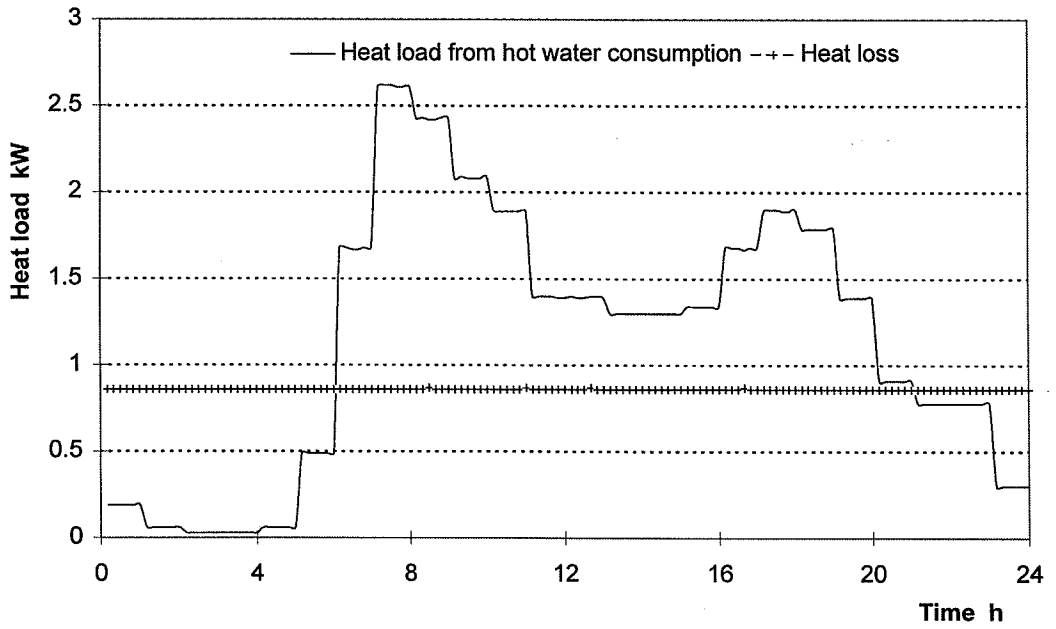

Figure 3.13 Heat load with typical working day load pattern.

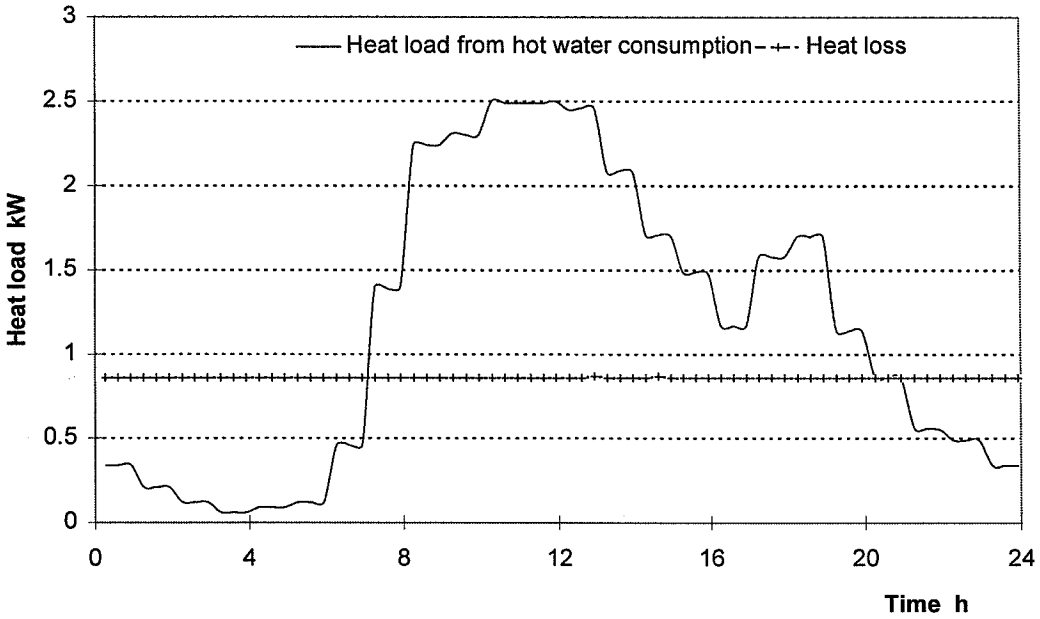

Figure 3.14 Heat load with weekend load pattern.

Based on a tank outlet temperature of 50°C and a control temperature of 45°C, the investigation of the effect of different load patterns on the heat loss was also carried out and the results are shown in Figures 3.13 and 3.14. It can be seen that the load patterns have no considerable influence on the heat loss and the heat loss from the network is at about 800 W throughout the day in both tapping pattern conditions.

3.5 Conclusion and discussion

In this chapter, analyses of the heat load of solar DHW systems have been presented. By literature studies, the investigation of the hot-water load, based on real measurements and statistical studies, were carried out. A dynamic model for distribution network has been developed to simulate the thermal process and calculate the heat loss from the distribution networks.

Based on measurements from the 80's, it was found that the average heat consumption for domestic hot water is about 5 kWh/day for an apartment in large apartment buildings, and 6 kWh/day for single-family houses under Danish conditions. Comparing the measurements made in the last two decades in Denmark, one notices a clearly decreasing tendency of the daily heat load. A decrease of the hot-water consumption of about 20% during the last decade has been reported. It was also found, from the measurements carried out in different regions in the world that the hot-water load and load pattern are very different from area to area. The variation of heat consumption during a day and an extended period was also investigated and a typical daily hot-water load pattern for Danish conditions is presented.

To investigate the heat loss from distribution networks, simulations were carried out under Danish hot-water load conditions. The results show that the heat loss from a circulation

type of DHW network may vary greatly from 40% to 50% of the total heat load, due to different operation temperatures. The hot-water load and pattern have no considerable influence on the heat loss. The time delay of the temperature changes at the consumer, corresponding to the tank temperature, was also studied. The results show that distance and heat capacities of the network make the major contributions.

From these simulation results it appears that at certain operation temperatures, the heat loss from a circulation type of distribution network is approximately constant. Therefore, in the solar DHW system simulation, the heat load caused by the heat loss can be calculated as a function of the tank outlet temperature.

Chapter 4

Component models of solar DHW systems

4.1 Introduction

Solar DHW systems are constructed from some basic components such as solar collector, connection pipes, heat exchanger, storage tank etc. Each of these components performs a certain function that plays an important role in the system operation. The thermal performance of such systems depends on the performance of each single component, the operation design and the hot-water consumption. In order to carry out a system simulation, it is necessary to develop the detailed dynamic models of these basic components.

The mathematic modeling of solar thermal systems has received a great interest during the last decades. So far, research on many different components has been conducted and many component models of different assessment can be found in literature. In this study the dynamic models of drain-back tanks (both as a separate tank and combined with a mantle tank) are developed. The other models presented in this chapter are based on the previous work.

Heat transfer and fluid flow are the basic process in the operation of a solar DHW system. The numerical models of the components are built up with the laws governing these processes and they are generally expressed in terms of differential equations. The exact solution of these equations involves a large amount of complicated computational work and is sometimes not feasible. It is therefore also necessary to have some simplified models which may give reasonable results and, at the same time, save the computational cost. In any case, the models should imitate and represent the physical reality.

In this chapter, the physical models and governing differential and/or algebraic equations are presented for each of the following components:

- Flat-plate collector
- Heat transfer media
- Connection pipe
- Spiral heat exchanger
- Drain-back vessel
- Storage tank
- Tank with built-in heat exchanger spiral

- Mantle tank with drain-back design
- Controller

4.2 Flat-plate collector

Collectors of the flat-plate type are very commonly used in the solar DHW systems all over the world. As the designation indicates, the solar collector collects solar radiation and converts it into heat. The modeling of this type of collector is the topic of many papers published during the last few decades.

Hottlel and Whillier (1955) did the pioneer work in collector modeling and several models refined in various directions have been developed (see Duffie [17], Svendsen [60], and Isakson [36]). The model presented here is based on these previous works.

4.2.1 Mathematical model

Low-flow condition

In order to determine the temperature profile, a collector can be assumed to be divided into a number of n segments along the flow direction. Each segment of the collector is considered to have a unique temperature and the same efficiency. The energy-balance equation for each segment i can thus be presented as:

$$A_{ci} \cdot C_{pc} \cdot \frac{dT_i}{dt} = A_{ci} \cdot G \cdot \eta + \dot{m}_c \cdot C_{pf} \cdot (T_{i-1} - T_i) \qquad (4.2.1)$$

For boundary segments we get:

$$A_{c1} \cdot C_{pc} \cdot \frac{dT_1}{dt} = A_{c1} \cdot G \cdot \eta + \dot{m}_c \cdot C_{pf} \cdot (T_{ci} - T_1) \qquad (4.2.2)$$

$$A_{cn} \cdot C_{pc} \cdot \frac{dT_n}{dt} = A_{cn} \cdot G \cdot \eta + \dot{m}_c \cdot C_{pf} \cdot (T_{n-1} - T_c) \qquad (4.2.3)$$

Here,	A_{ci}	area of collector segment *i*	m^2
	C_{pc}	thermal capacity of the collector	$J/K.m^2$
	C_{pf}	thermal capacity of the collector fluid	J/kg.K
	T_i	temperature of collector segment i	°C
	t	time	s
	G	solar irradiance	W/m^2
	η	collector efficiency	
	T_{ci}	inlet temperature of collector	°C
	T_c	outlet temperature of collector	°C
	$\dot{m}_c$	mass flow rate in the collector loop	kg/s

High flow condition

For high flow systems, the temperature change along the flow direction in the collector is approximately linear. Therefore, the energy balance of the collector can be expressed as:

$$A_c \cdot C_{pc} \cdot \frac{d\overline{T}_c}{dt} = A_c \cdot G \cdot \eta + \dot{m}_c \cdot C_{pf} \cdot (T_{ci} - T_c) \qquad (4.2.4)$$

Here, $\overline{T}_c$ mean temperature of collector °C
A_c area of the collector m^2

4.2.2 Collector efficiency

The efficiency of a collector is a comprehensive factor that depends on a number of design and operation parameters. A temperature dependent efficiency model is used in the collector model and it can be presented as:

$$\eta = \eta_0 - k_0 \frac{\overline{T}_c - T_a}{G} - k_1 \frac{(\overline{T}_c - T_a)^2}{G} \qquad (4.2.5)$$

where η_0 maximum collector efficiency
k_0 collector heat loss coefficient $W/m^2 K$
k_1 collector heat loss coefficient $W/m^2 K^2$

Solar irradiance absorbed

The quantity of solar energy collected by a flat-plate collector is highly dependent on the incidence angle of the radiation. The incident angle not only determines the incident irradiance on the collector surface, but also determines how efficiently this energy can be converted into heat. This is because the transmittance(τ) of the collector cover and the absorptance (α) of the absorber are highly dependent on the solar incidence angle[8].

The efficiency of a solar collector is usually reported at normal incidence. The corresponding reduction is computed from the incident angle modifier coefficient *IAM(θ):*

$$IAM(\theta) = (\tau \cdot \alpha)_\theta / (\tau \cdot \alpha)_n \qquad (4.2.6)$$

Here τ transmittance of the collector cover
α absorbtance of the absorber

The value of the incidence angle modifier can be approximated by the following expression:

$$IAM(\theta) = 1 - \left(\tan\left(\frac{\theta}{2}\right)\right)^{\beta_1} \tag{4.2.7}$$

Here, θ is the incident angle, and β_1 is a coefficient which depends on thickness and material of the cover.

Mean temperature of the collector

The temperature determination is the basic task for collector modeling. To simplify the model, the mean temperature of the collector fluid is often being used. For high flow systems, the mean temperature can be found from the following equation:

$$\overline{T}_c = \frac{T_{ci} + T_c}{2} \tag{4.2.8}$$

For low flow conditions, the temperature change along the flow direction is non-linear and the mean temperature of the collector fluid can be calculated by the following equation, (from Furbo [25]).

$$\overline{T}_c = a \cdot T_c + (1-a) \cdot T_{ci} \tag{4.2.9}$$

Here $a = -\frac{\dot{m}_c \cdot C_{pf}}{k_0 + k_1 \cdot (\overline{T}_c - T_a)} + \frac{1}{1 - e^{-(k_0 + k_1 \cdot (\overline{T}_c - T_a))/\dot{m}_c \cdot C_{pf}}}$

4.3 Heat transfer mediums

For a solar DHW system, the heat which is collected by the collector has to be transported to the storage tank for water heating. The heat transport is carried out by means of a heat transfer medium, and with the use of controlled pumps or buoyancy force. Naturally, the density, thermal conductivity and heat capacity of the medium are of importance for the heat transfer efficiency. In this study, the heat transfer media that have been used for the collector loop are water or water-propyleneglycol mixture. Thermal properties of both media are more or less temperature dependent.

4.3.1 Thermal properties of water

The following equations present the thermal properties of water as a function of temperature, from [21].

Density:

$$\rho = 1000.5 - 6.9 \cdot 10^{-2} \cdot T - 36.0 \cdot 10^{-4} \cdot T^2 \quad (\mathrm{kg/m^3})$$

Heat capacity:

$$C_p = 4209.1 - 132.8 \cdot 10^{-2} \cdot T + 143.2 \cdot 10^{-4} \cdot T^2 \quad \text{(J/kg K)}$$

Thermal conductivity:

$$\lambda = 0.5762 + 10.5 \cdot 10^{-4} \cdot T \quad \text{(W/mK)}$$

Kinematic viscosity:

$$\upsilon = 1.477 \cdot 10^{-6} \cdot \exp(-1.747 \cdot 10^{-2} \cdot T) \quad \text{(m}^2\text{/s)}$$

Pr number:

$$\text{Pr} = 39.5345 \cdot T^{-0.144} - 18.8396$$

Coefficient of expansion:

$$\beta = (0.8 \cdot T^{0.5348} - 1.9114) \cdot 10^{-4} \quad \text{(K}^{-1}\text{)}$$

Here, T is the temperature °C

4.3.2 Thermal properties of the mixture of glycol and water

Propyleneglycol-water mixtures are commonly used in the collector loop as a heat transport medium to prevent freeze problems. The thermal properties of this kind of liquids depend on both the proportions of the gradients and the temperature. The following equations present the thermal properties of propyleneglycol-water mixture as a function of the percentage of propyleneglycol and temperature, from [21].

Density:

$$\begin{aligned}\rho = {} & (999.65 + 152.3 \cdot 10^{-2} \cdot x - 96.6 \cdot 10^{-4} \cdot x^2) \\ & + (-1.7 - 146.1 \cdot 10^{-2} \cdot x + 76.7 \cdot 10^{-4} \cdot x^2) \cdot 10^{-2} \cdot T \\ & + (-38.4 + 62.1 \cdot 10^{-2} \cdot x - 30.8 \cdot 10^{-4} \cdot x^2) \cdot 10^{-4} \cdot T^2\end{aligned} \quad \text{(kg/m}^3\text{)}$$

Thermal capacity:

$$\begin{aligned}C_p = {} & (4255.5 - 958.5 \cdot 10^{-2} \cdot x - 941.7 \cdot 10^{-4} \cdot x^2) \\ & + (-168.9 + 843.5 \cdot 10^{-2} \cdot x - 35.0 \cdot 10^{-4} \cdot x^2) \cdot 10^{-2} \cdot T \\ & + (146.5 - 79.3 \cdot 10^{-2} \cdot x - 85.3 \cdot 10^{-4} \cdot x^2) \cdot 10^{4} \cdot T^2\end{aligned} \quad \text{(J/kg K)}$$

Thermal conductivity:

$$\lambda = (0.571 - 0.42 \cdot 10^{-2} \cdot x + 0.1 \cdot 10^{-4} \cdot x^2) + (12.6 - 31.3 \cdot 10^{-2} \cdot x + 12.2 \cdot 10^{-4} \cdot x^2) \cdot 10^{-4} \cdot T \quad \text{(W/mK)}$$

Kinematic viscosity:

$$\upsilon = (1.293 \cdot \exp(4.388 \cdot 10^{-2} \cdot x)) \cdot 10^{-6} \cdot \exp(-1.709 - 1.921 \cdot 10^{-2} \cdot x - 0.6 \cdot 10^{-4} \cdot x^2) \cdot 10^{-2} \cdot T \quad \text{(m}^2\text{/s)}$$

Here, T [°C] is temperature and x [%] is the percentage of the propyleneglycol.

4.4 Connection Pipes

Pipes are used to connect components in solar DHW systems. The most important parameters in the pipe model are flow and temperature. For active solar DHW systems, the flow is one of the design parameters and the task of pipe modeling is to present the thermal process under certain conditions.

The pipe model used in DHW systems is the same as the pipe model used in distribution networks. Detailed model description has been presented in section 3.3.4.1.

4.5 Heat exchanger spiral

When making effort to simulate the heat transfer process in the collector loop, the dynamic models of heat exchangers are important. The heat exchangers used in solar DHW systems are normally of a spiral type, since this type of exchanger is compact, easy to maintain and economic. Figure 4.1 shows a sketch of this kind of heat exchanger.

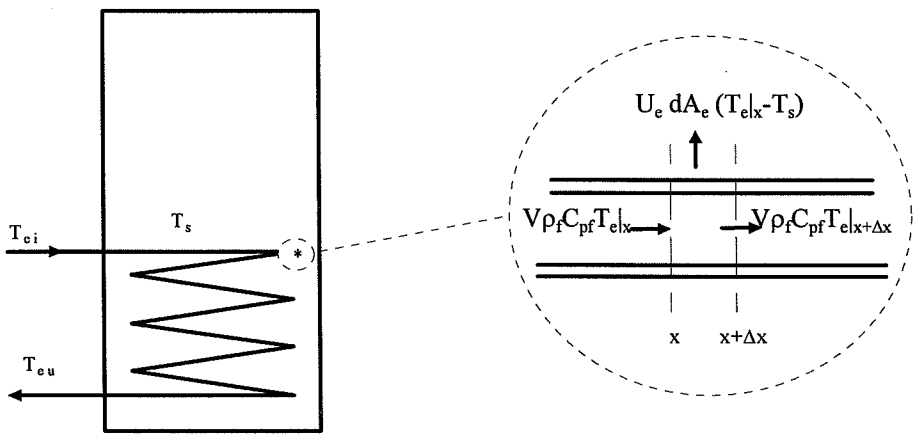

Figure 4.1 Sketch of a heat exchanger spiral situated at the bottom of a tank.

The heat exchanger in the collector loop is situated either in an additional heat exchange tank or directly in the storage tank. In both situations, the flow configuration may be classified as two-stream cross-counter flow. The amount of heat transferred by these heat exchangers depends on a number of design and operation parameters. For a system under certain operation condition, the design parameters of the heat exchanger are given, and the supply temperature is determined by the other part of the collector loop. Therefore, a model which determines the return temperature as a function of the temperature difference of heat exchanger fluid and tank water is important. The heat exchanger model presented here is based on [21].

4.5.1 Mathematical models

To determine the fluid temperature variation along the heat exchanger coil, the energy balance of the heat exchanger as a whole may be formulated by writing down the energy equations for a number of segments with the length Δx. So, the steady-flow energy equation for each segment can be presented as:

$$V \cdot C_{pf} \cdot \rho_f \cdot (T_e|_x - T_e|_{x+\Delta x}) = U_e \cdot dA_e \cdot (T_e|_x - T_s) \tag{4.5.1}$$

Where,	V	volume flow rate in the heat exchanger	m^3/s
	ρ_f	density of heat transfer fluid	kg/m^3
	T_e	temperature of the fluid in the heat exchanger	°C
	U_e	heat transfer coefficient of heat exchanger spiral	W/m^2K
	dA_e	surface area of the segment with length Δx	m^2
	T_s	the temperature of storage tank	°C

Let $T_e|_{x+\Delta x}$-$T_e|_x$=$dT_e|_x$, then Eqn. 4.5.1 can be written as:

$$-\frac{U_e \cdot dA_e}{V \cdot C_{pf} \cdot \rho_f} = \frac{dT_e|_x}{T_e|_x - T_s} \tag{4.5.2}$$

Integrate along the heat exchanger spiral.

$$\int_0^{A_e} -\frac{U_e \cdot dA_e}{V \cdot C_{pf} \cdot \rho_f} = \int_{T_{ei}}^{T_{eu}} \frac{dT_e|_x}{T_e|_x - T_s} \tag{4.5.3}$$

Rearrange yields:

$$-\frac{U_e \cdot A_e}{V \cdot C_{pf} \cdot \rho_f} = \ln\left(\frac{T_{eu} - T_s}{T_{ei} - T_s}\right) \tag{4.5.4}$$

Here, A_e surface area of the heat exchanger m^2
T_{ei} , T_{eu} the inlet and outlet temperature of the exchanger °C

Thus, the heat exchange capacity rate *H(W/K)* can be found:

$$\begin{aligned} H = U_e \cdot A_e &= -V \cdot C_{pf} \cdot \rho_f \cdot \ln\left(\frac{T_{eu} - T_s}{T_{ei} - T_s}\right) \\ &= V \cdot C_{pf} \cdot \rho_f \cdot \ln\left(\frac{T_{ei} - T_s}{T_{eu} - T_s}\right) \end{aligned} \tag{4.5.5}$$

4.5.2 Heat exchange capacity rate

Theoretical and experimental investigations on heat exchange capacity rate for heat exchanger spirals have been reported by several authors. Theoretically the heat exchange capacity rate can be calculated by the equation:

$$H = \frac{1}{R_{ei} + R_{ep} + R_{eu}} \tag{4.5.6}$$

Here, R_{ei} the thermal resistance of the inner surface of the heat exchanger pipe K/W
R_{eu} the thermal resistance of the outer surface of the heat exchanger pipe K/W
R_{ep} the thermal resistance of the heat exchanger pipe wall K/W

They can be found from the following equations:

$$R_{ei} = \frac{1}{\pi \cdot d_{ei} \cdot L_e \cdot h_{ei}} \tag{4.5.7}$$

$$R_{ep} = \frac{1}{2 \cdot \pi \cdot \lambda_p \cdot L_e} \cdot \ln(d_{eu}/d_{ei}) \tag{4.5.8}$$

$$R_{eu} = \frac{1}{\pi \cdot d_{eu} \cdot L_e \cdot h_{eu}} \tag{4.5.9}$$

Here, d_{ei} and d_{eu} are the inner and outer diameter of the coil pipe [m]. Similarly, h_{ei} and h_{eu} are the heat transfer coefficient of fluid to the pipe inner wall and the outer wall to the tank water [W/m^{2}K]. λ_p is the thermal conductivity of the coil pipe and according to Furbo [21], h_{ei} and h_{eu} can be calculated as:

$$h_{ei} = \frac{\lambda_f}{d_{ei}} \cdot 0.016 \cdot \mathrm{Pr}_m^{0.34} \cdot \mathrm{Re}^{0.82} \cdot \left(\frac{\mathrm{Pr}_m}{\mathrm{Pr}_w}\right) \tag{4.5.10}$$

$$h_{eu} = \frac{\lambda}{d_{eu}} \left\{ 0.60 + \frac{0.387 \cdot Gr^{0.192}}{(1+(0.559/\mathrm{Pr}_f)^{9/16})^{8/27}} \right\}^2 \tag{4.5.11}$$

Here,

λ_f	thermal conductivity of the heat transfer fluid	W/mK
λ	thermal conductivity of tank water	W/mK
$\mathrm{Pr_m}$	Prandtl number of the heat transfer medium at the average temperature inside the exchanger coil	
$\mathrm{Pr_w}$	Prandtl number of the heat transfer medium at the average temperature at the inner surface of the exchanger coil	
$\mathrm{Pr_f}$	Prandtl number of water at the mean temperature between the outer surface of the exchanger and the water in the tank	
Gr	the Grashof number for the characteristic length	

Based on the equations above, the heat exchange capacity rate of a specified heat exchanger with a certain inlet and storage tank temperature can be determined. To find the corresponding heat exchange capacity rate H, iteration methods could be used and the calculation starts with giving an estimated quantity of the average temperature of the heat exchanger fluid. By using the heat exchange capacity rate found in the previous step, the average and outlet temperature of the exchanger can be determined. Take the calculated exchanger temperature as a new estimate and repeat the last two computation processes until the calculated temperature equals to the estimated value. After this computation process the heat capacity rate value can be found.

Based on a large number of experiments with different heat exchanger spirals, volume flow rates and storage temperature, Jensen (1984)[37] has developed a computer model for smooth heat exchanger spirals situated at the bottom of hot water tanks. This model shows that the heat exchange capacity rate for a heat exchanger spiral situated at a hot water tank can be determined by the equation:

$$H = C_1 + C_2 \cdot \ln(T_{ei} - T_s) + (C_3 + C_4 \cdot \ln(T_{ei} - T_s)) \cdot T_s \qquad (4.5.12)$$

Here C_1, C_2, C_3, *and* C_4 are constants which only depend on the heat exchanger spiral, the heat transfer fluid and volume flow rate. These constants can be calculated by experimentally determined equations and detailed methods can be found in [37].

4.6 Separate drain-back tank

A drain-back tank works as a storage vessel of solar collector fluid in a drain-back system. Depending on the hot-water tank design, the drain-back tank can be either integrated with a mantle tank or separated as an additional tank. The later is normally a small tank which becomes part of the collector loop, see Figure 4.2(a).

When the collector loop starts to operate, the working fluid in the drain-back tank will be pumped into the collector and the quantity of fluid in the drain-back tank will be reduced until the collector has been filled up. The opposite process will happen during the stopping period. Therefore, in these starting and stopping conditions, the thermal capacity of the drain-back tank is a function of time and flow rate.

During operation, a drain-back tank is normally fully mixed, therefore it can be modeled as one temperature node.

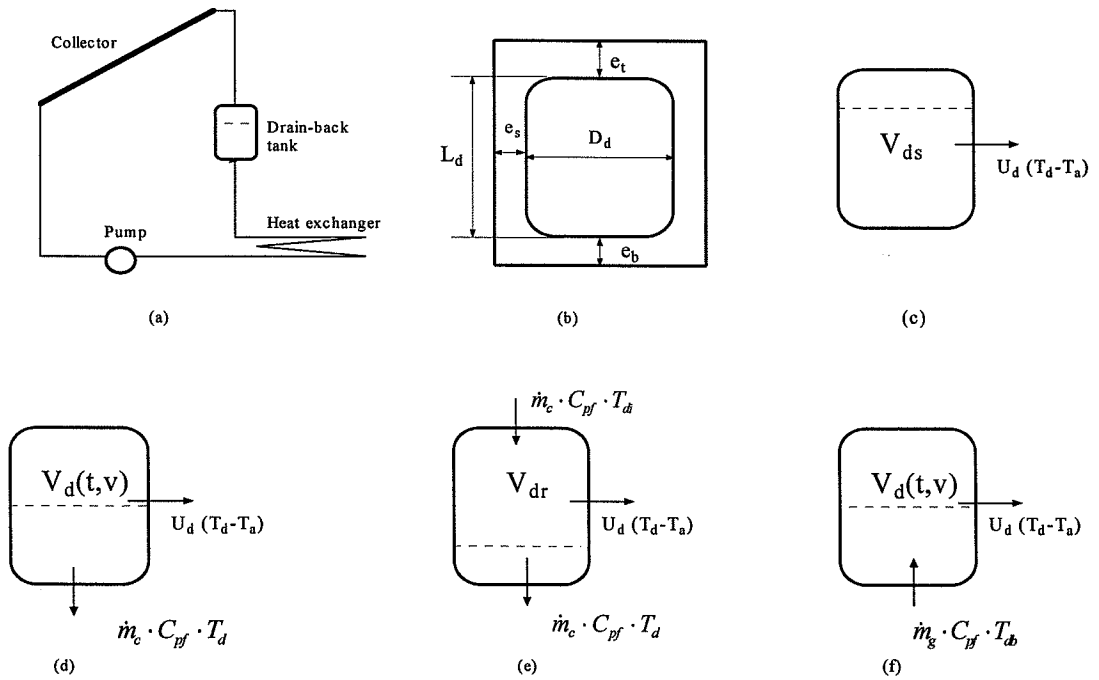

Figure 4.2 (a) collector loop with drain-back design. (b) Insulated drain-back tank. (c) Energy balance for a period without collector operation. (d) Energy balance for a starting period. (e) Energy balance for normal operation. (f) Energy balance for stopping period.

4.6.1 Mathematical model

A drain-back tank can be modeled as a fully mixed liquid tank with variable quantity of content fluid. To simplify the calculation, it was assumed that the temperature of the drain-back tank is uniform. However, the energy balance of a drain-back tank has to be analyzed under different operation conditions.

Period without collector operation

During the steady non-operation period, a drain-back tank is full with working fluid and the heat loss to the surroundings is the only energy exchange process. The energy balance of the drain-back tank may be presented as:

$$\frac{d}{dt}\left[(V_{ds}\cdot \rho_f \cdot C_{pf} + C_{pd})\cdot T_d\right] = -U_d\cdot(T_d - T_a) \qquad (4.6.1)$$

Rearrange

$$(V_{ds}\cdot \rho_f \cdot C_{pf} + C_{pd})\frac{dT_d}{dt} = -U_d\cdot(T_d - T_a) \qquad (4.6.2)$$

Where, V_{ds}	the maximum volume of the fluid	m^3
T_d	temperature of the drain-back tank	°C
U_d	total heat loss coefficient of the drain-back tank	W/K
C_{pd}	thermal capacity of the drain-back tank	J/K

Starting period

During the starting operation period, the fluid in a drain-back tank is pumped out to the collector, and the energy balance may be presented as:

$$\frac{d}{dt}\left[(V_d\cdot \rho_f \cdot C_{pf} + C_{pd})\cdot T_d\right] = -\dot{m}_c\cdot C_{pf}\cdot T_d - U_d\cdot(T_d - T_a) \qquad (4.6.3)$$

rearrange

$$\rho_f \cdot C_{pf}\frac{d}{dt}(V_d\cdot T_d) + C_{pd}\cdot\frac{dT_d}{dt} = -\dot{m}_c\cdot C_{pf}\cdot T_d - U_d\cdot(T_d - T_a) \qquad (4.6.4)$$

Here, V_d [m^3] is the volume of the fluid in the drain-back tank and it is decreasing during the starting period.

Normal operation period

For a normal operation period, one obtains:

$$\frac{d}{dt}\left[(V_{dr}\cdot\rho_f\cdot C_{pf}+C_{pd})\cdot T_d\right]=\dot{m}_c\cdot C_{pf}\cdot(T_{di}-T_d)-U_d\cdot(T_d-T_a) \qquad (4.6.5)$$

rearrange

$$(V_{dr}\cdot\rho_f\cdot C_{pf}+C_{pd})\frac{dT_d}{dt}=\dot{m}_c\cdot C_{pf}\cdot(T_{di}-T_d)-U_d\cdot(T_d-T_a) \qquad (4.6.6)$$

Where, V_{dr} [m^3] is the minimum volume of fluid in the drain-back tank, which is the volume of the fluid in the drain-back tank under normal operation. T_{di} [°C] is the inlet temperature.

Stopping period

Opposite to the starting period, during the stopping step, the fluid in the collector drains back to the drain-back tank by gravity force. The energy balance can be presented as:

$$\frac{d}{dt}\left[V_d\cdot\rho_f\cdot C_{pf}+C_{pd})\cdot T_d\right]=\dot{m}_g\cdot C_{pf}\cdot T_{db}-U_d\cdot(T_d-T_a) \qquad (4.6.7)$$

rearrange

$$\rho_f\cdot C_{pf}\frac{d}{dt}(V_d\cdot T_d)+C_{pd}\cdot\frac{dT_d}{dt}=\dot{m}_g\cdot C_{pf}\cdot T_{db}-U_d\cdot(T_d-T_a) \qquad (4.6.8)$$

Where, $\dot{m}_g$[kg/s] is the mass flow rate of the drain-back flow and the T_{db}[°C] is the temperature of the drain-back fluid. The volume of the fluid in the drain-back tank V_d is increasing during the stopping period.

4.6.2 Heat loss coefficient

As a part of the collector loop, a drain-back tank should be well insulated. Figure 4.3(b) shows an insulated drain-back tank. The overall heat loss coefficient of a drain-back tank can be calculated by the following equation:

$$U_d=L_d\cdot U_l+U_t+U_b \qquad (4.6.9)$$

Here, U_l *(W/m K)* is the heat loss coefficient of the tank side wall. Similarly, U_t *(W/K)* and U_b *(W/K)* are the heat loss coefficient of the tank top and the bottom wall. They can be found from the following equations.

$$U_l = \frac{\pi}{\frac{1}{2 \cdot \lambda_{ins}} \ln(1 + \frac{2 \cdot e_s}{D_d}) + \frac{1}{(D_d + 2 \cdot e_s) \cdot \alpha_{air}}} \tag{4.6.10}$$

$$U_t = \frac{\frac{\pi}{4} \cdot (D_d + e_s)^2}{e_t / \lambda_{ins} + 1/\alpha_{air}} \tag{4.6.11}$$

$$U_b = \frac{\frac{\pi}{4} \cdot (D_d + e_s)^2}{e_b / \lambda_{ins} + 1/\alpha_{air}} \tag{4.6.12}$$

Where, α_{air} is the natural convection coefficient from the drain-back tank insulation surface to the surroundings and approximately 7.7 W/m^2 K under indoor circumstance.

4.7 Normal hot-water tank

The design of thermal solar system involves, among other things, the selection of a heat storage. In solar DHW systems, the energy is stored as sensible heat and the water delivered to the consumer is also the medium of storing the heat. It has been proved that the solar fraction of a solar DHW system depends strongly on the heat storage design. Therefore, the heat storage tank is essential for the utilization of solar energy in domestic hot water heating.

The basic type of storage tank used in solar DHW system is shown in Figure 4.3. For this kind of storage tank the heat exchange between tank water and heat production unit is carried out outside the tank. During the operation, the cold water from the bottom of the tank is forced (by pump or buoyancy) to go through the collector (or the heat exchanger outside the tank) and back to the upper part of the tank. The advantage of using this kind of storage tank is the great reduction of the production, installation and maintenance costs.

The previous work on the modeling of this type of tank can be found in Duffie [17], Dutre [18], and Jensen [38] and Antonopoulo [2]. Figure 4.3 shows how the computer model is built for simulation of the tank.

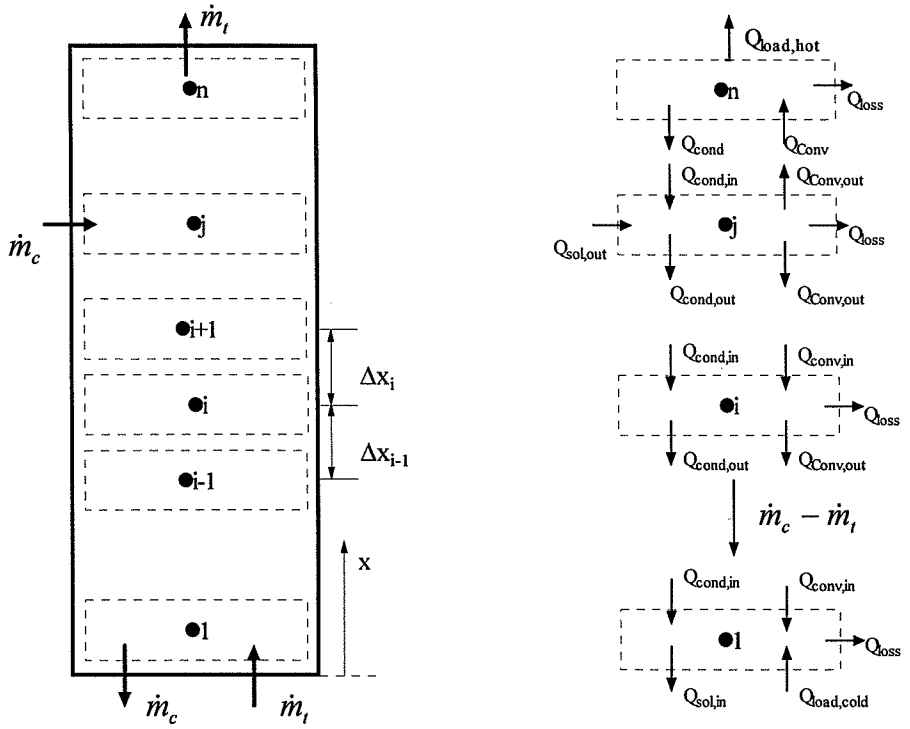

Figure 4.3 n-element stratified water tank

4.7.1 Mathematical model

For low flow operation, especially under natural circulation conditions, the tank water may operate with significant degrees of stratification. To explore the temperature gradient along the vertical direction, the tank water is modeled with *n* control elements along the tapping direction *x* and a uniform temperature is assumed in each of these control elements.

Generally, the energy balance in each control element *i* can be presented as:

$$\Delta Q_i = Q_{conv} + Q_{cond} - Q_{loss} \tag{4.7.1}$$

Here ΔQ_i is the energy stored within the layer *i*, Q_{conv} and Q_{cond} is the convective and diffusive heat fluxes entering or leaving the control volume. Q_{loss} presents the heat losses to the ambient.

The heat transfer caused by natural convection leads to mixing, therefore, it can be characterized by an equivalent heat conduction coefficient λ^{eq}. The combined heat transfer by conduction and natural convection is modeled as an effective conduction heat transfer. To determine the λ^{eq} value, at the end of each computational step, the temperature of each control volume should be scanned from the top to the bottom. If between two neighbor control volumes the temperature of the lower control volume is higher than the upper one, the λ^{eq} for lower control volume will be equal to a large value which may cause the fully mixture of these two control volumes. Otherwise, the λ^{eq} value is equal to zero.

In the present model, there are two streams flowing in and out of the tank. The flow to the collector (or exchanger) always leaves from the bottom element, and returns from the collector (or exchanger) to the element *j* which is situated in the upper part of the tank. The tapping flow comes to the bottom and leaves from the top element. The flow of tank water is directly controlled by the mass flow rate of these two streams.

Tapping period ($\dot{m}_t > \dot{m}_c$)

During major tapping periods, the tapping flow rate is larger than the flow to the collector and the stream inside the tank is in an up-flow condition. The tank model can be presented by a set of *n* differential equations:

For elements $1<i<j$

$$\begin{aligned}\frac{\partial}{\partial t}(V_i \cdot \rho \cdot C_p \cdot T_i) &= (\dot{m}_t - \dot{m}_c) \cdot C_p \cdot (T_{i-1} - T_i) \\ &- U_l \cdot \Delta x \cdot (T_i - T_a) \\ &+ A_t \cdot \left[(\lambda + \lambda_i^{eq}) \cdot \frac{T_{i+1} - T_i}{\Delta x_i} \right. \\ &\left. - (\lambda + \lambda_{i-1}^{eq}) \frac{T_i - T_{i-1}}{\Delta x_{i-1}} \right]\end{aligned} \tag{4.7.2}$$

For element $n>i>j$

$$\begin{aligned}\frac{\partial}{\partial t}(V_i \cdot \rho \cdot C_p \cdot T_i) &= \dot{m}_t \cdot C_p \cdot (T_{i-1} - T_i) - U_l \cdot \Delta x \cdot (T_i - T_a) \\ &+ A_t \cdot \left[(\lambda + \lambda_i^{eq}) \cdot \frac{T_{i+1} - T_i}{\Delta x_i} - (\lambda + \lambda_{i-1}^{eq}) \frac{T_i - T_{i-1}}{\Delta x_{i-1}} \right]\end{aligned} \tag{4.7.3}$$

For element $i=j$

$$\begin{aligned}\frac{\partial}{\partial t}(V_i \cdot \rho \cdot C_p \cdot T_i) &= C_p \cdot \left[\dot{m}_c \cdot (T_c - T_{i-1}) - \dot{m}_t \cdot (T_i - T_{i-1}) \right] \\ &+ A_t \cdot \left[(\lambda + \lambda_i^{eq}) \cdot \frac{T_{i+1} - T_i}{\Delta x_i} - (\lambda + \lambda_{i-1}^{eq}) \frac{T_i - T_{i-1}}{\Delta x_{i-1}} \right] \\ &- U_l \cdot \Delta x \cdot (T_i - T_a)\end{aligned} \tag{4.7.4}$$

For element $i=1$

$$\frac{\partial}{\partial t}(V_i \cdot \rho \cdot C_p \cdot T_i) = C_p \cdot \dot{m}_t \cdot (T_{cold} - T_i) + A_t \cdot (\lambda + \lambda_i^{eq}) \cdot \frac{T_{i+1} - T_i}{\Delta x_i} - U_b \cdot (T_i - T_a) - U_l \cdot \Delta x \cdot (T_i - T_a) \quad (4.7.5)$$

for element $i=n$

$$\frac{\partial}{\partial t}(V_i \cdot \rho \cdot C_p \cdot T_i) = C_p \cdot \dot{m}_t \cdot (T_{i-1} - T_i) + A_t \cdot (\lambda + \lambda_i^{eq}) \cdot \frac{T_{i-1} - T_i}{\Delta x_i} - U_t \cdot (T_i - T_a) - U_l \cdot \Delta x \cdot (T_i - T_a) \quad (4.7.6)$$

Where	V_i	volume of tank segment number *i*	m^3
	ρ	density of water	kg/m^3
	C_p	thermal capacity of water	J/kg K
	$\dot{m}_t$	tapping mass flow rate	kg/s
	A_t	cross section area of the tank	m^2
	λ	thermal conductivity of water	W/mK
	U_l	heat loss coefficient of tank side wall	W/m K
	U_b	heat loss coefficient of tank bottom wall	W/ K
	U_t	heat loss coefficient of tank top wall	W/ K

Operation period with ($\dot{m}_t < \dot{m}_c$)

For normal operation periods without major tapping, the flow to the collector might be the dominant stream. The tank model can then be presented by the following differential equations:

For elements $1<i<j$

$$\frac{\partial}{\partial t}(V_i \cdot \rho \cdot C_p \cdot T_i) = (\dot{m}_c - \dot{m}_t) \cdot C_p \cdot (T_{i+1} - T_i) - U_l \cdot dx \cdot (T_i - T_a) + A_t \cdot \left[(\lambda + \lambda_i^{eq}) \cdot \frac{T_{i+1} - T_i}{dx_i} - (\lambda + \lambda_{i-1}^{eq}) \frac{T_i - T_{i-1}}{dx_{i-1}} \right] \quad (4.7.7)$$

For elements $n>i>j$

$$\frac{\partial}{\partial t}(V_i \cdot \rho \cdot C_p \cdot T_i) = \dot{m}_t \cdot C_p \cdot (T_{i-1} - T_i) - U_l \cdot \Delta x \cdot (T_i - T_a) + A_t \cdot \left[(\lambda + \lambda_i^{eq}) \cdot \frac{T_{i+1} - T_i}{\Delta x_i} - (\lambda + \lambda_{i-1}^{eq}) \frac{T_i - T_{i-1}}{\Delta x_{i-1}} \right] \quad (4.7.8)$$

For element $i=j$

$$\frac{\partial}{\partial t}(V_i \cdot \rho \cdot C_p \cdot T_i) = C_p \cdot \dot{m}_c \cdot (T_c - T_i) + A_t \cdot \left[(\lambda + \lambda_i^{eq}) \cdot \frac{T_{i+1} - T_i}{\Delta x_i} - (\lambda + \lambda_{i-1}^{eq}) \frac{T_i - T_{i-1}}{\Delta x_{i-1}} \right] - U_l \Delta x \cdot (T_i - T_a) \quad (4.7.9)$$

For element $i=1$

$$\frac{\partial}{\partial t}(V_i \cdot \rho \cdot C_p \cdot T_i) = C_p \cdot \left[\dot{m}_c \cdot (T_{i+1} - T_i) + \dot{m}_t \cdot (T_{cold} - T_{i+1}) \right] + A_t \cdot (\lambda + \lambda_i^{eq}) \cdot \frac{T_{i+1} - T_i}{\Delta x_i} - U_b \cdot (T_i - T_a) - U_l \cdot \Delta x \cdot (T_i - T_a) \quad (4.7.10)$$

for element $i=n$

$$\frac{\partial}{\partial t}(V_i \cdot \rho \cdot C_p \cdot T_i) = C_p \cdot \dot{m}_t \cdot (T_{i-1} - T_i) + A_t \cdot (\lambda + \lambda_i^{eq}) \cdot \frac{T_{i-1} - T_i}{\Delta x_i} - U_t \cdot (T_i - T_a) - U_l \cdot \Delta x \cdot (T_i - T_a) \quad (4.7.11)$$

The heat loss from the tank can be calculated in the same way as the drain-back tank, presented in 4.4.2. The thermal conduction in the side wall of the tank is ignored in this model.

4.8 Storage tank with heat exchanger spiral

The majority of solar DHW systems installed in single-family houses in Denmark are systems with a combi tank. The water in the storage tank can be heated both by solar energy and by an auxiliary energy supply system whenever the solar energy is not sufficient for the energy

demand. Typically, for this kind of storage tank, there is a heat exchanger situated in the bottom part, normally of the spiral type, to transfer the solar heat. In the upper part of the tank, there is an auxiliary heating element to keep the top water at a certain temperature level. Figure 4.4 shows the sketch of a combi tank with heat exchanger spiral and auxiliary heating element.

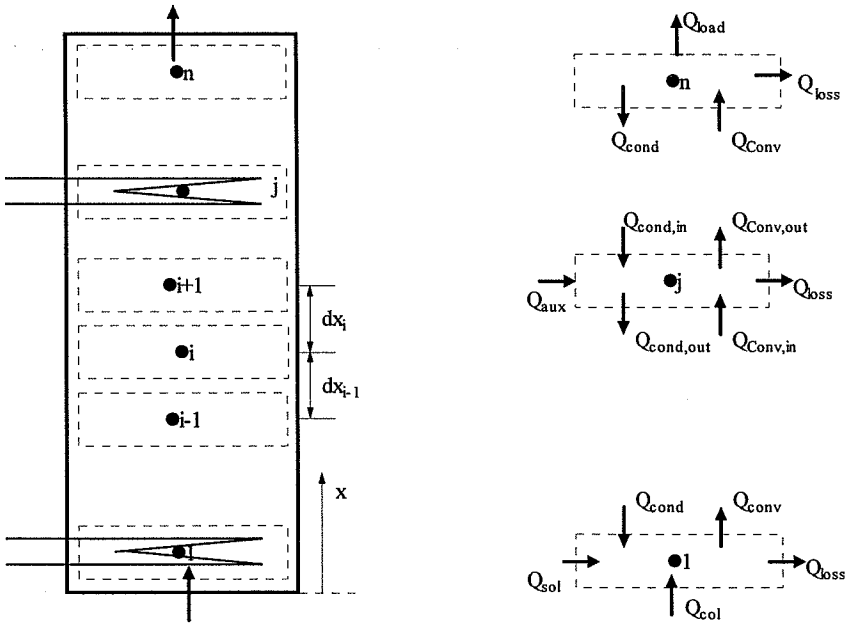

Figure 4.4 Sketch of a storage tank with heat exchanger spiral and auxiliary heating element.

Previous work about modeling of hot water tanks with heat exchanger spiral can be found in the literature, see Furbo [20], Duffie [17], Dutre [18], and Yang [64]. In this study, the dynamic model of the tank with heat exchanger spiral is based on the previous work of [20].

The mathematical model of the tank is represented by a stratified model with n segments with equal lengths in the vertical direction. Along the tapping flow direction x, the tank is then divided into n segments and uniform temperature is assumed in each of these segments. The model accounts for internal heat conduction between adjacent layers as well as for internal natural convection whenever an internal reversed temperature gradient occurs. A detailed description of the model can be found in [20].

4.9 Mantle tank with drain-back design

During the last decade, the temperature stratification in hot water storage tanks has been extensively studied. Results have shown that promoting thermal stratification in the storage tank improves the system performance considerably. Recently, researchers have found that mantle tanks based on low-flow conditions may result in a good stratification in the tank water and in a high thermal performance [23,55].

Basically, a mantle tank is an enlarged vertical contra flow two-stream heat exchanger. The heat transport medium from the collector enters the top of the mantle and returns from the

bottom to the collector. By means of conduction and natural convection, the heat is transferred to the tank water.

For the drain-back system design, mantle tanks make it possible to integrate the drain-back tank in the mantle, and therefore eliminate the additional drain-back tank in the collector loop. Basically a mantle tank with drain-back design is similar to the mantle tank in a normal system. However, since the mantle also functions as a drain-back tank, during the operation some of the working fluid in the mantle will be drawn to the collector and the top part of the mantle will be filled up with air. This phenomenon makes the thermal process in a drain-back mantle tank somewhat different from the one in a normal system. To analyse the mantle tank in this drain-back operation condition, it is necessary to have a detailed mathematical model.

The dynamic model of the mantle tank with normal operation design have been proposed by Berg[6]. During the periods with the collector loop not in operation, the mantle tank in a drain-back system works in the same manner as the one in a normal system. Therefore, the drain-back mantle tank model presented here only concerns the operation conditions. Figure 4.5 shows the sketch of the computer model of a drain-back mantle tank.

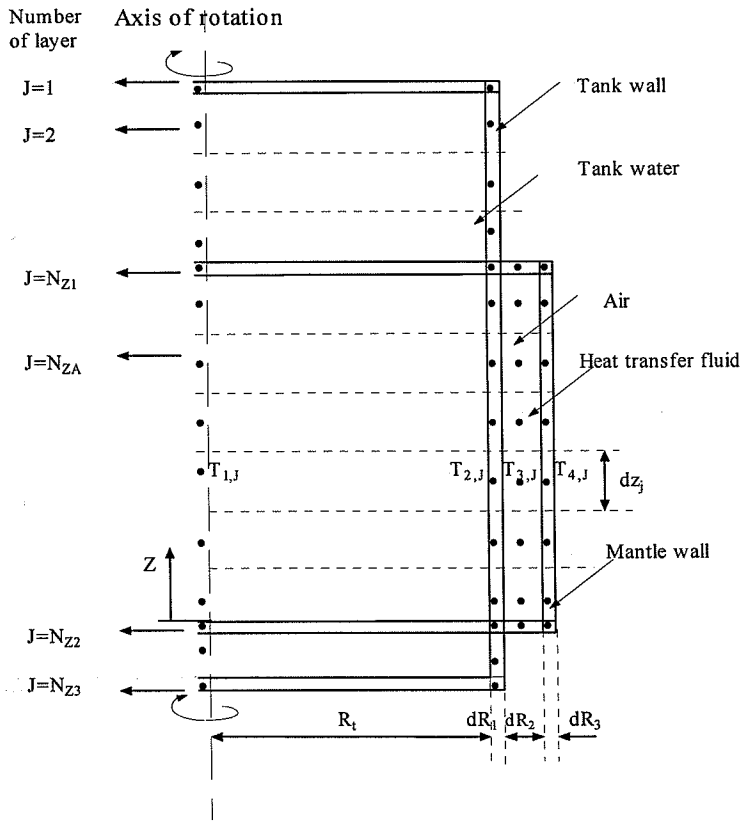

Figure 4.5 Sketch of a mantle tank model

4.9.1 The mathematical model

In cylindrical coordinates, the heat transfer in a mantle tank is a two-dimensional, non-steady process combined by convection and conduction. To determine the temperature profile, it is assumed that the tank is constructed with N_{Z3} segments along the vertical direction. Each of the segments j can be divided into 4 sections according to the possible temperature gradient. Therefore, one gets maximum $4\times N_{Z3}$ elements and it is assume that each element $n_{i,j}$ has an approximately uniform temperature. Here, N_{Z1} and N_{Z2} are the segment numbers of mantle top and bottom wall. N_{ZA} indicates the segment number of the bottom air layer in the mantle.

The energy balance of tank water and tank top and bottom wall in a drain-back mantle tank is the same as that in a normal mantle tank, and the detailed explanation can be found in [6]. Here, only the energy balance of the tank side wall and the air and fluid in the mantel are presented.

The energy balance of the side wall of the water tank *i=2*

The side wall of the water tank is partly covered by the mantle. The energy balance within the tank wall can be presented by the following differential equations:

For segments $1<j<N_{z1}$ and $N_{Z2}<j<N_{Z3}$

$$\begin{aligned} V_{2,j}\cdot C_{ps}\cdot \rho_s \cdot \frac{dT_{2,j}}{dt} &= 2\cdot R_t\cdot \pi\cdot dz_j\cdot h_{1,j}(T_{1,j}-T_{2,j}) \\ &-2\cdot(R_t+dR_1)\cdot\pi\cdot dz_j\cdot U_l\cdot(T_{2,j}-T_a) \\ &+(2\cdot R_t+dR_1)\cdot dR_1\cdot\pi\cdot\lambda_s\cdot\left[\frac{T_{2,j-1}-T_{2,j}}{(dz_{j-1}+dz_j)/2}-\frac{T_{2,j}-T_{2,j+1}}{(dz_j+dz_{j+1})/2}\right] \end{aligned} \qquad (4.9.1)$$

Where,	$V_{i,j}$	volume of element $n_{i,j}$	m^3
	$T_{i,j}$	temperature of element $n_{i,j}$	°C
	$h_{1,j}$	heat transfer coefficient between water and tank wall	W/m^2K
	R_t	inner radius of the water tank	m
	dz_j	the length of element j	m
	C_{ps}	thermal capacity of tank wall	J/kg K
	λ_s	thermal conductivity of tank wall	W/m K
	dR_1	thickness of tank wall	m
	U_l	heat loss coefficient of tank side wall	W/m K

For j=N_{Z1} and j=N_{Z2}

$$V_{2,j}\cdot C_{ps}\cdot \rho_s \cdot \frac{dT_{2,j}}{dt} = 2\cdot R_t \cdot \pi \cdot dz_j \cdot h_{1,j}(T_{1,j}-T_{2,j}) - \frac{4\cdot(R_t+dR_1)\cdot\pi\cdot dz_1\cdot\lambda_s}{dR_1+dR_2}\cdot(T_{2,j}-T_{3,j}) + (2\cdot R_t+dR_1)\cdot dR_1\cdot\pi\cdot\lambda_s\cdot\left[\frac{T_{2,j-1}-T_{2,j}}{(dz_{j-1}+dz_j)/2}-\frac{T_{2,j}-T_{2,j+1}}{(dz_j+dz_{j+1})/2}\right] \quad (4.9.2)$$

For $N_{z1+1}\geq j\leq N_{ZA}$

$$V_{2,j}\cdot C_{ps}\cdot \rho_s \cdot \frac{dT_{2,j}}{dt} = -2\cdot R_t \cdot \pi \cdot dz_j \cdot h_{1,j}(T_{2,j}-T_{1,j}) + 2\cdot(R_t+dR_1)\cdot\pi\cdot dz_j\cdot h_{a,j}\cdot(T_{3,j}-T_{2,j}) + (2\cdot R_t+dR_1)\cdot dR_1\cdot\pi\cdot\lambda_s\cdot\left[\frac{T_{2,j-1}-T_{2,j}}{(dz_{j-1}+dz_j)/2}-\frac{T_{2,j}-T_{2,j+1}}{(dz_j+dz_{j+1})/2}\right] \quad (4.9.3)$$

For $N_{ZA+1}<j<N_{Z2-1}$

$$V_{2,j}\cdot C_{ps}\cdot \rho_s \cdot \frac{dT_{2,j}}{dt} = -2\cdot R_t \cdot \pi \cdot dz_j \cdot h_{1,j}(T_{2,j}-T_{1,j}) + 2\cdot(R_t+dR_1)\cdot\pi\cdot dz_j\cdot h_{2,j}\cdot(T_{3,j}-T_{2,j}) + (2\cdot R_t+dR_1)\cdot dR_1\cdot\pi\cdot\lambda_s\cdot\left[\frac{T_{2,j-1}-T_{2,j}}{(dz_{j-1}+dz_j)/2}-\frac{T_{2,j}-T_{2,j+1}}{(dz_j+dz_{j+1})/2}\right] \quad (4.9.4)$$

Where, $h_{1,j}$	heat transfer coefficient between tank wall to tank water	W/m^2K
$h_{2,j}$	heat transfer coefficient between mantle fluid to tank wall	W/m^2K
$h_{a,j}$	heat transfer coefficient between air in the mantle to tank wall	W/m^2K

Air and fluid in the mantle *i=3*

Modeling the fluid in the mantle is based on the assumption of plug flow from the upper part down to the bottom of the mantle. The calculation time step is set up in such a way that in each time step the flow shifts the position of all fluid elements one segment downwards. At

the end of each time step, the fluid temperature in the mantle is scanned from top to bottom and the inlet fluid finds its way to the right segment matching the density of the fluid.

When the collector loop is in operation, the mantle is filled up both by air and working fluid. During the starting period, the air layer number N_{ZA} is increasing with the time until the collector is filled up and N_{ZA} maintains the same during the normal operation time. As the operation stops, the air layer number N_{ZA} will decrease with time until the fluid in the collector all drains back to the mantle.

The energy balance for the air and fluid in the mantle can be presented by the following equations:

For air gap element $j=N_{Z1+1}$

$$\begin{aligned} V_{3,j}\cdot C_{pa}\cdot \rho_a \cdot \frac{dT_{3,j}}{dt} &= 2\cdot(R_t+dR_1)\cdot\pi\cdot dz_j\cdot h_{a,j}(T_{2,j}-T_{3,j}) \\ &\quad -2\cdot(R_t+dR_1+dR_2)\cdot\pi\cdot dz_j\cdot h_{a,j}\cdot(T_{3,j}-T_{4,j}) \\ &\quad -(2\cdot R_t+2dR_1+dR_2)\cdot dR_2\cdot\pi \\ &\quad \cdot\left[h_{mt}\cdot(T_{3,j}-T_{3,j-1})+\lambda_a\cdot\frac{T_{3,j}-T_{3,j+1}}{(dz_j+dz_{j+1})/2}\right] \end{aligned} \tag{4.9.5}$$

For $N_{Z1+1}<j<N_{ZA}$

$$\begin{aligned} V_{3,j}\cdot C_{pa}\cdot \rho_a \cdot \frac{dT_{3,j}}{dt} &= 2\cdot(R_t+dR_1)\cdot\pi\cdot dz_j\cdot h_{a,j}(T_{2,j}-T_{3,j}) \\ &\quad -2\cdot(R_t+dR_1+dR_2)\cdot\pi\cdot dz_j\cdot h_{a,j}\cdot(T_{3,j}-T_{4,j}) \\ &\quad -(2\cdot R_t+2dR_1+dR_2)\cdot dR_2\cdot\pi\cdot\lambda_a\cdot\left[\frac{T_{3,j}-T_{3,j-1}}{(dz_{j-1}+dz_j)/2}\right. \\ &\quad \left.+\frac{T_{3,j}-T_{3,j+1}}{(dz_j+dz_{j+1})/2}\right] \end{aligned} \tag{4.9.6}$$

For j=N_{ZA}

$$V_{3,j}\cdot C_{pa}\cdot \rho_a \cdot \frac{dT_{3,j}}{dt} = 2\cdot(R_t + dR_1)\cdot\pi\cdot dz_j \cdot h_{a,j}(T_{2,j} - T_{3,j}) - 2\cdot(R_t + dR_1 + dR_2)\cdot\pi\cdot dz_j \cdot h_{a,j}\cdot(T_{3,j} - T_{4,j}) - (2\cdot R_t + 2dR_1 + dR_2)\cdot dR_2\cdot\pi\cdot\left[h_{ma}\cdot(T_{3,j} - T_{3,j+1}) + \lambda_a \cdot \frac{T_{3,j} - T_{3,j-1}}{(dz_{j-1} + dz_j)/2}\right] \quad (4.9.7)$$

For the element of mantle fluid $N_{ZA+1} < j < N_{Z2-1}$

$$V_{3,j}\cdot C_{pf}\cdot \rho_f \cdot \frac{dT_{3,j}}{dt} = -2\cdot(R_t + dR_1)\cdot\pi\cdot dz_j \cdot h_{2,j}(T_{3,j} - T_{2,j}) - 2\cdot(R_t + dR_1 + dR_2)\cdot\pi\cdot dz_j \cdot h_{3,j}\cdot(T_{3,j} - T_{4,j}) + (2\cdot R_t + 2dR_1 + dR_2)\cdot dR_2\cdot\pi\cdot\lambda_f \cdot\left[\frac{T_{3,j-1} - T_{3,j}}{(dz_{j-1} + dz_j)/2} - \frac{T_{3,j} - T_{3,j+1}}{(dz_j + dz_{j+1})/2}\right] \quad (4.9.8)$$

For $j=N_{ZA+1}$

$$V_{3,j}\cdot C_{pf}\cdot \rho_f \cdot \frac{dT_{3,j}}{dt} = -2\cdot(R_t + dR_1)\cdot\pi\cdot dz_j \cdot h_{2,j}(T_{3,j} - T_{2,j}) - 2\cdot(R_t + dR_1 + dR_2)\cdot\pi\cdot dz_j \cdot h_{3,j}\cdot(T_{3,j} - T_{4,j}) + (2\cdot R_t + 2dR_1 + dR_2)\cdot dR_2\cdot\pi\cdot\left[h_{ma}\cdot(T_{3,j-1} - T_{3,j}) - \lambda_f \cdot \frac{T_{3,j} - T_{3,j+1}}{(dz_j + dz_{j+1})/2}\right] \quad (4.9.9)$$

For $j=N_{Z2-1}$

$$\begin{aligned} V_{3,j}\cdot C_{pf}\cdot \rho_f \cdot \frac{dT_{3,j}}{dt} &= -2\cdot(R_t+dR_1)\cdot\pi\cdot dz_j\cdot h_{2,j}(T_{3,j}-T_{2,j}) \\ &\quad -2\cdot(R_t+dR_1+dR_2)\cdot\pi\cdot dz_j\cdot h_{3,j}\cdot(T_{3,j}-T_{4,j}) \\ &\quad +(2\cdot R_t+2dR_1+dR_2)\cdot dR_2\cdot\pi\cdot\left[\lambda_f\cdot\frac{T_{3,j-1}-T_{3,j}}{(dz_{j-1}+dz_j)/2}\right. \\ &\quad \left.-h_{mb}\cdot(T_{3,j}-T_{3,j+1})\right] \end{aligned} \tag{4.9.10}$$

Mantle wall i=4

Similar to the tank side wall without being covered by the mantle, the energy balance in the side wall of mantle can be presented as:

$$\begin{aligned} V_{4,j}\cdot C_{ps}\cdot \rho_s \cdot \frac{dT_{4,j}}{dt} &= 2\cdot(R_t+dR_1+dR_2)\cdot\pi\cdot dz_j\cdot h_{3,j}(T_{3,j}-T_{4,j}) \\ &\quad -2\cdot(R_t+dR_1++dR_2+dR_3)\cdot\pi\cdot dz_j\cdot U_{lm}\cdot(T_{4,j}-T_a) \\ &\quad +2\cdot dR_3\cdot\pi\cdot\lambda_s\cdot(R_t+dR_1+dR_2+0.5dR_3)\cdot \\ &\quad \left[\frac{T_{4,j-1}-T_{4,j}}{(dz_{j-1}+dz_j)/2}-\frac{T_{4,j}-T_{4,j+1}}{(dz_j+dz_{j+1})/2}\right] \end{aligned} \tag{4.9.11}$$

Here,

U_{lm}	the heat loss coefficient from side wall of mantel	W/m^2K
h_{mt}	heat transfer coefficient between mantle top wall and the air in the mantle	W/m^2K
h_{mb}	heat transfer coefficient between mantle bottom wall and the fluid	W/m^2K
h_{ma}	heat transfer coefficient between the air and fluid in the mantle	W/m^2K

4.9.2 Heat transfer coefficient

A mathematics model, describing the heat transfer coefficients in the mantle fluid, has been proposed by Shah (1996)[55]. The model is built up based on natural convection at a vertical wall and the following assumptions.

- the dominant flow is natural buoyancy driven flow
- the flow along the two inner sides of the mantle can be treated as external flow
- the thermal and dynamic boundary layers are set to be equal

These assumptions are normally valid only for small Prandtl-numbers. By using this model, the convective heat transfer coefficient can be described as:

$$h(z,T)=\frac{2\cdot\lambda_f}{E\cdot z^{1/4}} \tag{4.9.12}$$

where $$E=3.94\left[\frac{(20/21)\alpha_1^2+\upsilon\cdot\alpha_1}{g\cdot\beta\cdot(T_w-T_f)}\right]^{1/4}$$

Here,	z	the local height in mantle (from bottom of mantle)	m
	α_1	thermal diffusive	m^2/s
	ν	kinematic viscosity	m/s^2
	g	gravitational constant	m/s^2
	β	expansion coefficient	1/K
	T_w	wall surface temperature	°C
	T_f	fluid temperature	°C

Therefore, the heat transfer coefficient applied in the mantle $h_{2,j}$ and $h_{3,j}$ can be calculated by:

$$h_{2,j}=\frac{\lambda_f}{1.97}\cdot\left[\frac{g\cdot\beta\cdot(T_{3,j}-T_{2,j})}{((20/21)\cdot\alpha_1{}^2+\upsilon\cdot\alpha_1)\cdot z_j}\right]^{\frac{1}{4}} \tag{4.9.13}$$

$$h_{3,j}=\frac{\lambda_f}{1.97}\cdot\left[\frac{g\cdot\beta\cdot(T_{3,j}-T_{4,j})}{((20/21)\cdot\alpha_1{}^2+\upsilon\cdot\alpha_1)\cdot z_j}\right]^{\frac{1}{4}} \tag{4.9.14}$$

The heat transfer in the air gap in the top part of the mantle is combined with conduction and natural convection. To investigate the heat transfer coefficient, the air gap can be considered as a vertical enclosure. According to Mills [46], the convective heat transfer coefficient in the air gap can be calculated by:

$$h_a=\frac{\lambda_a}{dR_2}\overline{Nu} \tag{4.9.15}$$

$$\overline{Nu}=0.22\left(\frac{\mathrm{Pr}_a}{0.2+\mathrm{Pr}_a}\cdot Ra\right)^{0.28}\left(\frac{H_a}{dR_2}\right)^{-\frac{1}{4}} \qquad \text{if } 2<H_a/dR_2<10 \tag{4.9.16}$$

$$\overline{Nu}=\max\{Nu_1,Nu_2,Nu_3\} \qquad \text{if } H_a/dR_2>10 \tag{4.9.17}$$

$$Nu_1 = 0.0605 Ra^{1/3}$$

Where $$Nu_2 = \left\{1 + \left[\frac{0.104 Ra^{0.293}}{1 + (6310/Ra)^{1.36}}\right]^3\right\}^{1/3}$$

$$Nu_3 = 0.242\left(\frac{Ra}{H_a/dR_2}\right)$$

Here $$H_a = \sum_{j=N_{Z1+1}}^{N_{ZA}} dz_j \qquad (4.9.18)$$

Where, H_a the total height of air gap in the mantle m
dR_2 the thickness of mantle m
Pr_a Prandtl number of air
Ra Reyleigh number

Calculation example

Assumptions: The mantle thickness of the tank is 0.018 m, and the air gap in the top part of the mantle is 0.2 m high. We assume a temperature difference between tank wall and mantle wall of ΔT=10 K, and the mean temperature of the air is 40 °C. Then the thermal properties of the air can be found: λ=0.0281 W/mK, ν=17.44*10^{-6} m^2/s, Pr=0.69, ρ= 1.106 kg/m^3 and β=1/300 K^{-1}. The Rayleigh number can be calculated as:

$$Ra = Gr \cdot \mathrm{Pr} = \frac{\beta \cdot \Delta T \cdot g \cdot dR_2^3 \cdot \mathrm{Pr}}{\nu^2} = 4326.34$$

Since $H_a/dR_2 = 11$, Equation 4.9.17 applies:

$$Nu_1 = 0.9858, \qquad Nu_2 = 1.03, \qquad Nu_3 = 1.229$$

$$\overline{Nu} = \max\{0.9858,\ 1.03,\ 1.229\} = 1.229$$

$$h_a = \frac{\lambda_a}{dR_2}\overline{Nu} = \frac{0.0281 \times 1.229}{0.018} = 1.918 \text{ W/m}^2\text{K}$$

Therefore, under assumed conditions, the heat transfer coefficient in the air gap on top of the mantle is 1.918 W/m^{2}K.

The heat transfer coefficients between the fluid and tank wall are determined from the experiment results and a further improvement of the model is necessary. To set up an accurate mathematical model for the simulation of thermal behavior of mantle tanks, an ongoing project is carried out by Shah, L.J. at the Department of Buildings and Energy, Technical University of Denmark.

4.10 Controller

Except for the thermosyphon systems, the circulation flow in the collector loop of all solar DHW systems is on-off controlled by series combination of a differential thermostat and a safety thermostat. The high temperature sensor of the differential thermostat is located in the collector or the collector outlet and the low temperature sensor is normally located in the bottom layer of the storage tank. For the system with mantle tank, the low temperature sensor is situated in the bottom layer of the mantle.

In the Combi tank system, the auxiliary energy supply unit is also on-off controlled by using definable thermostats to keep the tank outlet temperature at a certain temperature level. The sensor of such thermostats is usually located in a layer in the upper part of the tank.

The mathematical description of the on-off controller in this section is based on [18].

4.10.1 Mathematical description

Differential thermostat

The input signal of the differential thermostat is the temperature difference of its high and low temperature sensors. For a solar DHW system, it is normally the temperature difference between the collector outlet and the tank bottom.

$$\Delta T = T_c - T_s$$

The controller is characterized by its starting and stopping temperature difference ΔT_{start} and ΔT_{stop} both are defined by the designer. The switching characteristic is shown in the figure 4.6.

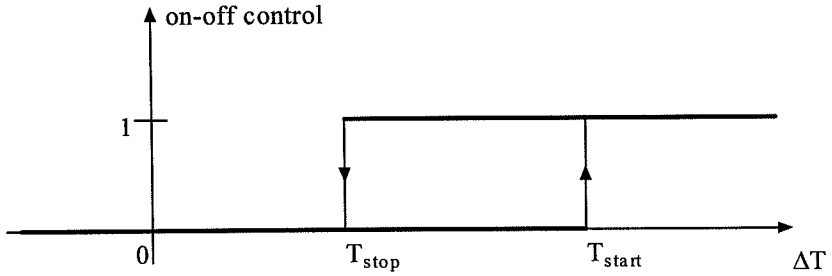

Figure 4.6 Switching characteristic of a differential thermostat.

Definable thermostats

The input signal of a definable thermostat is the sensor temperature in the upper part of tank T_{ts}. The controller is characterized by its temperature setting T_{hot}. The switching characteristic is shown in the figure 4.7.

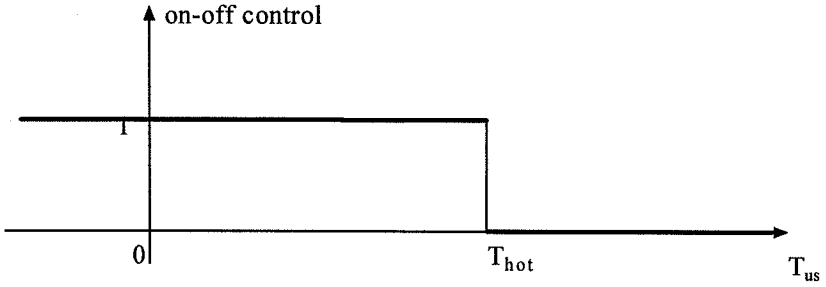

Figure 4.7 Switching characteristic of a definable thermostat.

4.11 Discussion

Dynamic models of components used in solar DHW systems have been presented in this chapter. These models can be used either in the performance investigation of single components or in the simulation and evaluation of whole systems. The dynamic models of drain-back tank (both as a separate tank and integrated with a mantle tank) were developed in this study. Other models which have been described here are based on the previous works.

The component models are generally expressed in number of differential equations. The numerical methods to solve these equations will be described in the sections of system simulation.

Chapter 5

Dynamic modeling and simulation of thermosyphon solar DHW systems

5.1 Introduction

The thermosyphon solar DHW system is one of the earliest systems designed for domestic water heating by solar energy. This type of system has gained popularity in many parts of the world, such as Eastern Asia, the Middle East, and Australia, because of its simplicity and its good economy compared with conventional methods of water heating. According to a report from the "1996 Chinese National Solar Thermal Application Conference", only in 1996 the total collector area of solar DHW systems that was installed in China amounted to about 2.0 million m^2. Thermosyphon systems make up a major portion of the total installations. However, the design of these systems is often based on limited experimental results and experience because of the complexity of the system operation.

In order to have a better understanding of the influence of the design parameters on the system performance, it is necessary to develop system simulation models. From series simulations it will be possible to make general recommendations on the optimum design of this type of systems.

Unlike other types of solar DHW systems, the operation of a thermosyphon system depends on a large number of design and weather parameters. The flow in the collector loop is essentially controlled and adjusted by the temperature distribution. This intrinsic self-control operation characteristic leads to the fact that the thermosyphon systems operate under an unsteady state flow condition which further complicates the analysis of thermosyphon systems.

For many decades, both experimental and theoretical research work have been carried out to improve such systems. Vaxman and Sokolv [62] have studied the influence of pipe insulation and height difference between the collector and the tank's bottom in a thermosyphon system. Shariah [58] presented the effect of most design parameters and operating strategies on the system performance for a thermosyphon system with combi tank. So far, many theoretical models [3, 43, 47, 49, 58, 62] with different complexity and precision have been introduced. To simplify the complexity, some treating techniques, which limited the application and accuracy, are commonly used in these models. Therefore, it is necessary to perform a further study on these models and carry out a comprehensive study for thermosyphon solar water systems.

In chapter 4, the component models of solar DHW systems have been described. Here only a thermosyphon loop model is presented. In order to apply the dynamic model as a tool for system design and analysis, the modular simulation program SOLSIM [52] was employed.

System simulations of thermosyphon systems are carried out under both Beijing and Danish weather conditions. The evaluation of how the design parameters and heat load affect the solar fraction is performed.

5.2 Configuration of thermosyphon systems

In the course of time, a number of different designs of thermosyphon systems have been developed all over the world. But basically, thermosyphon systems can be classified into two types according to the thermosyphon loop construction. They are the systems with collector loop connected with a heat exchanger spiral in the storage tank, and systems with the collector loop directly connected with the storage tank. Figure 5.1 shows the sketches of the typical design of these two types of systems.

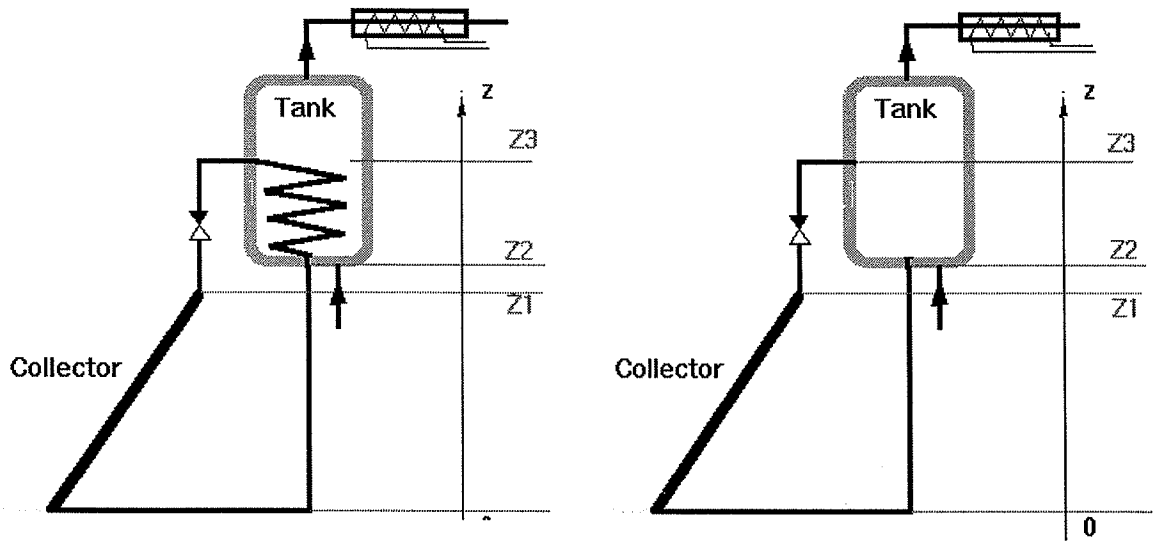

(a) (b)

Figure 5.1 Sketch of thermosyphon solar water heating systems.
(a) system with collector loop connected with heat exchanger spiral.
(b) system with collector loop directly connected with storage tank.

Figure 5.1(a) shows a thermosyphon system with the collector loop connected to a heat exchanger spiral in the tank. The basic working principle of this kind of systems is that whenever solar radiation adds energy on the collector, the heat transfer medium in the collector will be heated up and a density difference which causes the natural circulation flow

in the loop is established. By this natural circulation flow, the heat produced in the collector is transferred to the storage tank via a heat exchanger.

A thermosyphon system with collector loop directly connected with the storage tank is shown in Figure 5.1(b). In this type of system, the storage tank becomes part of the thermosyphon loop. When solar radiation which is absorbed in the collector heats up the water present in the collector tubes, this water becomes less dense than the cold water in the tank and thus rises to the highest point in the assembly, the top of the storage tank. At the same time, the cold water from the bottom of the tank flows into the collector and is in turn being heated. This process is repeated continuously, forming what is termed a thermosyphon water circulation pattern.

Since the flow in the collector loop is controlled by the density difference, the reverse flow may also happen during the night when the temperature of the collector and the riser pipe is lower than the temperature of the tank water. To avoid heat loss from the storage tank, a check valve is used in the system to prevent reverse flow.

The systems with the collector loop directly connected with a storage tank are most commonly used in developing countries such as China, India and Egypt, and the number of such systems in these countries makes up a major part of the world total. Therefore, thermosyphon systems with the collector loop directly connected to the storage tank was chosen for this study.

5.3 Thermosyphon loop model

The thermosyphon loop in a thermosyphon system generally consists of the collector array, a riser pipe, a storage tank (or internal heat exchanger for the system with built-in heat exchanger tank) and a downward pipe back to the collector inlet. The flow in the collector is controlled by the temperature distribution in each of the components in the loop. The flow rate is normally estimated by assuming instantaneously stable flow under the thermosyphon head.

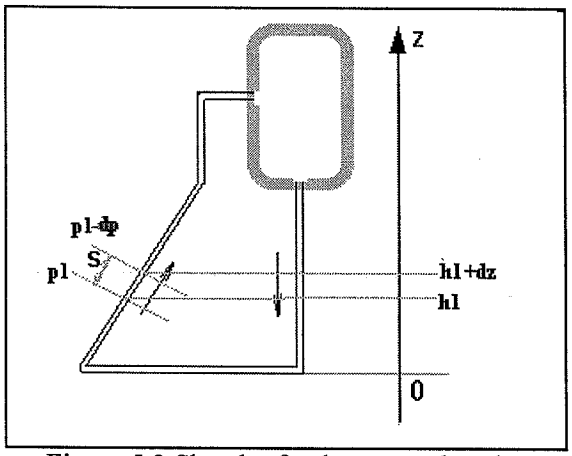

Figure 5.2 Sketch of a thermosyphon loop.

To simplify the calculation, the following assumptions are made:

- The flow is one-dimensional in the thermosyphon collector loop and
- Fluid flow friction losses in the tank are negligible.

From Bernolli's equation, the pressure loss along a streamline with length s in the flow direction can be presented as:

$$dp = \rho(T) \cdot g \cdot dz + \int_0^s \rho(T) \cdot g \cdot dh_f \qquad (5.3.1)$$

Where	P	pressure	Pa
	ρ	density of water	kg/m^3
	g	gravitational constant	
	z	height	m
	s	streamline distance	m
	h_f	fraction head loss	m

By integrating the pressure drop around the collector loop, Equation 5.3.1 becomes:

$$\oint dp = \oint g \cdot \rho(T) \cdot dz + \oint g \cdot \rho(T) \cdot dh_f \qquad (5.3.2)$$

Because of the conservation of energy, the integrated pressure loss around any loop must be zero.

$$\oint dp = 0 \qquad (5.3.3)$$

The pressure change caused by gravity is the source of power for the thermosyphon flow. The hydrostatic pressure around the loop is found to be:

$$\begin{aligned} \oint g \cdot \rho(T) \cdot dz = & \int_{z_3}^{z_2} g \cdot \rho(T_s) \cdot dz + \int_{z_2}^{0} g \cdot \rho(T_{dp}) \cdot dz \\ & + \int_{0}^{z_1} g \cdot \rho(T_c) \cdot dz + \int_{z_1}^{z_3} g \cdot \rho(T_{rp}) \cdot dz \end{aligned} \qquad (5.3.4)$$

Where,	z_1	height of collector outlet	m
	z_2	height of tank bottom	m
	z_3	height of outlet of riser pipe to the tank	m
Subscripts:			
	s	storage tank	
	dp	down come pipe	
	rp	riser pipe	
	c	collector	

The pressure drop around a thermosyphon loop is the sum of the pressure drop caused by friction loss in each component, and the local head loss caused by the fittings. The effect of these fittings such as bends, tees and valves is taken into account by an overall head loss

coefficient ζ. Therefore, the pressure drop caused by the friction head loss around the loop can be presented as:

$$\oint g \cdot \rho(T) \cdot dh_f = \Delta P_c + \frac{\rho(T) \cdot V^2}{2}(f \cdot \frac{l}{d} + \zeta) \tag{5.3.5}$$

Where,

ΔP_c	pressure drop in collector	Pa
f	friction loss coefficient	
l	length of the connecting pipes	m
V	flow rate	m/s
d	inner diameter of the connecting pipe	m
ζ	overall head loss coefficient caused by fittings	

The pressure drop caused by the collector array depends on many design parameters, which makes the theoretical calculation rather complicated. In the previous models, the collector array was often replaced by an equivalent length of pipe. However, experiment results have shown that the pressure drop in a collector as a function of the mass flow rate is largely different from the pipe model. Therefore, it is necessary to have a more accurate model to determine the pressure change through the collector array. Here, a model for flat plate collector (and collector array), based on both experiment and theoretical analysis, is used.

$$\Delta P_c = a(\overline{T}_c) \cdot \dot{m}^{b(\overline{T}_c)} \tag{5.3.6}$$

Where, a and b are two coefficients of the pressure drop in the collector. They depend on the properties and temperature of the fluid and structure of the collector. $\overline{T}_c$ is the mean temperature of the collector.

Assuming laminar flow is the governing flow condition in the thermosyphon loop, the friction coefficient for the connecting pipe f can be written as 64/Re (where Re is the Reynolds number). By using the mass flow rate expression, Equation 5.3.5 can be written as:

$$\oint g \cdot \rho(T) \cdot dh_f = a(\overline{T}_c) \cdot \dot{m}^{b(\overline{T}_c)} + \frac{8 \cdot \zeta}{\pi^2 \cdot \rho(\overline{T}) \cdot d^4} \cdot m^2 + \frac{128 \cdot \dot{m}}{\pi \cdot d^4}\left[\frac{\mu(\overline{T}_{dp}) \cdot l_{dp}}{\rho(\overline{T}_{dp})} + \frac{\mu(\overline{T}_{rp}) \cdot l_{rp}}{\rho(\overline{T}_{rp})}\right] \tag{5.3.7}$$

Here, $\mu(pa.s)$ is the dynamic viscosity of the liquid in the collector loop, and $\overline{T}$ indicates the mean temperature.

Similarly, for the thermosyphon loop with heat exchanger spiral, the hydrostatic pressure around the loop and the total friction head loss can be found from the following equations:

$$\oint g \cdot \rho(T) \cdot dz = \int_{z_3}^{z_2} g \cdot \rho(T_{he}) \cdot dz + \int_{z_2}^{0} g \cdot \rho(T_{dp}) \cdot dz + \int_{0}^{z_1} g \cdot \rho(T_c) \cdot dz + \int_{z_1}^{z_3} g \cdot \rho(T_{rp}) \cdot dz \tag{5.3.8}$$

and

$$\oint g \cdot \rho(T) \cdot dh_f = a(\overline{T}_c) \cdot \dot{m}^{b(\overline{T}_c)} + \frac{8 \cdot \zeta}{\pi^2 \cdot \rho(\overline{T}) \cdot d^4} \cdot m^2 + \frac{128 \cdot \dot{m}}{\pi \cdot} \left[\frac{\mu(\overline{T}_{dp}) \cdot l_{dp}}{\rho(\overline{T}_{dp}) \cdot d^4} + \frac{\mu(\overline{T}_{rp}) \cdot l_{rp}}{\rho(\overline{T}_{rp}) \cdot d^4} + \frac{\mu(\overline{T}_{he}) \cdot l_{he}}{\rho(\overline{T}_{he}) \cdot d_{he}^4} \right] \tag{5.3.9}$$

Here, subscript *he* indicates the heat exchanger; d_{he} and l_{he} are its inner diameter and total length, respectively. From Equations 5.3.2 - 5.3.7, the flow rate in the thermosyphon loop direct connected with the tank can be estimated.

5.4 Simulation program

The basic simulation program which was used for the system simulation is SOLSIM, which is a modular structured computer program for the simulation of solar heating systems. The computer model of thermosyphon loop was developed and added into the program. The major work in this study is to develop a software model which may accurately simulate thermosyphon systems, and is suitable for use in the simulation program SOLSIM. The code is written in *Pascal* [66].

The thermosyphon solar DHW systems simulated by the SOLSIM program are constructed by a number of components models. In each time step, the mass flow rate in the collector loop is determined by the temperature distribution in the component of the loop (by Equation 5.3.2). To start the simulation, an initial guess for the flow rate and temperature distribution in the collector loop is needed. After the flow has been determined, the energy balance on each component is calculated explicitly.

5.5 System simulation and optimization of design parameters for themosyphon systems

Themosyphon systems with the collector loop directly connected with the preheating storage tank are widely used in many parts of the world. There is a common interest to have a comprehensive study on this type of systems. Based on the dynamic model described in Section 5.3, simulations are carried out to investigate the effect of the design parameters on the thermal performance of the system.

5.5.1 Location and weather specification

As mentioned in chapter 2, the weather conditions which may influence the operation of solar DHW systems are very different from place to place. Here, Beijing and Denmark are chosen as the locations for the reference systems. Therefore, Beijing TRY and Danish DRY were used as the input weather data. Since thermosyphon systems are rarely used in Denmark, the simulation under Danish conditions is mainly used for a comparison of the system operation under different weather conditions.

Since thermosyphon systems are inherently difficult to protect against freezing, the systems can only be operated in the season when no freezing can occur. In both Beijing and Denmark, the beginning of May to the end of September may be considered as a safe period for thermosyphon systems. Therefore, the simulations were carried out only for the period from 1st of May to 30th of September.

5.5.2 Basic operation conditions and assumptions

The tapping pattern used in the simulation is designed according to the Chinese custom and living style. The peak load only appears in the evening during 7 pm to 9 pm. In each day, a certain percentage of the daily total hot-water demand is tapped at 7 am (10%), 8 am (10%), 12 am (20%), 5 pm (10%), 7 pm (30%) and 8 pm (20%). Since no measurements about the hot water load condition in China are available, the commonly accepted standard value 40 *l*/day per person are employed.

The cold-water temperature is assumed to be 18°C under Beijing conditions and 12 °C under Danish conditions throughout the simulation period. This assumption is based on the measurement results of cold-water temperature during the year from these two areas.

5.5.3 Dimension of the reference system

The basic design of the reference system is chosen from the typical one-family-use systems which are commonly marketed in China. A simple schematic diagram of the system is shown in Fig. 5.1(b). The system consists of a flat-plate collector, a vertical storage tank and connecting pipes. A check valve was added to the system to prevent reverse flow. An auxiliary electric heating element is also required to heat the water whenever the temperature flowing from the tank is below the desired hot water temperature. The daily hot water (45°C) demand from the system is 120 *l*. The basic design parameters for the system are shown in Table 5.1.

Table 5.1 Design parameters for the reference system

Design parameters	Parameters	Unit
Collector		
Area	1.2	m^2
Efficiency model	$\eta=0.78-4.85(T_m-T_a)/G-0.016(T_m-T_a)^2/G$	
Heat capacity	7000	J/m^2K
Tilt angle	40	°
Number of fluid tubes	8	-
Diameter of the fluid tube	8	mm
Connection pipes		
Material	copper	
Inner diameter	16	mm
Outer diameter	18	mm
Heat capacity	1033	J/m K
Length of riser pipe	0.6	m
Length of downward pipe	1.5	m
Storage tank		
Volume	0.10	m^3
Diameter	0.40	m
Height	0.80	m
Thickness of the wall	2	mm
Heat loss coefficient	1.4	W/K

A collector with 8 copper-aluminum Sunstrip absorber strips is used in the reference system. A simulation of the flow and pressure drop in the collector was carried out by the FLOWSOL program which has been developed in the Danish Solar Energy Testing Laboratory. It was found that with an average temperature of 40°C, the pressure drop through the collector can be calculated by $\Delta P_c = 2.31\dot{m}^{1.11}$.

5.5.4 Simulation results

Based on groups of system simulations, the effects of design parameters on the system performance were investigated and the solar fraction is of major interest in this study.

Collector area

The match of the collector area to the storage capacity is one of the most basic design parameters. Fig.5.3 shows the solar fraction as a function of the solar collector area under both Danish and Beijing weather conditions. It is clear that the increase of collector area causes a considerable increase in the solar fraction. When the collector area changes from 0.6 m^2 to 2.1 m^2, the solar fraction increases from 0.45 to 0.87 under Beijing conditions, and from 0.35 to 0.71 under Danish conditions. It can also be seen that if the collector area is larger than 1.8 m^2, the increase of solar fraction becomes relatively small. Since the collector is the major cost of thermosyphon systems, in the practical design, the optimum value of collector area should also take the economy into account.

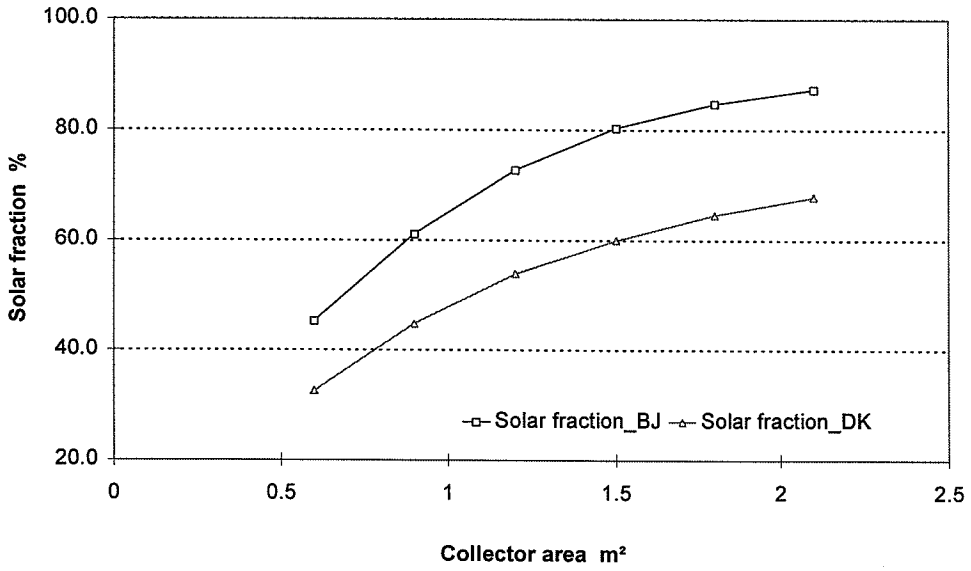

Figure 5.3 The solar fraction as a function of the collector area.

Collector tilt angle

It is known that the collector tilt angle has a direct influence on the total radiation on the collector panels. However, changing the tilt of the collector also has an impact on the heat loss coefficient of the collector [24]. To investigate the effect of the collector tilt on the solar fraction, the change of collector efficiency due to the variation of tilt angle should be taken into consideration. Based on the assumption of the temperature difference 40 K between solar collector and ambient temperature and the test result from [24], the maximum collector efficiency was corrected for different tilt angle. The variation of solar fraction with a collector tilt angle is shown in Fig.5.4. The maximum solar fraction was observed with collector tilt angle of 25° under Beijing conditions and 40° under Danish conditions. This different reaction of the system is mainly caused by the different geographic locations. However, it should be noted that collectors with 38° tilt in the Beijing area and 45° tilt in Denmark receive the greatest amounts of solar radiation over a one-year period. This result illustrates that the optimum angle of the system is dependent on the system location and the operation seasons.

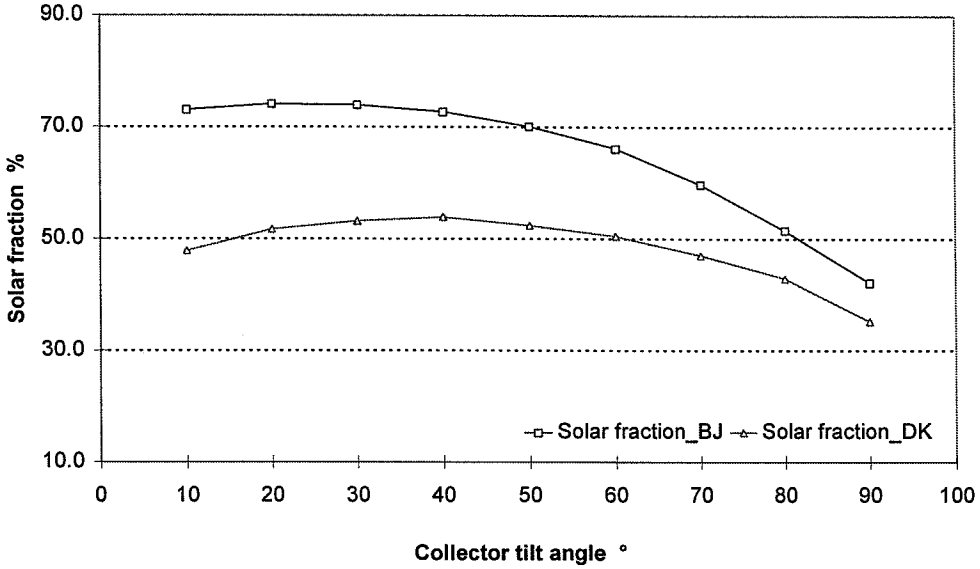

Figure 5.4 The solar fraction as a function of the collector tilt.

Collector efficiency

The effect of collector maximum efficiency on the solar fraction is shown in Fig.5.5. Obviously, as the efficiency of the collector increases, the solar fraction shows a corresponding increase.

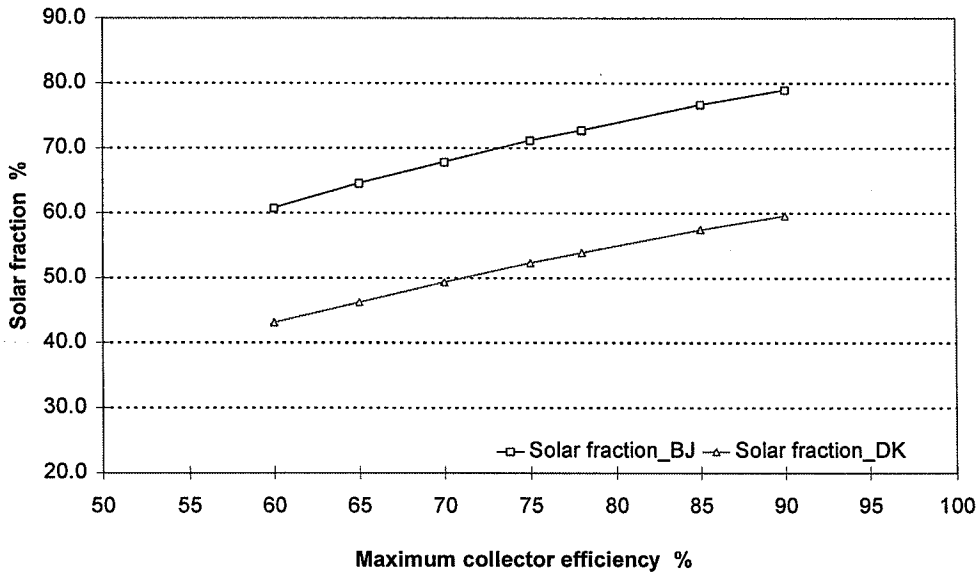

Figure 5.5 The solar fraction as a function of the maximum collector efficiency.

Collector heat loss coefficient

Figure 5.6 shows the effect of the collector heat loss coefficient on the solar fraction. As expected, the high heat loss coefficient results in a low solar fraction under both weather conditions. However, it can be seen that the decrease of solar fraction is faster under Danish conditions than under Beijing conditions. This is due to the fact that the average ambient temperature in Denmark during the simulation period is relatively low.

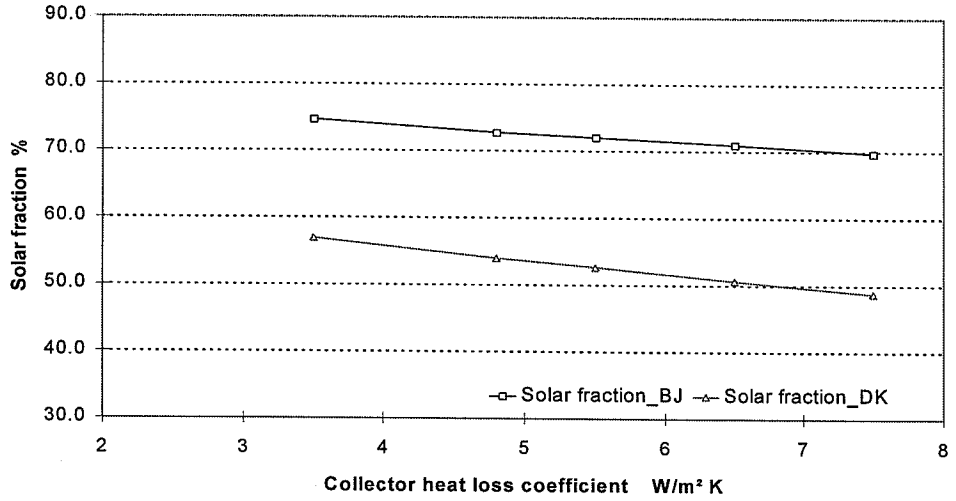

Figure5.6 The solar fraction as a function of the collector heat loss coefficient.

Hot water load

The predicted effect of the daily hot-water consumption on the solar fraction is shown in Fig.5.7. As the daily hot-water load increases, the solar fraction decreases rapidly. This is because with more hot-water load, more of the basic energy demand on hot water is needed.

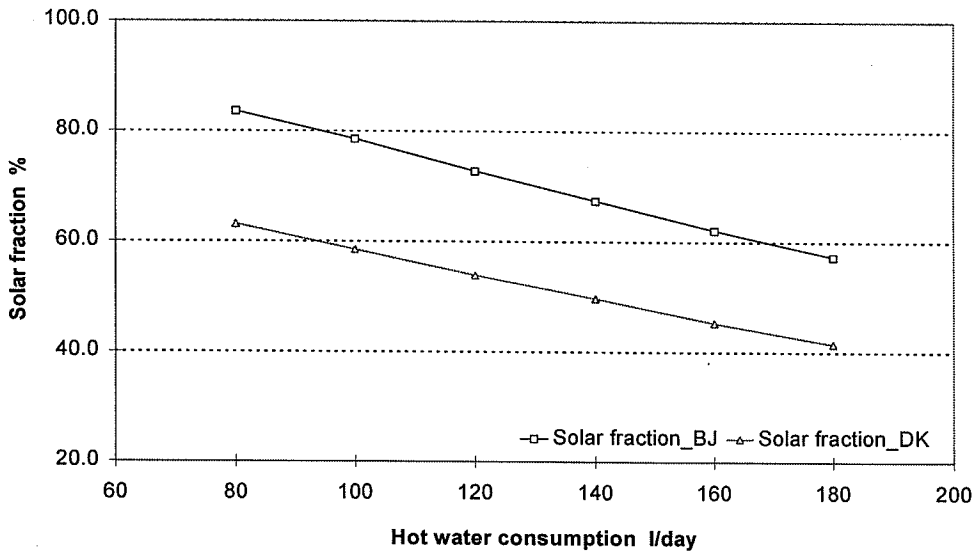

Figure 5.7 The solar fraction as a function of the hot-water load.

Diameter of the connecting pipes

As parts of the thermosyphon loop, connecting pipes have an important influence on the thermosyphon flow rate. Figure 5.8 shows the solar fraction as a function of the diameter of connecting pipes. Since the pipes are standardized, the variation of the pipe diameter is following the available sizes. It can be seen that the diameter of the connecting pipes should be larger than 15 mm. Similar results were reported by Shariah [58], but in the present simulation connection pipes with 8 mm diameter result in a relatively good performance compared to the result in [58]. This is mainly due to the fact that the connecting pipe in the reference system is relatively short and the peak loads only happen in the evening.

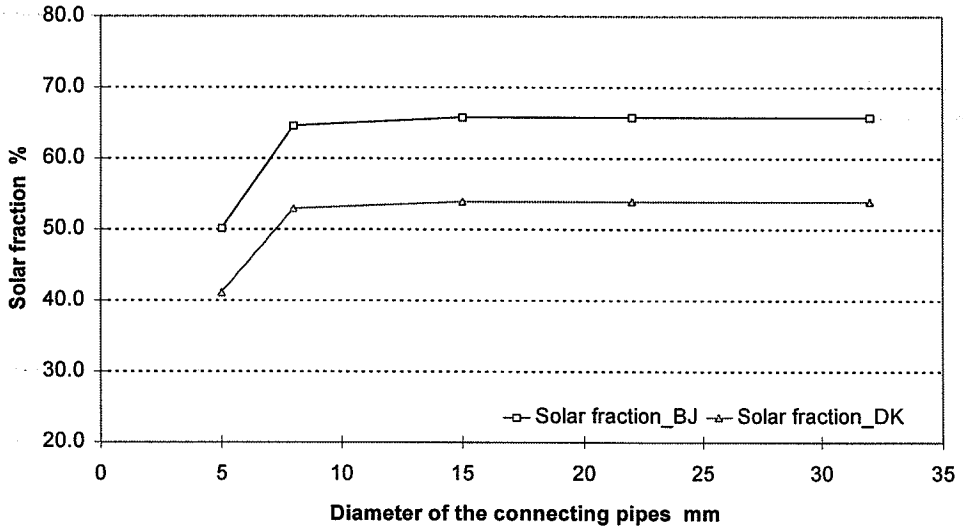

Figure 5.8 The solar fraction as a function of diameter of connecting pipes.

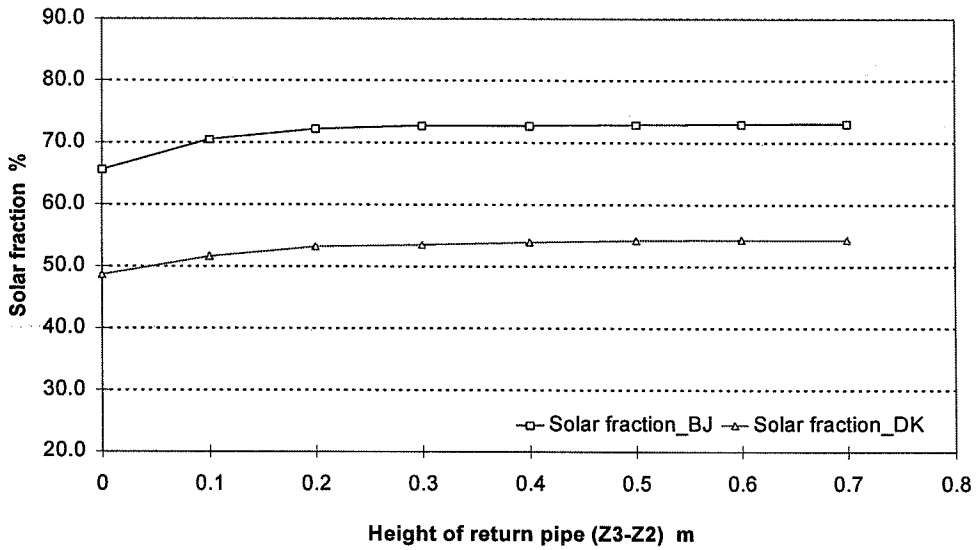

Figure 5.9 Solar fraction as a function of the height of the return pipe.

The height of the return pipe from the bottom of the tank

The effect of the height at which the return pipe from the collector enters the tank (z_3-z_2) on the solar fraction is shown in Fig. 5.9. The increase of the height of the return pipe starts from 0 and the solar fraction shows a corresponding increase at the beginning. The solar fraction is affected only very slightly when the height of the return pipe changes from 0.3 m to 0.7 m. Here it should be pointed out that the optimum height of the return pipe may also be influenced by the tank design.

The ratio of tank volume to daily hot water load

Figure 5.10 shows the solar fraction as a function of the ratio between the storage tank volume and the daily hot-water load volume. In the calculation, the volume of the tank is varied by changing the diameter of the tank. An increase in the ratio starting from 0.33 results in a rapid increase in the solar fraction. The maximum solar fraction is achieved when the ratio is between 0.85 and 1.0 and then a slight decrease is observed.

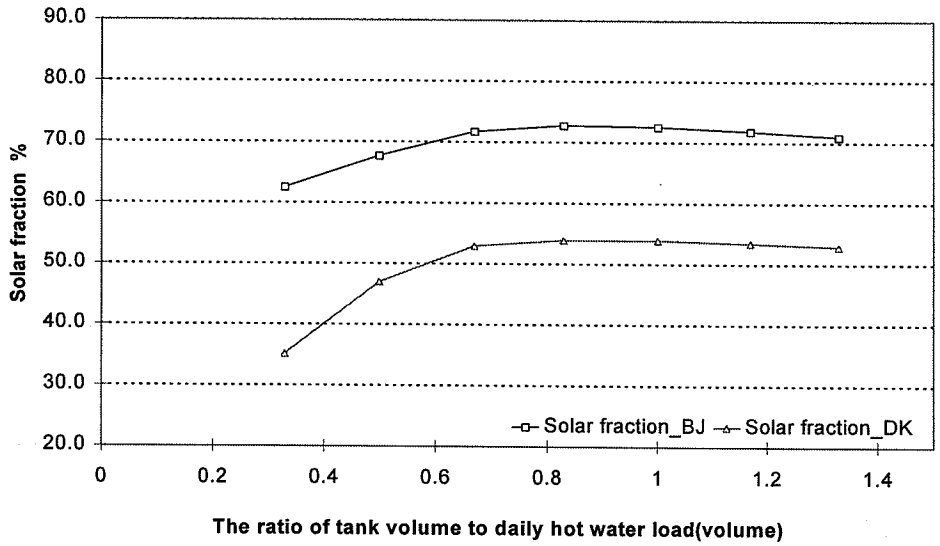

Figure 5.10 The solar fraction as a function of the ratio of tank volume to daily hot-water load volume.

Ratio of tank height to diameter

The effect of the ratio between tank height and tank diameter on the solar fraction is shown in Fig. 5.11. This ratio covers a tank height from 0.3 m to 1 m with such a tank diameter that the volume of the tank is constant at 100 *l*. The total heat loss from the tank is calculated according to different sizes of the tank, but the insulation thickness keeps the same in all the cases. It can be seen that the solar fraction is affected very slightly when the ratio changes between 0.5 and 3.0.

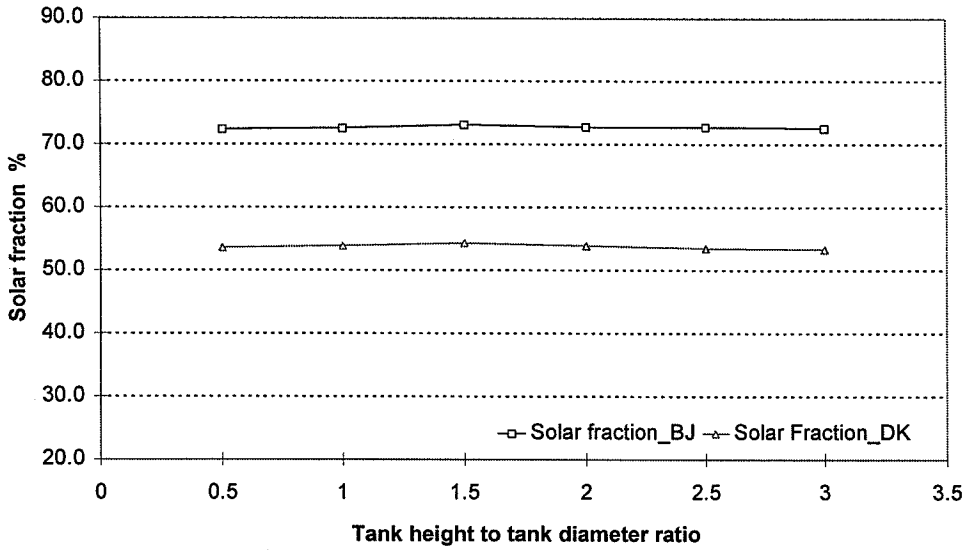

Figure 5.11 The solar fraction as a function of the ratio of tank height to tank diameter.

5.6 Conclusion and discussion

The model of a thermosyphon loop direct connected with a storage tank was developed. Based on the SOLSIM program, simulations were carried out for this type of thermosyphon systems under both Beijing (China) and Danish weather conditions. The results of the simulations showed that the solar fraction is influenced by various design and operation parameters.

The solar fraction can be increased by increase of the collector area. However, it should be noticed that the increase of collector area will cause a considerable increase of the system cost. The optimum collector area should take this into account.

During the period from May to September, the optimum tilt angle of the collector was found to be about 25° for the Beijing area, and 40° for Danish conditions.

The maximum efficiency and heat loss coefficients of the collector have a direct effect on the solar fraction. Results indicate that the increase of collector efficiency results in a corresponding increase of solar fraction. As the heat loss coefficient increases, the reduction of the solar fraction is faster under Danish conditions than under Beijing conditions.

The influence of the connecting pipe diameter is large when the diameter less then 15 mm, but no considerable effect was observed when the inner diameter of the pipe is larger than 15mm.

The daily hot water load has a considerable influence on the solar fraction. When the daily hot-water load increases, the solar fraction decreases. This effect is mainly due to the fact that the basic daily energy consumption for hot-water increases. Based on a definite hot water load, the ratio of tank volume to daily hot water load volume also has an influence on the

solar fraction. The optimum ratio of tank volume to daily hot-water load volume was found to lie between 0.8 and 1.

The ratio of the tank height to the diameter has no considerable effect on the solar fraction when it is between 0.5 and 3. The position of the hot water inlet to the tank from the collector has an effect on the solar fraction only when the height is below 0.3 m (from the bottom of the tank).

The system simulations in this chapter were carried out for thermosyphon systems with the tank direct connected with a thermosyphon loop. From the simulation results, recommendations can be made for optimum values of the most important design parameters for this type of systems.

Chapter 6

Dynamic modeling and simulation of drain-back solar DHW systems

6.1. Introduction

For solar DHW systems, the solar collector and/or parts of the connecting pipes have to work under outdoor climate conditions. In most parts of the world, freeze-protection naturally becomes one of the basic problems in the system design. To solve this problem, one common solution is the use of anti-freeze working liquid in the collector loop. However, other consequences of using anti-freeze liquid are the decrease of the system efficiency and pollution of the environment. Therefore, from an energy and environment point of view, the use of anti-freeze liquid should be avoided. The other possible solution to solve the freeze problem is the mechanical method, i.e. empty the collector before the temperature in the collector drops below a certain point. This is the basic design idea of drain-back solar DHW systems.

For years, many different designs of drain-back systems have been introduced into the market. In the 1996 report of the International Energy Agency Project Task 14 [16], several drain-back systems were introduced as "dream systems". Different from other designs, a drain-back system must include a drain-back tank in the collector loop, which can be either a special additional tank (as shown in Fig. 6.1) or integrated with a mantle tank. The basic working principle of these systems is that the solar collector fluid is working in the collector loop during the operation and drains back to the drain-back tank when the operation stops. It is the special operation design which eliminates the need for an anti-freeze fluid in the collector loop, thereby making it possible to improve the system performance by using water instead of glycol-water mixtures as the collector fluid.

To predict the thermal performance and optimize the design of such systems, it is necessary to know how the system will perform under various design and operation conditions. The cost of an experiment imposes the necessity of computer simulations to determine the thermal performance of the systems. Therefore, a simulation model for such systems, taking into account these varying conditions, is required.

A few investigations of drain-back systems are found in the literature. J.H. Davidson [14,15] has performed an experiment on the impact of the design of the components and of the operation conditions on the thermal ratings of a conventional drain-back solar water system

(the heat exchanger was in the drain-back tank). Based on the test results they made a comparison of experimental and simulated thermal ratings of drain-back systems in 1993. L.B. Hansen & S. Furbo (1995) [27] carried out experimental investigations on drain-back systems and found out some basic design rules for those systems.

In this chapter, dynamic models of drain-back systems with both a built-in heat exchanger spiral tank and a mantle tank are studied. The system models were verified by means of comparing the simulated results to the measurements from an experiment that was carried out in the laboratory of the Department of Buildings and Energy, Technical University of Denmark. A number of predictions of the influence on annually performance have been made by applying the present simulation procedure for a wide range of quantities of the system design parameters.

6.2 Drain-back system with built-in heat exchanger spiral tank

Hot-water tanks with a built-in heat exchanger spiral are commonly used in solar DHW systems. For a drain-back system with this kind of storage tank, an additional drain-back tank has to be added into the collector loop. A simple schematic diagram of a drain-back system with a built-in heat exchanger spiral tank is shown in Fig. 6.1. The system basically consists of a flat-plate collector array, a drain-back tank, a storage hot-water tank and a control system. Water is used as the solar collector fluid in the collector loop. When the collector loop is in a non-operation condition, the major part of the working fluid is stored in the drain-back tank and the collector is filled up with air. The storage tank is designed as a combi tank and an auxiliary electric heating element is situated in the upper part of the tank.

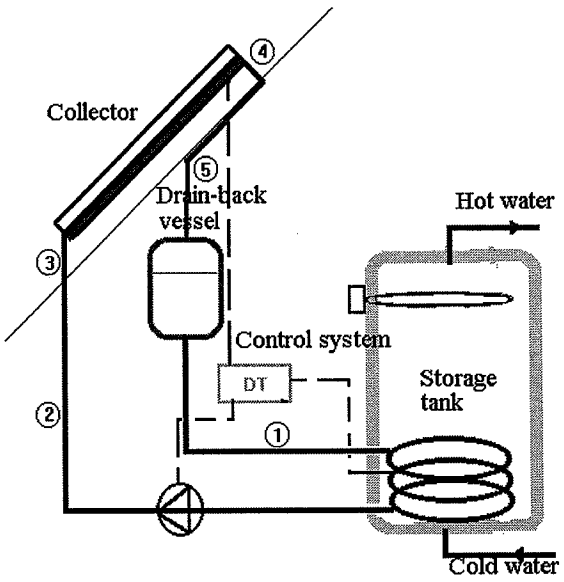

Figure 6.1 Sketch of the drain-back system with a built-in heat exchanger spiral tank.

6.2.1 Modeling of the system

The basic design of a drain-back system as shown in Fig. 6.1 is similar to a normal active solar DHW system. The dynamic models of the components in a drain-back system have been described in chapter 4. The general mathematical model of the system is a set of differential equations that can give detailed information about thermal processes under certain boundary conditions.

Under normal operation conditions, a drain-back system can be analyzed in a manner similar to a normal system. However, special attention has to be paid to the starting and stopping period, since the thermal capacity of some components in a drain-back collector loop is a function of time and flow rate under those conditions.

For a time period, the collected energy removed by the working fluid is either delivered to the storage tank, or stored in the collector loop and dissipated as heat loss. According to the temperature distribution, the collector loop can be divided into two parts, a collector with connection pipes (including heat exchanger) and a drain-back vessel. Since the temperature drop along the connection pipes is usually small during operation periods, the pipes were modeled as single nodes with negligible temperature drop along the pipe.

Therefore the energy balance over a time interval *dt* on the collector segment can be given by the following expression.

$$\frac{\partial(A_c \cdot C_{pc} \cdot \overline{T}_c + C_{pl} \cdot T_d + \sum_{i=2}^{3} C_{pi} \cdot T_{eu} + \sum_{i=4}^{5} C_{pi} \cdot T_c + C_{pe} \cdot T_e)}{\partial t} = \eta \cdot G \cdot A_c + \dot{m}_c \cdot C_p \cdot (T_d - T_c)$$
$$- \dot{m}_c \cdot C_p \cdot (T_d - T_{eu}) - U_{pi} \cdot l_1 \cdot (T_d - T_0) - U_{pi} \cdot l_2 \cdot (T_{eu} - T_a)$$
$$- U_{pu} \cdot l_3 \cdot (T_{eu} - T_a) - U_{pu} \cdot l_4 \cdot (T_c - T_a) - U_{pi} \cdot l_5 \cdot (T_c - T_0) \qquad (6.2.1)$$

Here $\eta = \eta_0 - k_1 \cdot (\overline{T}_c - T_a)/G - k_2 \cdot (\overline{T}_c - T_a)^2/G$

$$\overline{T}_c = 0.5 \cdot (T_{eu} + T_c)$$

$$T_e = 0.5 \cdot (T_d + T_{eu})$$

where

T_d	outlet temperature of drain-back vessel	°C
T_{eu}	outlet temperature of heat exchanger	°C
T_c	outlet temperature of collector	°C
T_0	room temperature	°C
U_{pi}	pipe heat loss coefficient (indoor)	W/m K
U_{pu}	pipe heat loss coefficient (outdoor)	W/m K
C_{pi}	thermal capacity of pipe i	J/K
C_{pe}	thermal capacity of heat exchanger	J/K
l_i	length of pipe i	m

Subscribe

1,2,3,4,5	pipe 1,2,3,4,5
e	heat exchanger

The energy balance of the drain-back tank can be presented as :

$$\frac{\partial(V_d \cdot \rho_f \cdot C_{pf} \cdot T_d + C_{pd} \cdot T_d)}{\partial t} = \begin{cases} -\dot{m}_c \cdot C_{pf} \cdot T_d - U_d \cdot (T_d - T_a) & \text{if } \dot{m}_c \cdot \int_0^t dt \le M_c \\ \dot{m}_g \cdot C_{pf} \cdot T_d - U_d \cdot (T_d - T_a) & \text{if } \dot{m}_g > 0 \\ \dot{m}_c \cdot C_{pf} \cdot (T_c - T_d) - U_d \cdot (T_d - T_a) & \text{otherwise} \end{cases} \quad (6.2.2)$$

Where, $\dot{m}_g$ the drain-back mass flow rate kg/s

M_c mass content of the collector array kg

The dynamic models of the heat exchanger and the storage tank have been described in chapter 4. Together with the collector loop model, the system model consists of a set of differential equations.

6.2.2 Simulation program

To apply the dynamic model described above as a tool for system simulation design and analysis, a simulation program [66] which is based on a program [20] for normal active solar DHW systems has been developed. For the purpose of easy usage, the mathematical equations of the model are programmed in FORTRAN 77.

6.2.2.1 Method to solve the energy equations

As mentioned before, the dynamic model of a system consists of a set of energy equations which are generally expressed in terms of differential equations. To solve these differential equations, discretization methods are the common numerical solution. These methods include Taylor-series formulation, Euler's method and the Runge-Kutta method, which are commonly used in heat transfer calculations.

By means of the Taylor-series formalism, the system differential equations may be written in the finite-difference form, and the resulting equations are consistent with a heat balance over a short interval. Therefore, for a system model we derive *n* finite-difference equations. In order to solve these *n* finite-difference equations, here, the implicit method was used. The advantage of using this method is that no uncontrollable oscillations of the result will occur, even if the time step is increased significantly.

Then the *n* finite-difference equations can be rearranged in the following form.

$$A(i) \cdot T_{i-1} + B(i) \cdot T_i + C(i) \cdot T_{i+1} = D(i)$$

With proper consideration of the boundary condition, the equation systems can be written in a matrix form as:

$$\begin{bmatrix} B_1 & C_1 & & & \\ \cdot & \cdot & \cdot & & \\ & A_i & B_i & C_i & \\ & & \cdot & \cdot & \cdot \\ & & & A_n & B_n \end{bmatrix} \cdot \begin{bmatrix} T_1 \\ \cdot \\ T_i \\ \cdot \\ T_n \end{bmatrix} = \begin{bmatrix} D_1 \\ \cdot \\ D_i \\ \cdot \\ D_n \end{bmatrix}$$

For such an equation system, the solution with Gauss elimination can be carried out using a rapid algorithm. The algorithm goes through two steps: elimination and substitution.

Elimination is carried out by multiplying the equations with a factor and adding them to some of the other equations in such a way that some of the coefficients in the matrix becomes zero. This is done in a certain order until all coefficients to the left of the main diagonal have been eliminated. Then the equation system can be transformed into:

$$\begin{bmatrix} 1 & E_1 & & & \\ & \cdot & \cdot & & \\ & & 1 & E_i & \\ & & & \cdot & \cdot \\ & & & & 1 \end{bmatrix} \cdot \begin{bmatrix} T_1 \\ \cdot \\ T_i \\ \cdot \\ T_n \end{bmatrix} = \begin{bmatrix} F_1 \\ \cdot \\ F_i \\ \cdot \\ F_n \end{bmatrix}$$

Elimination can be expressed by the recursive formulae:

$$G_1 = B_1; \qquad E_1 = C_1/G_1; \qquad F_1 = D_1/G_1;$$

For I=2, ...,n-1:

$$G_i = B_i - A_i E_{i-1}; \qquad E_i = C_i/G_i; \qquad F_i = (D_i - A_i F_{i-1})/G_1;$$

$$G_n = B_n - A_n E_{n-1}; \qquad F_n = (D_n - A_n F_{n-1})/G_n$$

The back-substitution starts by solving equation n directly. When T_n is known, it can be inserted into equation n-1 to isolate T_{n-1}, and so forth until all temperatures are found.

6.2.3 Model verification and system evaluation

Before using the theoretical model as a tool for system design and analysis, it should be verified in order to obtain reliable results. The dynamic model of drain-back systems with a

built-in heat exchanger tank has been verified by comparing the predictions of the simulation to experimental data.

The measurement of a drain-back system from SolarNor AS was carried out at the test facility of Department of Buildings and Energy, Technical University of Denmark. The thermal performance of the system has been measured for the period of May to November, 1997.

The simulation model was modified by comparing the simulated temperatures and energy quantities to the measured quantities. By using this simulation model, the yearly thermal performance of the system was investigated with the Danish Test Reference Year (TRY) as the input weather data.

6.2.3.1. Configuration and specification of the tested system

Photographs of the system are shown in Figures 6.2 and 6.3. The system consists of four solar collector modules, a heat storage tank (with a built-in heat exchanger), a control system, a drain-back tank, and two circulation pumps.

The solar collector is placed on a 45° tilted plate with an azimuth angle of +10°. The total transparent area of the collector modules is 5.48 m^2. Each collector module consists of a transparent cover made of a polycarbonate (PC) twin wall sheet, and an absorber plate of PPO-material (NORYL PX507, developed by General Electric Plastics). The PPO absorber plate contains a large number of channels filled with ceramic particles. The function of the ceramic particles is to provide good thermal contact between the heat transfer fluid and the energy absorbing surface of the absorber plate. The supply pipe of the heat transfer fluid is placed below the row of collector modules. Through an inlet pipe centrally placed in the absorber plate, the fluid is lifted to an internal distribution channel at the top of the module. Driven by the gravity, the heat transfer fluid trickles through the absorber channels and is finally collected by an internal channel placed at the collector bottom.

In the collector loop, water is used as the heat transfer fluid with a total volume of 21 *l*. As a drain-back system, the collector loop, which is open, contains air besides water. During periods without collector operation, the major part of the heat transfer fluid is stored in the drain-back tank, and the solar collector and parts of the connection pipes are filled with air. Whenever the operation of the collector starts, the air in the collector will be forced out of the collector from the top to the bottom and back to the upper part of the drain-back tank.

The solar collector, drain-back tank and storage tank are connected through well insulated pipes of PVC material with a total length of 15 m. The heat loss coefficient from the connecting pipes is about 0.13 W/mK. Two circulation pumps (Grundfos type UPS 25-60) with a total power of 101W (measured) were used in the collector loop. The volume flow rate during the operation is about 0.233 *l/sec.*

The storage tank (SOLARNOR OSO 16RVE 300) of the system is a combi-tank with a total volume of 285 *l*. It is essentially a vertical cylindrical steel tank (diameter 0.5 *m*) with a built-in spiral heat exchanger at the bottom, and an auxiliary electric heating element (3 kW) in the

Figure 6.2 Solar collector modules.

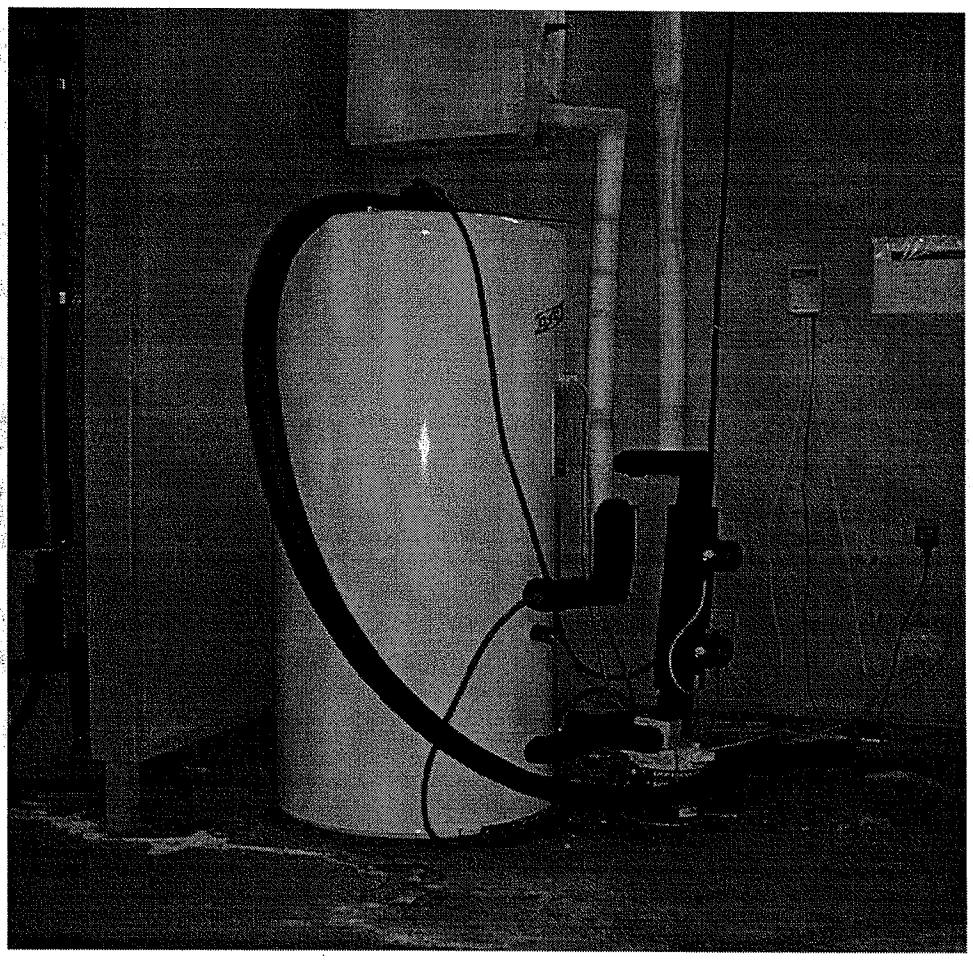

Figure6.3 Storage tank and part of the collector loop.

upper part. The tank is well insulated with 40 *mm* of polyurethane foam on the side and top walls. The basic design parameters of the tank are shown in Appendix 1.

The control system used in the test system is a Solar Controller M205 which is a differential thermostat control system with temperature sensors at the bottom of the storage tank and in the lower part of the absorber surface of the collector. The start and stop temperature difference were set up to 10 K and 2 K. Furthermore, the operation is controlled in such a way that the pump stops 20 seconds every 15 minutes during operation periods. This is to solve the air problems in the collector. The power consumption of the control system is metered as 3.0 W when the pump in the collector loop is in operation, and 1.6 W when it is not.

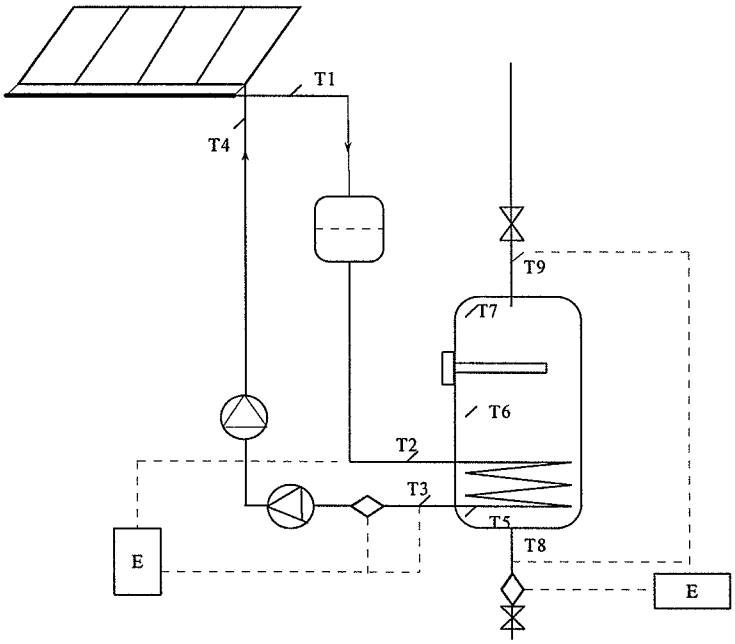

Figure 6.4 Sketch of the test system with measuring point.

6.2.3.2. Experimental conditions

The measurements were carried out from May 1997. The temperatures in the collector loop and storage tank were measured by means of thermo-elements of the copper/constantan type (TT). The thermo-elements in the storage tank are placed in a glass rod in the middle of the tank, and the three measurement points are placed at 0.16 *m*, 0.754 *m* and 1.382 *m* from the top of the tank. Fig. 6.4 shows the system with the measuring points.

The flows in the solar collector loop and tapping loop are measured by means of Clorius Combimeter energy and flow meters. The amount of energy that is transferred from the collector to the storage tank is determined from the measured flows in the collector loop, and the difference of the inlet and outlet temperature of the heat-exchanger spiral. Similarly, the

energy tapped from the storage tank is calculated from the tapping flow and the temperature difference between the tapped hot water and the inlet cold water.

The outdoor ambient temperature and solar radiation on a south-facing surface with a 45° tilt angle are measured and recorded as mean quantities over a period of 5, 10 and 60 minutes. respectively. The temperature in the room where the storage tank is situated is also recorded.

During the test period, the hot water was tapped 3 times a day, at 7 am, 12 am and 7 pm. The energy quantity of 2.44 *kWh* was tapped at each tapping.

The sums of the measured energy quantities in each month from May to November 1997 are shown in Table 6.1. There are some days missing in May, June, July, and November because of both operation and measurement problems. The net utilized solar energy here is defined as the energy tapped from the storage tank minus the total energy consumption for the electric heating element, circulation pump and control system. The solar fraction is defined as the ratio of the net utilized solar energy to the energy for hot water consumption.

Table 6.1 Measured monthly sum of the energy quantities

Month	Available days	Solar energy supplied to the tank kWh	Energy tapped from tank kWh	Auxiliary energy used kWh	Net utilized solar energy kWh	Solar fraction %
May	6-31	93	184	129	55	29.9
June	1-13	89	85	30	55	64.7
July	20-31	76	71	23	48	67.6
Aug.	1-31	212	214	66	148	69.1
Sep.	1-30	123	186	111	75	40.3
Oct.	1-15 17-31	77	202	137	65	32.1
Nov.	1-4 6-30	34	205	195	10	4.9

6.2.3.3. Models used in the system simulation

Collector loop

The efficiency of the collector that was used in the simulation model was based on both the measurements report [30] from the *Institut für Thermodynamik und Wärmetechnik, Universität Stuttgart,* and the results from the test period.

From [30] the efficiency of the collector is expressed as:

$$\eta = 0.711 - 4.405 \cdot (T_m - T_a) / G - 0.036 \cdot (T_m - T_a)^2 / G$$

The simulation program uses a linear expression for the efficiency at a temperature difference of 45K. Therefore, the efficiency of the collector may be written as:

$$\eta = 0.711 - 6.025 \cdot (T_m - T_a) / G$$

From the test data of the system, it was found that the efficiency of the collector is relatively low compared with the result of [30]. Therefore, the collector efficiency model is modified based on the test data, and represented as:

$$\eta = 0.68 - 6.03 \cdot (T_m - T_a) / G$$

The incident angle modifier of the efficiency was determined (from [30]) as :

$$IAM(\theta) = 1 - \left(\tan(\frac{\theta}{2}) \right)^{2.6}$$

Where, IAM incidence angle modifier coefficient

θ incidence angle

Irregular variations of the flow in the collector loop were observed from the measurements, because of both the special operation strategy and air problems in the collector. Figure 6.5 shows the measured flow rate in the collector loop during the period 7/11-13/11, 1997. Experience showed that during periods with collector operation, it was impossible to force all the air out of the collector. In the simulation model, an average constant flow is used.

Storage tank

The mathematical model of the tank is represented by a stratified model with 8 segments along the vertical direction. Uniform temperature is assumed in each of these segments. The heat exchanger is placed at the bottom segment, whereas the electric heating element is situated at the third segment from the top.

The heat exchange capacity rate of the heat exchanger was determined from the model proposed by Jensen [37]. According to the measurement, the heat exchange capacity rate of the heat exchanger at the bottom of the tank may be presented as:

$$H = 1.01 + 5.05 \cdot T_1$$

Where, H the heat exchange capacity rate of the heat exchanger, W/K

T_1 temperature of the bottom segment, °C

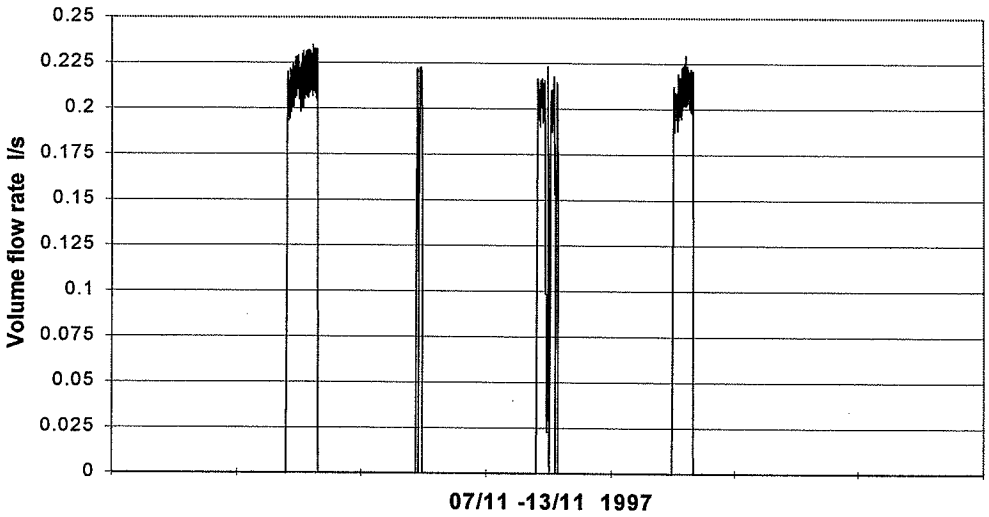

Figure 6.5 Measured flow rate in the collector loop in the period 7/11 -13/11 1997.

6.2.3.4. Comparison of simulated and tested results

With the design parameters of the system and the calculation model introduced above, simulations were carried out for the period 7/11 to 13/11, 1997. The computer model of the system was validated with measured energy and temperature data. The comparison of the simulation results and measurements are made for the most important parameters such as solar energy supplied to the tank, auxiliary energy for the electric heating element, the energy tapped from the tank, the net utilized solar energy (1), and the temperature change in the collector loop and storage tank. Here the net utilized solar energy (1) is defined as the energy tapped from the storage tank minus the auxiliary energy supplied to the tank.

To compare the simulation results with the measurements, the solar irradiation, ambient temperature, inlet water temperature to the tank, and the tapping flow are used as simulation inputs. The temperature distribution both in the collector loop and the storage tank are the corresponding output.

The solar irradiation on the collector plate and ambient temperature during the simulation period are shown in Figures 6.6 and 6.7. The solar irradiation data were calculated from the measurements on a surface with a 45° tilt angle facing south.

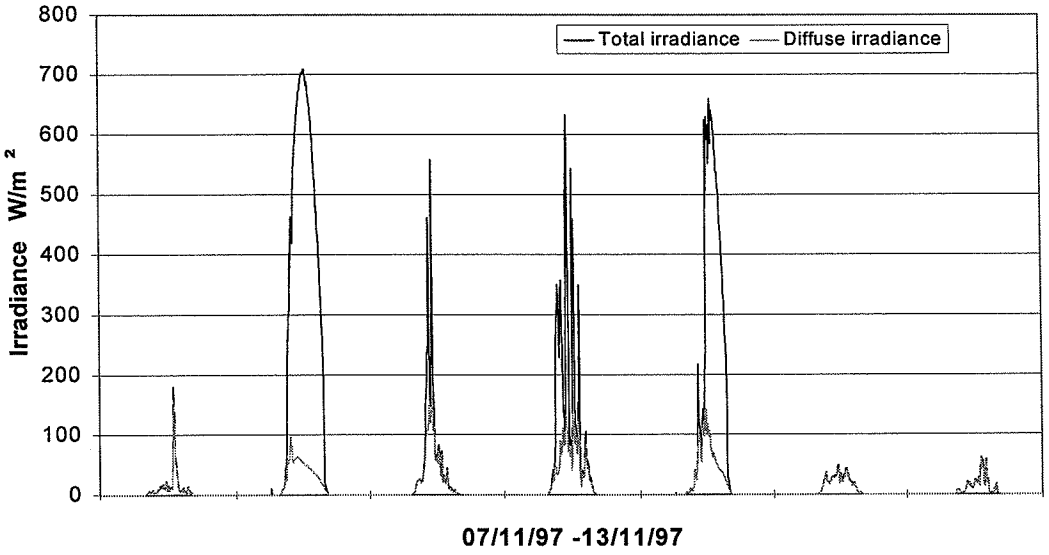

Figure 6.6 Solar irradiation on the collector in the period of 07/11 -13/11 1997.

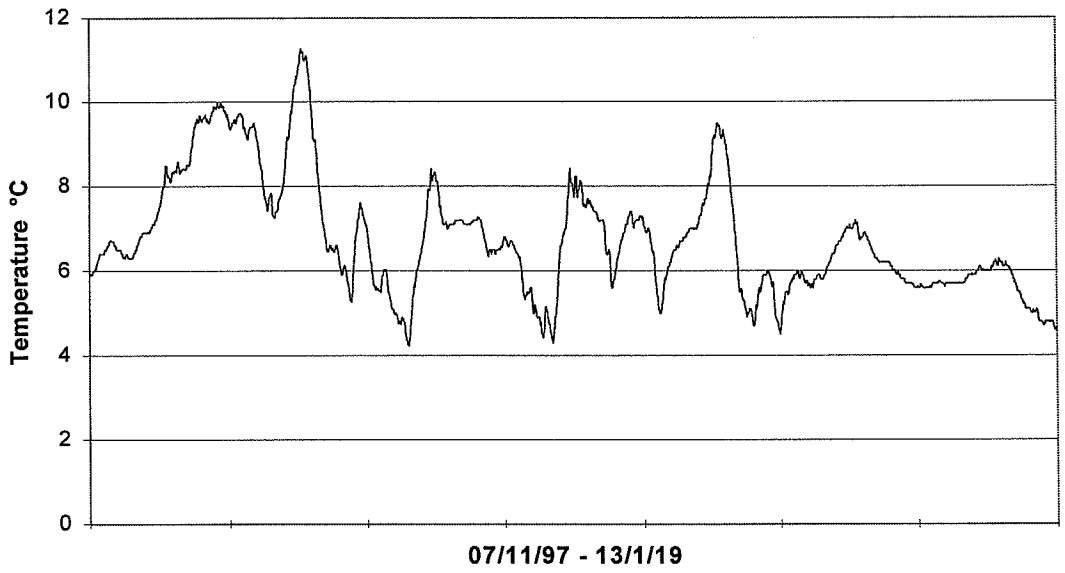

Figure 6.7 Outdoor ambient temperature in the period 07/11 -13/11 1997.

Comparison of measured and simulated temperatures of the fluid coming from the drain-back tank and the temperature of the fluid from the heat exchanger spiral to the collector are shown in Figure 6.8. The horizontal line indicates that the collector loop was in non-operation condition. The great temperature difference between the measurement and the simulation results during this non-operation period is due to the fact that the temperature sensor is installed at the outlet pipe of the drain-back tank and the heat exchanger spiral. Figure 6.8 illustrates that the simulated temperature of the fluid from the drain-back tank and the heat exchanger spiral has the correct dynamic responses.

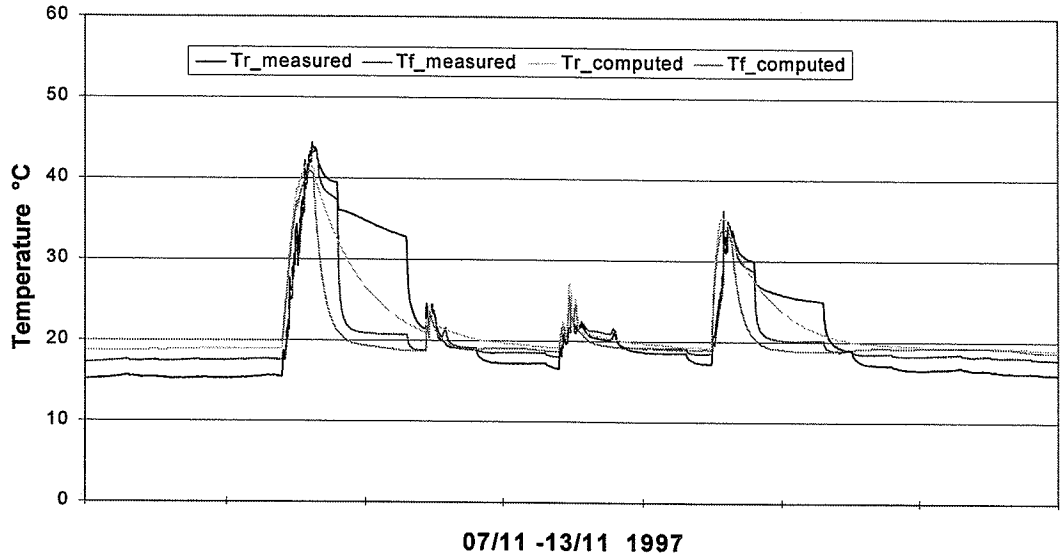

Figure 6.8 The inlet and outlet temperature of the heat exchanger spiral situated at the bottom of the tank.

The measured and simulated temperature at the top of the storage tank is presented in Figure 6.9. The simulated temperature was approximately constant at 49.9°C, while the measured temperature is varying between 49°C and 51°C. This is due to the fact that the definable thermostat in the program is set at a constant temperature.

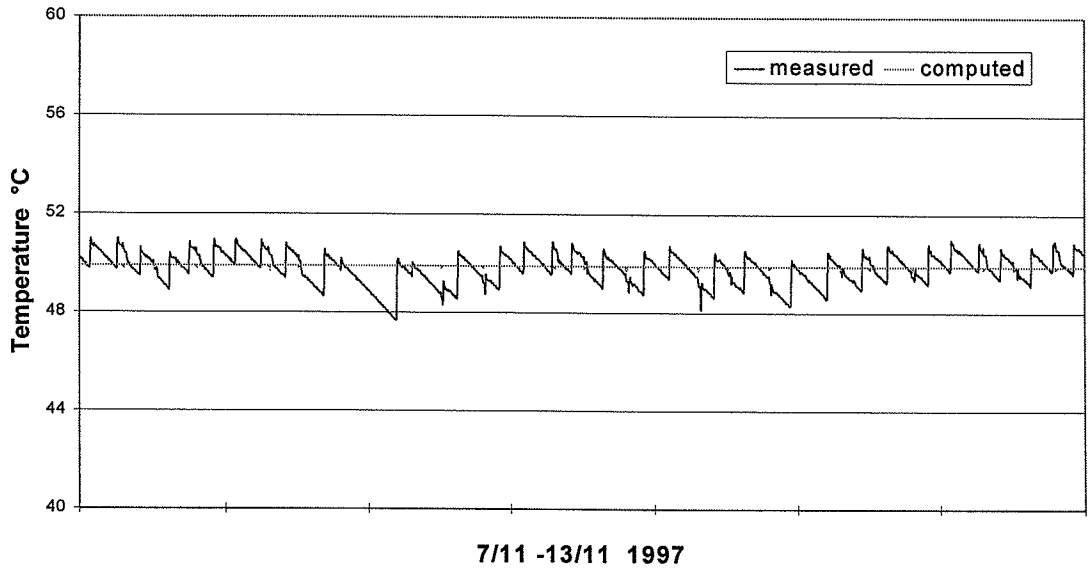

Figure 6.9 The temperature at the top of the storage tank during the simulation period.

Figure 6.10 illustrates the measured and simulated solar energy supplied to the storage tank (5 minutes values). It can be seen that the measured and the simulated values show good agreement.

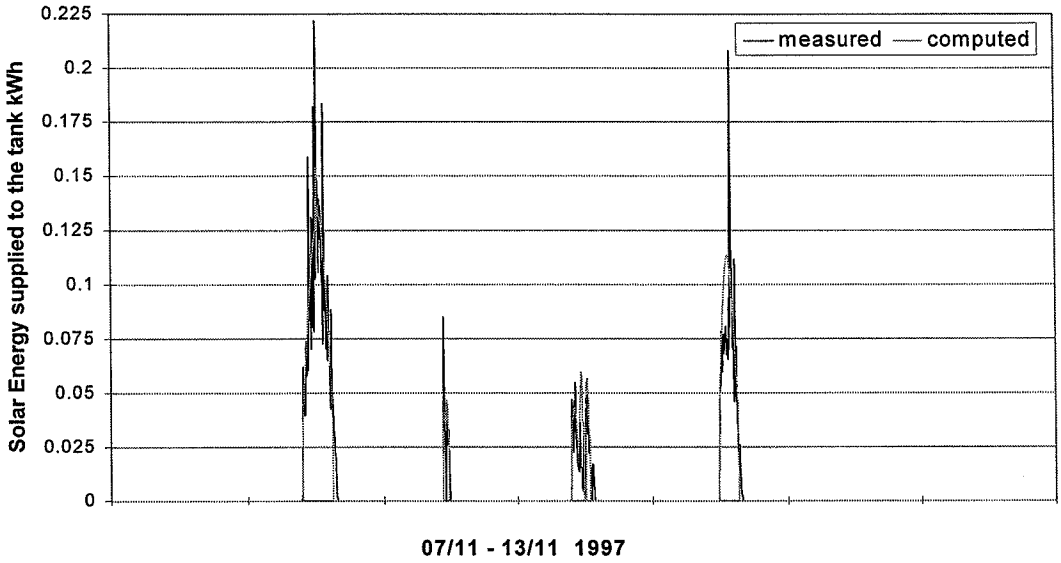

Figure 6.10 Solar energy supplied to the storage tank (5 minutes values).

The measured and simulated daily energy quantity tapped from the storage tank is shown in Figure 6.11, and the comparison of measured and simulated values for the daily energy supplied from the collector to the storage tank is shown in Figure 6.12. Similarly, Figure 6.13 illustrates the measured and calculated daily supply of auxiliary energy to the storage tank. The comparison of measured and calculated net utilized solar energy (1) is shown in Figure 6.14. It appears that there is a good agreement between the measured and simulated energy quantities.

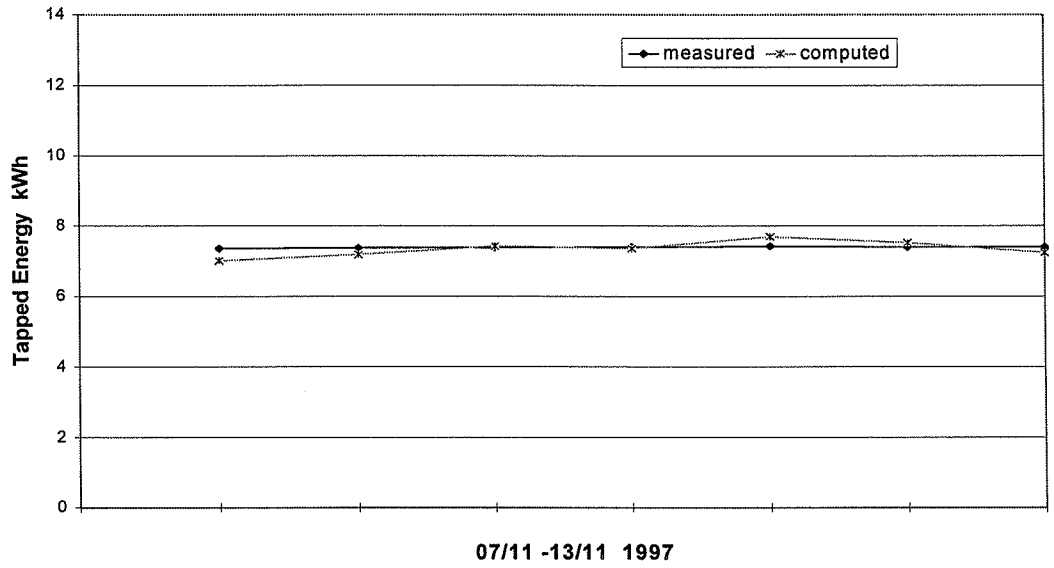

Figure 6.11 Energy tapped from the storage tank during the simulation period (daily values).

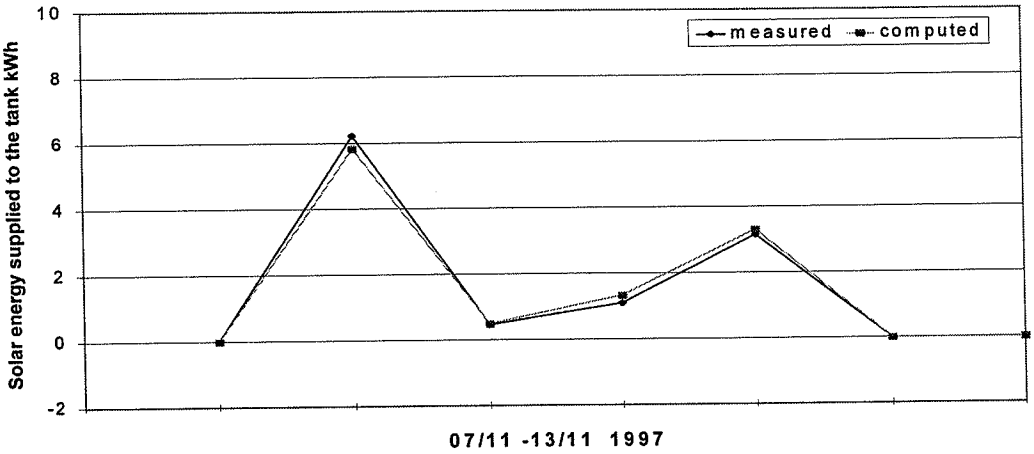

Figure 6.12 Solar energy supplied to the tank during the simulation period (daily values).

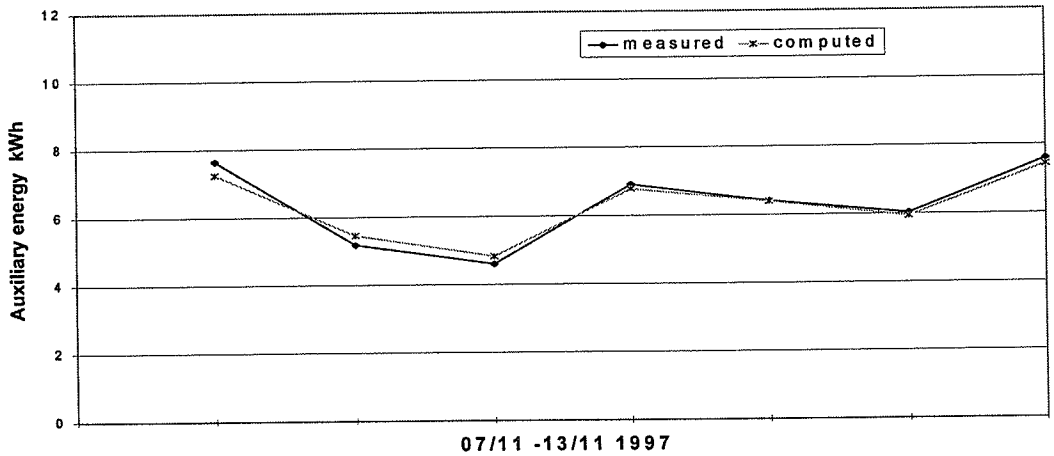

Figure 6.13 Auxiliary energy supplied to the tank during the simulation period (daily values).

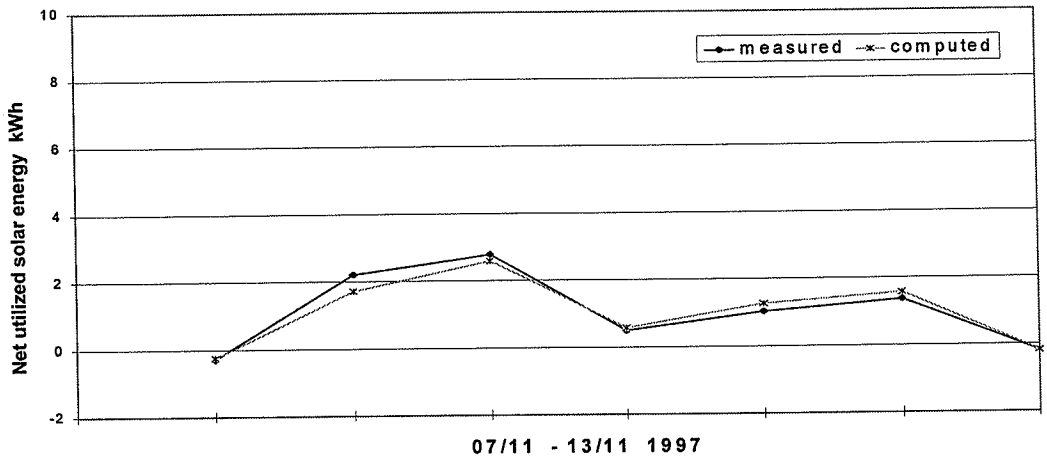

Figure 6.14 Net utilized solar energy during the simulation period (daily values).

Table 6.2 shows the sum of the energy quantities over the simulation period and the deviation between the simulated and measured values. It shows that the deviations are smaller than the precision of the measured energy quantities [57] and the simulation results are acceptable.

Table 6.2 Energy quantities during simulation period

Period 1997 07/11-13/11	Solar energy to the tank (kWh)	Auxiliary energy used (kWh)	Tapped energy from tank (kWh)	Net utilized solar energy (kWh)
Measured	10.9	44.4	51.8	7.4
Calculated	11.0	44.2	51.4	7.3
Deviation %	0.6	-0.4	-0.6	-1.9

6.2.3.5. Simulated yearly thermal performance of the tested system

On the basis of this verified simulation model, the long-term (yearly) thermal performance of the system was simulated under Danish weather conditions by using the Danish TRY. The simulations were carried out for two operation conditions:

1. The daily hot water (50°C) consumption is 160 liters and the auxiliary heating element heats the water in the top of the tank to 50.5 °C.
2. The daily hot water (45°C) consumption is 200 liters and the auxiliary heating element heats the water in the top of the tank to 45.5 °C .

Under both conditions, the inlet cold water is 10 °C and the hot water is tapped three times a day at 7 am, 12 am and 5 pm with one third of the daily total quantities in each tapping.

The calculated monthly values of solar irradiation on the collector, solar energy supplied to the storage tank, auxiliary energy from the electric heating element, energy tapped from the tank, net utilized solar energy, etc. are shown in Tables 6.3-6.4. The net utilized solar energy is defined as the energy tapped from the tank, minus the total energy consumption for the electric heating element, circulation pump and control system. The net utilized solar energy (1) is defined as the energy tapped from the tank minus the auxiliary energy for the electric heating element.

It appears from the Tables 6.3 and 6.4 that the yearly energy gain from solar energy (net utilized solar energy) of the test system changes from 930 kWh to 1160 kWh under different operation and tapping conditions, corresponding to solar fractions of 34.7% to 39.4%, respectively. The tables also show that there is a large difference between the net utilized solar energy and net utilized solar energy (1) for the tested system. This is due to the relatively large energy consumption of the circulation pumps.

Table 6.3 Simulated yearly thermal performance of the system (operation condition 1)

Month	Solar irradiation on collector kWh	Solar energy supplied to tank kWh	Energy tapped from tank kWh	Auxiliary energy supplied to tank kWh	Energy for pump kWh	Energy for control system kWh	Net utilized solar energy (1) kWh	Net utilized solar energy kWh	Solar fraction (1) %	Solar fraction %
Jan.	146	22	228	219	3	1.3	9	5	3.9	2.1
Feb.	324	59	206	164	6.6	1.3	42	34	20.3	16.5
Mar.	409	75	228	174	9.1	1.5	54	43	23.5	18.9
Apr.	733	159	221	103	17.5	1.7	117	98	53.1	44.5
May	858	199	228	76	21	1.8	152	130	66.8	56.8
June	976	241	221	46	23.4	1.8	174	149	79.0	67.6
July	860	220	228	61	23.8	1.9	167	141	73.1	61.9
Aug.	821	226	228	61	23.4	1.8	167	142	73.2	62.1
Sep.	586	156	221	103	18	1.7	118	98	53.5	44.6
Oct.	372	92	228	158	11.2	1.5	70	58	30.8	25.3
Nov.	210	42	221	193	6.3	1.3	28	20	12.6	9.1
Dec.	187	34	228	208	5.4	1.3	20	14	8.9	5.9
Total	6482	1524	2685	1566	168.6	18.8	1119	931	41.7	34.7

Table 6.4 Simulated yearly thermal performance of the system (operation condition 2)

Month	Solar irradiation on collector kWh	Solar energy supplied to tank kWh	Energy tapped from tank kWh	Auxiliary energy supplied to tank kWh	Energy for pump kWh	Energy for control system kWh	Net utilized solar energy(1) kWh	Net utilized solar energy kWh	Solar fraction (1) %	Solar fraction %
Jan.	146	23	250	230	3.2	1.3	20	16	8	6.2
Feb.	324	62	226	172	6.9	1.3	54	46	24.0	20.4
Mar.	409	79	250	181	9.5	1.5	69	58	27.4	23.1
Apr.	733	171	242	102	18.3	1.7	140	120	57.7	49.5
May	858	217	250	70	22.8	1.8	180	156	72.1	62.3
June	976	260	242	40	24.8	1.9	202	175	83.3	72.3
July	860	240	250	55	25.3	1.9	195	168	78.1	67.2
Aug.	821	243	250	55	25.2	1.9	195	168	78.0	67.2
Sep.	586	170	242	98	19.2	1.7	144	123	59.4	50.8
Oct.	372	99	250	163	12	1.5	88	74	35.0	29.6
Nov.	210	45	242	202	6.7	1.3	40	32	16.5	13.1
Dec.	181	37	250	218	5.7	1.4	32	25	12.8	9.9
Total	6482	1646	2943	1586	179.5	19.1	1357	1159	46.1	39.4

6.2.3.6. Improvement of the measured system

To make improvements on the tested system, investigations are carried out for one of the important parameters - the flow in the collector loop. By adjusting the setting of the two circulation pumps, different circulation flow rates in the collector loop are obtained. Further, it was observed that the circulation flow rates are also influenced by the temperature of the fluid in the collector loop. The measured results with a temperature about 30°C in the collector loop are shown in Table 6.5.

Because of the special design of the collector modules, the flow in the collector loop also influences the water content of the collector during operation. By measuring the volume of the water in the drain-back tank, it was observed that the water content of the collector varies between 0.9 *l/m*^{2} and 1.5 *l/m*^{2}, corresponding to flow rates in the collector loop from 4.6 *l/min.* to 15.6 *l/min.* This means that the air in the collector cannot be forced out completely during operation. The air in the collector will result in a poor flow distribution, and in a reduction of the collector efficiency. With the present design it is therefore important to use a high flow rate in the collector loop. A possible solution to the air problem could be a reverse flow direction from bottom to top in the collector.

Table 6.5 Pumps set up and corresponding flow rate for the tested system

Condition	Pump 1	Pump 2	Total power W	Flow rate l/s	Collector water content l/m^2
1	stage 1	stage 1	51.2	0.077	0.96
2	stage 1	stage 2	66.0	0.13	0.98
3	stage 2	stage 2	80.8	0.17	1.15
4	stage 2	stage 3	101.2	0.22	1.26
5	stage 3	stage 3	122.4	0.26	1.46

Based on the assumption that the collector efficiency is not influenced by the flow rate, simulations were carried out to determine the yearly thermal performance under different flow-rate conditions. The results are shown in Fig. 6.15. It appears that the net utilized solar energy (1) increases as the flow rate increases, whereas the net utilized solar energy decreases. This is due to the fact that the energy consumption of the pumps increases with increasing flow rate. Consequently, an improvement of the thermal performance of the system might be achieved by using an upwards flow direction in the collector, and by reducing the circulation flow rate in the collector loop. This change would also make it possible to use a mantle tank instead of a spiral heat exchanger tank, and further improve the performance of the system.

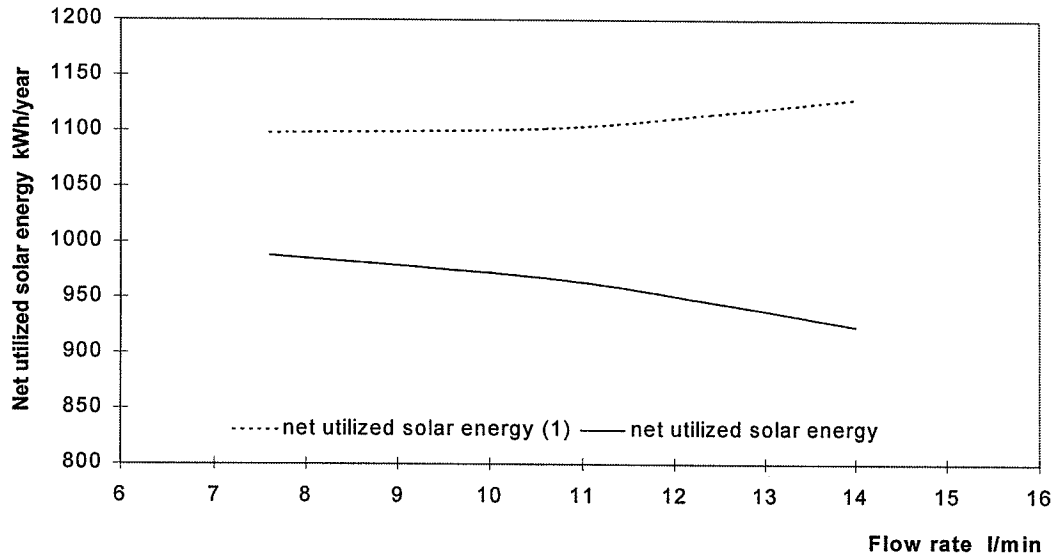

Figure 6.15 Net utilized solar energy as a function of flow rate in the collector loop.

6.3 Drain-back system with mantle tank

Research has shown that the design of the heat storage in a solar DHW system has a significant influence on the system thermal performance and the improvement of the system heavily depends on the storage tank design. Recent work on solar DHW systems has found that the system based on mantle tank and low flow operation results in a very good thermal performance compared to systems with other configuration [55].

For a drain-back solar DHW system, a mantle tank makes it possible to leave out the additional drain-back tank in the collector loop, thereby making the system more compact than the other types of drain-back systems. Basically, the design of a drain-back system with a mantle tank is the same as a normal mantle tank system. It consists of a collector array, a circulation pump, connecting pipes, and a mantle tank. The only difference is that the collector loop contains both solar collector fluid and air. During periods when the collector is in operation, the air in the collector loop will be forced to the top of the mantle. When the pump in the collector loop stops, the air will go to the upper part of the collector loop, and the collector and parts of the connection pipes will be filled with air. A sketch of a drain-back solar DHW system with a mantle tank is shown in Figure 6.16.

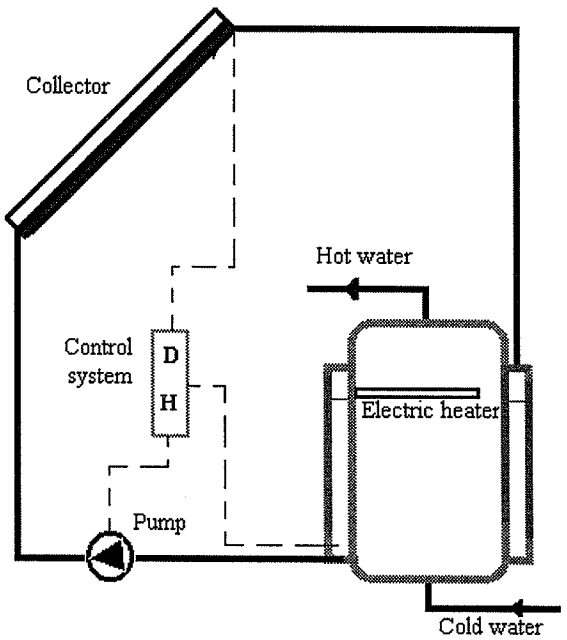

Figure 6.16 Sketch of the drain-back system with mantle tank.

6.3.1 System model and simulation program

The dynamic models of the components in a drain-back solar DHW system with a mantle tank have been described in chapter 4. For the purpose of applying these dynamic models for system design and analysis, as well as for the purpose of easy usage, a simulation program was written in *Pascal* [66]. This program was based on an earlier program [6] that was originally developed for the simulation of normal mantle tank systems.

As mentioned in section 4.9, the heat transfer in a mantle tank is a two-dimensional, non-steady process. The system simulation involves solving a large set of ordinary differential equations. Here, discretization methods were applied in the solution procedure. Because of the large matrix involved in the calculation, the simulation time is relatively long. To perform a one-year simulation takes about 5 hours on a 486 DX2/66 personal computer.

6.3.2 Model Verification

A drain-back system with mantle tank from Batec AS has been tested at the test facility of Department of Buildings and Energy, Technical University of Denmark throughout the year 1995. By applying the design parameters of the system, the dynamic model of a drain-back system with a mantle tank has been verified by comparing the simulation predictions to the measurements.

The parameters which are used for system model modification are the temperatures and energy quantities. By using this verified simulation model the yearly thermal performance of the tested system has been investigated with the Danish Design Reference Year as the input weather data.

6.3.2.1. Configuration and specification of the tested system

A sketch of the tested system with measuring points is shown in Figure 6.17. Basically, the system consists of two solar collector modules, a heat storage tank, a control system, and a circulation pump in the collector loop. The solar collector is placed on a 45° tilted plate facing south and the total transparent area of collector modules is 4.38 m^2. Each collector module consists of a 3.3 *mm* hardened iron-free transparent glass cover, and an aluminum-copper Sunstrip absorber.

The storage tank of the system is a mantle tank with a total volume of 250 *l* (+50 *l* in the mantle). It is essentially a vertical cylindrical steel tank (inner diameter 0.45 *m*) from the upper part to the bottom covered by a mantle. There are two auxiliary heating systems which are designed for the system. The spiral heat exchanger is situated in the upper part of the tank, and the electric heating element (1180 *W*) in a side loop connected with the upper part of the mantle. The basic idea of this design is to use the existing auxiliary heating system in the winter period and the electric heating element during the summer time. The electric auxiliary heating is designed in such a way that the electric heating element heats up the liquid in the side loop, and the heat is transferred to the mantle by the thermosyphon principle. The tank is well insulated with 45 *mm* of polyurethane foam on the side wall, but

originally not well insulated on the top. The basic design parameters of the tank are shown in Appendix 2.

In the collector loop, water is used as heat transfer fluid with a total volume of 50 *l*. During periods without collector operation, the heat transfer fluid (water) is stored in the mantle and the solar collector and part of the connection pipes is filled up with air. Whenever the operation of the collector starts, the air in the collector will be forced to the upper part of the mantle.

The solar collector and storage tank are connected through foam-insulated copper pipes (diameter 15/13 *mm*) with a total length of 21 *m*. The heat loss coefficient from the connecting pipes is about 0.17 *W/mK*. A circulation pump (Grundfos type UPS 25-40) with a total power of 35 *W* (measured) was used in the collector loop. The volume flow rate during the operation is about 0.8 *l/min*.

The control system used in the test system is a differential thermostat control system with temperature sensors at the bottom of the mantle and the outlet of the collector. The temperature differences for the start and stop operation were set to 15 *K* and 2 *K*, respectively. The power consumption of the control system is metered as 5.2 W.

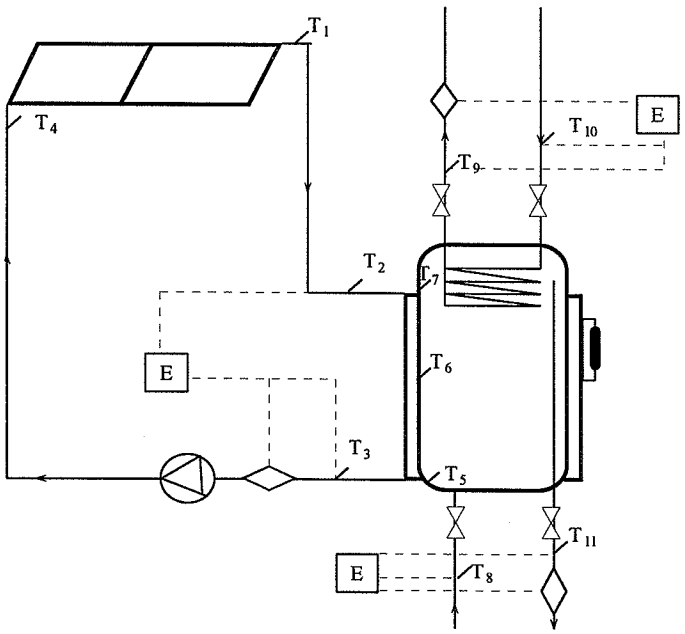

Figure 6.17 Sketch of the drain-back system with mantle storage tank.

6.3.2.2. Experiment conditions

The measurement was carried out throughout the year 1995. The temperatures in the collector loop and storage tank were measured by means of thermoelements of the copper/constantan type (TT). Fig. 6.17 shows the measuring points in the system. The thermoelements in the storage tank are placed in a glass rod in the middle of the tank, and the three measurement points are placed at 0.032 *m*, 0.622 *m* and 1.322 *m* from the top of the tank.

The flows in the solar collector loop and tapping loop are measured by means of Clorius Combimeter energy and flow meters. The energy that was transferred from the collector to the storage tank is determined from the measured flows in the collector loop, and the differences of the inlet and outlet temperature of the mantle. Similarly, the energy tapped from the storage tank is calculated from the tapping flow and the temperature difference between the tapped hot water and the inlet cold water.

The weather parameters such as the outdoor ambient temperature and solar radiation on a south-facing surface with a 45° tilt angle are measured and recorded as 10 minutes mean values. Similarly the temperature of storage room and cold water temperature are also recorded.

A simplified tapping program was designed for the tested system. The hot water was tapped 4 times a day, at 7 am, 12 am, 5 pm and 7 pm and the energy quantity of 2.0 *kWh* was tapped at each tapping.

Table 6.6 shows the sums of the measured energy quantities of each month in 1995. It should be noticed that there are some days missing in January, March, November and December because of operation and measurement problems.

Table 6.6 Measured monthly sum of energy quantities

Month	Solar irradiation on collector	Solar energy supplied to tank	Energy tapped from tank	Auxiliary energy supplied to tank	Energy for pump	Energy for control system	Net utilized solar energy(1)	Net utilized solar energy	Solar fraction (1)	Solar fraction
	kWh	kWh	kWh	kWh	kWh	kWh	kWh	kWh	%	%
Jan.	64	11	95	100	0.8	2.0	-5	-8	-5.3	-8.4
Feb.	157	37	210	217	2.4	3.49	-7	-13	-3.3	-6.2
Mar.	297	111	219	148	3.0	3.49	71	65	32.4	29.7
Apr.	498	181	242	108	6.2	3.74	134	124	55.4	51.2
May	676	215	248	74	7.8	3.87	174	162	70.2	65.3
June	598	209	239	70	8.3	3.74	169	157	70.7	65.7
July	770	260	250	29	9.8	3.87	221	207	88.4	82.8
Aug.	806	262	249	21	9.0	3.87	228	215	91.6	86.3
Sep.	305	116	187	89	4.4	3.12	98	90	52.4	48.1
Oct.	329	115	240	156	4.2	3.87	84	76	35.0	31.7
Nov.	34	10	56	57	0.5	0.75	-1	-2	-1.8	-3.6
Dec.	46	9	106	121	0.4	1.62	-15	-17	-14.2	-16.0
Total	4580	1536	2341	1190	56.8	37.4	1151	1057	49.2	45.2

* Missing days: January 1-15, March 13 - 15, September 26 -30, November 7-30 December 14-31.

6.3.2.3. Models used in system simulation

Collector loop

The efficiency of the collector was determined by the laboratory test in *Department of Buildings and Energy, Technical University of Denmark* [*33*]. From the test report [33] the efficiency of the collector is expressed as:

$$\eta = 0.75 - 4.85 \cdot (T_m - T_a) / G - 0.016 \cdot (T_m - T_a)^2 / G$$

Since the result from [33] is based on a glycol-water mixture working liquid, the collector efficiency model is modified by theoretical analysis, and accounts for the thermal properties of the water. The simulation program uses a linear expression for the efficiency at a temperature difference of 50 *K*. Therefore, the efficiency of the collector may be presented as:

$$\eta = 0.78 - 5.4 \cdot (T_m - T_a) / G$$

The incident angle modifier of the efficiency was determined (from [33]) as :

$$IAM(\theta) = 1 - \left(\tan(\frac{\theta}{2})\right)^{4.2}$$

Where, IAM incidence angle modifier

θ incidence angle

Storage tank

In the simulation model the tank is divided into 31 layers from the top to the bottom. The mantle starts at 0.162 *m* from the top of the tank, and ends at 0.05 *m* from the bottom of the tank. When the collector loop is in operation, the air layer in the mantle is down to 0.35 *m* from the top of the tank. The auxiliary spiral heat exchanger is situated in the tank 0.54 *m* from the top of the tank and the side loop for electric heating is connected with the mantle at 0.395 *m* and 0.74 *m* from the top of the tank.

The storage tank is originally insulated with 45 *mm* of PUR foam at the side and top wall and 20 *mm* of PUR foam at the bottom. An additional insulation layer, 0.1 *m* mineral wool, was added at the top of the tank from the middle of March 1995, because of the large heat loss from the top of the tank due to the thermal bridges caused by the connecting pipes.

6.3.2.4. Comparison of simulated and tested results

With the design parameters of the system and the calculation model introduced above, simulations are carried out for two periods to cover both a winter and a summer situation. The

two simulation periods are March 4-11, 1995 with auxiliary heating from the heat exchanger spiral, and June 6-16, 1995 with auxiliary heating from the electric heating element.

The computer model of the system is validated with measured energy and temperature data. The comparisons of the simulation results and measurements are done for the most important parameters, namely the solar energy supplied to the tank, the auxiliary energy for the electric heating element, the energy tapped from the tank, the net utilized solar energy and the temperature changes in the collector loop and storage tank.

In order to make comparisons of the simulation results to the measurements, the weather parameters, the storage room temperature, the inlet cold water temperature and the tapping flow are used as simulation inputs. Figures 6.18 - 6.21 show the solar irradiation on the collector plate and the ambient temperature during these two simulation periods.

Comparisons of measured and simulated temperatures of the fluid coming from the collector to the mantle, and from the bottom of the mantle to the collector, are shown in Figures 6.22 and 6.23. Here, the horizontal line indicates that the collector loop was in a non-operation condition. The temperature difference between the measurement and the simulation during this non-operation period is due to the fact that the temperature sensors are installed at connecting inlet and outlet pipes of the mantle. It can be seen that the simulated temperature of the fluid from the collector and the mantle shows the correct dynamic responses during the operation period.

The water temperature in the top part of the tank is one of the important parameters in system operation. Figures 6.24-6.25 show the measured and simulated tank top temperature in the two simulation periods. It appears from the Figure 6.24 that the tank top temperature varies between 49°C and 51°C during the winter period when the heat exchanger spiral was used for auxiliary heating. However, Figure 6.25 shows that the tank top temperature was varying from 40°C to 55°C during the summer period when the electric heating element was used for auxiliary heating. Such a significant temperature drop is undesirable for the comfort of the consumer. The main reason for this large variation of the tank top temperature during the summer period is the time control strategy of the heating element. During this period, the electric heating element only operated from 5 am to 11 pm every day. It can be seen that in both simulation periods the simulated and measured tank top temperatures are in good agreement.

Energy quantities such as energy tapped from storage tank, solar energy supplied to the tank and net utilized solar energy are the major interests of the system simulation. Here the net utilized solar energy is defined as the energy tapped from the storage tank minus the auxiliary energy supplied to the tank. The measured and simulated daily energy tapped from the storage tank is shown in Figures 6.26 - 6.27 and the comparison of measured and simulated energy supplied from the collector to the storage tank is shown in Figures 6.28 and 6.29. Similarly, Figures 6.30 and 6.31 illustrate the measured and calculated daily supply of auxiliary energy to the storage tank. The comparison of measured and calculated net utilized solar energy is shown in Figures 6.32-6.33. It can be seen that these simulated energy data show good agreement with the measured quantities.

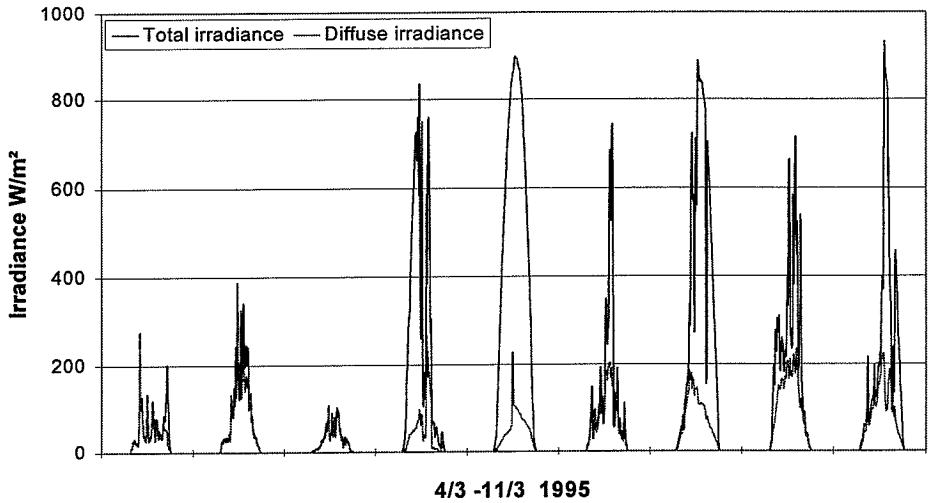

Figure 6.18 Solar irradiation on the collector (date: 4/3 -11/3 1995).

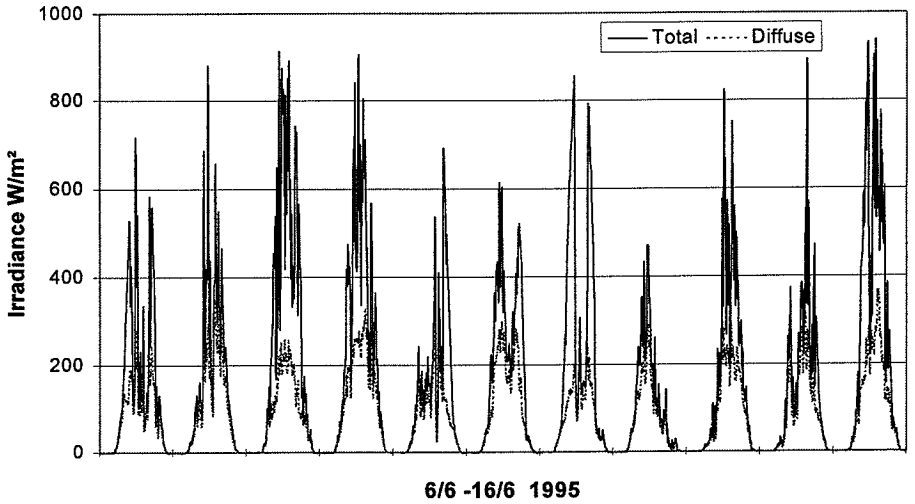

Figure 6.19 Solar irradiation on the collector (date: 6/6 -16/6 1995).

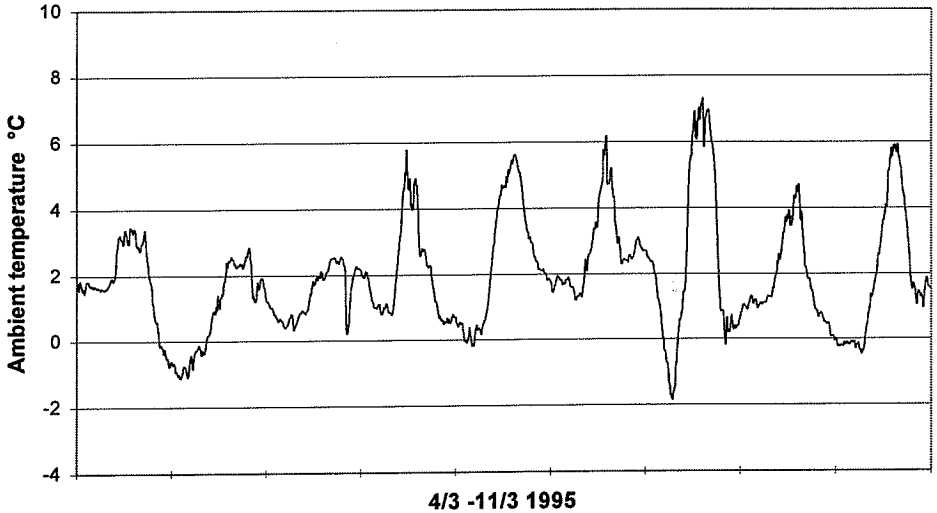

Figure 6.20 Ambient temperature (date: 4/3 - 11/3 1995).

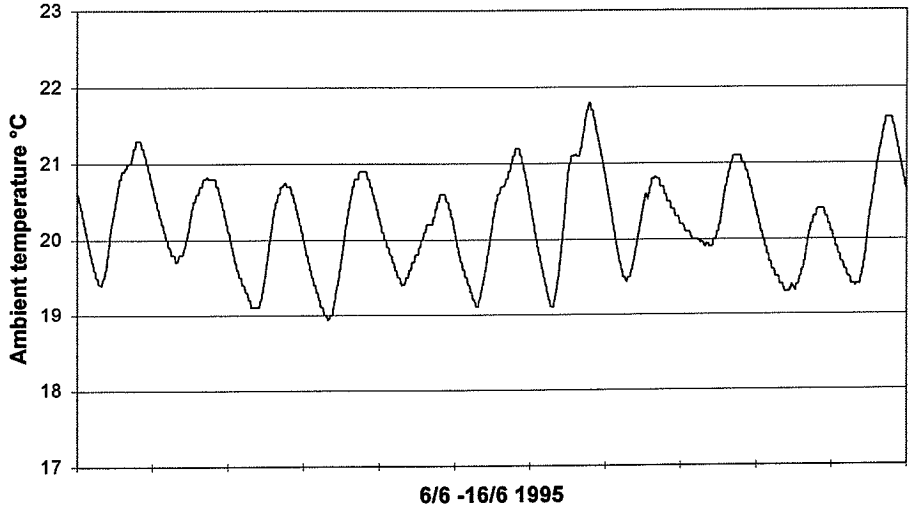

Figure 6.21 Ambient temperature (date: 6/6 - 16/6 1995).

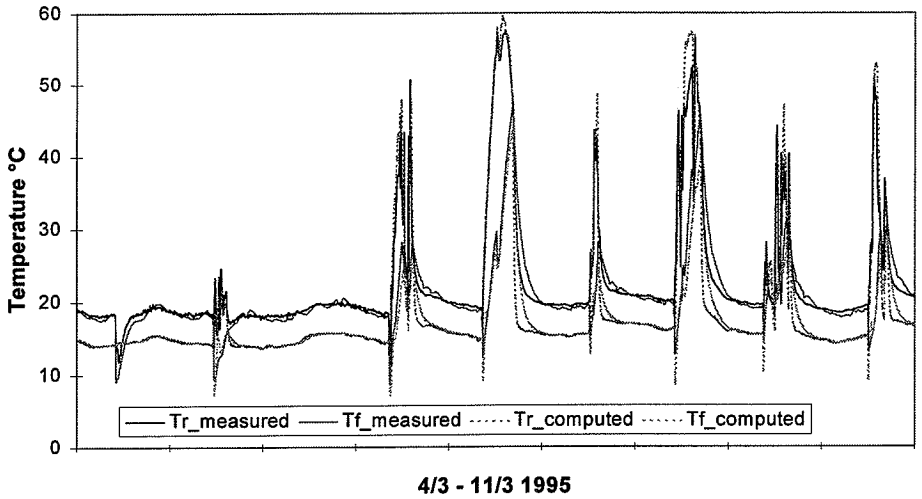

Figure 6.22 The inlet and outlet temperature of the mantle (4/3 -11/3).

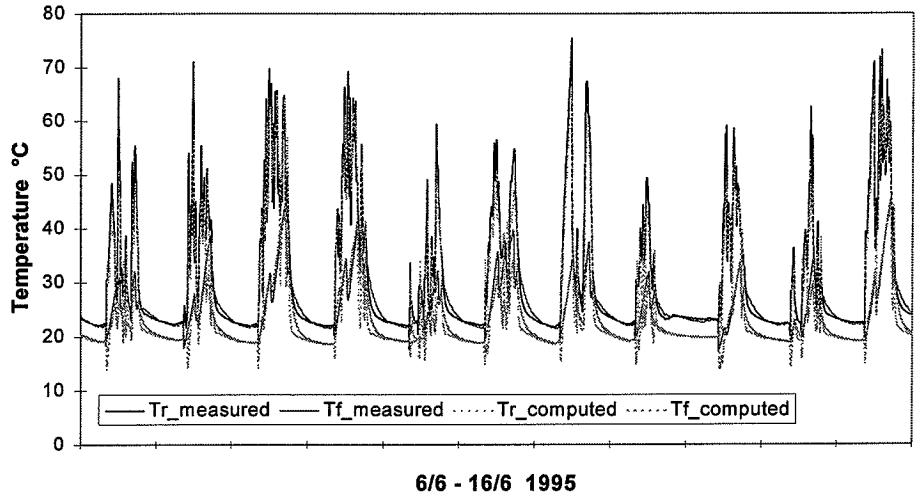

Figure 6.23 The inlet and outlet temperature of the mantle (6/6 -16/6).

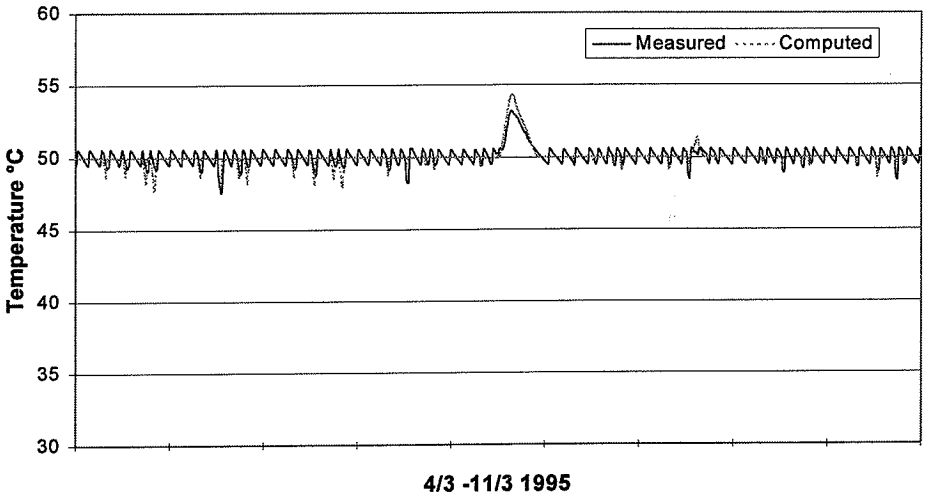

Figure 6.24 The temperature at the top of the tank (4/3 -11/3).

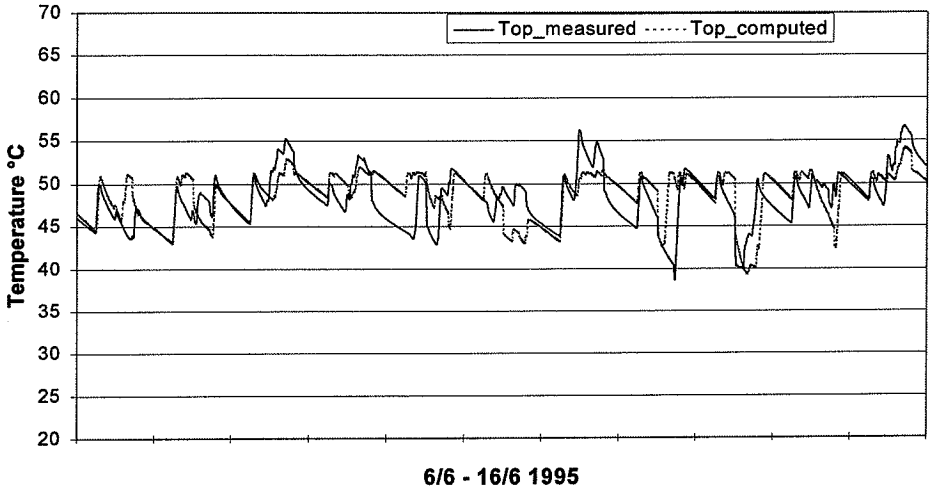

Figure 6.25 The temperature at the top of the tank (6/6 -16/6).

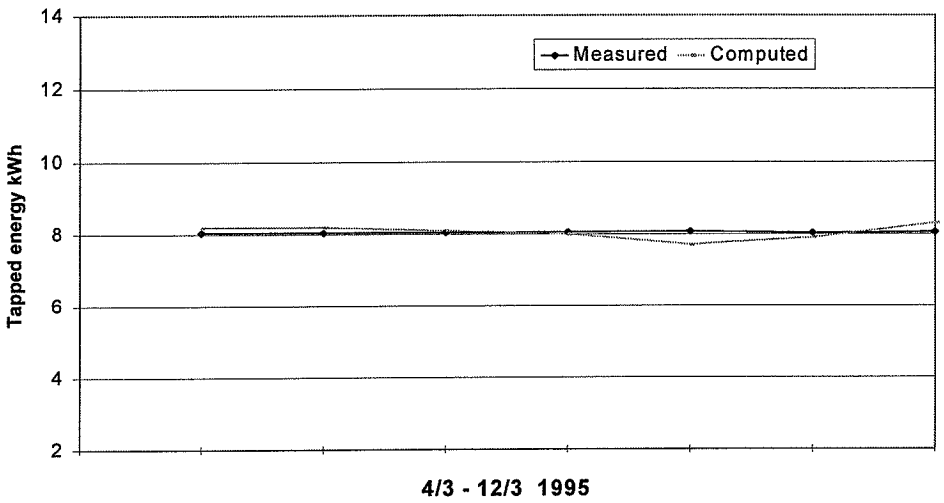

Figure 6.26 Energy tapped from the storage tank (4/3 -11/3).

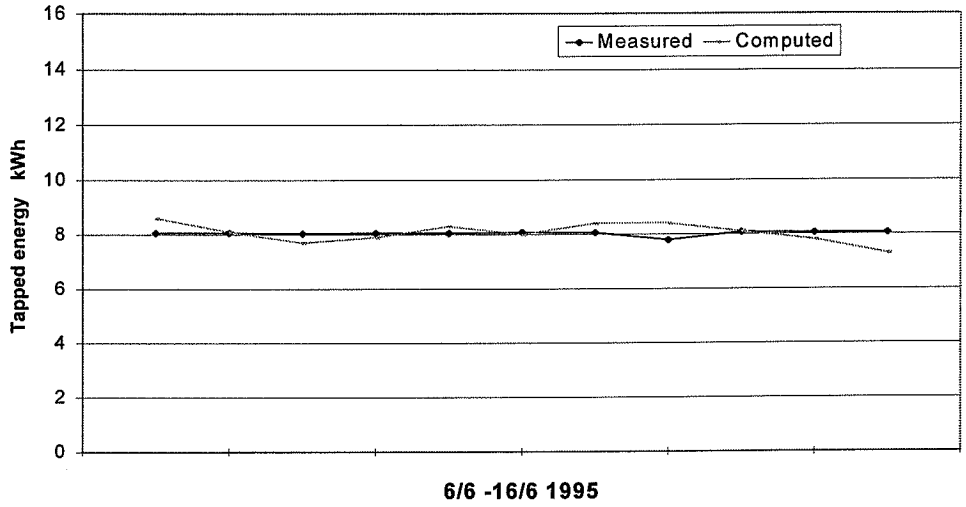

Figure 6.27 Energy tapped from the storage tank (6/6 -16/6).

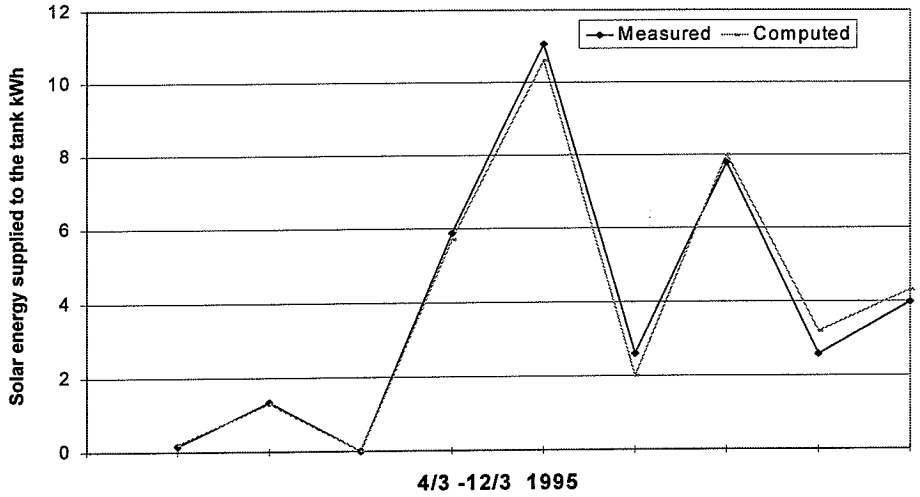

Figure 6.28 Solar energy supplied to the tank (4/3 - 11/3).

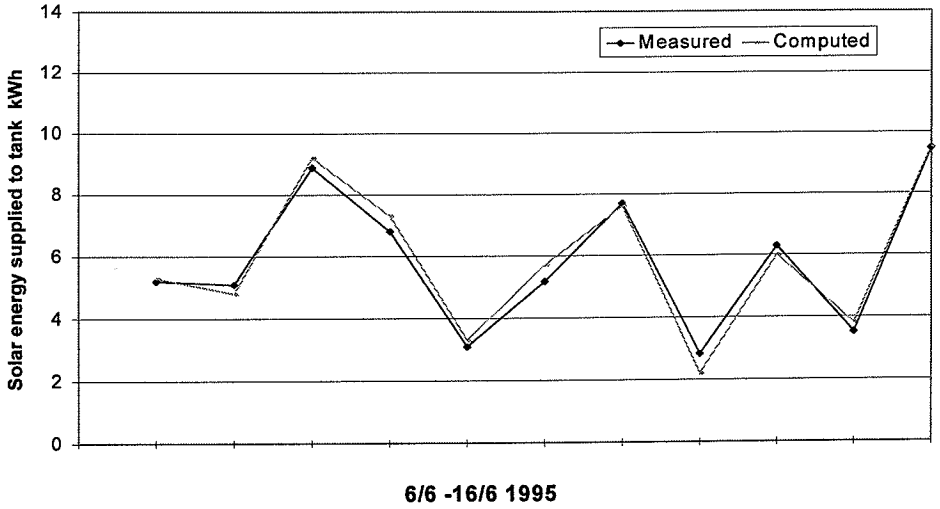

Figure 6.29 Solar energy supplied to the tank (6/6 - 16/6).

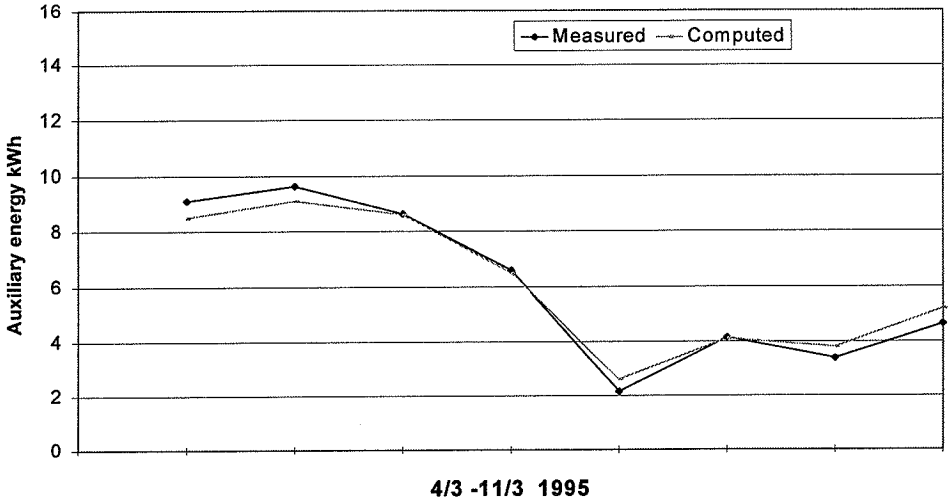

Figure 6.30 Auxiliary energy supplied to the tank (4/3 -11/3).

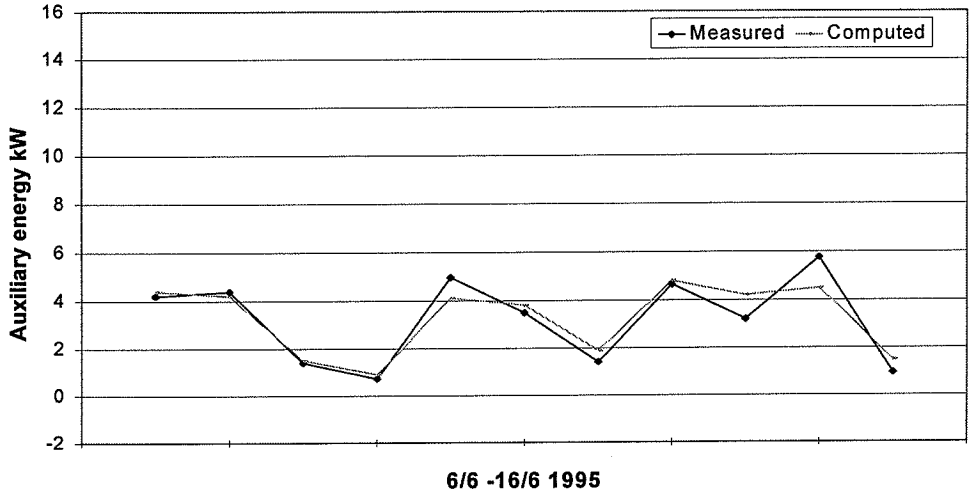

Figure 6.31 Auxiliary energy supplied to the tank (6/6 -16/6).

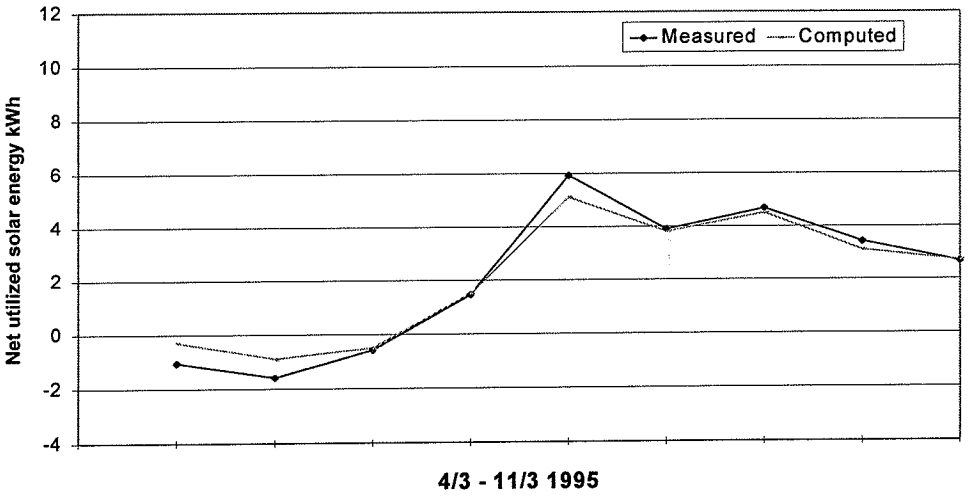

Figure 6.32 Net utilized solar energy (4/3 - 11/3).

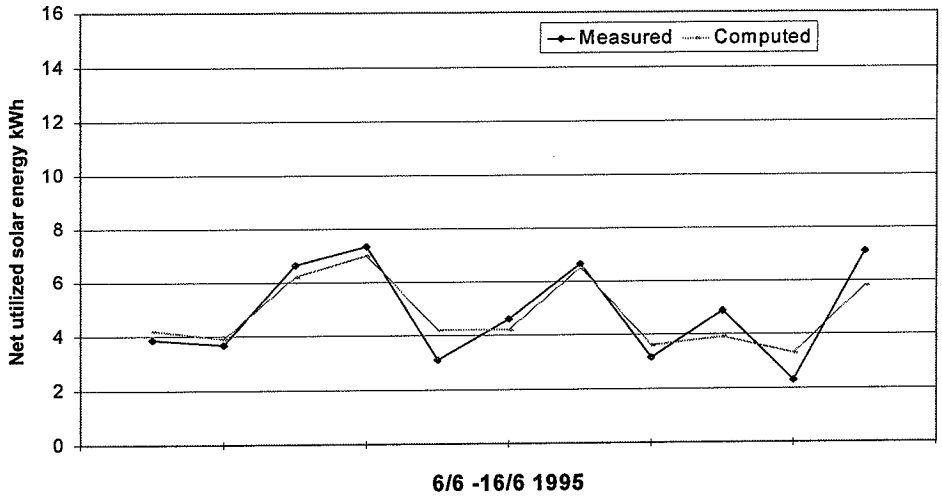

Figure 6.33 Net utilized solar energy (6/6 - 16/6).

Table 6.7 shows the sum of the energy quantities over these two simulation periods and the deviation between the simulated and measured values. It can be seen that the deviations between measured and calculated energy quantities are in a reasonable small range. According to [57], the precision of the measured energy quantities is about 5%. It is clear that the deviations are smaller than the accuracy of the measured energy quantities, and the simulation results are acceptable.

Table 6.7 Energy quantities during simulation periods

	Solar Energy to the tank (kWh)		Auxiliary energy used (kWh)		Tapped energy from tank (kWh)		Net utilized solar energy (kWh)	
	4/3-11/3	6/6-16/6	4/3-11/3	6/6-16/6	4/3-11/3	6/6-16/6	4/3-11/3	6/6-16/6
Measured	35.4	64.1	53.7	36.0	72.5	88.4	18.8	52.4
Calculated	35.3	64.7	54.0	35.8	73.0	88.6	19.0	52.8
Deviation %	-0.3	0.9	0.6	-0.6	0.7	0.2	1.0	0.8

Table 6.8 Simulated yearly thermal performance of the system

Month	Solar irradiation on collector kWh	Solar energy supplied to tank kWh	Energy tapped from tank kWh	Auxiliary energy supplied to tank kWh	Energy for pump kWh	Energy for control system kWh	Net utilized solar energy (1) kWh	Net utilized solar energy kWh	Solar fraction (1) %	Solar fraction %
Jan.	146	37	228	208	0.9	3.87	20	15	8.8	6.7
Feb.	242	69	206	154	1.3	3.49	52	47	25.2	22.9
Mar.	402	121	228	132	2.2	3.87	96	90	42.1	39.4
Apr.	591	182	221	76	3.4	3.74	145	138	65.6	62.4
May	764	236	228	38	4.1	3.87	190	182	83.3	79.8
June	730	233	221	34	4.3	3.74	187	179	84.6	81.0
July	723	237	228	29	4.5	3.87	199	190	87.3	83.6
Aug.	681	244	228	28	4.3	3.87	200	191	87.7	84.1
Sep.	474	172	221	74	3.4	3.74	147	139	66.5	63.3
Oct.	300	110	228	138	2.2	3.87	90	84	39.5	36.8
Nov.	164	51	221	183	1.1	3.74	38	33	17.2	15.0
Dec.	97	24	228	218	0.6	3.87	10	6	4.4	2.4
Total	5317	1718	2685	1313	32.2	45.6	1372	1294	51.1	48.2

6.3.2.5 Simulated yearly thermal performance

On the basis of this verified simulation model, the yearly thermal performance of the tested system was simulated under Danish weather conditions by using Danish DRY. The simulation was carried out under the following operation conditions.

- The daily hot-water consumption is 160 *l*, and the auxiliary heating element heats the water in the top of the tank to 50.5°C.
- The hot water is tapped three times a day at 7 am, 12 am and 7 pm with one third of the daily total in each tapping.
- The inlet cold water is 10°C and the room temperature is 20°C. The temperature of the tapped water is 50°C.

The calculated monthly values of solar irradiation on the collector, solar energy supplied to the storage tank, auxiliary energy from electric heating element, energy tapped from the tank, net utilized solar energy, etc. are shown in Table 6.8. Here, the net utilized solar energy is defined as the energy tapped from the storage tank minus the total energy consumption for the electric heating element, circulation pump and control system, and net utilized solar energy (1) is defined as the energy tapped from the storage tank minus the energy consumption for the electric heating element. It can be seen that the yearly solar fraction of the system may be up to 48%.

6.4 System simulation and optimization of Drain-back systems

The dynamic models of two drain-back solar DHW systems have been discussed in sections 6.2 and 6.3, based on both theoretical analyses and measurement results from the laboratory test. There are also possibilities of constructing drain-back systems in some other ways. However, these two types of design can be considered as the representatives and prototypes of most drain-back systems. In order to understand these two types of system more thoroughly and to make a possible recommendation for optimum design of these types of systems, it is necessary to perform a general investigation on the influences of design parameters on the system performance.

As mentioned before, computer simulations have proved to be a cost-effective method for the prediction of system performance. By means of a series of simulations, it will be possible to make general recommendations on the optimum design of the system.

The yearly solar fraction is one of the most important elements in solar DHW system evaluation. The optimization procedure in this study follows the orthogonal optimization process and the yearly solar fraction of the system is the main focus.

6.4.1 Basic operation conditions and assumptions

As stated previously, the thermal performance of solar DHW systems is strongly influenced by the operation conditions. In this part of the study, Denmark is chosen for the system location and therefore the Danish DRY is used as input weather data for all the simulations.

A simplified tapping program, based on the measurement results [45] for Danish conditions, is employed. In each day, a certain percentage of the daily total hot-water demand is tapped at 7 am (23%), 9 am (19%), 12 am (20%), 5 pm (18%) and 7 pm (20%).

The temperature of the storage room is assumed as 20°C throughout the year and the inlet cold-water temperature is 10°C.

Table 6.9 Basic design parameters of the reference systems

Parameters	Quantity	Unit
Solar Collector		
Area	4.0	m^2
Efficiency model	$\eta = 0.78 - 5.33 \cdot \frac{T_m - T_a}{G}$	
Heat capacity	7000	$J/m^2 K$
Tilt angle	45	°
Azimuth	0	°
Heat transfer fluid	water	
Volume content of the collector	0.86	l/m^2
Storage tank		
Volume	250	*l*
Diameter	0.45	m
Height	1.57	m
Tank material	Steel	
Thickness of the tank wall	3	mm
Electric heating element power	3000	W
Water volume over electric heating element	100	l
Thermostat temperature	50	°C
Insulation material	PUR foam	
Insulation thickness on top wall	60	mm
Insulation thickness on side wall	40	mm
Thermal conductivity of the insulation material	0.03	W/m K
Drain-back tank		
Volume	8	l
Water content (stop condition)	6	l
Heat loss coefficient	0.2	W/K
Connection pipes		
Pipe material	copper	
Inner diameter	13	mm
Outer diameter	15	mm
Length of the pipe, indoors	10	m
Length of the pipe, outdoors	1.2	m
Power of circulation pump	35	W
Control system		
Start difference	10	K
Stop difference	2	K

6.4.2 Dimension of the reference systems

Sketches of two reference systems are shown in Figure 6.1 and Figure 6.16. The reference systems are designed to supply domestic hot water for one-family use, and the daily hot-water consumption is 160 *l*. The design parameters for these two systems are shown in Table 6.9. In order to have a comparison of these two types of systems, the basic design values are chosen to be the same for both systems.

Heat exchanger

The volume of the hot-water tanks for both systems is 250 *l* and the inner diameter of the tank is 0.45 *m*. For the mantle tank, the mantle enclosing the water tank starts at 0.406 *m* from the top of the tank and ends at 0.058 *m* from the bottom. The inner diameter of the mantle is 0.486 *m*, and the total volume of the mantle enclosure is 26 *l*. For the tank with a heat exchanger spiral, a 9 *m* steel heat exchanger coil (diameter 18/20 *mm*) is used, and the heat exchanger is situated at the bottom of the tank. A volume flow rate of 0.8 *l/min* is used in the collector loop for both systems.

6.4.3 Simulation results

The influence of the design and operation parameters on the yearly solar fraction for both types of drain-back systems are shown in Figs. 6.34 - 6.47. All the simulations are based on the same operation conditions which are specified in section 6.4.1.

The yearly solar fraction as a function of the solar collector area is shown in Figure 6.34. As the collector area increases, the solar fraction of both systems increases as expected. Since the area of the collector decides how much solar irradiation can be received by a solar DHW system, the increase of the solar collector area will increase the solar energy gain as well as the solar fraction. However, Fig. 6.34 shows that the solar fraction follows a non-linear increase with the increase of collector area which indicates that the system efficiency decreases as the collector area increases. It can be seen that when the collector area changes from 8 m^2 to 10 m^2, the solar fraction is only slightly affected.

The effects of the maximum solar collector efficiency and the collector heat loss coefficient on the solar fraction are shown in Figure 6.35 and Figure 6.36. It is clear that for both types of systems, the increase of the maximum collector efficiency will cause a corresponding increase of the solar fraction and that a high heat loss coefficient of the collector will result in a low solar fraction. The simulation results also show that the solar fraction for both types of system have the same changing tendency with the change of collector efficiency.

The influence of the fluid content in the solar collector array on the solar fraction is shown in figure 6.37. It should be noticed that the fluid content of the collector has an impact not only on the thermal capacity of the collector but also on the fluid volume in the drain-back tank and the air volume in the mantle. The simulations were carried out based on the assumptions that the collector efficiency will not be influenced by the fluid content and that the thermal capacity of the collector without working fluid is the same. The volume of the separate drain-back tank is varying with the fluid content of the collector, but the mantle volume of the mantle tank keeps the same, that is, during the operation the fluid level in the mantle is

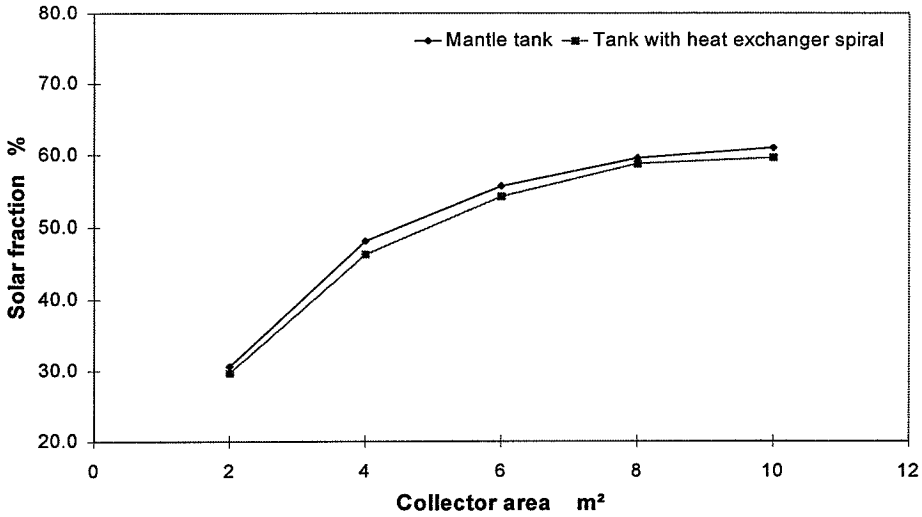

Figure 6.34 The yearly solar fraction as a function of collector area.

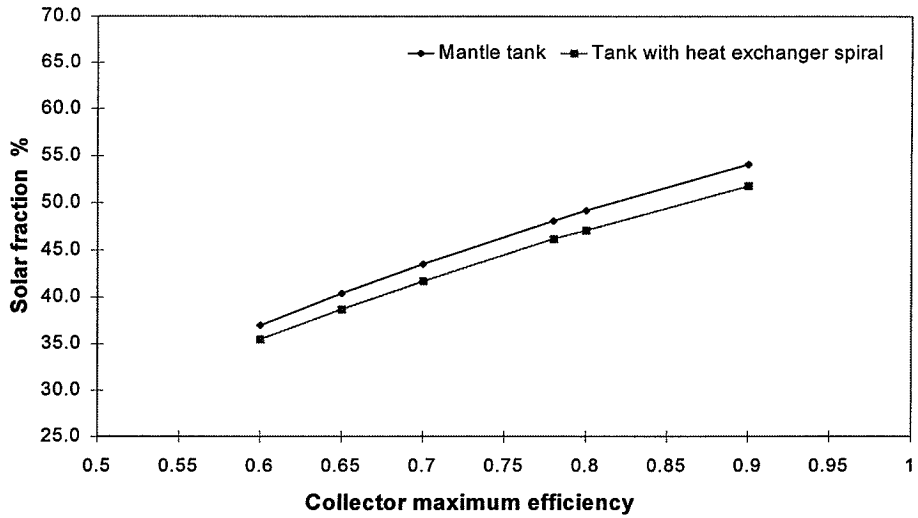

Figure 6.35 The yearly solar fraction as a function of collector maximum efficiency.

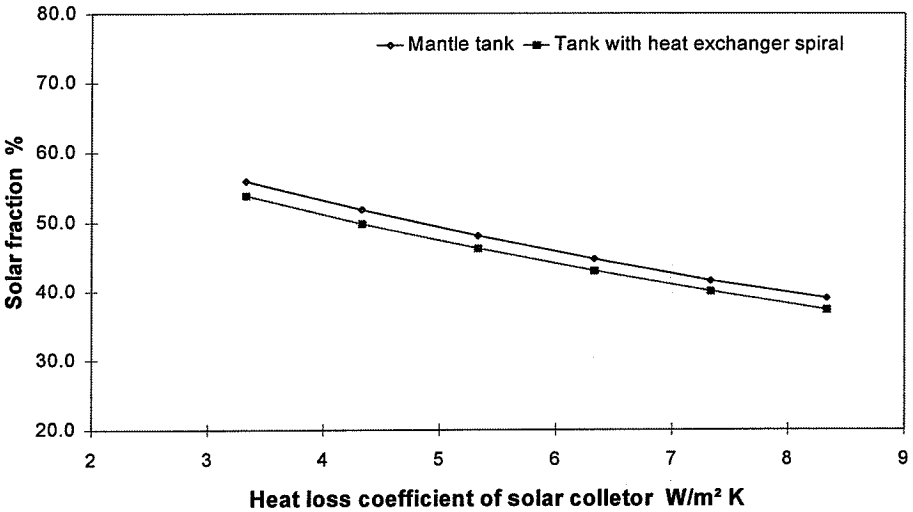

Figure 6.36 The yearly solar fraction as a function of the heat loss coefficient of the collector.

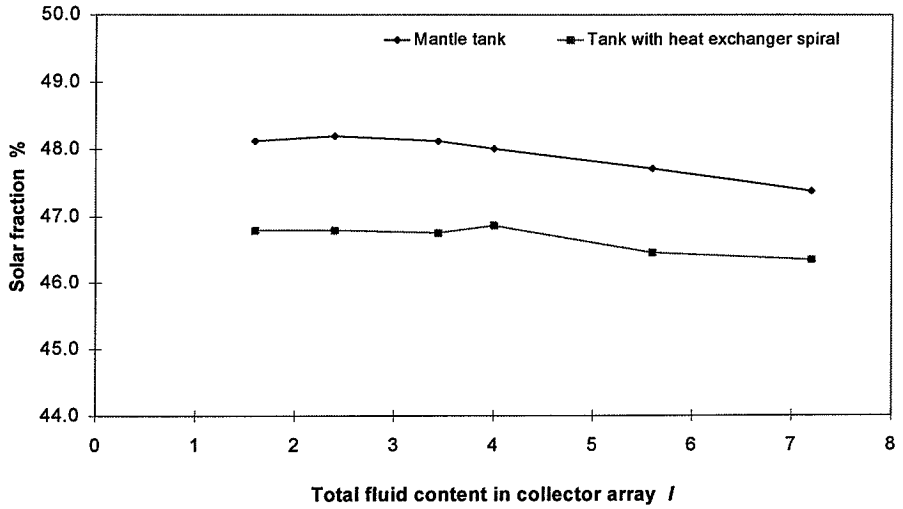

Figure 6.37 The yearly solar fraction as a function of the volume content of the collector.

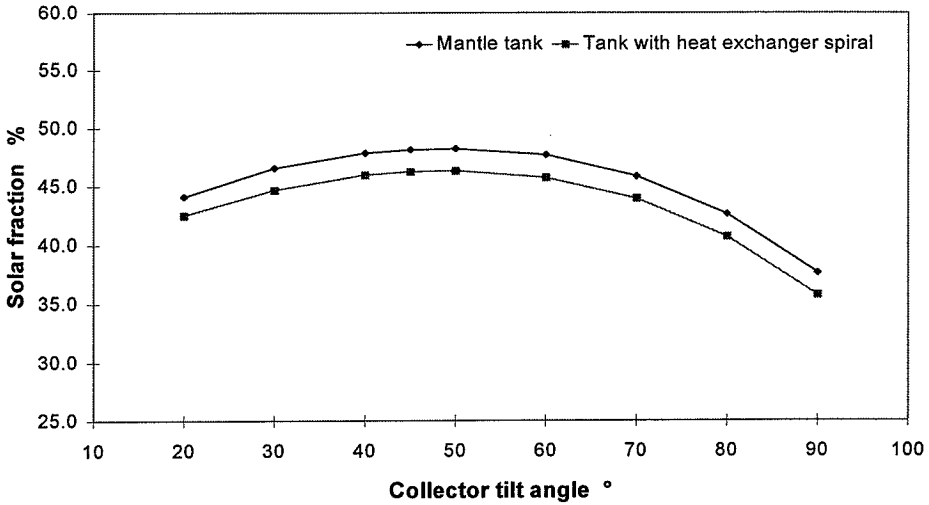

Figure 6.38 The yearly solar fraction as a function of the collector tilt angle.

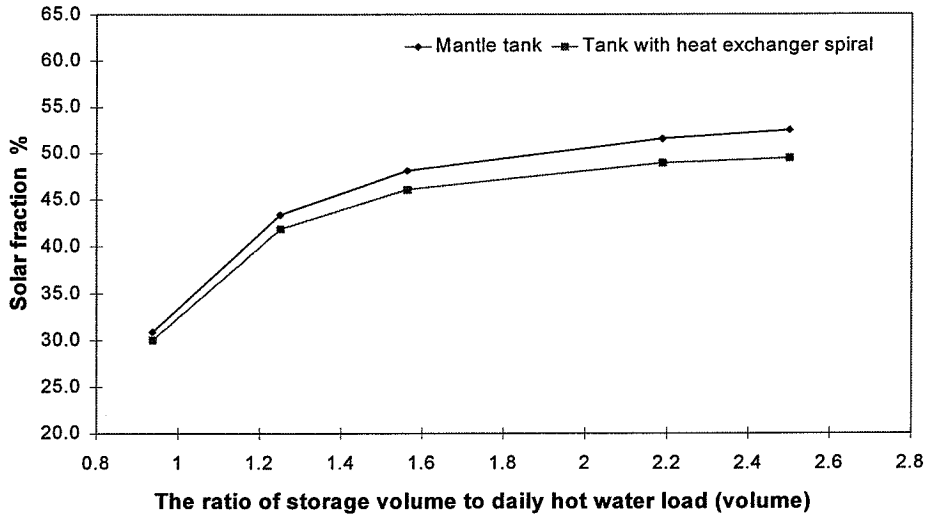

Figure 6.39 The yearly solar fraction as a function of the ratio of storage volume to daily hot-water load.

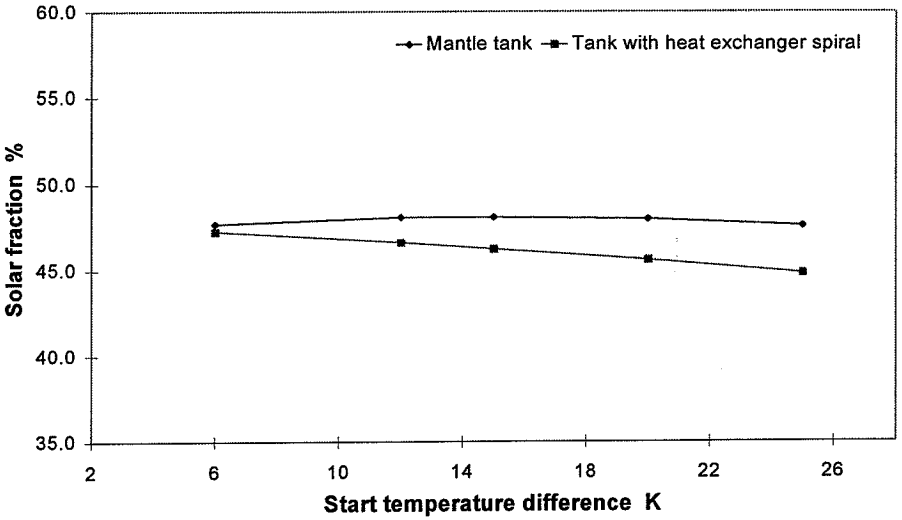

Figure 6.40 The yearly solar fraction as a function of the start temperature difference.

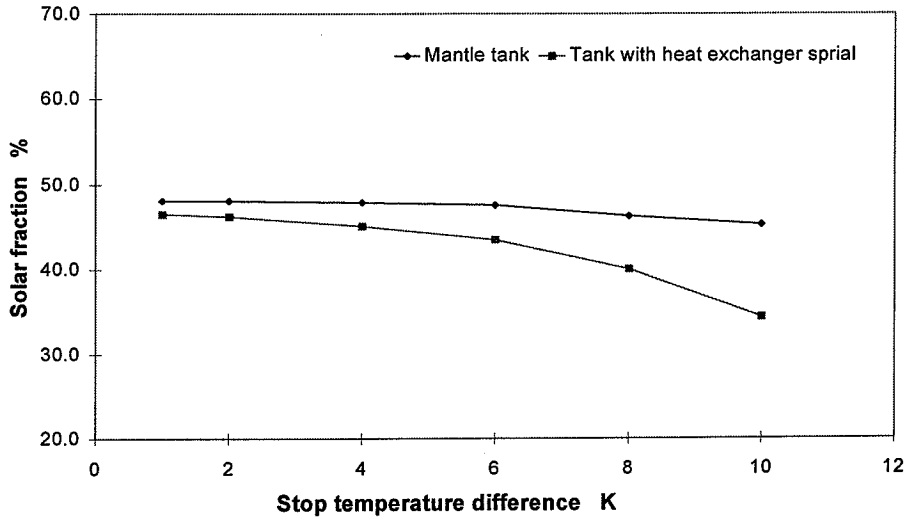

Figure 6.41 The yearly solar fraction as a function of the stop temperature difference.

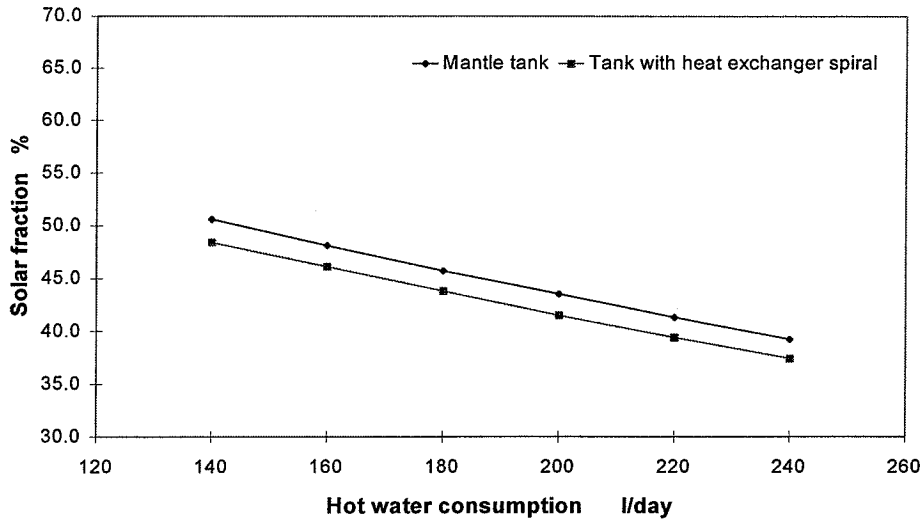

Figure 6.42 The yearly solar fraction as a function of the daily hot-water consumption.

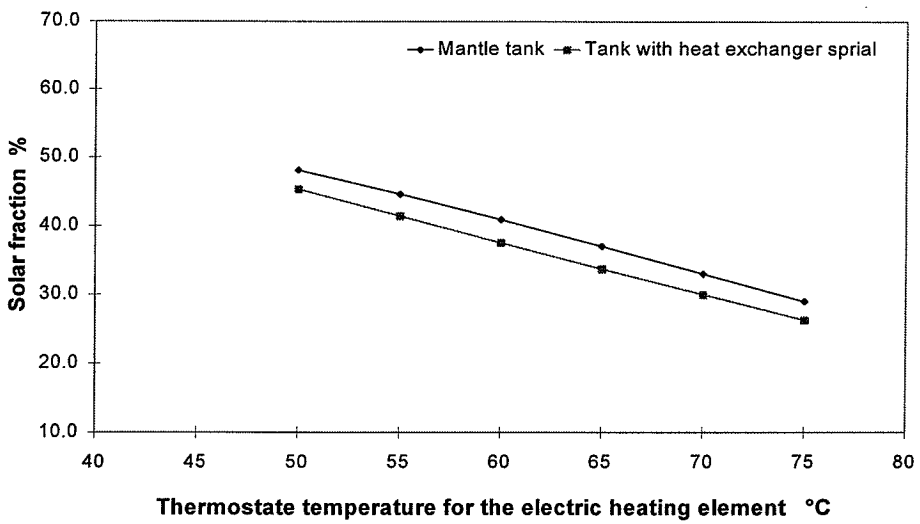

Figure 6.43 The yearly solar fraction as a function of the thermostate temperature of the elctric heating element.

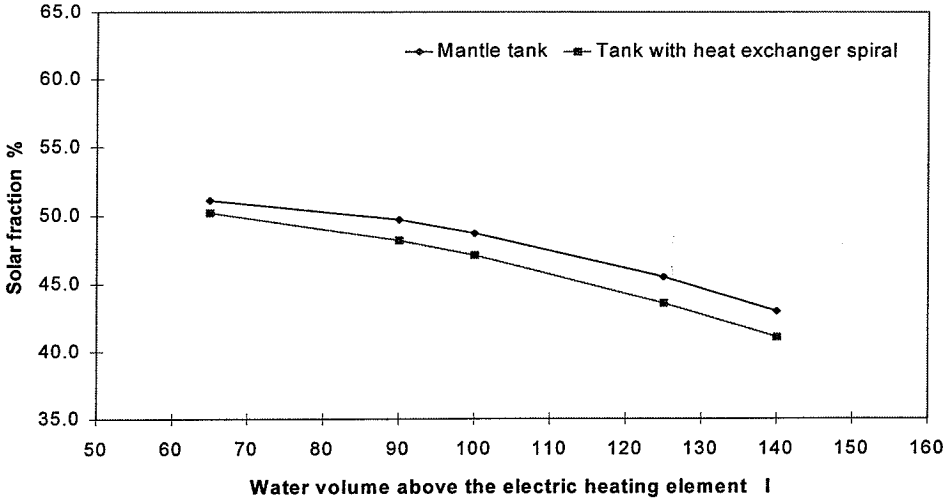

Figure 6.44 The yearly solar fraction as a function of the volume of water heated by electric heating element.

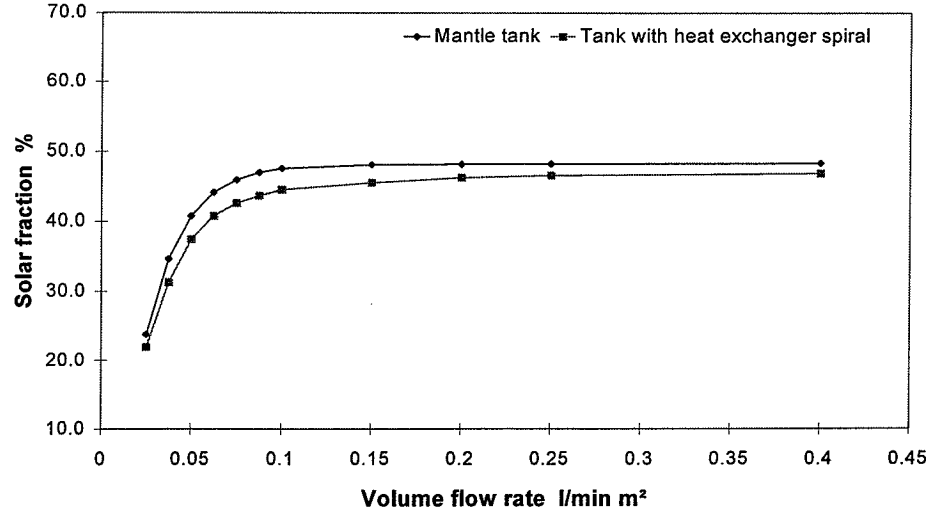

Figure 6.45 The yearly solar fraction as a function of the volume flow rate in the collector loop.

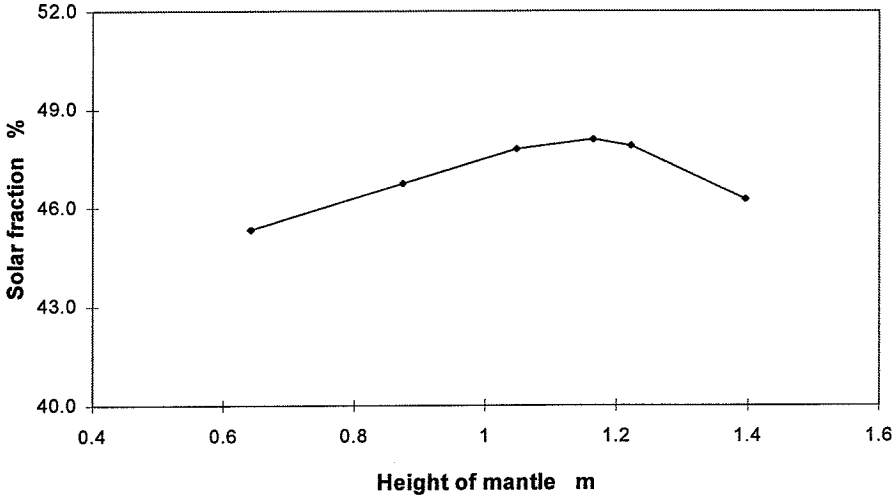

Figure 6.46 The yearly solar fraction as a function of the extent of the mantle.

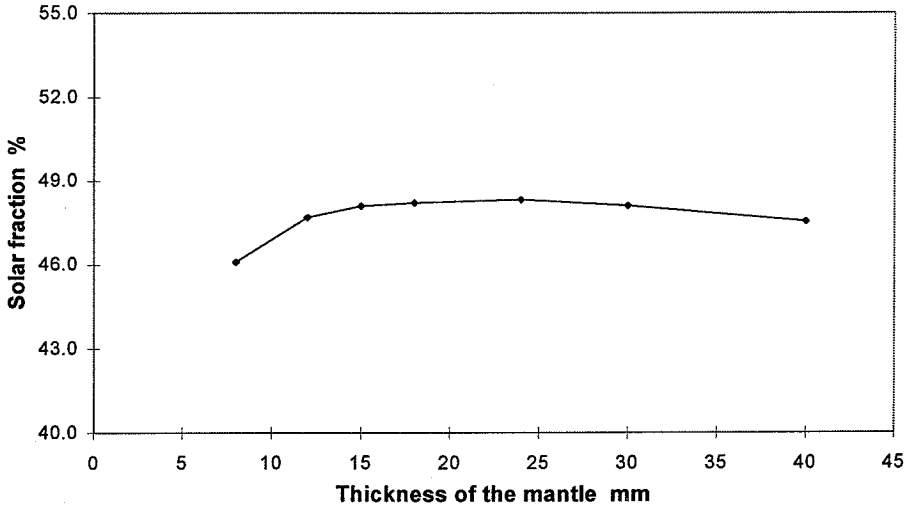

Figure 6..47 The yearly solar fraction as a function of the thickness of the mantle.

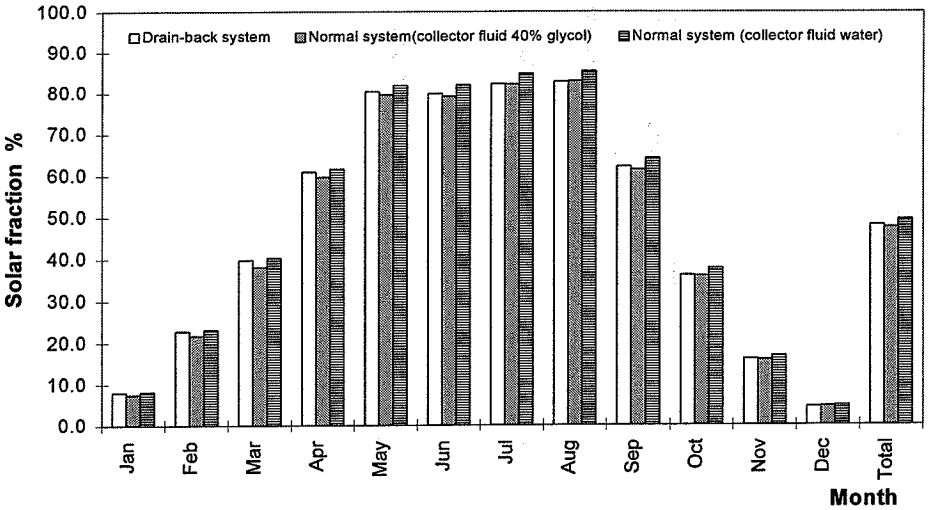

Figure 6.48 Comparison of monthly solar fraction of drain-back system and normal system with mantle tank.

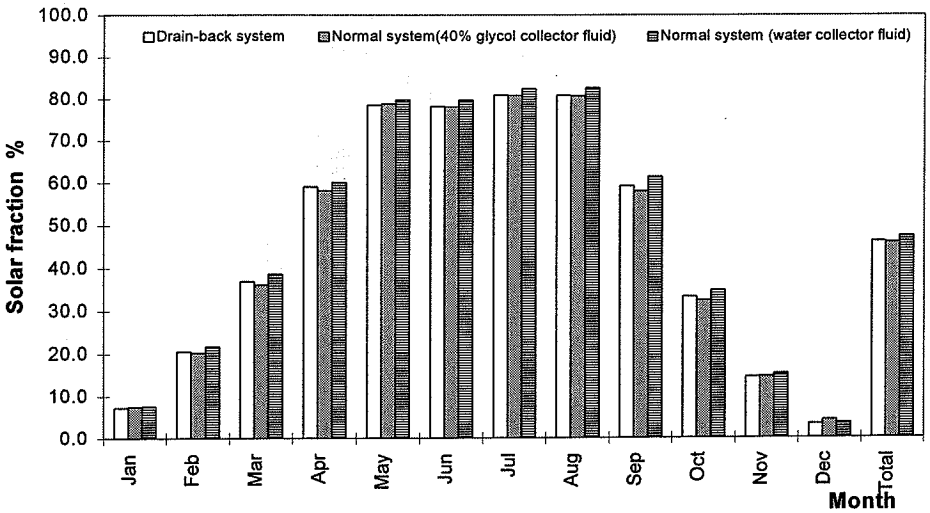

Figure 6.49 Comparison of monthly solar fraction of drain-back system and normal system with tank with built-in heat exchanger spiral.

different for different fluid content in the collector array. It can be seen from the results that the solar fraction is slightly effected when the total collector fluid content changes from 1.6 *l* to 4.0 *l* for both systems. When the fluid content in collector array is larger than 4.0 *l*, a further increase of the collector fluid content results in a corresponding decrease of the solar fraction.

Figure 6.38 shows the change in the solar fraction associated with changes of the collector tilt angle. It appears that the maximum solar fraction can be achieved with a collector tilt angle between 45°-50°, and that both types of the system have the same corresponding change with the change of the tilt angle.

The predicted effect of the ratio of storage volume to the daily hot-water load on the solar fraction is shown in Figure 6.39. In the calculation, the volume of the tank is varied by changing the height of the hot-water tank (for the mantle tank the height of the part that is covered by the mantle). For both systems, the solar fraction increases as the ratio of storage volume to daily hot-water load increases. This is because with more storage capacity, more of the daily energy demand for hot water can be met by solar energy. This increase is greater at the beginning between 1 and 1.6; a very small increase is maintained after the ratio of storage volume to daily hot-water load reaches 1.6.

The effect of the start and stop temperature difference on the solar fraction is shown in Figure 6.40 and Figure 6.41. For both systems, the solar fraction is affected only slightly when the start temperature difference changes from 6 *K* to 25 *K*. This is due to the fact that the heat capacity of the solar collector without fluid is very low, so the increase of the starting temperature difference will not cause any considerable time delay of the pump operation. Similarly, for the mantle tank system, the change of the stopping temperature difference only has a small influence on the solar fraction. But for the system with spiral heat exchanger tank, the increase of the stopping temperature difference results in a rapid decrease of the solar fraction. One of the reasons for this different reaction in the two types of system is the design of the drain-back tank. When the collector loop operation stops, the temperature of the fluid which drains back to the drain-back tank is still higher than the bottom temperature of the tank. Therefore as the stopping temperature increases, the energy stored in the drain-back tank will increase. For a system with a separate drain-back tank, the energy stored in the drain-back tank will be dissipated as heat loss and a small stopping temperature difference makes it possible to minimize the energy loss. However, that effect will not influence mantle tank systems, simply because the drain-back tank is integrated with the mantle.

The yearly solar fraction as a function of the daily hot-water load is shown in Figure 6.42. As the daily hot-water load increases, the solar fraction of both systems decreases. This is due to the fact that the basic daily energy consumption for hot water increases more than the solar energy gains from the hot-water load.

Figure 6.43 shows the effect of the thermostat temperature of the electric heating element on the solar fraction. As expected, a high thermostat temperature will cause a low solar fraction. This is because a high temperature in the tank results in a large heat loss and high collector inlet temperature which leads to a low collector efficiency.

The effect of the location of the auxiliary heater on the solar fraction is shown in Figure 6.44. As expected, high solar fraction occurs when the auxiliary heater is positioned high in the tank. The reduction in the solar fraction is slower when the volume of the water above the electric heater increases from 80 *l* to 100 *l*, then from 100 *l* onward it is reduced. This is because the increase of the electric heating volume in the storage tank results in a large heat loss and high temperature level in the lower part of the tank which will further influence the collector inlet temperature and collector efficiency.

The effect of the volume flow rate in the collector loop on the solar fraction is substantial for both systems, as shown in Figure 6.45. The simulations were based on the assumption that the collector efficiency is not influenced by the flow rate. An increase in the flow rate starting from 0.1 $l/m^2 \cdot min$ results for both systems in a rapid increase in solar fraction at the beginning. For the mantle tank system, a maximum solar fraction can be achieved when the volume flow rate is between 0.15 and 0.2 $l/m^2 \cdot min$, and only a very slight influence was found with a flow rate larger than 0.2 $l/m^2 \cdot min$. For the system with a heat exchanger spiral tank, a small increase of solar fraction is recorded when the flow rate is larger than 0.2 $l/m^2 \cdot min$. The same results were observed by Furbo [23] for normal systems. The reason is that as the flow rate increases, the heat exchange capacity rate increases.

An investigation of the effect of the mantle height on the solar fraction was carried out as well. Figure 6.46 shows the solar fraction as a function of the mantle extent. The bottom of the mantle is maintained at the same place in the simulations, so the variation in the extent of the mantle is achieved by changing the location of the mantle top. An increase of mantle height starting from 0.62 *m* from the bottom of the hot water tank results in a steady increase in the solar fraction. The maximum value of solar fraction is observed with the mantle height at 1.17 *m* from the bottom of the tank. Then, a rapid decrease is recorded with the increase of the mantle height. Since the electric heater is situated at the level of 0.94 *m* from the bottom of the tank, this result indicates that the mantle should partly cover the electric heating part of the tank. Further investigation shows that the fluid level in the mantle during the operation time is about 0.93 *m* from the bottom of the tank with a mantle height of 1.17 *m*. As the mantle height is over 1.17 m, the fluid level in the mantle during operation is over the height of the electric heating element, and a decrease of solar fraction is observed. This result indicates that the optimum mantle height should take the drain-back fluid volume into account and the fluid level in the mantle during operation time should be a bit lower than the electric heater level.

The predicted effect of the thickness of the mantle on the solar fraction is shown in Figure 6.47. An increase of the thickness starting from 8 *mm* results in a rapid increase of the solar fraction at the beginning, when the thickness changes from about 8 to 15 *mm*, whereas the solar fraction is affected only very slightly when the mantle thickness increases further from 15 *mm* to 30 *mm*. Even further increase of the thickness of the mantle results in a slight decrease of solar fraction. For a normal DHW system with mantle tank, different results were reported by Furbo [23], where the thickness of the mantle does not have a particular influence on the thermal performance. The reason for the different influence on drain-back systems is that the fluid level in the mantle during operation changes with the variation of the mantle thickness. With the mantle thickness of 8 *mm*, during operation the fluid level in the mantle

drops to 0.65 *m* from the bottom of the tank. Therefore, the solar fraction change caused by mantle thickness also comes from the fluid level change in the mantle.

Simulations were also carried out to investigate the effect of different system designs and collector fluids on the solar fraction. Figure 6.48 shows the monthly solar fraction of three mantle tank systems with the same basic design. All the design parameters for these three systems are the same as shown in Table 6.9, except the collector fluid type and the drain-back operation. Two types of collector fluid are used in two normal designed systems, namely a 40% glycol-water mixture and pure water. Since the collector efficiency is influenced by the type of collector fluid, different collector efficiencies for using water or glycol-water mixture fluid are used in the simulations. Based on measurements and theoretical calculations, the collector efficiencies that were used for the simulations were $\eta = 0.75 - 5.5 \cdot (T_m - T_a)/G$ for the collector with glycol-water mixture fluid and $\eta = 0.78 - 5.33 \cdot (T_m - T_a)/G$ for the collector using water as working fluid. According to the report of Thomsen 1997 [61], the flow rate in the collector loop is a function of fluid temperature with a certain pump power, and the degree of flow rate change is largely dependent on the thermal property of the fluid. Since the flow rate change will influence the thermal performance of the system, the different changing patterns of the flow rate by using different collector fluids should also be taken into account. Based on [61], the flow rate in the collector loop was set constant for the systems using water as working fluid. However, the flow rate as a function of the collector temperature was used in the simulation for the system using the glycol-water mixture as a working liquid; this function can be presented as V = 0.027 T - 0.04. Here V (*l/min*) is the volume flow rate and T(°*C*) is the outlet temperature of the collector.

From Fig. 6.48, it is clear that normal systems using water as collector fluids show a high solar fraction throughout the year. The drain-back system achieves a slightly higher solar fraction than the normal system using glycol as a collector fluid, but compared to normal systems using water as a collector fluid, the drain-back system ends up with a relatively low solar fraction. From these results it can be seen that it is the difference in the thermal properties of water and glycol-water mixture that makes the major contribution to the advantage of using drain-back systems. It should be noticed that the reason for the difference in the solar fraction between drain-back systems and normal systems with water collector fluid could be that the fluid in the mantle is working at different levels.

Similarly, Figure 6.49 shows the monthly solar fraction of three systems with a built-in heat exchanger spiral tank. One of the systems is a drain-back design and the other two are normal systems. Glycol-water mixture and water are used as collector fluid in the two latter systems. All three systems have the same basic design as shown in Table 6.9. It is obvious that normal systems using water as a collector fluid show the best performance, and that the solar fraction change among the systems follows the same rules as for a mantle tank system. The reason for the decrease of the solar fraction for drain-back systems as compared to normal systems is the heat dissipation from the drain-back tank.

It should also be pointed out that water used as a collector fluid in normal systems is not realistic. The simulations carried out here are only for theoretical study.

6.5. Conclusion and discussion

Dynamic models of drain-back solar DHW systems with both built-in heat exchanger spiral tank and mantle tank have been developed. The models are verified by using simulated temperatures and energy quantities against measured results from experiments carried out in the laboratory.

The simulations were carried out for two test systems by applying the measured input data. The results show that the simulated and measured temperatures and energy quantities have good agreement. The deviations between simulated and measured energy quantities are small and acceptable. The model verification results illustrate that the system model is applicable for system design and analysis.

Based on the verified models, the system evaluation and the optimization of design parameters were performed for both types of drain-back system under Danish geography and weather conditions. This was done by means of a number of group simulations. The yearly solar fraction was chosen as the critical parameter of the evaluation and optimization process.

For both types of systems, the solar fraction can be increased by increasing the collector area. However, from a certain point on, the increase of the collector area results in a rapid decrease of the system efficiency. Therefore, the optimum value of the collector area should also take the economy into account.

The simulation results show that an increase of the collector efficiency will result in a steady increase of the solar fraction, and a high heat loss coefficient of the collector will result in a low solar fraction. The fluid content of the collector also has an effect on the solar fraction. A collector with small fluid content will result in good system performance.

The maximum yearly solar fraction can be achieved with the collector tilt angle between 45°-50° under Danish conditions. The ratio of storage volume to daily hot water load has a considerable influence on the solar fraction. The optimum ratio of storage volume to daily hot water load is found to be about 1.6 for both types of systems. The system evaluation shows that the starting and stopping temperature differences have no significant influence on the drain-back system with a mantle tank, but that the stopping temperature difference has a strong effect on the system with a built-in heat exchanger tank. This indicates that for drain-back systems with a separate drain-back tank, the stopping temperature difference should be set to not more than 2 *K*.

The effect of the daily hot-water load on the yearly solar fraction shows that the larger the daily hot-water load is, the lower the solar fraction. The simulation results also show that it is important to have a suitable position for the auxiliary heating element. An increase of the tank volume heated by the electric heater will result in a reduction of the solar fraction. Under the condition of fulfilling the requirements of the consumer, the volume of the water being heated by the electric heating element should be as small as possible.

The influence of the volume flow rate in the collector loop is significant. It was observed that the optimum flow rate for a drain-back system with mantle tank is about 0.15 $l/min \cdot m^2$. For a

system with a built-in heat exchanger spiral tank, the flow rate should not be less than 0.25 $l/min \cdot m^2$.

For a drain-back system with a mantle tank, the design of the mantle has a great impact on the solar fraction. Both mantle height and thickness design should consider the influence of the level of heat transfer fluid in the mantle. Therefore, the mantle should be designed in such a way that the fluid level in the mantle during the operation is a bit below the level of the electric heating element.

The comparison of drain-back systems with normal systems illustrates that systems with drain-back design achieve a slightly improved solar fraction. Further investigation shows that it is the different thermal properties of the heat transfer fluid that make the major contribution to this improvement.

Chapter 7

Impact of the time scale of input climatic data on system simulation

7.1 Introduction

As described in chapter 2, the operation of solar energy systems depends upon the climatic variables such as solar radiation, ambient temperature, relative humidity and wind speed. For both small and large time scales, these variables are irregular functions of time and locations. It is the irregularity of the climate that complicates the theoretical analysis of solar DHW systems.

For long-term system simulation, the commonly used input climatic data are hourly mean values such as the data from TRY or DRY. This is mainly due to the fact that long-period, short-term weather data, such as five or ten-minute measurements, are not available in most cases. However, the variations of the irradiance, due to the clouds, are not taken into consideration when the hourly mean values are used. Therefore, using the hourly data for system simulation may, to some degree, lead to an error on the operation time and thermal performance for the active solar DHW systems. This is so particularly in areas with maritime climate, where the weather may often change greatly within one hour during some seasons.

In 1991, Furbo and Carlsson [23] carried out an investigation on the influence of input weather data on the simulated thermal performance of small low-flow DHW systems. The calculation was based on a short period (6 weeks) of 2-minute measurements, and 2 to 60 minute average values of the weather data were used in the simulations. It was found that as the time scale for input weather data reduces from 60 minutes to 2 minutes, the net utilized solar energy increases steadily.

To investigate the influence of the time scale of input weather data on the result of long-term system simulation, it is necessary to perform a further study on a yearly basis. In this study, the 10-minute climatic data that was measured at the Department of Buildings and Energy, Technical University of Denmark, during 1996 was employed. The weather data were averaged for periods of different duration: 10, 20, 30, and 60 minutes. Simulations were carried out based on these different time scales of input weather data.

Simulations were performed for two types of normal active solar DHW systems with both pre-heating tank design and combi tank design. The influence on yearly net utilized solar energy and solar fraction is of major interest.

7.2 Ten-minute climatic data file for Denmark 1996

To investigate the effect of different time scales of the input weather data on the result of a simulation, short-term (5 to 10 minutes) measurements of climatic data are needed. Here, a ten-minute climatic data file was formulated from 10-minute measurements in Denmark, 1996.

The data base for the Climatic Data File 1996 (CDF96') is the 10-minute measurements from a test facility of the Department of Buildings and Energy at the Technical University of Denmark during the period of 1996. The weather parameters which were originally recorded are ambient temperature, total radiation, and diffuse radiation on a south-faced surface with a tilt angle of 45°. Since a large amount of the measurements is missing in the period from January to May 1996, measurements on a horizontal surface from a nearby test station were used as replacement. Therefore, from January to May the radiation data in CDF96' were converted from the measurements with the horizontal surface.

A checking procedure was performed and used for the original data. Short periods with data missing were found on many days, but in most cases these missing data periods are less than an hour. In these cases, the neighboring data was used to fill up the missing period. A few whole days of the measurements were missing in the months of August and September. For these few days, the measurements from the neighboring day were employed.

The weather parameters that are included in the CDF96' are ambient temperature and solar radiation on a south faced surface with a tilt angle of 45°. The solar radiation data include the total, direct and diffuse radiation. Among these three parameters, total radiation and diffuse radiation are taken from real measurements.

7.3 Comparison of CDF96' to Danish TRY and DRY

Danish TRY and DRY, which have been introduced in chapter 2, are formulated on a long-term (15-30 years) basis, and it is believed that the weather data from TRY or DRY can present the typical weather conditions in Denmark. In order to make an evaluation on the quality of CDF96', a comparison of the monthly solar radiation and mean ambient temperature from TRY, DRY and CDF96' is carried out. Table 7.1 shows the monthly total radiation on a south facing surface with 45° tilt, and the ambient temperature from these three climatic data files. The radiation data from TRY and DRY were converted from the radiation on a horizontal surface.

From Table 7.1, it can be seen that the solar radiation data from CDF96' are relatively low in January, February and May as compared to TRY and DRY data. On the other hand, the radiation in August and September is relatively high in 1996. The monthly mean ambient temperature during the winter period was 1.5 K - 3 K lower for CDF96' than the data from TRY or DRY, but during the months from April to November the temperature is similar to the TRY or DRY data. The yearly total radiation on a south facing surface with 45° tilt was found to be 1108.5 kWh/m^2 from CDF96' and 1161.9 kWh/m^2 from DRY.

Table 7.1 Monthly total radiation on a south facing 45° tilted surface and mean ambient temperature from TRY, DRY and CDF96'

Period	Solar radiation (kWh/m^2)			Mean ambient temperature °C		
	TRY	DRY	96'CDF	TRY	DRY	CDF96'
Jan	26.9	32.3	16.7	-0.6	-0.5	-2.1
Feb	57.8	53.1	36.3	-1.1	-1.1	-3.8
Mar	75.2	87.9	85.0	2.6	1.7	-0.9
Apr	134.6	128.7	150.9	6.6	5.6	6.5
May	157.6	168.1	105.4	10.6	11.3	8.6
Jun	179.3	159.0	142.8	15.7	14.3	13.2
Jul	158.1	157.1	153.9	16.4	16.7	14.6
Aug	150.8	149.5	168.0	16.7	16.2	17.2
Sep	107.7	103.3	125.5	13.7	12.5	10.8
Oct	68.3	65.8	64.5	9.2	9.1	9.0
Nov	38.6	36.0	30.0	5.0	4.8	4.0
Dec	34.4	21.3	29.7	1.7	1.5	-1.6
Year	1189.0	1161.9	1108.5	8.1	7.7	6.3

7.4 Influence of the time scale of input weather data on simulation results

Simulations were carried out for two reference solar DHW systems under different operation conditions to investigate the influence of the time scale of input weather data on the calculated thermal performance. The weather data from CDF96' were averaged for periods with different duration: 10, 20, 30, 60 minutes. For each system and operation design a group of simulations were carried out by using these weather data with a different average time scale.

7.4.1 Reference systems

Two reference solar DHW systems with different tank designs were chosen for the investigations. They are a system with a built-in heat exchanger spiral tank and one with a mantle tank. Low-flow operation was used in the mantle tank system, and the volume-flow rate in the collector loop was set as 0.8 *l/min.* For the system with the built-in heat exchanger spiral tank a volume-flow rate of 4 *l/min.* was employed.

Basically, the reference systems were designed as one-family systems and a daily hot-water (50°C) load of 160 *l* is assumed. The inlet cold water temperature is set as 10 °C throughout the year. A simplified tapping program was used in the simulations. The hot water was tapped three times a day at 7 am, 12 am, and 7 pm, and one third of the daily total hot-water load was tapped in each tapping. The main design parameters of these two systems are shown in Tables 7.2 and 7.3.

Table 7.2 Basic design parameters of the reference systems

Parameter	Quantity	Unit
Solar collector		
Area	4.0	m^2
Efficiency model	$\eta = 0.75 - 5.4 \frac{T_m - T_a}{G}$	
Heat capacity	7000	$J/m^2 K$
Tilt angle	45	°
Azimuth	0	°
Pipe in collector loop		
Pipe material	copper	
Inner diameter	13	mm
Outer diameter	15	mm
Insulation material	PUR foam	
Insulation thickness	10	mm
Length of the pipe from tank (indoor)	3.5	m
Length of the pipe from tank (outdoor)	1.5	m
Length of the pipe return to tank (outdoor)	1.5	m
Length of the pipe return to tank (outdoor)	3.5	m
Power of circulation pump	35	W
Control system		
Start difference (low flow system)	5	K
Stop difference (low flow system)	2	K
Start difference	5	K
Stop difference	0.4	K

Table 7.3 Design parameters of tanks

Parameter	Mantle tank		Tank with heat exchanger spiral	
Tank material	St 37-2		St 37-2	
Volume	192	l	192	l
Height/diameter	1020/500	mm	1020/500	mm
wall thickness	4	mm	4	mm
Mantle				
Volume	8	l		
Height/diameter	463/530	mm		
wall thickness	4	mm		
Heat exchanger spiral				
material			St 37-2	
diameter			1/2''	
length			12	m
Volume of hot water above electrical heating element	96	l	97	l
Insulation				
Insulation material	PUR foam		PUR foam	
thickness of insulation	50	mm	50	mm

7.4.2 Simulation results

Simulations are first carried out for the system with a mantle tank, both as a pre-heating tank and as a combi-tank, and the results are shown in Table 7.4. It is clear that the time scale of input weather data has an impact on the simulation results. As the time scale increases, the net utilized solar energy reduces constantly for both the pre-heating and the combi tank design. Here, the net utilized solar energy is defined as the energy tapped from the storage tank minus the total energy consumption for electric heating element and circulation pump. On a yearly basis, the difference of the net utilized solar energy between using 10 min. and 60 min. input weather data are 16.8 *kWh* for the pre-heating system, and 21.3 *kWh* for the combi tank system. Figure 7.1 shows the extra solar fraction achieved on a monthly basis by decreasing the time scale of the input weather data from 60 min. to 10 min. Here, the extra solar fraction is defined as the ratio of the increase of net utilized solar energy by using 10 min input water data instead of 60 min to the energy tapped from the tank. It can be seen that the influence is relatively strong on the combi tank system and the maximum extra solar fraction of 1.3% was observed in the month of September. The yearly extra solar fraction gain was found to be 0.79% for the combi tank system and 0.62% for the pre-heating system.

Table 7.4 Calculated net utilized solar energy for a mantle tank system (CDF96' weather data)

Period	Net utilized solar energy (kWh) (pre-heating tank)				Net utilized solar energy (kWh) (combi-tank)			
	10 min	20 min	30 min	60 min	10 min	20 min	30 min	60 min
Jan	26.8	26.7	26.6	26.2	-2.2	-2.3	-2.4	-2.9
Feb	42.6	42.4	42.2	41.7	18.1	17.9	17.8	17.1
Mar	100.8	100.5	100.3	99.4	70.3	70.1	69.7	68.7
Apr	173.9	173.5	173.3	172.5	152.1	151.7	151.4	150.1
May	129.8	129.6	129.2	128.2	96.8	96.5	96.1	94.8
Jun	178.9	178.7	178.3	177.4	152.2	151.8	151.4	150.3
Jul	189.9	189.6	189.2	188.4	168.0	167.5	167.0	165.8
Aug	210.1	209.9	209.7	208.9	193.5	193.2	192.9	191.9
Sep	169.3	169.0	168.6	167.1	142.7	142.4	141.7	139.8
Oct	99.2	98.8	98.4	97.4	66.0	65.5	65.1	63.5
Nov	48.2	48.0	47.7	47.1	21.1	20.9	20.7	19.9
Dec	42.3	42.1	41.8	40.7	16.5	16.3	16.0	14.8
Year	1411.8	1408.8	1405.3	1395.0	1095.1	1091.3	1087.4	1073.8

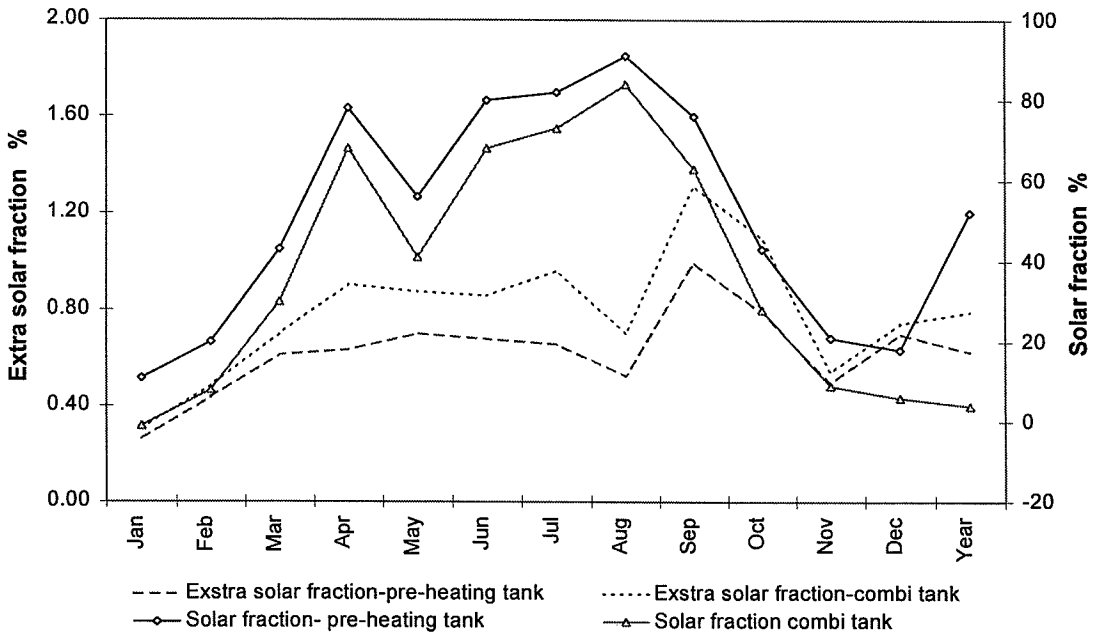

Figure 7.1 Calculated solar fraction and extra monthly solar fraction for system with mantle tank.

The same investigation simulations were also performed for the system with the heat exchanger spiral tank, and the results are shown in Table 7.5. Obviously, the larger the time scale of the input weather data is, the smaller the net utilized solar energy. The net utilized solar energy gain by reducing the time scale of the input weather data from 60 min to 10 min is 15.6 *kWh* for the combi tank system and 12.1 *kWh* for the pre-heating tank system. However, compared to the results from the system with a mantle tank, the influence of the weather data on the thermal performance of the spiral heat exchanger tank system is relatively small.

Table 7.5 Calculated net utilized solar energy for the system with a built-in heat exchanger spiral tank (CDF96' weather data)

Period	Net utilized solar energy (kWh) (pre-heating tank)				Net utilized solar energy (kWh) (combi tank)			
	10 min	20 min	30 min	60 min	10 min	20 min	30 min	60 min
Jan	22.1	22.0	21.9	21.5	-4.1	-4.1	-4.1	-4.5
Feb	34.3	34.2	34.1	33.7	13.5	13.3	13.3	12.9
Mar	84.3	84.0	83.7	83.0	58.7	58.4	58.1	57.5
Apr	159.7	159.6	159.3	158.7	138.7	138.6	138.2	137.8
May	109.0	108.8	108.5	108.6	81.5	81.4	80.8	80.8
Jun	162.1	161.9	161.7	161.0	137.3	137.0	136.6	135.7
Jul	173.7	173.4	173.0	171.9	152.1	151.6	151.3	149.5
Aug	197.2	196.9	196.6	195.9	180.2	179.8	179.5	178.1
Sep	146.8	146.6	146.4	145.0	121.1	120.8	120.6	119.0
Oct	79.7	79.4	79.3	78.8	52.9	52.5	52.4	51.7
Nov	38.4	38.1	38.0	37.5	16.2	16.0	15.8	15.3
Dec	30.8	30.8	30.5	29.9	9.5	9.4	9.2	8.8
Year	1238.1	1235.7	1233.1	1225.5	957.6	954.3	951.7	942.5

It has been proved that an increase of hot-water load has a strong effect on the net utilized solar energy. In order to investigate the influence of the hot-water load on the extra net utilized solar energy, by using 10 min. input weather data instead of 60 min. data, simulations were carried out for the two reference systems with different hot-water load conditions. Here, the extra net utilized solar energy is defined as the ratio of the net utilized solar energy difference between using 10 min. and 60 min. weather data to the calculated net utilized solar energy from the 60-minute weather data.

Figure 7.2 shows the extra net utilized solar energy as a function of the hot-water load. It can be seen that the increase of hot-water load results in a decrease of the extra net utilized solar energy under all conditions. However, the figure shows that the change of the extra net

utilized solar energy with the hot-water load is different for the pre-heating tank systems and the combi tank system. For both reference systems with a combi tank design, the change of the extra net utilized solar energy with the variation of hot water load is significant. As the hot water load increases from 50 *l* to 100 *l*, the extra net utilized solar energy decreases from 3.4% to 2.3% for the system with mantle tank, and from 2.5% to 1.8% for the system with a heat-exchanger spiral tank. When the hot-water load is beyond 100 *l*, a relatively slow reduction of the extra net utilized solar energy is observed. For the two reference systems with the pre-heating tank design, the extra net utilized solar energy is only slightly influenced when the water load changes from 50 *l* to 200 *l*.

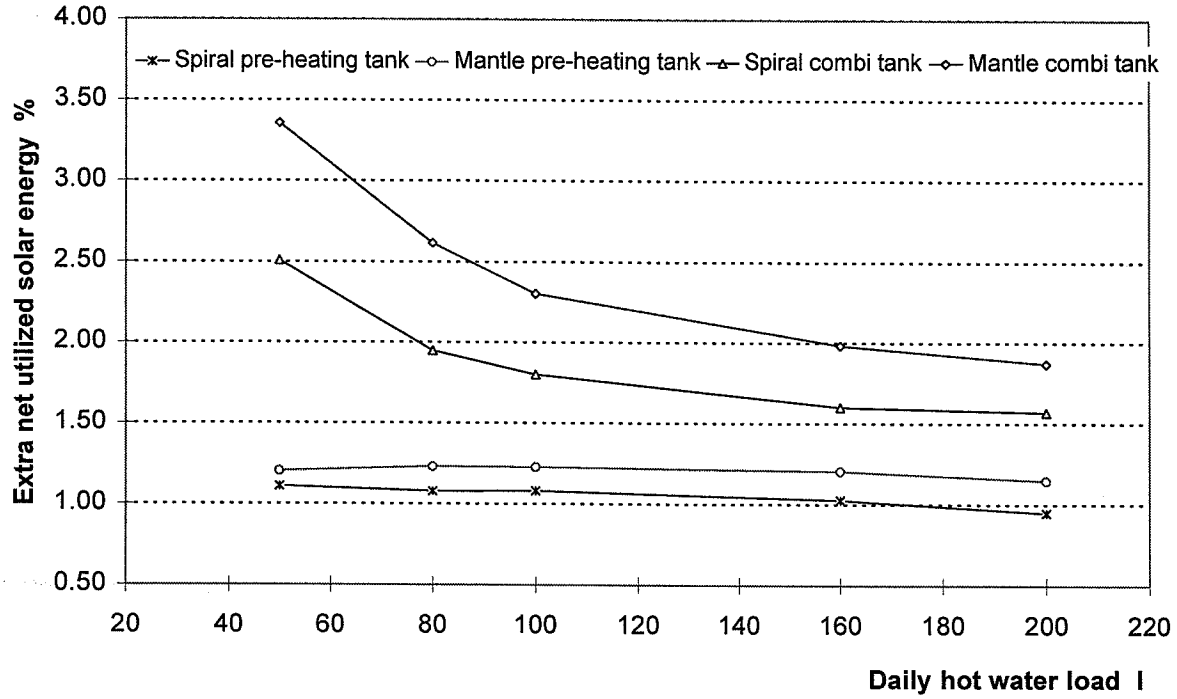

Figure 7.2 Extra yearly net utilized solar energy as a function of hot water load.

In [23], Furbo and Carlson have found that the extra net utilized solar energy by reducing the time step of weather data from 60 to 2 minutes depends strongly on the solar fraction of the system. To gain further insight into the impact of the solar fraction on the extra solar fraction, a large group of simulations, based on the reference systems and different hot-water load conditions, were carried out. Figures 7.3 - 7.6 show the simulation results for the two systems with both pre-heating tank design and combi tank design. The figures show the extra monthly net utilized solar energy achieved by reducing the time scale of the input weather data from 60 to 10 minutes, as a function of solar fraction.

For the pre-heating systems, it can be seen from Fig. 7.3 and Fig. 7.4 that the extra net utilized solar energy follows a definite changing pattern as the solar fraction increases. When the solar fraction increases from 10% to 30%, the extra net utilized solar energy decreases very rapidly. The reduction is relatively slow when the solar fraction is more than 30%. For the systems with a solar fraction of 50%, the extra net utilized solar energy is about 1% to

1.2%. It can also be seen that the extra solar fraction may be up to 4% for the pre-heating system with very low solar fraction.

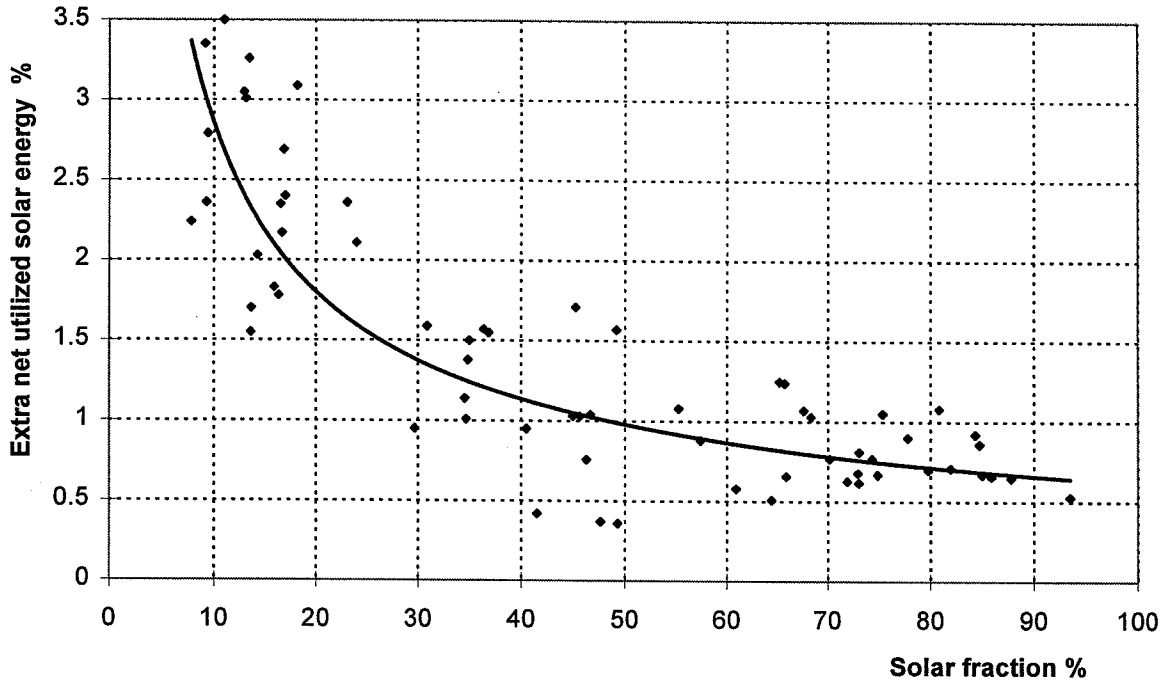

Figure 7.3 Extra net utilized solar energy as a function of solar fraction (system with pre-heating heat exchanger spiral tank).

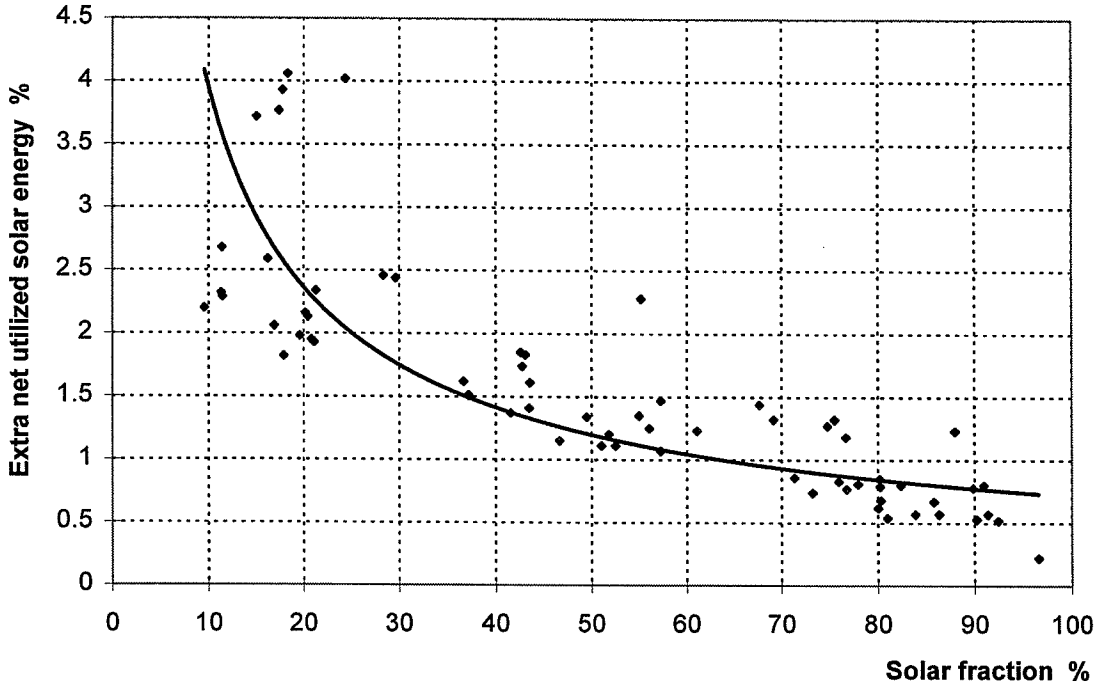

Figure 7.4 Extra net utilized solar energy as a function of solar fraction (system with pre-heating mantle tank).

Fig. 7.5 and Fig. 7.6 show the extra net utilized solar energy as a function of solar fraction for the combi tank systems. It is obvious that the extra net utilized solar energy shows a clear changing pattern with the increase of the solar fraction. The great effect of the solar fraction on the extra net utilized solar energy appears when the solar fraction is below 30%. As the solar fraction changes between 30% and 90%, a small decrease of the extra net utilized solar energy was observed. For the system with solar fraction of about 50%, the extra net utilized solar energy is approximately 1.6% to 1.9%.

The tendency curves of the extra net utilized solar energy as a function of solar fraction for the two types of systems are shown in Figure 7.7. It is obvious that the time scale of input weather data has the strongest influence on the system with a combi mantle tank and low flow operation design. With a solar fraction of 10%, the extra net utilized solar energy may be up to 6.5%.

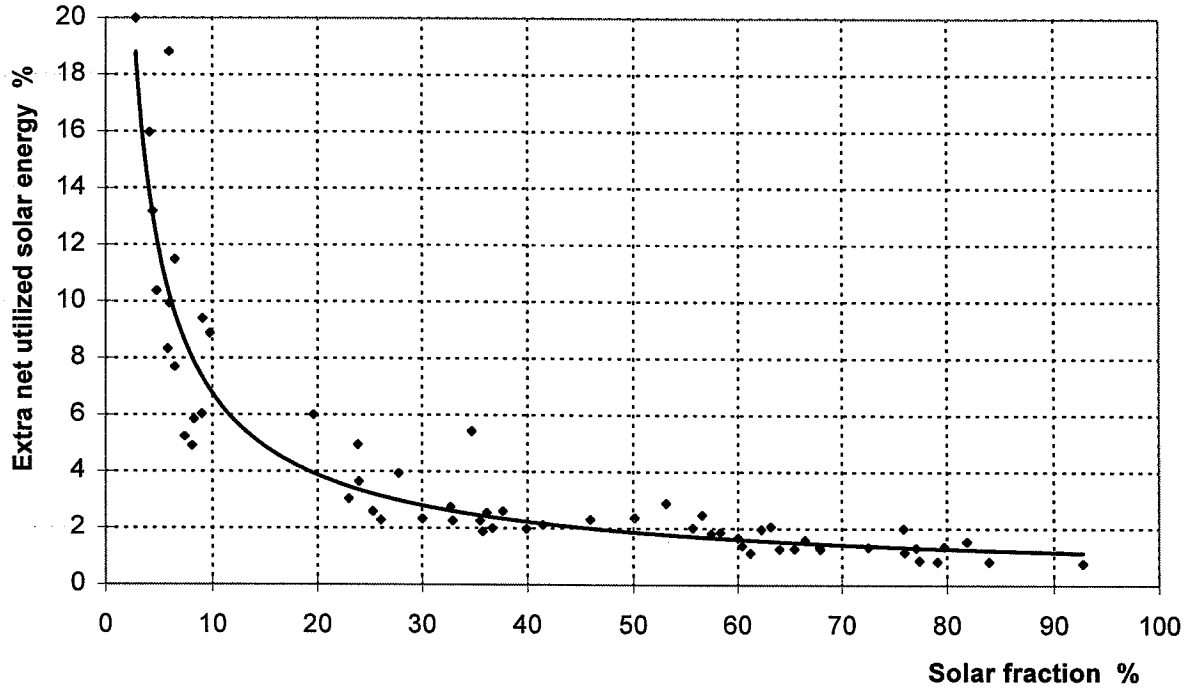

Figure 7.5 Extra net utilized solar energy as a function of solar fraction (system with combi mantle tank).

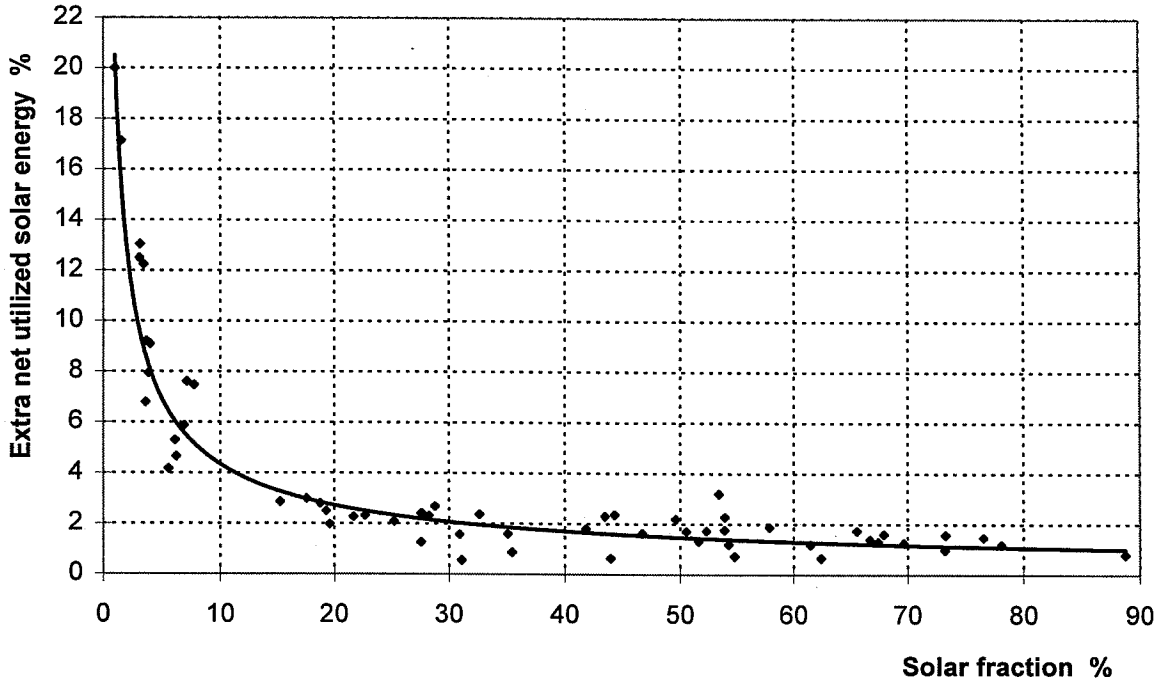

Figure 7.6 Extra net utilized solar energy as a function of solar fraction (system with combi heat exchanger spiral tank).

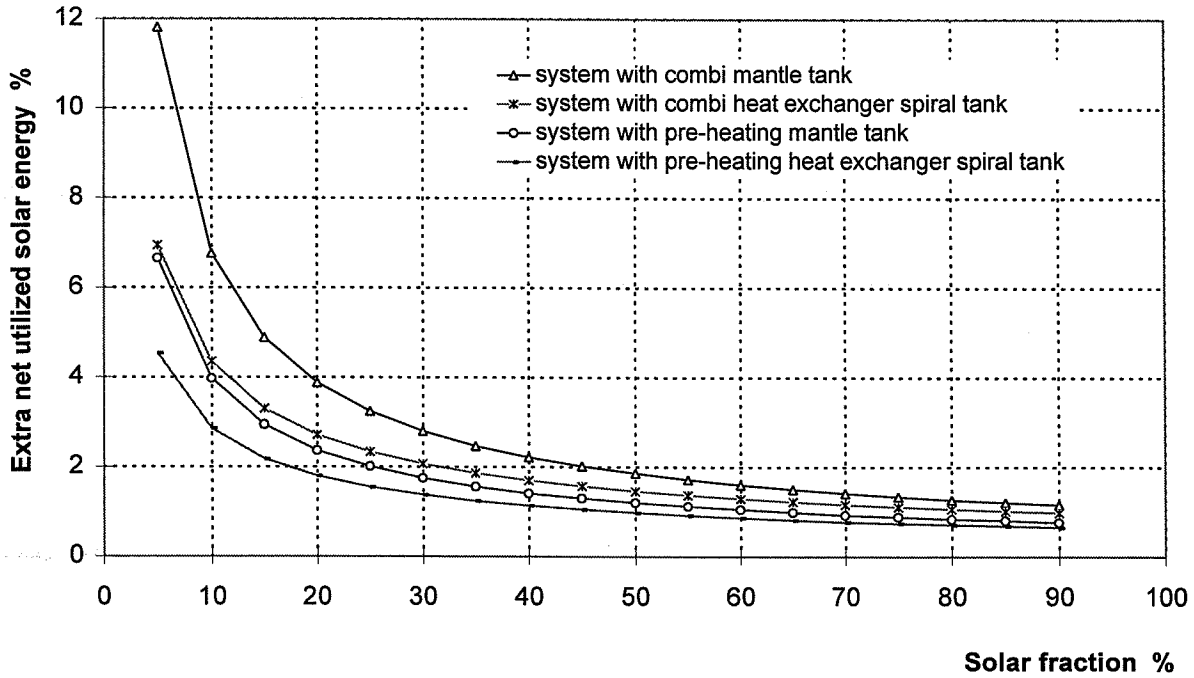

Figure 7.7 Extra net utilized solar energy as a function of solar fraction for all systems.

It should be pointed out that the investigation of the extra net utilized solar energy here is based on 10 *min.* to 60 *min.* input weather data. Additional small increase of extra net utilized solar energy and extra solar fraction could be further achieved by using an even smaller time scale of input data. Based on the simulation results presented in Tables 7.4-7.5, the extra net utilized solar energy as a function of time scale of input weather data was studied and the results are shown in Figure 7.8. It is clear that the extra yearly net utilized solar energy shows a linear increase with the decrease of the time scale of input weather data. For the combi tank systems, the yearly extra net utilized solar energy could be up to 2.3% for the low flow mantle tank system and 1.9% for the system with heat exchanger spiral tank. For the pre-heating system, the extra net utilized solar energy of 1.5% and 1.2% was observed for the mantle tank system and the spiral heat exchanger tank system.

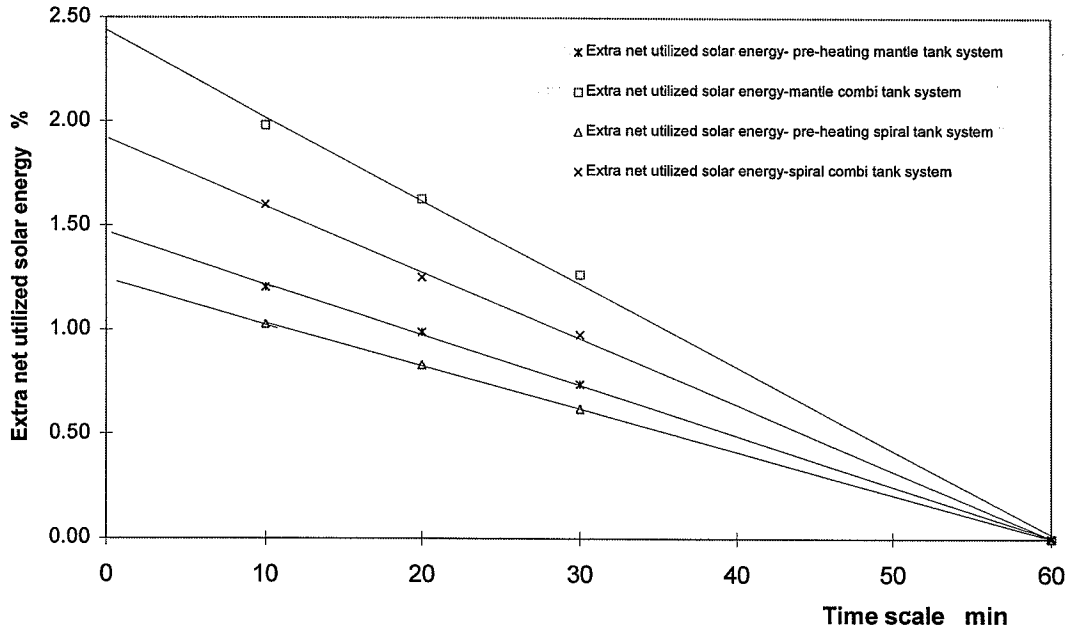

Figure 7.8 Extra yearly net utilized solar energy as a function of time scale of input weather data.

8.5 Conclusion and discussion

The impact of the time scale of the input weather data on the simulation results has been studied for solar DHW systems. To carry out the investigation, a 10-minute climatic data file CDF96' was formulated based on the 10-minute measurements in Denmark, 1996. Different time scales of input weather data from 10 minutes to 60 minutes have been used in the group of simulations.

Simulation results show that the time scale of input weather data has a relatively small influence on the calculated thermal performance. As the time scale of input weather data increases, the simulated net utilized solar energy decreases. However, the degree of impact is different for different systems. For systems with mantle tanks and low flow operation, the extra net utilized solar energy, achieved by reducing time scale of input weather data from 60

minutes to 10 minutes, is larger than that for the systems with heat exchanger spiral tanks and normal flow rate.

The daily hot-water load also has an influence on the extra net utilized solar energy. For the combi tank system, a rapid reduction of extra net utilized solar energy is observed as the daily hot-water load increases. However, the influence is small for the systems with a pre-heating tank design.

The extra net utilized solar energy strongly depends on the solar fraction of the system. The smaller the solar fraction, the greater the extra percentage of net utilized solar energy. When the solar fraction is below 30%, the increase of extra net utilized solar energy is increasingly significant with the decrease of the solar fraction. The increase of extra net utilized solar energy for the solar fraction from 90% to 30% is relatively small.

For the systems with a combi tank design, the extra net utilized solar energy for a solar fraction between 40% and 50% is about 1.6% to 2%. For the pre-heating system, an extra net utilized solar energy of 1% to 1.3% is observed for solar fractions between 40% and 50%.

All the results presented above are achieved from the investigation of the time scale of input weather data from 10 min to 60 min. It should be noticed that an additional small increase of the extra net utilized solar energy and extra solar fraction would be achieved by using even small time scale input weather data. It is believed that the extra net utilized solar energy for solar fraction between 40% and 50% may be up to 1.9% to 2.3% for the combi tank system and to 1.2% to 1.5% for the pre-heating system.

Chapter 8

Conclusions and outlook

8.1 Conclusions

The object of this study was dynamic modeling, simulation and optimum design of solar DHW systems, with respect to different weather conditions, and accurate dynamic behavior of the heat load. Special attention was paid to systems with thermosyphon and drain-back design.

A Beijing TRY that is based on limited 4-year hourly (or 6-hourly) measurements and long-term daily (and/or monthly) values was developed by statistical analysis and "Danish methods". It was shown that the cubic-spline interpolation method is suitable to generate hourly data from the limited available data that include daily maximum and minimum values. Typical months for the Beijing TRY are selected from 4-year hourly data, but the selection was done by comparison with 13-year monthly data. It has been shown that it is possible to control the quality of a TRY that is based on short-period hourly data, in a reasonable range by employing long-term daily (and/or monthly) data. The Beijing TRY formulated in this study can be used as input weather data for the simulation of solar energy systems and the calculation of heat balance for heating and ventilation systems under Beijing weather conditions.

Theoretical models that describe the flow and thermal processes in a domestic hot-water distribution network were developed. Different from other pipe network models, the present model takes the fact into consideration that the flows in the DHW distribution networks are also controlled by the temperature variation. To determine the flow distribution in the network, quasi-steady state calculations are performed in each time step. The linear-theory method, which is recommended by several authors for steady state analysis of pipe networks, was employed in the solution procedure. The advantage of applying the liner-theory method is that it is possible to simply supply an initial guess of all flow rates equal to unity for the first iteration. However, the weak point of using this method is that in some cases a great number of iterations must be applied before convergence is achieved, which makes the simulation time consuming.

Simulations were carried out to investigate how the operation parameters such as tank outlet temperature, hot-water load and load patterns effect the heat loss from the distribution networks. It was found that the thank outlet temperature has a significant influence on the heat loss from the circulation type of distribution networks, while the hot-water load and load pattern have no considerable effect on the heat loss. Therefore, one important conclusion is

that for system simulations, the heat loss from a distribution network may be formulated as a function of the tank outlet temperature alone.

Dynamic models for drain-back tanks, both as separated tank and combined with a mantle tank, were developed in this study. Models for other components that are used in solar DHW systems were also presented. Furthermore, by combining the dynamic models of the components, system models which permit the simulation of heat production and distribution in the solar DHW systems are constructed. After being verified, these system models were shown to be usable for the prediction of system performance and the optimization of design parameters.

Thermosyphon solar DHW systems with a collector loop that is directly connected with a storage tank are still most commonly used in many parts of the world. A refined thermosyphon loop model was developed in this study, and an iterative method was used for the solution procedure to determine the flow conditions. System simulations were performed to investigate the impact of design parameters on the thermal performance of the system, both under Beijing and Danish weather conditions. It was found that only the collector tilt and the heat loss coefficient of the collector effect the system thermal performance differently for those two areas. However, under the same system configuration and operation conditions, the solar fraction is generally smaller for the Danish conditions. It was also shown here that system simulations are able to predict accurately the optimum values for the collector tilt, the diameter of connection pipes, the height of the return pipe, and the ratio of tank volume to daily hot-water load. However, accurate optimal values for parameters such as the collector area and the maximum efficiency of the collector, need comprehensive analyses from both technical and economy points of view.

Another type of solar DHW systems that was investigated in this study is the ones with a drain-back design. System models for drain-back systems both with spiral heat exchanger tank and mantle tank were developed. For the mantle tank systems, a very detailed tank model has been modified and used in the system simulation. On the one hand, this makes the simulated results more accurate, but on the other hand, it also makes the simulation very time consuming. The strong point of the drain-back system models presented in this study is that they all have been verified by means of measured data from laboratory tests, which makes the simulation result more reliable than the ones from purely theoretical models.

By applying these verified system models, a number of simulations were carried out for these two types of drain-back systems under Danish weather conditions. The results present that the thermal performance of these two types of system shows a similar dynamic response to the variations of most design parameters, except the control temperature difference. With the same basic system design, this study shows that systems with a mantle tank design result in a relatively good thermal performance. From the simulation results, recommendations on optimum value of design parameters, such as, flow rate in the collector loop, collector tilt, heat storage volume and mantle design etc., can be given for these types of systems.

To investigate the impact of drain-back design and the different working fluids on the system thermal performance, simulations were also carried out for parallel systems with normal and with drain-back design. When the same working fluid was used, systems with normal design

result in a relatively good thermal performance. However, the usage of water instead of water-glycol mixture as working fluid improves the system performance to some degree. As a consequence, systems with drain-back design show a slight advantage in the system thermal performance.

Another object of this study was to investigate the impact of the time scale of input weather data on the simulated thermal performance. By applying mean values of input weather data with different duration, it was found that the time scale of input weather data has an effect on the simulation results. The smaller the time scale is, the higher the thermal performance. The degree of this effect is also influenced by the system and the operation design. For systems with combi tank and low flow operation, the time scale of the input weather data has a relatively strong influence on the simulation results, if compared to systems with a preheating tank design. However, generally the time scale of input weather data, in the range of 10 to 60 *min*, has only a small influence on the simulated thermal performance. Therefore, accurate simulation results could be achieved by amending the result from commonly used 60 min input weather data with a correction coefficient.

It can be concluded that the system models developed in this study are applicable for system simulation and analysis. Using these models is a suitable, efficient and economical way for the optimum design of solar DHW systems. The simulation programs that were developed or modified in this study may be used as tools for the systems design and analysis.

8.2 Outlook

In the present study, the Beijing TRY has been constructed based on the limited 4 years' hourly measurements. Because of this limitation, an important checking procedure on the radiation data (according to the "Danish method") could not be performed, and large deviations of some important parameters could have appeared in some of the months. Further analysis and improvement of the Beijing TRY are needed when long-period hourly measurements are available.

A dynamic model of DHW distribution networks was developed. A remaining challenge for the dynamic modeling of the heat load could be the detailed modeling of the regulation of each individual consumer. A drawback of the presently used program for the dynamic simulation of distribution networks is that it cannot deal with extreme conditions such as a control valve that is closed completely within a short period. Further programming work should be put forward to solve these problems.

There are many different kinds of solar DHW systems based on different working principles; here, only systems with thermosyphon and drain-back design were investigated. The types of thermosyphon and drain-back systems which were chosen for this study are common, but they are not necessarily the best design of these kinds of systems. Further investigation on the thermal performance of systems with different designs could be of interest.

Last, but not least, it is necessary for the optimum design of solar DHW systems, to perform studies that are incorporating an economic point of view.

System simulation has proved to be a powerful and efficient method for system design and analysis. The growing availability of faster computer systems will allow very accurate models to be used in the simulations, and that might lead to a growing importance of system simulation in the practical development of solar DHW systems.

Nomenclature

Upper case

A_c	area of the collector	m^2
A_{ci}	area of collector segment i	m^2
A_e	surface area of heat exchanger spiral	m^2
A_t	cross section area of the tank	m^2
B_0	solar constant	W/m^2
B_{s0}	extraterrestrial irradiance	W/m^2
C	Hazen-Williams coefficient	
C_1,C2	constant of heat exchanger coil	
C3,C_4	constant of heat exchanger coil	
C_p	thermal capacity of water	J/kgK
C_{pc}	thermal capacity of the collector	J/m^2K
C_{pd}	thermal capacity of drain-back tank	J/K
C_{pf}	thermal capacity of the fluid	J/kgK
C_{pi}	thermal capacity of pipe i	J/K
C_{ps}	thermal capacity of tank wall material	J/kgK
C_{pw}	thermal capacity of water and pipe	J/mK
D	outer diameter	m
D_d	outer diameter of drain-back tank	m
D_p	outer diameter of pipe	m
G	solar irradiance	W/m^2
Gr	the Grashof number for the characteristic length of heat exchanger pipe	
G_{0d}	daily extraterrestrial irradiation on horizontal surface	Wh/m^2
H	heat exchange capacity rate	W/K
H_a	the total height of air gap in mantle	m
I_{dir}	direct radiation on horizontal surface	W/m^2
I_{DN}	beam radiation	W/m^2
IAM	incident angle modifier coefficient	
$K(u_1)$	time and department number dependent factor	
$K(u_2)$	time and department number dependent factor	
L	length of pipe	m
L_e	length of heat exchanger pipe	m
M_c	mass content of collector array	kg
P	pressure	Pa
Pr	Prandtl number	
Pr_a	Prandtl number of air	
Pr_m	Prandtl number of the heat transfer medium at the average temperature inside the exchanger coil	
Pr_w	Prandtl number of the heat transfer medium at the average temperature at the inner surface of the exchanger coil	
Pr_f	Prandtl number of water at the mean temperature between the outer surface of the exchanger and the water in the tank	
Q_z	total net heat demand in time period *Z*	Wh
Q_b	heat demand for an apartment	Wh

Q_{cond}	heat exchange by conduction	W
Q_{conv}	heat exchange by convection	W
Q_{loss}	heat loss	W
R	thermal resistance	
R_a	Reyleigh number	
R_{ei}	the thermal resistance of inner surface of the heat exchanger pipe	K/W
R_{eu}	the thermal resistance of outer surface of the heat exchanger pipe	K/W
R_{ep}	the thermal resistance of the heat exchanger pipe wall	K/W
Rf	pipe resistant coefficient	
R_t	inner radius of water tank	m
S	standard deviation	
$\overline{T}$	mean temperature	°C
T	temperature	°C
T_0	room temperature	°C
T_a	ambient temperature	°C
T_c	collector outlet temperature	°C
$\overline{T}_c$	mean temperature of collector	°C
T_{ci}	collector inlet temperature	°C
T_d	temperature of drain-back tank	°C
T_{db}	temperature of drain-back fluid	°C
T_{di}	inlet temperature of drain-back tank	°C
T_e	temperature of the fluid in the heat exchanger	°C
T_{ei}	inlet temperature of the heat exchanger	°C
T_{eu}	outlet temperature of the heat exchanger	°C
T_i	inlet temperature of component	°C
T_m	mean temperature	°C
T_s	temperature in storage tank	°C
T_u	outlet temperature of component	°C
U_b	heat loss coefficient of the tank bottom wall	W/K
U_d	total heat loss coefficient from drain-back tank	W/K
U_e	heat transfer coefficient of heat exchanger spiral	$W/m^2 K$
U_l	heat loss coefficient of the tank side wall	W/m K
U_p	heat loss coefficient of the pipe	W/m K
U_t	heat loss coefficient of the tank top wall	W/K
V	volume flow rate	m^3/s
V_d	volume of the fluid in a drain-back tank	m^3
V_i	volume of tank segment i	m^3
Y	year number	

Lower case

a	coefficient	
b	coefficient	
d	inner diameter of connecting pipe	m
d_{ei}	inner diameter of heat exchanger pipe	m
d_{eu}	outer diameter of heat exchanger pipe	m
dn	day number in a year	

dR_1	the thickness of tank wall	m
dR_2	the thickness of mantle	m
dR_3	the thickness of mantle wall	m
e_b	thickness of insulation on bottom wall	m
e_s	thickness of insulation on side wall	m
e_t	thickness of insulation on top wall	m
f	friction loss coefficient	
g	gravitational constant	
Δh	energy head loss through a pipe	Pa
h	energy head	Pa
h_1	heat transfer coefficient between tank wall to tank water	W/m^2K
h_2	heat transfer coefficient between mantle fluid to tank wall	W/m^2K
h_3	heat transfer coefficient between mantle fluid to mantle wall	W/m^2K
h_a	heat transfer coefficient between air in the mantle to tank wall	W/m^2K
h_{ei}	heat transfer coefficient of inner wall of heat exchanger	W/m^2 K
h_{eu}	heat transfer coefficient of outer wall of heat exchanger	W/m^2 K
h_f	friction head loss	m
h_i	heat transfer coefficient	W/m^2K
h_{mt}	heat transfer coefficient between mantle top wall and the air in the mantle	W/m^2K
h_{mb}	heat transfer coefficient between mantle bottom wall and the fluid	W/m^2K
h_{ma}	heat transfer coefficient between the air and fluid in the mantle	W/m^2K
l	length of connecting pipe	m
l_i	length of element i	m
$\dot{m}$	mass flow rate	kg/s
$\dot{m}_c$	mass flow rate in collector loop	kg/s
$\dot{m}_g$	drain-back mass flow rate	kg/s
$\dot{m}_t$	tapping mass flow rate	kg/s
k_0	collector heat loss coefficient	W/m^2K
k_1	collector heat loss coefficient	W/m^2K^2
k_T	clear sky index	
q	draw-off mass flow rate	kg/s
q(T)	energy exchange with surrounding	kg/s
r	sun-earth distance correction fact	
s	stream line distance	m
v	volume flow rate	m^3/s
t	time	s
z	height	m
z_1	height of collector outlet	m
z_2	height of tank bottom	m
z_3	height of riser pipe connected to the tank	m

Greek

α	absorptance of the absorber	
α_1	natural convection coefficient	W/m^2 K
α_{air}	heat transfer coefficient between surface and air	W/m^2 K

β	expansion coefficient	K^{-1}
β_1	coefficient	
η	collector efficiency	
η_0	maximum collector efficiency	
λ	thermal conductivity	W/mK
λ^{eq}	equivalent thermal conductivity	W/mK
λ_{ins}	thermal conductivity of insulation material	W/mK
λ_f	thermal conductivity of heat transfer fluid	W/mK
λ_p	thermal conductivity of pipe	W/mK
λ_s	thermal conductivity of tank wall material	W/mK
ν	kinematic viscosity	m^2/s
δ	declination	o
ϕ	latitude	o
ρ	density	kg/m^3
ρ_f	density of heat transfer fluid	kg/m^3
ρ_s	density of tank wall material	kg/m^3
γ	solar altitude	o
θ	incident angle	o
τ	transmitance of collector cover	
ω	hour angle	o
ω_0	sun set hour angle	o
ζ	overall head loss coefficient by fittings	
ψ	incident angle coefficient	

Reference

(1). Andersen, B., Eidorff, S., Hallgreen, L. Lund, H. *Danish Test Reference Year, TRY Meteorological Data for HVAC and Energy*, Report No 174, March 1986. Thermal Insulation Lab. Technical University of Denmark

(2). Antonopoulos, K. A. and Rogndakis, E.D., *A correlation for the optimum collector flow rate in one tank forced circulation solar water heater*, Renewable Energy vol.1, No.3/4, pp373-379, 1991

(3). Arbel, A. and Sokolov, M., *Improving load matching characteristics of a thermosyphonic solar system by thermostatically controlled circulation*, Solar Energy, vol.52, No.4, pp347-358, 1994

(4). Barr, A.B., Mcginn, S.M. and Cheng, S.B., *A comparison of methods to estimated daily global solar irradiation from other climatic variables on the Canadian prairies*, Solar energy, Vol.56, No3, pp213-224,1996

(5). Benonysson, A., *Dynamic modeling and operational optimization of district heating systems,* Ph.D. thesis, Laboratory of Heating and Air Conditioning, Technical University of Denmark, 1991. ISBN 87-88038-24-6

(6).Berg, P., *Højtydende solvarmeanlæg med små volumenstrømme,* Teoretiske undersøgelser Report No. 209, Laboratoriet for Varmeisolering, Danmark Tekniske Universitet, March 1990 (in Danish).

(7). Berkovsky,B.M., and Polevikov,V.K., *Numerical study on problems on high-intensive free convection*, in Heat Transfer and Turbulent Buoyant Convection, eds. D.B. Spalding and N.Afgan, Hemisphere, Washington,D.C.(1977).

(8). Bourges, B. *Climatic data handbook for Europe*, Kluwer Academic Publishers, The Netherlands. 1992. ISBN 0-7923-1716-5

(9). Bøhm, B., *Optimum operation of district heating systems,* Laboratory of Heating and Air Conditioning, Technical University of Denmark, 1994 (ISBN 87-88038-29-7).

(10). Calsson, P.F., *Solvarmeanlæg til brugsvands-og rumopvarmning,* Thermal Insulation Lab., Technical University of Denmark, Report No. 277 July 1995.

(11). Casey, T. J., *Water and wastewater engineering hydraulics*, Oxford University Press, 1992.

(12). Committee on the Challenges of Modern Society North Atlantic Treaty Organization, *Test Reference Year(TRY) Final Report,* Office of conservation energy research and development administration August 1977.

(13). Cross, H. *Analysis of flow in networks of pipe conduits or conductors*, Univ. of Illinois Bull. 286 (1936).

(14). Davidson, J.H., Carlson,W. T. and Duff, W.S., *Impact of Component Selection and Operation on Thermal Ratings of Drain-Back Solar Water Heaters*, Journal of Solar Energy Engineering, November 1992, Vol. 114/219

(15). Davidson, J.H., Carlson,W. T. and Duff, W.S., *Comparison of Experimental and Simulation Thermal Ratings of Drain-Back Solar Water Heaters*, Journal of Solar Energy Engineering, May 1993, Vol. 115/101

(16). Duff, W., *Advanced Solar Domestic Hot Water System,* a report of the Task 14 Advanced Solar Domestic Hot Water Systems Working Group, April 1996.

(17). Duffie, J.A. and Beckman, W. A., *Solar engineering of thermal processes,* John Wiley& Sons, New York, 1991.

(18). Dutre,W. *Simulation of water based thermal solar systems*, Kluwer Academic Publishers Dordrecht, the Netherlands(1991)

(19). Furbo, S. and Shah, L.J., *Laboratory Test of small SDHW systems*, North Sun'97, pp 153-160, June 9-11,1997. Espoo-Otaniemi, Finland.

(20). Furbo, S., *Varmelagring til solvarmeanlæg,* report number 162,(Sept. 1984), Thermal Insulation Lab. Technical University of Denmark (in Danish).

(21). Furbo, S., Undervisningsnotat, *Varmelager til solvarmeanlæg,* Institut for Bygninger og Energi , Danmarks Tekniske Universitet, Notat U-002, 1997. ISSN 1396-4046.

(22). Furbo, S. and Shah, L. J., *Optimum solar collector fluid flow rates*, EuroSun' 96 Proceedings, 10. Internationales Sonnenforum, 1996.

(23). Furbo, S. and Carlsson, P., *The thermal performance of small low flow solar heating systems* , Thermal Insulation Lab., Technical University of Denmark, Report No. 91-22 November 1991.

(24). Furbo, S. and Holck,O., *Efficiencies of solar collector for different tilts* Thermal Insulation Lab. Technical University of Denmark, Report No.95-07 May 1995

(25). Furbo, S., *Fordele Ved Små Volumenstrømme I solvarmeanlæg*, Meddelelse Nr. 188, Marts 1987, Laboratoriet For Varmeisolering Danmarks Tekniske Højskole.(in Danish)

(26). Furbo, S. and Ellehauge, K., *Undersøgelse af solvarmeanlæg fra Thermo Dynamics Ltd,* Thermal Insulation Lab. Technical University of Denmark, Report No.206, May 1994

(27). Hansen, L.B. and Furbo, S., *Solvarmeanlæg med Tømning*, Thermal Insulation Lab., Technical University of Denmark, Report No.257 March 1995 (in Danish).

(28). Hansen, T. H., *Optimization of large networks for natural gas,* Institute for Numerical Analysis, Technical University of Denmark, Repor NI-99-09, 1988.

(29). Hansen, T. H., *Optimization of pipe networks,* Institute for Numerical Analysis, Technical University of Denmark, April 1988.

(30). Hahne, E., *Prüfbericht Kollektortest*, nach DIN 4757,Teil 4(6.1994), Hersteller: Solar Nor AS, Type: SolarNor, Herstelljahr: 1996. Institut für Thermodynamik und Wärmetechnik Universität Stuttgart. (in Geman)

(31). Harrison, S. J. and Carpenter,A. M., *Recent Result of the S-2000 SDHW Monitoring Project,* Proceedings of SESC 1994, Ottwa,Ontario.

(32). Hazen, A. and Williams G. S., *Hydraulic Tables*, New York, 1920.

(33). Holck, O., *Prøvning af solfangeres effektivitet foretaget for prøvestationen for Solenergi solfangerfabrikant:Batec,* Report 93-15, Laboratoriet for Varmeisolering, Danmark Tekniske Universitet, May 1993 (in Danish).

(34). Holmberg, S., *Flow rates and power requirements in the design of water services*, Kungl. Tekniska Högskolan i Stockholm, 1987.

(35). Homonnay, G. and Barna, B., *District heating research and development in Hungary*, Nordic Council of Ministers, Energy research cooperation, June 1991.

(36). Isakson, P., S*olar collector model for testing and simulation,* Royal Institute of Technology Building Services Engineering, final report for BRF project Nr 900280-1, ISSN 0284-141x, 1995.

(37). Jensen, S. Ø., *Varmeovergang for Varmevekslere Neddykket i Vand,* Rapport 84-10, Laboratoriet for Varmeisolering, Danmark Tekniske Universitet, Maj 1984. (in Danish)

(38). Jensen, F. F. and Schadow, A., *Lagermodel med sammenhængende temperaturprofil* , Eksamensprojekt, juni 1994, Laboratoriet for Varmeisolering, Danmarks Tekniske Universitet.

(39). Jiang and J. Jia, *Simulation of dynamic performance of district heating systems*, Proceeding of the International Seminar on HVAC, Tsinghua-HVAC-91, Beijing, 1991.

(40). Knight, K.M., *A methodology for the synthesis of Hourly Weather Data,* Solar energy, Vol.46, No2, pp109-120,1991.

(41). Lawaetz, H., *Brugsvandsopvarming. Kort Gennemgang af DIN 4708,* Varme-og Installationsteknik, Teknologisk Institut, Denmark,1984,(in Danish).

(42). Lawaetz, H., *Vamtvandsforbrug i Boliger. Målinger af Vand-og Energiforbrugets Størrelse og Fordeling*, Varme-og Insttallationsteknik, Teknologisk Institut, Denmark, 1985 (ISBN 87-7511-544-1).

(43). Lin W.X. and Lu E.R., *The solar water heating system with natural circulation assisted by an auxiliary electric heater- performance modeling*, Energy conservation and management, Vol.31, No.5 (1991)

(44). Lund, H. *The Design Reference Year User Manual*, Report of task 9: Solar radiation and Parameter Studies, February 1995. Report No. 274 Thermal Insulation Lab., Technical University of Denmark

(45). Mazin, M. and Maleki, M., *Optimering af varmt brugsvandssystem* , Laboatoriet for Varmeisolering, Danmarks Tekniske Universitet, Juli 1995 (in Danish)

(46). Mills, A. F., *Heat Transfer*, University of California at Los Angeles, 1992. ISBN 0-256-07642-1

(47). Morrison, G.L.M. and Braun, J.E., *System modeling and operation characteristics of thermosyphon solar water Heaters*, Solar Energy, Vol 34, No.4/5,pp 389-405,1985

(48). Morrison, G.L., *Solar Radiation Data for INDONESIA,* Solar Energy, Vol.49, No1, pp65-76,1992.

(49). Morrison, G.L. and Sapsford, C.M., *Long-term performance of thermosyphonic solar systems,* Solar Energy, Vol.37, pp323-330,1988.

(50). Nielsen, H. B., *An efficient method for analyzing pipe networks,* Institute for Numerical Analysis, Technical University of Denmark, 1987.

(51). Otto W., Nielsen, J.E. and Dalsgaard Jacobsen T. *Ydelsesstatistik for mindre brugsvandsanlæg erfaringer fra det femte års målinger 1996.* Danish solar Energy Testing Laboratory,1997.

(52). Rahbek, J., and S. Svensen, *SolSim,Simuleringsprogram for solvarmeanlæg* ,Thermal Insulation Lab. Technical University of Denmark, Report No. 273, 1995.

(53). Press. W. H., Flannery, B. P., Teukolsky, S. A. and Vetterling, W., *Numerical Recipes in Pascal,* Cambridge University press, ISBN 0-521-37516-9, 1989.

(54). Schultz, J.M., *Effektiv brugsvandsopvarmning,* Thermal Insulation Lab., Technical University of Denmark, Report No. 226, December 1991.

(55). Shah, L. J. and Furbo, S., *Optimization of mantle tanks for low flow solar heating systems,* Proceedings of EuroSun'96(1996).

(56). Shah, L.J.,*Små low flow solvarmeanlæg med kappebeholdere*, Rapport R-009-1997, Institut for Bygninger og Energi, Danmark Tekniske Universitet, 1997. (in Danish)

(57). Shah, L. J. *Undersøgelse af små solvarmeanlæg til brugsvandsopvarmning*, Rapport R-1 Februar 1996.

(58). Shariah, A.M., Hittle, D.C. and Lof, O.G. *Computer simulation and optimization of design parameters for thermosyphon solar water heater,* Joint Solar Engineering Conference, San Francisco PP393-399 (1994)

(59). Stephenson, D. *Pipeline design for water engineers,* Elsevier Scientific Publishing Company, New York, 1976.

(60). Svendsen, S., *Solfangers effektivitet,* report number 109,(1981), Thermal Insulation Lab., Technical University of Denmark (in Danish).

(61). Thomsen,K., Kundsen,S. and Weitze,C.A., *Aktiv Solvarme*, Polyteknisk Midtvejsprojekt, Institut for Bygninger og Energi, Danmark Tekniske Universitet, 1997. (in Danish)

(62). Vaxman, M. and Scoklov, M. *Effects of connecting pipes in thermosyphonic solar system*, Solar Energy, , No.5 (1986).

(63).Werner, S., *The heat load in district heating systems,* Chalmer University of Technology, Goteborg, Sweden, 1984. ISBN 91-7032-145-0

(64). Yang, L.B., *District heating house stations with hot-water storage* , Ph.D. thesis, Laboratory of Heating and Air Conditioning, Technical University of Denmark, 1994. ISBN 87-88038-30-0.

(65). Zhao, H.P. *Analysis, Modelling and Operational Optimization of Distric Heating System*, Ph.D. thesis, Laboratory of Heating and Air Conditioning, Technical University of Denmark, 1995. ISBN 87-88038-31-9.

(66). Lin, Q. *Simulation programs for Ph.D. study of analysis, modeling and optimum design of solar domestic hot water systems,* Rapport SR-98-18, Department of buildings and Energy, Technical university of Denmark, July 1998.

APPENDIX 1

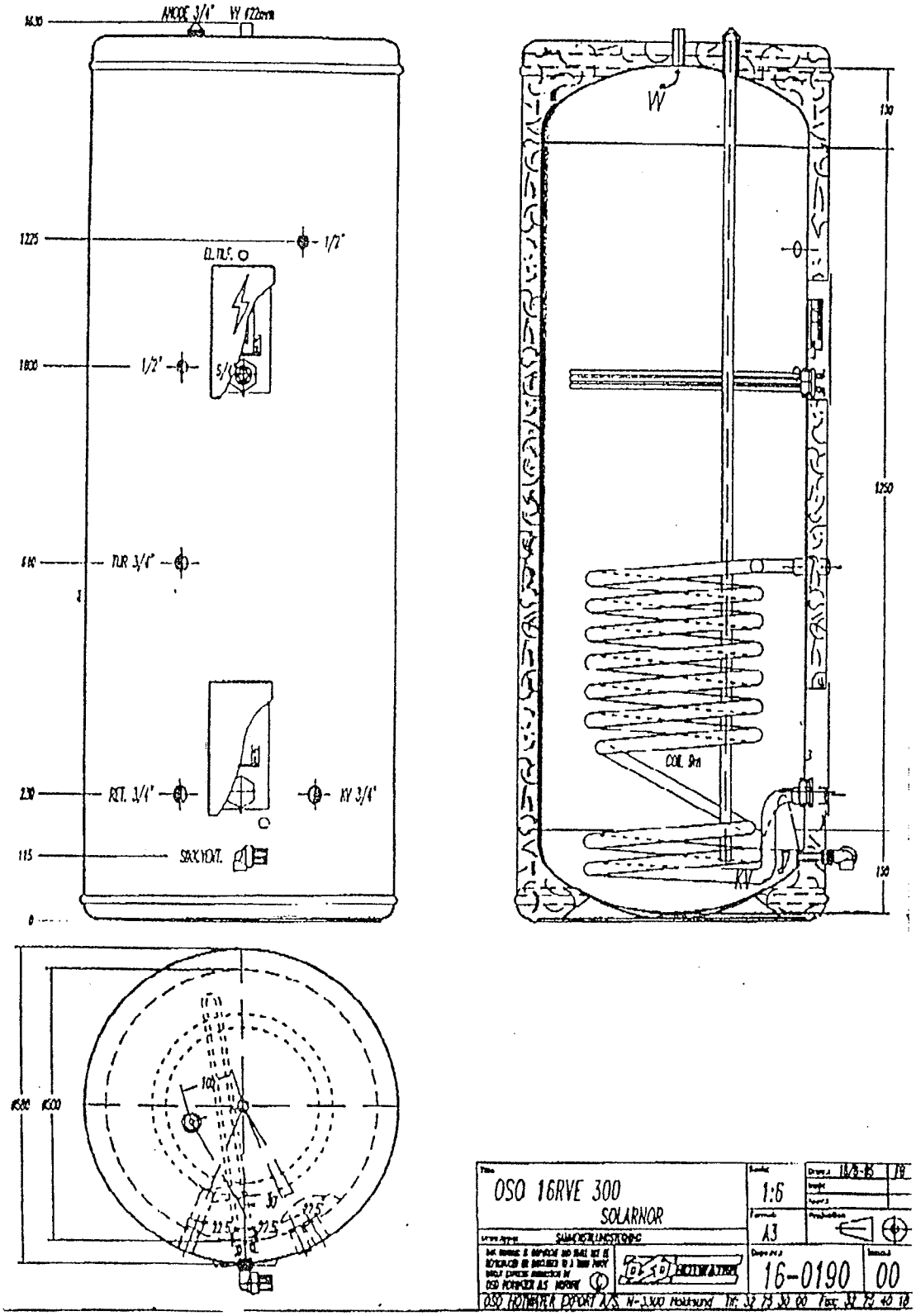
ANODE 3/4" W Ø22mm
1225
1/2"
EL.ELS.
1800
1/2"
S/T
TUR 3/4"
230
RET. 3/4"
KV 3/4"
115
SUG/VENT.
0
W
1250
COIL 9m
KV
OSO 16RVE 300
SOLARNOR
1:6
A3
16-0190
00
OSO HOTWATER DOOR AS N-1300 Hauøsund

APPENDIX 2